FOUNDATION FOR RESEARCH AND TECHNOLOGY – HELLAS
INSTITUTE OF ELECTRONIC STRUCTURE AND LASER

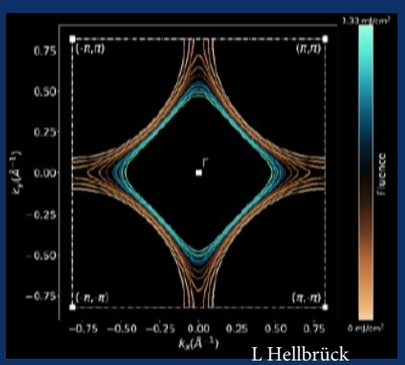

L Hellbrück

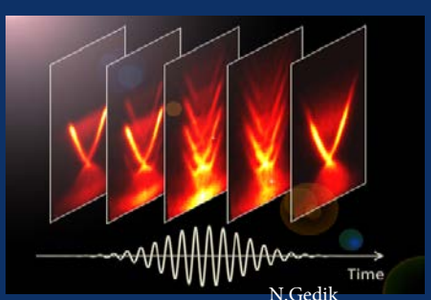

N.Gedik

Abstract Proceedings

ULTRAFAST DYNAMICS & METASTABILITY

ULTRAFAST BANDGAP PHOTONICS

2024

XI Symposium

Professor Michael K.Rafailov

University of Alberta

Professor Rolf Binder

University of Arizona Tucson

Professor Ilias E Perakis

The Foundation Research & Technology – HELLAS
University of Alabama at Birmingham

Abstract Proceedings comprising summaries of research papers prepared for two closely related Conferences dedicated to studies of nonequilibrium states in condenced matter– Ultrafast Bandgap Photonics and Ultrafast Dynamics and Metastability which forming the Symposium. The Symposium builds a bridge between cutting edge modern physics and emerging applications which are desperately in need. Symposium is vertically integrated, covering the area of interaction of high intensity and relatively low energy pulses with condensed matter, from fundamental physics to practically applicable energy sources, devices and technologies.

This workshop is the 11th in a series of International symposia, conferences and workshops on Ultrafast Dynamics and closely related and application technology driven y Ultrafast Bandgap Photonics which we are running from 2013. University of Crete and Foundation for Research and Technology - FORTH are hosting the 11th Symposium on the island of Crete-the 3rd time

The Symposium is organized by sections that are focused either on research field or on phenomena. The division is pretty much conditional, while providing direct access to general topics of interest for the research community and applications as well. Phenomenology topics, like ultrafast dynamic in heterostructures and spin-and orbital ultrafast phenomena may overlap areas of studies like noneqilibrium high temperature superconductivity and ultrafast magnetism, creating multiple entries into the Proceedings General reviews of Ultrafast Dynamics and Ultrafast Bandgap Photnics progresss as well as the most interesting recent discoveries are presented here as the keynote papers. Material oranized in sections and each section divided by sessions. Each section has the keynote papers, where results and considerations of most common interest topics are presented, while the Astract Proceedings is compiled based on generally alphabetic list of the speakers in Program -as it was presented at the Symposium. Plus to Table of Contents the Abstract Prosceeding has list of authors where the authors of submitted papers are listed with their papers associated page numbers.

The Abstract Proceeding is actually a snapshot of most interesting and noticeable research results in Ultrafast Dynamics and Ultrafast Bandgap Photonics which one can get in 2024. a snapshot of up to date research results and progress in Ultrafast Dynamics and Metastability and the applications in Ultrafast Bandgap Photonics. It is an Encyclopedia of Ultrafast Dynamics, Metastability and Ultrafast Bandgap Photonics that presents the status quo in the disciplines ranging from Theoretical Physics to Ultrafast Laser and covering practically all phenomena of interests in interaction of light with complexly organized condensed matter in form of low dimentional structures of different origins as well as bulk materials in different ambient contitions including temperature, static pressure, electric and magnetic potentials, biased irradience and so on.

Ultrafast Dynamics and Ultrafast Bandgap Photonics XI Symposium in Crete Abstract Proceeding book- with ***574*** Authors, ***133*** Speakers and more than ***1500*** authors in references listed in the papers below is practically represent the community of researchers actively working in the field now and as a matter of fact is the leading source of most recent information on the reserch results. Representing all Continents and most of the Countries involved in research in Ultrafast Dynamics and Ultrafast Bandgap Photonics the XI Symposium and its Abstract Proceedings could be considered as an important milestone in the development of Ultrafast Dynamics and Ultrafast Bandgap Photonics which now entering the most exciting stage - the stage of important technology applications raising from many years of great research results: specifically in the field of ultra-broadband electronics, high-temperature superconductivity, spintronics, material development, semiconductors, low dimentional and remote sensing.

In Loving Memory of Elena

Content
Crete 2024 Speakers and Titles

Long-lived photon echoes in semiconductor nanostructures: from Exciton to resident electron spin and nuclei spin dynamics

I. A. Akimov
Technische Universität Dortmund, 44221 Dortmund, Germany

Coherent optical response provides rich information about the energy structure and dynamical properties of the studied system and can be used for applications in quantum memories where light-matter interaction is exploited to store and retrieve optical fields in the form of photon echoes. Excitons in semiconductor nanostructures can be excited resonantly by sub-ps optical pulses on a very short timescale enabling access to large bandwidths but unavoidably leading to short radiative lifetime, which imposes limitations for optical storage time. Using the spin degrees of freedom, it is possible to extend the timescale of coherent optical response by several orders of magnitude and to explore the fascinating field of coherent optics with spins. In our earlier work, this concept has been achieved for localized charged excitons in CdTe quantum well structures and donor-bound excitons in bulk ZnO crystals [1, 2, 3]. It is based on resonant excitation of negatively charged exciton (trion) with a sequence of optical pulses in the presence of a transverse magnetic field. This allowed us to transfer the optical coherence of trions into the electron spin coherence of resident electrons with a significantly longer relaxation time and to extend the timescale of photon echo by 2-3 orders of magnitude from 50 ps to 50 ns [1, 2, 3]. For realistic quantum memory protocols, it is necessary to apply resonant optical pulses with an area of π, i.e. to perform robust Rabi flops. This is very difficult in semiconductor quantum wells and bulk crystals due to the strong damping of Rabi oscillations by excitation-induced dephasing [4]. Therefore, it is advantageous to use quantum dots (QDs) with strong localization potential which ensures robust coherence properties. In our recent studies, we have shown multiple Rabi rotations of trions in InGaAs quantum dots observed by photon echo spectroscopy with spatially shaped laser pulses [5]. Moreover, we have demonstrated that additional control pulses can be used as tuning knobs for adjusting the magnitude and timing of the coherent emission in a wide range up to several hundreds of picoseconds [6,7]. Finally, we revealed homogeneous optical anisotropy in an ensemble of symmetric self-assembled InGaAs quantum dots, i.e. optical and spin coherences in an ensemble of QDs subject to a transverse magnetic field can be initialized by linearly polarized optical fields in a deterministic way and most of the quantum optical approaches developed for single QDs can be transformed into ensembles [8]. These achievements in QD ensembles embedded in microcavity allowed us to perform the next step, the demonstration of long-lived spin-dependent echoes in charged QDs (see Fig.1).

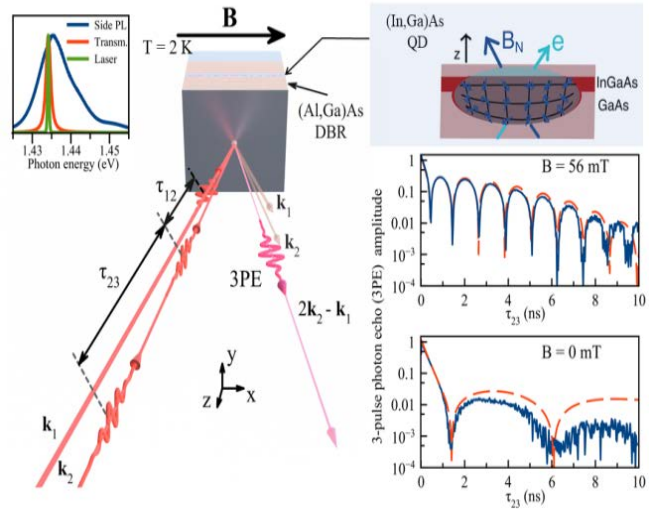

Fig. 1. Long-lived spin dependent echo in (In,Ga)As/GaAs quantum dots (QDs)*. Sketch of the photon echo experiment. (In,Ga)As quantum dots are embedded in a microcavity with GaAs/AlAs distributed Bragg reflectors (DBR). Three-pulse photon echo (3PE) results from resonant excitation of charged excitons (trions) with a sequence of three optical pulses delayed in time by τ_{12} and τ_{23}. External magnetic field* **B** *is applied in plane of the sample. Temperature T=2 K.* ***Left inset****: Low temperature photoluminescence (PL, blue line) and transmission (red line) spectra of the sample. The PL spectrum is shown for lateral emission from the edge of the sample in the direction parallel to its plane, e.g. along x-axis. The laser spectrum is shown with a green line.* ***Right inset****: Schematic diagram of an (In,Ga)As QD within a GaAs matrix. Small blue arrows at the nodes of the lattice represent random orientations of nuclear spins within the quantum dot. The arrow "*$\mathbf{B_N}$*" corresponds to the effective magnetic field of nuclear fluctuations acting on the resident electron spin "***e***."* ***Right****: Dependence of three-pulse photon echo on τ_{23} in a transverse magnetic field B = 56 mT (top) and in zero magnetic field (bottom). Blue lines show the experiment and red lines are calculations in the nuclear spin fluctuation model. The oscillatory decay reflects the spin dynamics of resident electrons in the resulting magnetic field* $\mathbf{B_{tot}}=\mathbf{B}+\mathbf{B_N}$.

Here, we have shown that despite strong inhomogeneous broadening, it is possible to perform a robust and efficient transfer between the optical and spin coherences and to observe long-lived spin-dependent photon echoes in an ensemble of charged self-assembled QDs. Without the magnetic field, the photon echo decays with $T_2 = 0.45$ ns which is determined by the radiative lifetime of trions$T_1 = 0.26$ ns.In the presence of the transverse magnetic field of about 50 mT, the decay of the photon echo signal is given by the spin dephasing time of the ensemble of resident electrons $T_{2,e} \sim 4$ns[9] as shown in the Fig.1 (top right). Moreover, the long-lived oscillatory response is also observed in a zero magnetic field (data

These oscillations occur due to spin precession of the resident electron spins in the effective fluctuating nuclear field, whose direction and magnitude are different in each quantum dot. We evaluated the mean field of nuclear spin fluctuations as 6.4 mT. The spin initialization for resident electrons in the photon echo protocol depends on the direction and magnitude of the effective nuclear field and therefore extends the possibilities for exploring the hyperfine interaction in semiconductor QDs [10].

References

[1] L. Langer, S.V. Poltavtsev, I.A. Yugova, D.R. Yakovlev, G.Karczewski, T.Wojtowicz, J. Kossut, *Physical Review Letters* **109**, 157403 (2012).
[2] L. Langer, S.V. Poltavtsev, I.A. Yugova, M. Salewski, D.R. Yakovlev, G. Karczewski, T. Wojtowicz, *Nature Photonics* **8**, 851 (2014).
[3] M. Salewski, S.V. Poltavtsev, I.A. Yugova, G.Karczewski, M. Wiater, T. Wojtowicz, D.R. Yakovlev. *Phvsical Review* X **7**, 031030 (2017).
[4] S.V Poltavtsev, M Reichelt, I.A. Akimov, G Karczewski, M Wiater, T Wojtowicz, D.R. Yakovlev ,Phvsical Review B **96**, 075306(2017).
[5] S Grisard, H Rose, AV Trifonov, R Reichhardt, DE Reiter, M Reichelt, C Schneider, M Kamp, *Physical Review B* **106**, 205408 (2022).
[6] A. N. Kosarev. H. Rose. S.V. Poltavtsev. M. Reichelt, C. Schneider, M. Kamp, S. Höfling, M.Bayer, *Communications Physics* **3**, 228 (2020).
[7] S. Grisard, A.V. Trifonov, H. Rose, R. Reichhardt, *ACS Photonics* **10**, 3161 (2023).
[8] A. V. Trifonov, I.A. Akimov, L.E. Golub, E.L. Ivchenko, I.A. Yugova, A.N. Kosarev, S.E. Scholz, C. Sgroi, Phvsical Review B **104**, L161405 (2021).
[9] A. N. Kosarev, A.V. Trifonov, I.A. Yugova, I.I. Yanibekov, S.V. Poltavtsev, A.N. Kamenskii, S.E. Scholz. *Communications Physics* **5**, 144 (2022).
[10] A. V. Trifonov, I.A. Yugova, A.N. Kosarev, Y.A. Babenko, A. Ludwig, A.D. Wieck, D.R. Yakovlev,*Physical Review* B **109**, L041406 (2024).

Exchanging quantum information with a nuclear spin ensemble: there and back again

M. Atatüre

University of Cambridge, Cambridge CB30HE, UK

Quantum nodes comprising multiple qubits coupled to photons can serve a range of quantum information applications including quantum repeaters and photonic cluster-state generation. An optically active solid-state spin qubit serving as broker to exchange information between a photon and several register qubits is one promising implementation. Multiple such spin-photon interfaces have demonstrated functionality including in diamond, silicon carbide and rare-earth doped YVO4 crystal. Many initial implementations involve an electronic spin in dipolar coupling to a small number of proximal nuclear spins, where their distance controls their coupling rate. III-V compound semiconductor quantum dots have superior optical properties including brightness, purity and coherence, and have efficient coupling to information-carrying single photons. However, they lack additional spins to act as register qubits for the electron spin qubit. Quantum dots offer an opportunity for a contrasting perspective to the few proximal spin implementations, namely the nuclear spin ensemble comprising the quantum dot itself. The resident electron spin qubit is Fermi-contact linked to a group of roughly 100,000 nuclei, which, if not managed, serves as a source of noise detrimental to the qubit's performance [1]. However, if these nuclei are sufficiently manipulated, they can potentially serve as an information reservoir by leveraging their collective behavior [2]. This concept bears similarities to spin-wave-based photonic memories in solid states or ferromagnetic magnon modes. Advances in controlling dense nuclear spin ensembles relied on dynamic nuclear polarization, reducing their magnetic-field fluctuations and allowing for electron-mediated collective nuclear excitations [3]. The final goal of a nuclear quantum register combines a controllable electron spin with a tailored nuclear ensemble.In this talk we will discuss the reversible quantum state transfer between an electron spin qubit and a collective excitation of 13,000 nuclear spins in a GaAs QD. We present a method to construct a collective nuclear state by polarizing Ga isotopes. Consequently, one of the Ga isotopes is set in our register's ground state, forming a coherent nuclear dark state with 60% polarization.

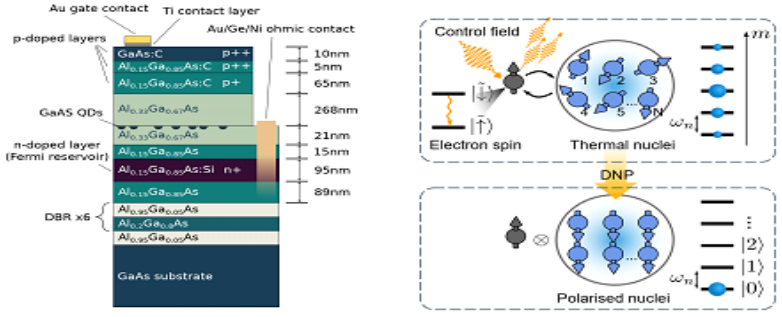

Fig. 1. Left Electrically gated heterostructure *device containing GaAs quantum dots.*
Right*: Illustration of electron-mediated control mechanism of the nuclear spin ensemble.*

Our electro-nuclear coherent control facilitates arbitrary state transfers from the electron spin qubit to the single magnon spin-wave states. We show that the register reaches a storage time of 130(16) µs, aligned with limitations from residual quadrupolar broadening.

References

[1] J. M. Taylor, C. M. Marcus, M. D. Lukin, *Physical Review Letters* **90**, 206803 (2003).
[2] B. Urbaszek, X.Marie,T.Amand, O.Krebs, P. Voisin, F. P. Maletinsky, A.Hogele, A. Imamoglu, *Review of Modern Physics* **85**, 79 (2013).
[3] D.A. Gangloff, G Ethier-Majcher, C.Lang, E.Denning, J.H.Bodey, D.Jackson, E.Clarke, M.Hugues, C.Le Gall, M.Atature, *Science* **364**, 62 (2019).

Photo-ionization and high-harmonic generation in zinc oxide Irradiated by intense mid-infrared femtosecond laser pulse

T. Apostolova[1], B. Obreshkov[2]
[1]*Institute for Advanced Physical Studies, 1618 Sofia, Bulgaria*
[2]*Institute for Nuclear Research and Nuclear Energy, 1784 Sofia, Bulgaria*

We theoretically investigate photo-ionization and high harmonic generation in the bulk of zinc oxide irradiated by intense femto-second laser pulses with mid-infrared wavelength (3 μm) in a wide range of laser intensities. For laser intensities below threshold for avalanche breakdown of ZnO we find that high harmonic generation (HHG) is strongly affected by the multiple band structure of the irradiated semiconductor. More specifically, it is shown that the sub-cycle response of multiple valence band holes to photo-ionization results in transient intra-band current responsible for the high-harmonic emission process. The intra-band mechanism is weakly dependent on the static band structure of ZnO and reflects the time-dependent characteristics of photo-ionization and photo-excitation process in a non-equilibrium plasma of electron-hole pairs. The corresponding HHG spectra resulting from photo-ionization for parallel and perpendicular laser polarization are calculated. For the parallel polarization, the power spectrum of both intra- and inter-band currents is dominated by bremsstrahlung and lacks clear harmonic structure (Fig.1a). For the perpendicular polarization, the inter-band current displays clear odd harmonic peaks below the absorption edge. The harmonic structure above the band edge is not so well defined. It consists of broad and overlapping harmonic peaks on top of the continuous background (Fig.1b). The non-adiabatic response of valence band holes manifests in the emergence of clean odd-harmonic structure in the intra-band current.

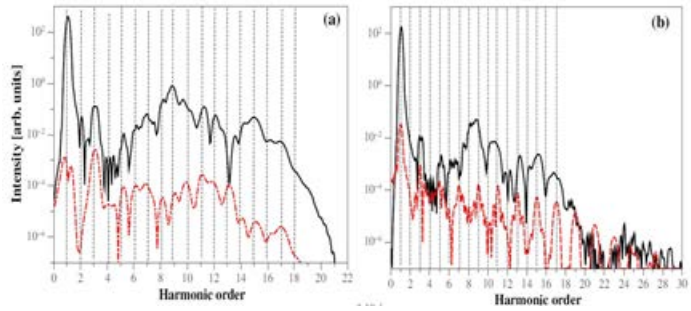

Fig. 1. Power spectrum of intra- (dashed red line) and inter-band (solid black line) currents *in the bulk of ZnO for peak laser intensity 10^{12}W/cm^2, laser wavelength 3 μm and pulse duration of 60fs.*
***Left*: a** *- the laser is polarized parallel to the optical axis;*
***Right*: b** *- the laser polarization direction is perpendicular to the optical axis.*

Taking into account the realistic, multiple band structure of the solid our theoretical calculations of HHG spectra show good semi-quantitative agreement with the experimental data [1],[2] without including ultra-fast de-phasing process. Clean and well-defined odd-order harmonic peaks extending beyond the band edge of ZnO are obtained for laser linearly polarized perpendicular to the optical axis of the crystal.

References
[1] S. Ghimire, A. D. DiChiara, E. Sistrunk, P. Agostini, L. F. DiMauro, D. A. Reis, *Nature Physics* **7**, 138 (2011).
[2] User experiment at ELI-ALPS lead by T. Apostolova; participants D. Velkov, M. Thoma (experiment ID :LIUPM162_MIR_ULTRAHIGH_TA.
* Acknowledgement(s): authors acknowledge support from the Air Force Office of Scientific,(grant number FA8655-24-1-7014) and awarded access to PetaSC Discoverer supercomputer resources, (T.A.) COST Action CA20129 and awarded by ELI user experiment ELIUPM162_MIR_ULTRAHIGH_TA; author (T.A.) is grateful to D. Velkov and M. Thoma for conducting the experiment.
** The abstract scientific content is not published yet and it was submitted to Physical Review A (9th of April 2024) and arXiv.
***Author (T.A.) acknowledges support from CFSR (New Bulgarian University).

A two-stage onset of helimagnetism in $Cr_{1/3}NbS_2$

Y. Ahn[1], W. Zhang[1], S. Mozaffari[2], D. Sapkota[2]
H. S. Arachchige[2], R. Xue[2], I. Mazin[3], K. Sun[1], D. G. Mandrus[4], L. Zhao[1]
[1] *University of Michigan, Ann Arbor, MI 48109, USA*
[2] *University of Tennessee, Knoxville, TN 37996, USA*
[3]*George Mason University, Fairfax, VA 22030, USA*
[4]*Oak Ridge National Laboratory, Oak Ridge, TN 37831, USA*

Chiral helimagnetism in $Cr_{1/3}NbS_2$ has served as an interesting host for studies of novel magnetic orders as well as tunable electrical properties relevant to its mesoscale magnetic textures [1]. However, the current understanding of helimagnetism has been indirectly inferred based on the measurement of material physical properties with an absence of the comprehensive understanding of the evolution of the helical magnetism [2]. Here, we demonstrate the second harmonic generation (SHG) spectroscopy as an outstanding method to investigate a chiral helimagnet $Cr_{1/3}NbS_2$. Combining SHG wide-field imaging and rotational anisotropy (RA) SHG scanning measurements, we reveal the existence of two chiral structural domain states and the formation of six helimagnetic domain states (Fig. 1(a)) upon an unexpected rotational symmetry breaking across the phase transition. The spatially resolved RA SHG patterns directly show that the six domain states

are related by vertical mirror and three-fold rotation symmetries, corresponding to the structural chirality and magnetism, respectively, in $Cr_{1/3}NbS_2$. We will also discuss the observation of the rotation symmetry breaking, ascribed to an existence of magnetic anisotropy, in striking contrast to a widely accepted assumption of negligible anisotropy in helical magnets.

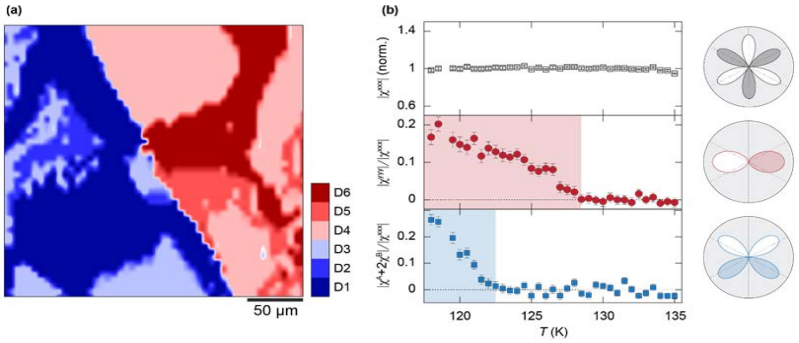

Fig. 1. (a) Map of helical magnetic order at 80 K, *visualizing the formation of helical order parameters with different directions in* $Cr_{1/3}NbS_2$.
(b) *Temperature dependence of nonlinear optical susceptibility tensors, corresponding to structure (**top**) and magnetism (**middle and bottom**) contributions.*

Furthermore, we observe two characteristic temperatures at which distinct nonlinear optical susceptibility tensors evolve. The probed susceptibility tensors are characterized by different symmetry properties, demonstrating that the helimagnetism in $Cr_{1/3}NbS_2$ undergoes two phase transitions. I will finally discuss potential pathways of helimagnetic phase transitions from the paramagnetic states.

References

[1] T. Moriya, T. Miyadai, *Solid State Communications* **42**, 209 (1982).
[2] N. J. Ghimire, M. A. McGuire, D. S. Parker, B. Sipos, S. Tang, J.-Q. Yan, B. C. Sales, D. Mandrus, *Physical Reivew* B **87**, 104403 (2013).

Exciton-polaritons with halide perovskites

W. Bao
Rensselaer Polytechnic Institute, Troy, NY 12180, USA

Recently, semiconducting lead halide perovskites with a composition of ABX_3 (where A is commonly $CH_3NH_3^+$ (MA^+) or Cs+; B is Pb^{2+}; X is Cl^-, and Br^-) have emerged as contenders to GaAs for polaritonic but at room temperature, due to their large exciton binding energy, high photoluminescence (PL) quantum yield, tunable bandgap and high room-temperature nonlinear interaction strength. With chemical vapor deposition (CVD), single-crystalline inorganic halide perovskites have shown polariton condensation. However, due to the limitations of the current growth methods and the fragile nature of perovskites, only small single crystals can be integrated into the optical cavities. Critically, the small sizes prohibit the studies of large-scale phenomena, such as superfluidity formation, XY spin Hamiltonian, and topological effects, due to the limited lattice size and the restricted propagation lengths.In this talk, I will first introduce our approach [1] to overcome the above size limitation and obtain various types of large halide perovskite single crystals inside optical nanocavities. Due to the uniform confined environment, the solution growth approach shows uniformity, comparable to the MBE-grown GaAs quantum well, enabling submillimeter-large single crystals with superb excitonic quality. These crystals with strongly interacting Wannier-Mott excitons allowed us to successfully demonstrate a polaritonic XY spin Hamiltonian at room temperature. Further, we show that a lattice with many coherently coupled condensates up to 10 x 10 can be achieved. This is a critical step towards the ultimate goal of realizing a room-temperature polaritonic platform on par with MBE-grown GaAs at low temperatures. In addition, we show that the dispersion of the perovskite system has unique advantages for future studies on synthetic non-Abelian gauge fields and topological physics.

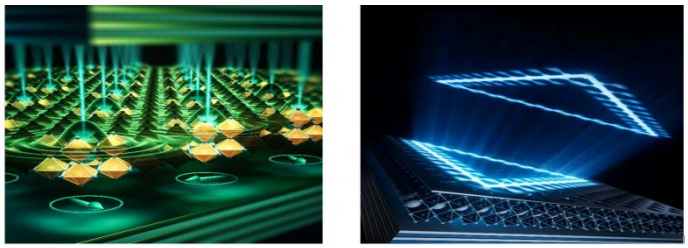

Fig. 1. Left: Schematic of polaritonic XY *spin Hamiltonian*
Right*: Schematic of polaritonic valley Hall laser.*

Lastly, I will introduce our recent two works using halide perovskite on topological valley Hall polariton condensation [2] and polariton superfluidity [3].

References

[1] R. Tao, K. Peng, L. Haeberlé, Q. Li , D. Jin , G. R. Fleming , S. Kéna-Cohen , X. Zhang, W.Bao, *Nature Materials* **21**, 761 (2022).
[2] K. Peng, W. Li, M. Sun, J. Rivero, C. Ti, X. Han, L. Ge, L. Yang, X. Zhang, W. Bao, *Nature Nanotechnology* (to be published), (2024).
[3] K. Peng, R.Tao, L. Haeberlé, Q. Li, D. Jin, G. R. Fleming, S. Kéna-Cohen, X. Zhang, W. Bao, *Nature Communications* **13**, 7388 (2022).

All-optical attoclock for detecting topology in solids

I. Babushkin[1], R. Silva[2], A. Demircan[1], U. Morgner[1], M. Ivanov[3]
[1]*Leibniz University, 30176 Hannover, Germany*
[2]*Max Born Institute, 12489 Berlin, Germany*
[3]*Instituto de Ciencia de Materiales de Madrid -ICMM, 28049 Madrid, Spain*

Photoionization in strong optical fields of atoms, and molecules, as well as analogous processes of transitions from valence to conduction band in solids, are at the heart of attosecond science. The so called attoclock [1] was suggested as a method to measure attosecond-scale dynamics of electrons during photoionization in strong optical fields. As an electron tunnels out of the atomic potential through the barrier created by laser field, the time spent on tunneling is mapped by the nearly circularly polarized laser field on the final direction of the electron motion (Fig. 1a). In this scheme, the rotating electric field plays the role of a "hand of a clock", with one degree rotation corresponding to just 2.7fs/360°=7.5 attoseconds for an infrared driver at 800 nm. Experiments demonstrated effective delays in the range of 10-10^2 attoseconds, with the observed deflection stemming also from the action of the core potential [2], with the tunneling delay still under discussion [3]. Irrespectively of the underlying physics, applying this idea directly to tracking electron injection across the bandgap in bulk dielectrics is highly challenging due to obvious limitations in directly measuring the electrons. In [4] it was suggested that the attoclock principle can be implemented in an all-optical setup by measuring the polarization of light emitted by the electrons during injection into a conduction band. Indeed, the light radiated by the electrons directly reflects their acceleration. Therefore, polarization of radiated light for different harmonics can capture the attosecond-scale dynamics of electrons. This approach can thus be called an "all-optical attoclock."

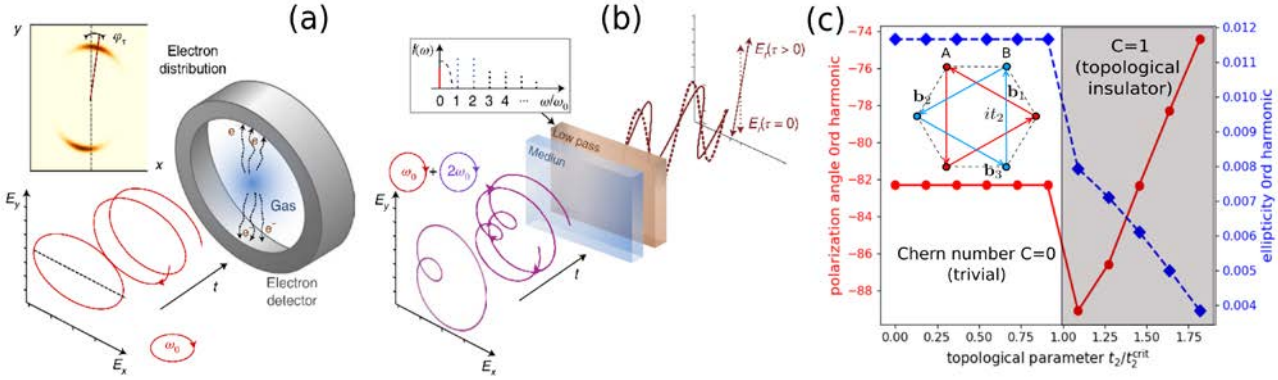

Fig. 1. Electronic [1] (a) and all-optical [4] (b) attoclock. *(**c**) Polarization and ellipticity of THz light (0^{th}harmonic) in a Haldane topological insulator in dependence on the coupling parameter t_2 (**see inset**) for a two-color driver shown in (**b**).*

Here we show how an all-optical attoclock can be used to study the Berry curvature and the overall topology of conduction bands in solids, using a combination of two co-rotating fields with frequencies ω and 2ω, see Fig.1b. The Berry curvature manifests itself as the presence of an effective magnetic field, which modifies electron trajectories and therefore the polarization of the radiated light. Using both effective semiclassical model and semiconductor Bloch equations we show that the topology can be "recorded" in the polarizations of low-order harmonics. As an example, in Fig. 1c we show 0^{th} harmonic [located in terahertz (THz) range] of a two-color field, shown in Fig. 1b. The calculations are done for the Haldane model of a topological insulator (see inset to Fig. 1c), showing that the transition between topologically trivial and topologically nontrivial phase (different by the values of the Chern number C) is clearly visible in the polarization of the harmonics. This contributes to the field of topological strong field physics [5], extending our ability to measure and control matter with light. We note that, whereas high harmonics were recently considered [6] to detect topology, our mechanism is focused namely on the lowest harmonics.

References

[1] P Eckle, M. Smolarski, P. Schlup, J. Biegert, A. Staudte, M. Schöffler, H.G. Muller, R. Dörner, *Nature Physics* **4**, 565 (2008).
[2] L Torlina, F. Morales, J Kaushal, I. Ivanov, A. Kheifets, *Nature Physics* **11**, 503 (2015).
[3] C. Hofmann, A. Bray, W. Koch, H. Ni, N.I. Shvetsov-Shilovski,*The European Physical Journal D* **75**, 208 (2021).
[4] I. Babushkin, Á.J. Galán, J.R.C. de Andrade, A. Husakou, F. Morales, M. Kretschmar, T. Nagy, *Nature Physics* **18**, 417 (2022).
[5] R.E.F.Silva, A. Jimenez-Galan, B.Amorim, O Smirnova, *Nature Physics* **13**, 849 (2019).
[6] D. Baykusheva, A.Chacó, J.Lu, T.P. Bailey, J.A. Sobota, H.Soifer, P.S. Kirchmann, C.Rotundu, C.Uher, T.F.Heinz, D.A. Reis, S. Ghimire, *Nano Letters* **2021**, 21 (2021).

* Acknowledgement(s) : I.B., A.D. and U.M. acknowledge support from Cluster of Excellence PhoenixD (EXC 2122, project ID 390833453).

Robust and time-optimal quantum control from geometric space curves

E. Barnes
Virginia Tech, Blacksburg, VA, 24061, USA

Quantum information technologies demand highly accurate control over quantum systems. Achieving this requires control techniques that perform well despite the presence of decohering noise and other adverse effects. I will present a general technique for designing control fields that dynamically correct errors while performing operations using a close relationship between quantum evolution and geometric space curves. This approach provides access to the global solution space of control fields that accomplish a given task, facilitating the design of experimentally feasible gate operations for a wide variety of applications. This approach unifies and generalizes prior methods for dynamically decoupling a qubit from its environment. Noise-cancelling pulses can be derived by designing space curves with certain geometric properties and then computing their curvatures.

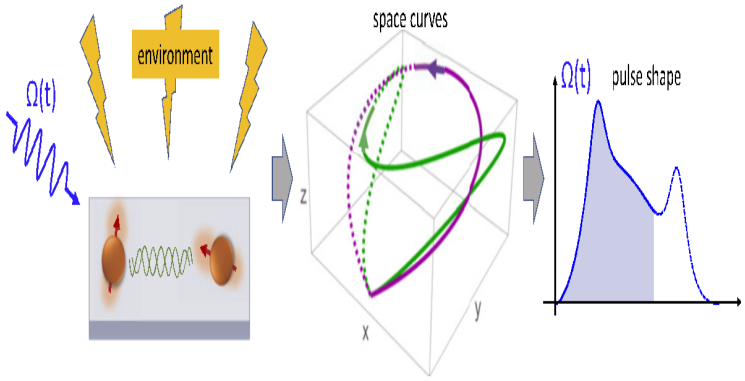

Fig. 1. Geometric space curves provide a general method to design quantum gates *that are robust to environmental noise and other sources of error. The evolution of a driven quantum system subject to low-frequency noise* ***(left)*** *can be described using space curves* ***(middle)****. Two examples of space curves in three dimensions are shown. These curves represent the deviation away from the ideal evolution induced by noise.The coordinate origin of the space in which the curve lives represents the ideal evolution and astime evolves and noise errors accumulate, the curve moves away from this point. The dimension of this space is determined by the size of the Lie algebra spanned by the operators in the system Hamiltonian,including control and noise terms. The control Hamiltonian is encoded in the shape of the curve. As the curve is traversed, the local curvature at each point determines the strength of the control fields at that point in the evolution. For example, the* ***green curve*** *in the middle yields the pulse shown on the* ***right.*** *The* ***arrows*** *on the curve indicate the direction in which the curve is traversed, while the* ***solid (dashed)*** *lines in the curve and pulse represent the past (future) as time evolves. We can thus reverse-engineer the evolution by first constructing a space curve and then computing the control Hamiltonian from its shape.Choosing the space curve to return to the origin at the end of the evolution* ***(middle)*** *yields noise- cancelling control pulses* ***(right)****.*

I will present noise-cancellation conditions for a variety of different noise types, including pulse amplitude, detuning and phase noise, Stark shift errors, etc. I will also discuss applications of this method to qubit platforms based on electron spins, superconducting circuits, trapped ions, and Rydberg atoms.

References

[1] E. Barnes, F.A. Calderon-Vargas, W. Dong, B. Li, J. Zeng, F. Zhuang, *Quantum Science and Technology* **7**, 023001 (2022).
[2] H.T. Nelson, E. Piliouras, K. Connelly, E. Barnes, *Physical Review* A **108**, 012407 (2023).
* Acknowledgments: This work was supported by the Office of Naval Research (grant no. N00014-21-1-2629).

Momentum-resolved study of ultrafast scattering in Photo-excited graphite

F. Barantani[1*], I. Madan[1], A. A. Sapozhnik[1], F. Iyikanat[2], B. Weaver[1]
F. J. G. de Abajo[3], T. LaGrange[1], F. Carbone[1]
[1]*École Polytechnique Fédérale de Lausanne, 1015 Lausanne, Switzerland*
[2]*ICFO-Institut de Ciencies Fotoniques,08860 Castelldefels, Spain*
[3]*ICREA-Institució Catalana de Recerca i Estudis Avançats, 08010 Barcelona, Spain*

The investigation of emerging collective modes provides direct information on the microscopic interactions at the origin of materials' properties. While ultrafast methods allow real-time monitoring of phonons, magnons, and excitons, their behavior is typically measured only within a limited region of momentum space, close to the center of the Brillouin zone. Extending these studies to encompass the entire Brillouin zone offers a more complete understanding of the interactions. Particularly fascinating are scenarios that involve finite momentum transfer, such as processes between particles in different valleys [1].In this study, we delve into both inter- and intra-valley scattering in photo-excited graphite [2-4] and evaluate their impact on interband plasmonic excitations [5]. To do so, we develop and employ time and momentum-resolved electron energy loss spectroscopy (tr-q-EELS), a novel experimental approach implemented in an ultrafast transmission electron microscope [6]. Additionally, we selectively modulate relaxation pathways by adjusting the pump photon energy.

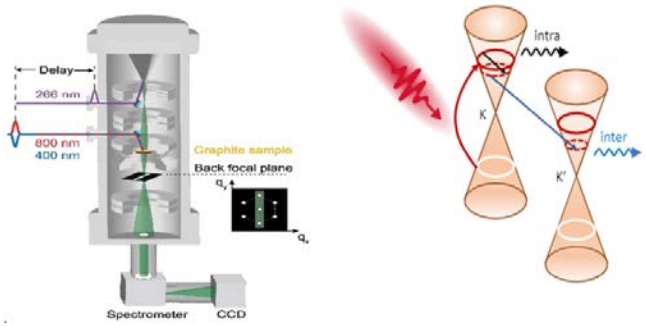

***Fig. 1. Left**: **Experimental setup of momentum- and time-resolved EELS** in an ultrafast TEM.*
***Right**: Sketch of the inter- and intravalley scattering processes for the relaxation of photo-excited electrons in graphite.*

Ab-initio calculations establish a direct link between our experimental observations and the excitation of strongly coupled optical phonons occurring at specific location in the Brillouin zone. Our novel approach opens the way to ultrafast collective mode spectroscopy at finite momentum within tabletop measurements.

References
[1] J. Madéo, M.K.L Man, C. Sahoo, M. Campbell, V. Pareek, E.L. Wong, A. Al-Mahboob, N.S. Chan, A. Karmakar, B. M. K. Mariserla, X. Li, T. Heinz T. Cao, K. M. Dani, *Science* **370**, 1199 (2020).
[2] T. Kampfrath, L. Perfetti, F. Schapper, C. Frischkorn, M. Wolfe, *Physical Review Letters* **95**, 187403 (2005).
[3] M. J. Stern, L.P.R. de Cotret, M.R. Otto, R.P. Chatelain, J.P. Boisvert, M. Sutton, B.J. Siwicket, *Physical Review* B **97**, 165416 (2018).
[4] M. X. Na, A. K. Mills, F. Boschini, M. Michiardi, B. Nosarzewski, R. P. Day, E. Razzoli, A. Sheyerman, M. Schneider, G. Levy, S. Zhdanovich T. P. Devereaux, A. F. Kemper, D. J. Jones, A. Damascelli, Science **366**, 1231(2019).
[5] F. Carbone, O. H. Kwon, A. H. Zewail, *Science* **325**, 181 (2009).
[6] L. Piazza, D.J. Masiel, T. LaGrange, B.W. Reed, B. Barwick, F. Carbone, *Chemical Physics* **423**, 79 (2013).
* *Currently at The University of Texas at Austin, Austin, TX78712, USA.*

Ultrafast spectroscopy of coherent phonon across the pressure-driven Insulator to metal phase transition in V_2O_3

T. Gauthier[1], N. Godin[1], G. Privault[1], B. Corraze[2], J. Tranchant[2], L. Cario[2], D. Babich[2], E. Janod[2]
R. Bertoni[1]
[1]*Université de Rennes, 35000 Rennes, France*
[2]*Nantes Université, 44322 Nantes, France*

Nowadays, material science is moving towards the understanding of material in out-of-equilibrium states by making use of perturbative approaches to investigate their dynamical response under strong stimuli. From that perspective, the use of ultrashort light pulse seems to be relevant as it can selectively address different degrees of freedom inside solid-state materials and more particularly the electronic ones [1]. Such methodology may help to decipher the physical phenomena originating from electronic correlations, like Mott transition, and completes the more conventional approach where phase diagrams of materials are investigated at equilibrium in the temperature/pressure frame.The combination of ultrafast optical spectroscopy and high-pressure experiment sounds like a wise choice to investigate materials experiencing phase transition under hydrostatic pressure such as the canonical Mott insulator V_2O_3 [2]. We use an innovative setup to monitor the ultrafast out-of-equilibrium dynamics of V2O3, especially the coherent structural photo-response, across the pressure driven Insulator to Metal transition (IMT). The obtained results demonstrate the possibility to use the spectroscopy of coherent phonons as a thermodynamical phase marker in a nanometric V_2O_3 thin film.

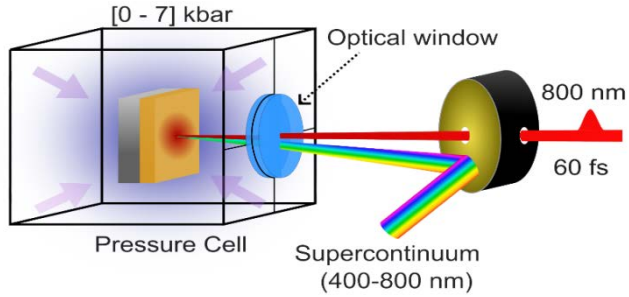

***Fig.1.** Simplified scheme of the experimental setup.*

In addition, the variation of frequency of the ultrafast coherent phonon mode (A_{1g} character) seems to reflect the manifestation of a peculiar coupling between lattice and electronic degrees of freedom near first-order transition lines with a clear drop of frequency around the critical pressure.

References
[1] D. N. Basov, R. D. Averitt, D. Hsieh, *Nature Materials* **16**, 1077 (2017).
[2] G. Privault, G. Huitric , M. Herve, E. Trzop, J. Tranchant , B. Corraze, Z. Khaldi, L. Cario , E. Janod, J.-C. Ameline , N. Godin R. Bertoni, *The European Physical Journal. Special Topics* **232**, 2195 (2023).

Terahertz pumping of antiferrodistortive phonons in $LaAlO_3$

M. Basini[1,2], V. Unikandanunni[3], F. Gabriele[4], M. Cross[5], M.C. Hoffmann[5], F. Forte[4], M. Cuoco[4] S.Bonetti[6]
[1]*Stockholm University,114 19 Stockholm, Sweden.*
[2] *ETH Zürich, 8092 Zürich, Switzerland.*
[3]*Bern University, 3012 Bern, Switzerland.*
[4]*Università degli Studi di Salerno, 84084 Fisciano, Italy.*
[5]*SLAC National Accelerator Laboratory, Menlo Park, CA 94025, United States.*
[6] *Ca' Foscari University of Venice, 30123 Venice, Italy.*

The perovskite family of oxides (ABO_3) shows a wide range of functionalities due to the strong interplay between spin, orbital, and lattice interactions. This is in particular reflected in the different structural instabilities found in these systems. An example is the oxygen octahedra tilting and distortions, which are associated with structural phase transition, in particular, with the cooling from the undistorted, high-temperature cubic phase. The idea to control structural instabilities by a coherent drive of the material's intrinsic vibrations (i.e. phonons) was exploited in the last decades using ultrashort laser pulses, and the emergence of new phases [1-6] was observed. In these studies, the change in the material properties was primarily linked to the externally driven displacement of Raman modes, and in particular the ones responsible for a distortion of the equilibrium crystal structure. One can then expect that when a Raman phonon is driven by an external excitation, a larger displacement would lead to a more significant change in the material properties.Here, we present evidence of a new mechanism for the excitation of lower energy Raman active, phonon in the centrosymmetric $LaAlO_3$, which makes use of an intense THz electric field. In particular, we observed a coherent dynamics in low-temperature measurements of the optical response to a THz pulse excitation. Our measurements show the apparent excitation of an IR-inactive Eg mode at 1.1 THz, as well as a continuum of low frequency oscillations with peaks at 0.35 THz and 0.8 THz, never reported before. Importantly, for a given pump pulse energy, the THz pulse is actually significantly more efficient in driving the Eg mode than an optical radiation (1300 nm), this last acting through Impulsive Stimulated Raman Scattering (ISRS). We point out that, given the absence of IR active phonons in the spectral range of the THz pulse, the reported mechanism is not consistent with a Ionic Raman Scattering (IRS) [7.8]. At this stage, we hypothesize that the Eg phonon is parametrically driven by the coupling with the strain induced by the THz in the material, this last displaying ferroelastic properties [9,10]. The proposed model is able to qualitatively reproduce the low frequency dynamics as well as the Eg excitation. Our investigation shows an efficient new path for the excitation of Raman-active phonon to large amplitude, and would open new directions for the control of the structural phases and related macroscopic properties.

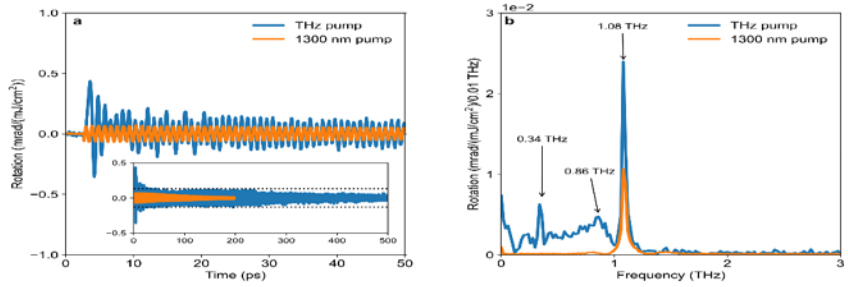

Fig. 1.Pump-probe response *(probe polarization rotation) in time (**a**) and frequency (**b**) domain of $LaAlO_3$[100] at 8K. The FFT was evaluated in the range 0-50ps. The sample was excited by means of an 1300nm pump (**red**) and broad band OH1-geneated THz pump (**blue**). Inset of panel (**a**) shows pump-probe response till later delay times up to 500 ps.*

The proposed model is able to qualitatively reproduce the low frequency dynamics as well as the Eg excitation. Our investigation shows an efficient new path for the excitation of Raman-active phonon to large amplitude, and would open new directions for the control of the structural phases and related macroscopic properties.

References

[1] M. Rini, R.I. Tobey, N. Dean, Y. Tomioka, Y. Tokura, R. W. Schoenlein, A. Cavalleri, *Nature* **449**, 72 (2007).
[2] T.F.Nova , A. S. Disa, M. Fechner, A.Cavalleri, *Science*, **364,** 6445, 1075 (2019).
[3] X.Li, T.Qiu, J. Zhang, E.Baldini, J.Lu, A. M. Rappe, K. A. Nelson, *Science* **364**, 1079 (2019).
[4] A.S. Disa, M. Fechner, T.F. Nova, B. Liu, M. Först, D. Prabhakaran, P.G. Radaelli, A. Cavalleri, *Nature Physics*, **16**, 937 (2020).
[5] D. Afanasiev, J. R. Hortensius, B. A. Ivanov, A. Sasani, E. Bousquet, Y. M. Blanter, R. V. Mikhaylovskiy, A. V. Kimel, A. D. Caviglia *Nature Materials*, **20,** 607(2021) .
[6] M. Basini, M. Pancaldi, B. Wehinger, M. Udina, T. Tadano, M. C. Hoffmann, A. V. Balatsky, S. Bonetti,. *Nature* **628**, 534 (2024).
[7] J. R.Hortensius, D. Afanasiev, A. Sasani, E. Bousquet,A. D. Caviglia *npj Quantum Materials* **5**, 95(2020).
[8] M.J.Neugebauer. D.M.Juraschek. M.Savoini, P.Engeler, L.Boie, E.Abreu, N.A.Spaldin, S.L.Johnson, *Physical Review Research* **3**, 013126 (2021).
[9] S. Kustov, I. Liubimova, E.K.H. Salje. *Applied Physics Letters* **112,** 042902 (2018).
[10] C. A. Mizzi, B. Guo, L.D. Marks, *Physical Review Materials* **5**, 064406 (2021).
* Acknowledgement(s): we acknowledge S. Johnson, M. Fechner, S. Maehrlein**,** M. Trigo and J. Johnson for useful discussions.

Time-resolved low-energy photoelectron diffraction for the study of Ultrafast adsorbate-surface interactions

M. Bauer
Kiel University, 24118 Kiel, Germany

Various types of surface-sensitive time-domain techniques have, in the past, provided detailed and comprehensive insights into ultrafast adsorbate-surface interactions involving the charge and vibrational degrees of freedom that are relevant for surface chemical reactions. Time-domain surface electron diffraction techniques hold the potential to greatly enrich this research, as they can provide quantitative and direct information on how structural orders in adsorbate layers are transiently affected by such interactions [1-3]. In this context, ultrafast low-energy electron diffraction (ULEED) would be the first choice technique due to its exceptional surface sensitivity and the available and established methods for the quantitative analysis of the data. However, electron dispersion and Coulomb interaction broadens the probing electron pulse and considerably limits the time resolution of ultrafast electron diffraction techniques in general, and it is particularly critical for the low electron energies typically used in LEED. To at least partially compensate for this problem, attempts have been made to minimize the propagation distance of the electron pulses from the source to the sample surfaces. However, even with sophisticated designs, the time scale below one picosecond has not been reached yet [4]. In this talk, I will present a surface-sensitive and ultrafast electron diffraction experiment capable of probing structural dynamics in adsorbate layers with a temporal resolution of 100 fs-see Fig.1. In our experiment we analyze the energy-momentum distribution of low-energy photoelectrons excited by a near ultraviolet (NUV) ultrafast laser pulse in graphite that are diffracted as they pass through an ordered tin-phthalocyanine adsorbate layer. The propagation distance of the (photo-) electron pulse prior diffraction is limited by the inelastic mean free path of the electrons in the substrate to typical values of a few nanometers, so that a significant temporal broadening is omitted. We experimentally demonstrate a time resolution of this ultrafast low energy photoelectron diffraction (ULEPD) technique of 100 fs, yet limited by the pulse width of the NUV laser pulse. The analysis of the transient changes in the photoelectron diffraction intensity from the SnPc overlayer indicates the excitation of the adsorbate layer on a characteristic time scale of several ps. We associate the observed changes to vibrational disorder in adsorbate layer as a result of coupling to the phonon bath in graphite, which is transiently excited during the cooling-down of the photo-excited hot carrier distribution. Remarkably, the ULEPD signal contains also direct information on the hot photocarrier dynamics in the substrate providing unique capabilities to directly correlate ultrafast processes associated with the electronic and structural degrees of freedom at surfaces.

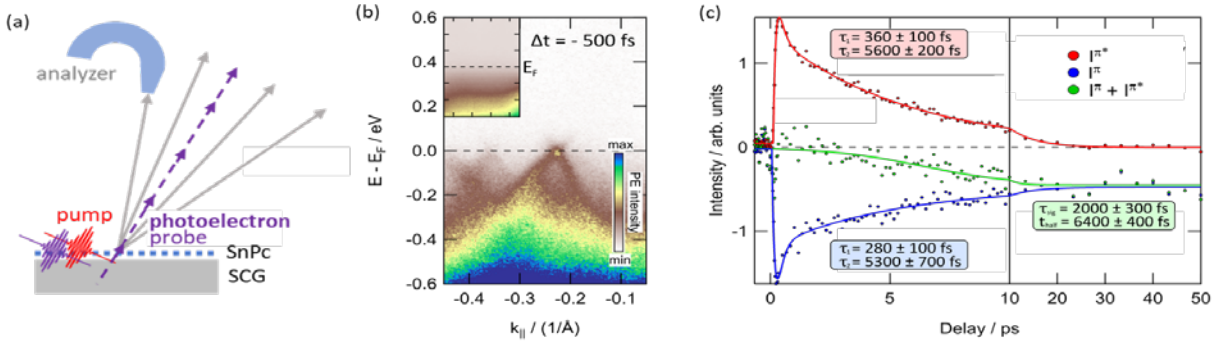

Fig. 1. (a) Experimental scheme for ULEPD. ***(b)*** *ULEPD signal of SnPc/graphite 500 fs before photoexcitation. The inset shows the same energy-momentum field of view for the pristine graphite sample.* ***(c)*** *ULEPD transients extracted from energy regions above (**red**) and below (**red**) E_F. The green data results from the sum of these transients and represent structural changes in the adsorbate layer due to vibrational disorder. Lines are fits to the data.*

In the future we plan to use a momentum microscope for the detection of the photoelectron diffraction signal. Similar to ULEED it will enable us to access the full two-dimensional ULEPD signal of an adsorbate layer, including ultrafast diffuse scattering information [5, 6]. The use of XUV-pulses from high-harmonic generation sources or free electron lasers for the generation of the probe photoelectron pulse will furthermore considerably extend the accessible momentum field of view.

References

[1] A. Hanisch-Blicharski, A. Janzen, B. Krenzer, S. Wall, F. Klasing, A. Kalus, T. Frigge, M. Kammler, M. Horn-von Hoegen, *Ultramicroscopy* **127**, 2 (2013).
[2] M. Gulde, S. Schweda, G. Storeck, M. Maiti, H. K. Yu, A. M. Wodtke, S. Schafer, C. Ropers, *Science* **345**, 200 (2014).
[3] T. Frigge, B. Hafke, T. Witte, B. Krenzer, C. Streub¨uhr, A. Samad Syed, V. Mik˘si´c Trontl, I. Avigo, P. Zhou, M. Ligges, D. Von Der Linde, U. Bovensiepen M.Horn- Von Hoegen, S. Wippermann, A. L¨ucke, S. Sanna, U. Gerstmann, W. G. Schmidt, *Nature* **544**, 207 (2017).
[4] G. Storeck, K. Rossnagel, C. Ropers, *Applied Phyics. Leters.* **118**, 221603 (2021).
[5] M. J. Stern, L. P. R. de Cotret, M. R. Otto, R. P. Chatelain, J.-P. Boisvert, M. Sutton, B. J. Siwick, Physical Review B **79**, 165416, (2017).
[6] H. Seiler, D. Zahn, M. Zacharias, P. N. Hildebrandt, T. Vasileiadis, . W. Windsor, Y. Qi, C. Carbogno, C. Draxl, R. Ernstorfer, F. Caruso, *Nano Letters* **21** 6171 (2021).
* Acknowledgement(s) : authors (M.B.) acknowledge support from DFG, (grant 433458487).

Exciton polaritons in two-dimensional-semiconductor heterostructures

R. Binder, J.R. Schaibley, M. Spotnitz, N.H. Kwong
University of Arizona, Tucson, AZ 87721, USA

Semiconductor structures, including bulk, quantum wells, two-dimensional (2D) layers, and microcavities, support formation of exciton-polaritons, i.e., eigenmodes or quasi-particles composed of excitons and light. The fact that excitons in 2D semiconductors, such as various monolayer transition-metal dichalcogenides (TMDs), e.g., $MoSe_2$ or WS_2, have very strong binding energies (on the order of 500 meV, as opposed to about 5 meV in bulk GaAs) makes them ideal candidates for strong light-matter coupling and thus strong polaritonic effects, including, for example, a modification of the group velocity or large changes in the effective mass. Exciton-polaritons ("polaritons" for short) can also provide optical nonlinearities that may be exploited in communication network devices. Polaritons are always open-pumped-dissipative systems, which means that non-trivial non-Hermitian effects can be possible. The open-pumped-dissipative character also affects possible condensation phenomena, such as formation of a Bose-Einstein condensate or a polaritonic Bardeen-Cooper-Schrieffer (BCS) state. While exciton-polaritons can often be viewed as composite particles combining two particles (exciton and photon), with the exciton behaving like a point Boson (at least at low excitation densities), interesting physical effects can also result from the fact that the exciton itself is a composite particle (comprising an electron and a hole). This may not only lead to deviations from the bosonic nature but can enable non-trivial effects like valley-dependent electron-hole (e-h) exchange interactions, which can affect optical nonlinearities [9]. In this talk, we review our recent research activities on the linear and nonlinear optical properties of 2D semiconductors in various geometries: free-standing monolayer, monolayer in dielectric heterostructures, plasmonic heterostructure (i.e., monolayer in proximity to metal surface), and microcavities containing 2D-monolayers. We show that the specific heterostructure design has a substantial influence on the exciton-polariton characteristics, and enables design of specific target properties, such as strong ultrafast optical nonlinearity [1] and strong reduction of group velocity [2], or strong modification (even qualitative modification) of the polaritons' effective mass and related transport effects [3]. While the main focus of the talk will be on plasmonic devices that allow for ultrafast (sub-picosecond) modulations, we also touch briefly on recently obtained insights into the lasing properties of TMD microcavities, extending work that focuses on GaAs quantum well microcavity lasers [4-6]. Fig.1 shows the plasmonic modulator device that consists of a TMD monolayer in the vicinity of a metal surface. This structure supports surface-plasmon polaritons (SPPs), but also mixed modes in which excitons from the monolayer are coupled to the SPP. We call these latter modes exciton-surface-plasmon-polaritons (E-SPPs).

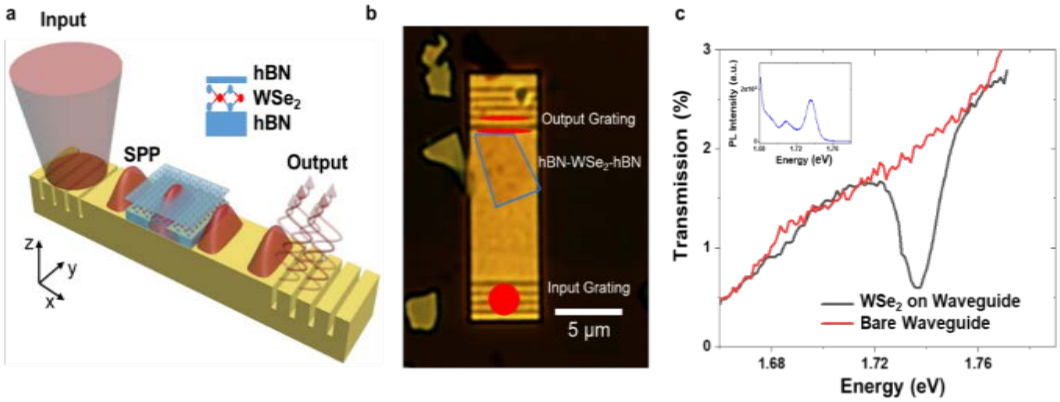

Fig. 1 (a) Sketch of plasmonic device with input and output coupler grating**; **(b)** optical image of device**; (c)** transmission data**.[1].

The E-SPP dispersion is shown in Fig.2. Fig. 3 shows experimental data of the optical nonlinearity seen in a pump-and-probe configuration. The differential transmission has a peak in frequency (close to the E-SPP resonance), and exhibits an ultrafast (femtosecond) initial temporal decay, corresponding to a modulation bandwidth of ~1.5 THz, followed by a picosecond decay.

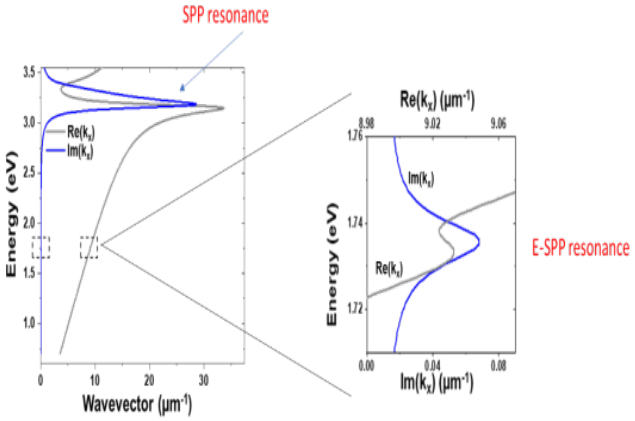

Fig.2. Calculated dispersion relation (left) *with close-up of exciton-surface-plasmon-polariton* ***(E-SPP)*** *resonance* ***(right).*** *[1].*

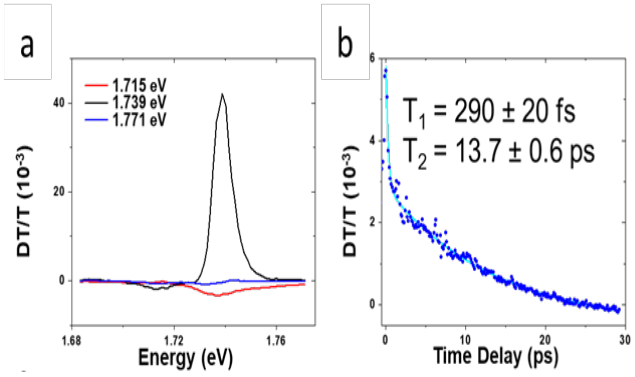

Fig.3 Differential transmission *induced by pump divided by transmission without pump* ***(DT/T). (a)*** *Frequency dependence for three different pump frequencies.* ***(b)*** *Time dependence for pump frequency of 1.736 eV showing ultrafast (290 fs) initial recovery. [1].*

Fig.3 shows experimental data of the optical nonlinearity seen in a pump-and-probe configuration. The differential transmission has a peak in frequency (close to the E-SPP resonance), and exhibits an ultrafast (femtosecond) initial temporal decay, corresponding to a modulation bandwidth of ~1.5 THz, followed by a picosecond decay. Fig.4 shows theoretical predictions for the enhancement of the optical nonlinearity that is expected when the exciton resonance is closer to the SPP resonance.

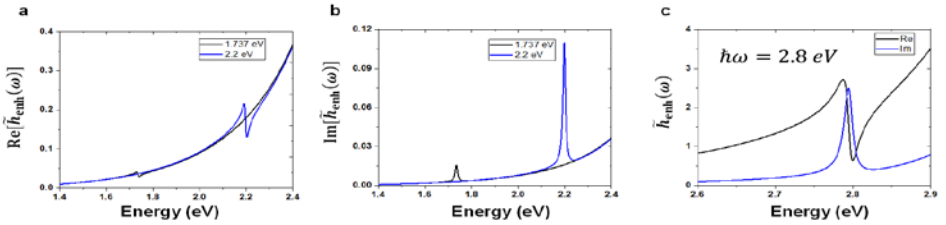

Fig.4.Real (a) and imaginary (b) part of calculated plasmonic enhancement *factor for two different exciton frequencies.* ***(c)*** *Real* ***(black)*** *and imaginary* ***(blue)*** *part for exciton frequency of 2.8 eV .[1].*

Fig.5 shows ultranarrow (micro-eV) resonances that can be induced with a stationary pump field tuned close to the exciton resonance, if pump and probe have the same linear polarization.

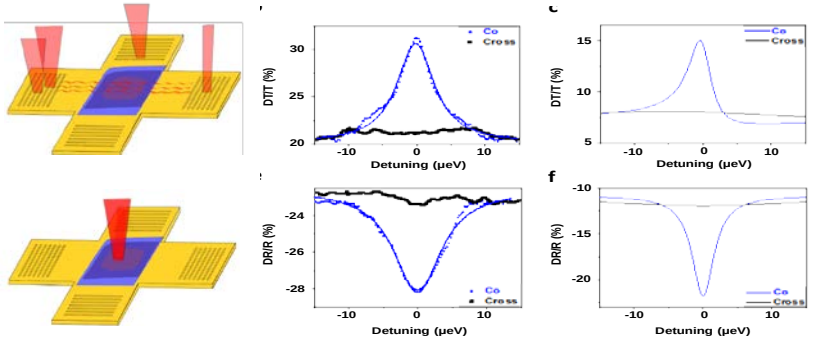

Fig. 5. (a) *and* ***(d):*** *depiction of two different pump- probe configurations;* ***(b)*** *experimental differential transmission for configuration* ***(a)*** *for linearly co-polarized and cross-polarized pump and probe;* ***(e)*** *experimental differential reflection for configuration* ***(d),*** ***(c)*** *and* ***(f)*** *same as* ***(b)*** *and* ***(e),*** *respectively, but showing theoretical results.[2].*

The ultranarrow resonance leads to slow-light behavior, and using an interferometric measurement we found a slow-down factor of 1,300, i.e., the group velocity of the E-SPP was smaller than the speed of light in vacuum by a factor of 1,300 [2].

References

[1] M. Klein, B. H. Badada, R. Binder, A. Alfrey, M. McKie, M. R. Koehler, D. G. Mandrus, T. Taniguchi, K. Watanabe, B. J. LeRoy, J. Schaibley *Nature Communications* **10**, 3264 (2019).
[2] M. Klein, R. Binder, M.R. Koehler, D.G. Mandrus, T. Taniguchi, K. Watanabe, J.R. Schaibley, *Nature Communications* **13**, 6216 (2022).
[3] R. Binder, J. R. Schaibley, N. H. Kwong, *Physical Review* B **109**, 125301 (2024).
[4] J. Hu, Zh. Wang, S. Kim, H. Deng, S. Brodbeck, Ch. Schneider, S. Hoefling, N.H. Kwong, R. Binder, *Physical Review* X **11**, 011018 (2021).
[5] R. Binder, N.H. Kwong, *Physical Review* B **103**, 085304 (2021).
[6] M.Spotnitz, N.H. Kwong R. Binder, *Physical Review* B **104**, 115305 (2021).
[7] M.Em. Spotnitz, N. H. Kwong, R. Binder, *Physical Review* B **107**, 125309 (2023).
[8] N. H. Kwong, M. Em. Spotnitz, R. Binder, *Physical Review* B **109**, 045306 (2024).
[9] N. H. Kwong, J.R. Schaibley, R. Binder, *Physical Review* B **104**, 245434 (2021).

* Acknowledgements: RB gratefully acknowledges financial support from NSF under grant number DMR 1839570, and CPU time at HPC, University of Arizona. JRS acknowledges funding from AFOSR Grant number: FA9550-20-1-0217.

Valley-controlled photoswitching of a Metal-insulator surface texture

H. Böckmann[1], J G. Horstmann[1], F. Kurtz[1], M. Buriks[2], K. Gadge[2], S. R. Manmana[2], S. Wippermann[3]
C. Ropers[2]
[1] *Max Planck Institute for Multidisciplinary Sciences, 37077 Göttingen, Germany*
[2] *University of Göttingen, 37073 Germany*
[3] *Philipps University of Marburg, 35037 Marburg, Germany*

Phase competition and coexistence are hallmarks of strongly-correlated materials [1] and directly related to intriguing phenomena such as colossal magnetoresistance [2] and high-temperature superconductivity [3]. Active control over phase textures further promises nanoscale tunable electronic material properties [4]. Light allows for tilting the balance between distinct correlated states and phases with a prominent example given by the optical switching of an insulator to a metal. However, optical excitation generally lacks the specificity to select sub-wavelength domains. In this work, we employ valley-selective photodoping of correlated electronic states to demonstrate control over the domains and texture of a quasi-one-dimensional Peierls insulator [5]. Specifically, we exploit the anisotropic absorption of nanowire domains by tuning both the photon energy and the polarization to the transition matrix elements most strongly coupled to the structural transformation.

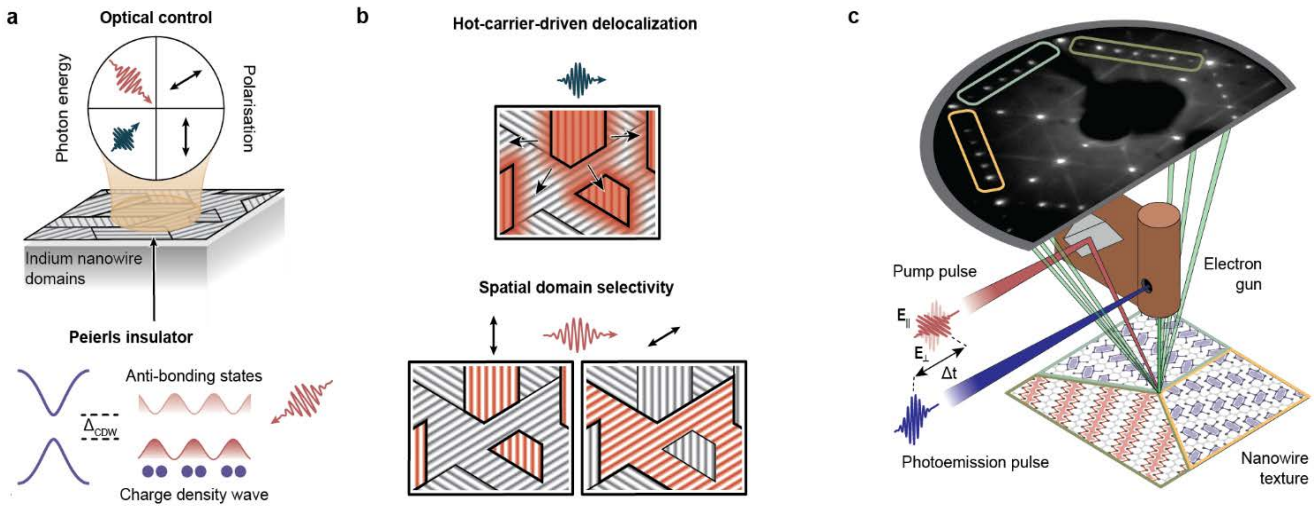

Fig.1. Optical surface electronic texture control via valley-selective photodoping.
a. Top*: schematic of optical control parameters that drive selective surface domain switching.*
Bottom: *the Peierls transition in a one-dimensional atomic chain yields the formation of a periodic lattice distortion and charge density wave (CDW) with a characteristic energy gap.*
b. Top*: light-induced electronic quench of the CDW phase. A population of states at the CDW gap yields a homogeneous phase change across the surface via delocalized energetic charge carriers.*
Bottom*: direct bandgap excitation (valley-selective) minimizes dissipation which manifests in domain- specific switching (**red wires**) with pronounced phase coexistence and local carrier confinement.*
c. *Experimental setup of ultrafast LEED. The domain-specific quench of the structural distortion manifests in a loss of corresponding reflex intensity.*

We find that averting dissipation facilitates domain-specific carrier confinement, control over nanotextured phases, and a prolonged lifetime of the metastable metallic state. Augmenting existing manipulation schemes, valley-selective photoexcitation will enable the activation of electronic phase separation beyond thermodynamic limitations, facilitating optically-controlled hidden states, engineered heterostructures, and polarization-sensitive percolation networks.

References

[1] E. Dagotto, *Springer Series in Solid-State Sciences* **136,** *(*2003*).*
[2] M. Uehara, S. Mori, C. H. Chen, S.-W. Cheong, *Nature* **399**, 560 (1999).
[3] P. A. Sharma , N. Hur, Y. Horibe, C. H. Chen, B. G. Kim, S. Guha, M. Z. Cieplak, S.-W. Cheong, *Physical Review Letters* **89**, 167003 (2002).
[4] J. Cao , E. Ertekin, V. Srinivasan, W. Fan, S. Huang, H. Zheng, J. W. L. Yim, D. R. Khanal, D. F. Ogletree, J. C. Grossman, J. Wu *Nature Nanotechnology* **4**, 732 (2009).
[5] H. Böckmann (*to be published*) (2024).

Dynamics in the non-equilibrium state: Towards a more complete understanding how the charge, spin, and Lattice degrees of freedom interact

U. Bovensiepen
University of Duisburg-Essen, 47048 Duisburg, Germany

One key challenge in the analysis of ultrafast experiments is the assignment of a particular pump-induced observation to a specific degree of freedom that may cooperate or compete with another one. A seminal example is the analysis of e-ph interaction by Allen [1]. Using specific probing and resonant pumping methods, which are typically available in the experimental toolbox nowadays, very detailed microscopic understanding was developed, see, for example, the work on the interface hybrid phonons regarding energy transfer across metal-oxide interfaces [2] and hot electron injection and transport in heterostructures [3]. In this talk recent developments exploiting ultrafast soft x-ray spectroscopy carried out at the femtoslicing facility at BESSY II, Berlin, and the spectroscopy and coherent scattering (SCS) instrument at the European XFEL, Hamburg, will be presented. The experimental opportunities and related challenges [4], key observations of ultrafast spectral changes at Ni or Fe L_3 and O K absorption edges in metals [5,6], charge transfer insulators [7], and films of Fe(II) spin-crossover complexes [8] will be discussed. Thereby, the manifold scientific opportunities which exploit the element and site specificity of the spectroscopy to shed light on non-equilibrium dynamics in condensed matter will be highlighted. Moreover, dichroic experiments, which provide specific access to broken symmetry ground states, will be addressed.

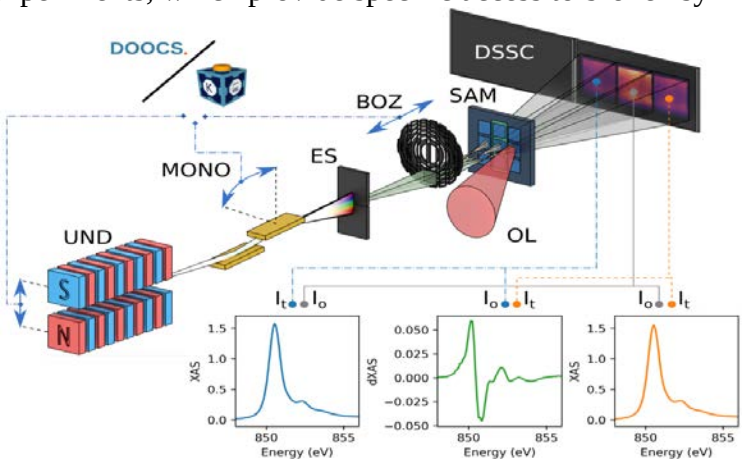

Fig. 1. Scheme of the SCS instrument at European XFEL *which allows for shot-to-shot normalization in combination with pump-probe experiments. A key element is the beam-splitting off-axis zone plate (**BOZ**) which splits the monochromatized (**MONO**) pulsed x-ray beam generated by the SASE3 undulator system (**UND**) after passing an exit slit (**ES**) into three beams. Subsequently, they pass the sample (**SAM**) which consists of three membranes. The center one is bare membrane window. The two other ones contain the sample of interest. The right one is pumped by laser excitation. The corresponding transmitted intensities are detected at the detector **DSSC** and shot-to-shot normalization provides excellent signal-to-noise ratio in time dependent x-ray experiments. The figure was originally published in [4].*

Moreover, dichroic experiments, which provide specific access to broken symmetry ground states, will be addressed.

References

[1] P. B. Allen, *Physical Review Letters* **59**, 1460 (1987).
[2] N. Rothenbach, M. E. Gruner, K. Ollefs, C. Schmitz-Antoniak, S. Salamon, P. Zhou, R. Li, M. Mo, S. Park, X. Shen, S. Weathersby, J. Yang X. J. Wang, R. Pentcheva, H. Wende, U. Bovensiepen, K. Sokolowski-Tinten, A. Eschenlohr, *Physical Review* B **100**, 174301 (2019).
[3] M. Heckschen, Y. Beyazit, E. Shomali, F. Kuehne, J. Jayabalan, P. Zhou, D. Diesing, M. E. Gruner, R. Pentcheva, A. Lorke, B. Sothmann U. Bovensiepen, *PRX Energy* **2**, 043009 (2023).
[4] L. Le Guyader, A. Eschenlohr, M. Beye, W. Schlotter, F. Döring, C. Carinan, D. Hickin, N. Agarwal, C. Boeglin, U. Bovensiepen, J. Buck R. Carley, A. Castoldi, A. D'Elia, J.-T. Delitz, W. Ehsan, R. Engel, F. Erdinger, H. Fangohr, P. Fischer, C. Fiorini, A. Föhlisch, L. Gelisio M. Gensch, N. Gerasimova, R. Gort, K. Hansen, S. Hauf, M. Izquierdo, E. Jal, E. Kamil, S. Karabekyan, T. Kluyver, T. Laarmann, T. Lojewski D. Lomidze, S. Maffessanti, T. Mamyrbayev, A. Marcelli, L. Mercadier, G. Mercurio, P. S. Miedema, K. Ollefs, K. Rossnagel, B. Rösner N. Rothenbach, A. Samartsev, J. Schlappa, K. Setoodehnia, G. Sorin Chiuzbaian, L. Spieker, C. Stamm, F. Stellato, S. Techert, M. Teichmann M. Turcato, B. Van Kuiken, H. Wende, A. Yaroslavtsev, J. Zhu, S. Molodtsov, C. David, M. Porro, A. Scherz, *Journal of Synchrotron Radiation* **30** 284 (2023).
[5] R. Y. Engel, O. Alexander, K. Atak, U. Bovensiepen, J. Buck, R. Carley, M. Cascella, V. Chardonnet, G. S. Chiuzbaian, C. David, F. Döring A. Eschenlohr, N. Gerasimova, F. de Groot, L. Le Guyader, O. S. Humphries, M. Izquierdo, E. Jal, A. Kubec, T. Laarmann, C.-. Lambert, J. Lüning J. P. Marangos, L. Mercadier, Giuseppe Mercurio, P. S. Miedema, K. Ollefs, B. Pfau, B. Rösner, K. Rossnagel, N. Rothenbach, A. Scherz J. Schlappa, M. Scholz, J. O. Schunck, K. Setoodehnia, C. Stamm, S. Techert, S. M. Vinko, H. Wende, A. A. Yaroslavtsev, Z. Yin, M. Beye *Structural Dynamics* **10**, 054501 (2023).
[6] T. Lojewski, M. F. Elhanoty, L. Le Guyader, O. Gråsäs, N. Agarwal, C. Boeglin, R. Carley, A. Castoldi, C. David, C. Deiter, F. Döring, R. Engel F. Erdinger, H. Fangohr, C. Fiorini, P. Fischer, N. Gerasimova, R. Gort, F. deGroot, K. Hansen, S. Hauf, D. Hickin, M. Izquierdo, B. E. Van Kuiken Y. Kvashnin, C.-H. Lambert, D. Lomidze, S. Maffessanti, L. Mercadier, G. Mercurio, P. S. Miedema, K. Ollefs, M. Pace, M. Porro J. Rezvani, B. Rösner, N. Rothenbach, A. Samartsev, A. Scherz, J. Schlappa, C. Stamm, M. Teichmann, P. Thunström, M. Turcato A. Yaroslavtsev, J. Zhu, M. Beye, H. Wende, U. Bovensiepen, O. Eriksson, A. Eschenlohr, *Material Research Letters* **11**, 655 (2023).
[7] T. Lojewski, D. Golez, K. Ollefs, L. Le Guyader, L. Spieker, N. Rothenbach, R. Y. Engel, P. S. Miedema, M. Beye, G. S. Chiuzbaian, R. Carley R. Gort, B. E. Van Kuiken, G. Mercurio, J. Schlappa, A. Yaroslavtsev, A. Scherz, F. Döring, C. David, H. Wende, U. Bovensiepen, M. Eckstein P. Werner, A. Eschenlohr, *arXiv:2305.10145*, (2023).
[8] L. Kämmerer, G. Kämmerer, M. Gruber, J. Grunwald, T. Lojewski, L. Mercadier, L. Le Guyader, R. Carley, C. Carinan, N. Gerasimova D. Hickin, B. E. Van Kuiken, G. Mercurio, M. Teichmann, S. Kumar Kuppusamy, A. Scherz, M. Ruben, K. Sokolowski-Tinten, A. Eschenlohr K. Ollefs, C. Schmitz-Antoniak, F. Tuczek, P. Kratzer, U. Bovensiepen, H. Wende, *arXiv:2312.01483*, (2023).

* Acknowledgement: Funding by the Deutsche Forschungsgemeinschaft (DFG, German Research Foundation) – Project-ID 278162697 – SFB 1242 is gratefully acknowledged.

Light-induced quench of macroscopic condensates probed via Time-resolved ARPES

D. Armanno[1], J. M. Parent[1], A. Longa[1], G. Jargot[1], F. Légaré[1], N. Gauthier[1], F. Boschini[2]
[1] *Institut National de la Recherche Scientifique, Varennes, QC J3X 1S2, Canada*
[2] *University of British Columbia, Vancouver, BC V6T 1Z4, Canada*

Time- and angle-resolved photoemission spectroscopy (TR-ARPES) is a powerful technique that provides direct access to the light-induced ultrafast dynamics of the electronic band structure of quantum materials with both momentum and energy resolutions [1]. When probing the transient response of long-range condensates (e.g., superconductors), TR-ARPES studies have conventionally employed near-infrared light excitation to drive an ultrafast quench of macroscopic condensates [1]. In this context, it is worth noting that near-infrared light carries photon energies several orders of magnitude larger than those usually associated with the underlying order parameters (eV vs. meV energy scales). The TR-ARPES endstation at the Advanced Laser Light Source (ALLS) user facility provides mid-infrared optical excitation capabilities (0.15-0.8 eV range) along with a 6-eV probe (soon to be upgraded to >10 eV extreme ultraviolet via high-harmonic generation) [2]. Furthermore, the ALLS TR-ARPES endstation can map a large area in momentum space by using 6-eV probe pulses, in combination with a new state-of-the-art hemispherical analyzer (ASTRAIOS 190, SPECS) with single octupole deflector technology and sample biasing [3]. We demonstrate the momentum mapping capabilities of our TR-ARPES system by presenting the Fermi surface mapping of optimally doped $Bi_2Sr_2CaCu_2O_{8+\delta}$ (Bi2212), a prototypical high-T_c cuprate superconductor, in Figure 1(a), where we prove the ability to reach up to ~90% of the antinodal $(0,\pi)$ distance. Figure 1(b) shows that 300 meV pump excitation induces an ultrafast filling of the superconducting gap, similar to what has been reported upon near-infrared excitation [4]. We will discuss how mid-infrared light, with photon energy well below the charge transfer gap of Bi2212, quenches the superconducting condensate over a wide momentum range.

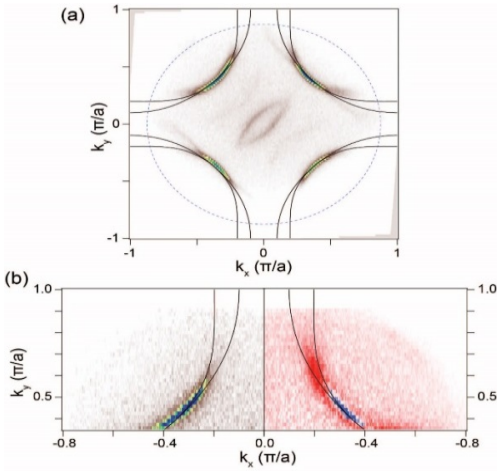

Fig. 1. (a): Fermi surface *mapping of optimally-doped Tc~91 K Bi2212. The* ***solid*** *lines show the bonding and antibonding bands. The* ***dashed blue*** *circle shows the momentum space that can be accessed using 6 eV photons.* ***(b):*** *photoexcited Fermi surface (**left**) and differential Fermi surface (**right**) at zero pump-probe delay upon 300 meV excitation.*

We will then present some preliminary TR-ARPES results on Ta_2NiSe_5, where we investigate how mid-infrared light excitation might offer valuable insights into the presence of an underlying excitonic condensate.

References

[1] F. Boschini, M. Zonno, A. Damascelli, *Review of Modern Physics* **96**, 015003 (2024).
[2] A. Longa, J.-M. Parent, B. K. Frimpong, D. Armano, N. Gauthier, F. Legare, F. Boschini, G. Jargot, *(in print)* (2024).
[3] N. Gauthier, J. A. Sobota, H. Pfau, A. Gauthier, H. Soifer, M. D. Bachmann, I. R. Fisher, Z.-X. Shen, P. S. Kirchmann, *Review of Scientific Instruments* **92**, 123907 (2021).
[4] F. Boschini, E. H. da Silva Neto, E. Razzoli, M. Zonno, S. Peli, R. P. Day, M. Michiardi, M. Schneider, B. Zwartsenberg, P. Nigge, R. D. Zhong J. Schneeloch, G. D. Gu, S. Zhdanovich, A. K. Mills, G. Levy, D. J. Jones,C. Giannetti, A. Damascelli, *Nature Materials* **17**, 416 (2018).

Dynamical routes renormalization of the magnonic spectrum beyond Linear spin wave theory via nonlinear magnonics

D. Bossini
University of Konstanz, 78457 Konstanz, Germany

In the absence of external magnetic felds, the Hamiltonian of a magnetic material contains the exchange interaction, which is of electrostatic origin, and the spin-orbit coupling, whose magnitude depends on the atomic charge [1]. Linear spin wave theory provides a representation of the entire spectrum of

collective magnetic excitations, i.e. magnons, under the following assumptions: i) the interactions are constant; ii) the number of magnons in the system are negligible; iii) the magnon-magnon interaction and scattering are not present [1-3]. However, the electric field component of laser pulses is able to perturb electrostatic interactions, charge distributions and, at the same time, can create a magnonic population. A fundamental open question therefore concerns the possibility to optically renormalise the magnon spectrum and the spin Hamiltonian. In practice this means either modifying the amplitude, frequency and lifetime of the magnons, in comparison with the predictions of linear spin wave theory, whose predictions are confirmed by equilibrium spectroscopic methods (e.g. Raman, infrared absorption). Activating a coupling between different magnon modes by means of laser pulses induces spin dynamics elusive of linear spin wave theory as well.Here, we discuss a route to achieve nonlinear coherent spin dynamics in solid state magnets. We rely on an electric-dipole excitation of high-energy magnons near the edges of the Brillouin zone, called two-magnon (2M) mode [4-6]. This process enables to trigger magnon pairs in a spin-conserving fashion by perturbing the exchange interaction [4-6]. We note that this transition is in the mid-infrared spectral range and therefore the exploration of the spin dynamics, triggered by its resonant and off-resonant pumping, requires a laser source operating in the mid-infrared spectral range. Furthermore, the abilities to tune the central photon energy of the laser pulses, to fully control the polarization and spectrum of the excitation pulses is also key for this experimental investigation. To meet these extremely challenging demands, we have developed an home-made laser system, based on the Yb:YAG thin disk technology, able to generate femtosecond laser pulses with photon energy tunable in the 37 THz- 50 THz range [7]. The mid-infrared beam was used to excite the weak ferromagnet α-Fe_2O_3 (hematite) at room temperature. In this material the 2M mode is centered at 46 THz. The transient spin dynamics is monitored by measuring the second-order magneto-optical effects [8] with a near-infrared laser beam, tuned to the transparency region of hematite. The data reveals the activation and a surprising amplification of coherent low-energy zone-centre magnons, i.e. the two magnetic resonances, which are not directly driven. Strikingly, the spectrum of these low-energy magnons differs from the observations obtained with equilibrium spectroscopic methods, which are on the other hand consistent with spin wave theory. The light-spin interaction thus results in a room-temperature renormalisation of the magnon spectra: a five-fold and three- fold increases of the amplitudes and 4% frequency shifts of their ground-state values were measured. We rationalise the observation in terms of a novel resonant scattering mechanism, in which zone-edge magnons couple nonlinearly to the zone-centre modes. This process provides effectively a resonant to the light scattering mechanism, which is canonically employed to trigger coherent magnons in solids (impulsive stimulated Raman scattering [9-11]). In a quantum mechanical model, we analytically derive the corrections to the spectrum due to the photoinduced magnon population. The effect of the magnon-magnon scattering can be also added to the analytical formalism, although it significantly complicates the analytical treatment. On the other hand, atomistic spin dynamics simulations were performed, relying on a stochastic version of the Landau-Lifschitz-Gilbert equation for a weak ferromagnet. The numerical results demonstrate that exciting zone-edge magnons results in a blueshift of one of the magnetic resonances of hematite, in particular the q-AFM mode. This is consistent with the experimental observation. Our results present a milestone on the path towards a coherent all-optical engineering of Hamiltonians in solids, as an arbitrary tuning of the quasiparticles eigen frequencies would result in optically driving instabilities and phase transitions.

References

[1] J. Stohr, H.C. Siegmann, *Magnetism from Fundamentals to Nanoscale Dynamics*, Springer, Berlin, Heidelberg (2006).
[2] C. Kittel, *Quantum theory of solids*, Wiley, New York (1987).
[3] O. Gomonay, D. Bassini, *Journal of Physics* D: *Applied Physics* **54,** 374004 (2021).
[4] T. Moriya, Y. Tanabe, S. Sugano, *Physical Review Letters* **15**, 1023 (1965).
[5] T. Moriya, *Journal of Applied Physics* **39**, 1042 (1968).
[6] R. Loudon, *Advances in Physics* **17**, 243 (1968).
[7] C. Schönfeld, L. Feuerer, A.-C. Heinrich, A.Leitenstorfer, D. Bossini, *Laser Photonics Rev*iew, Wiley, New York, 2301152 (2024).
[8] K. Grishunin,E. A. Mashkovich, A. V. Kimel, A. M. Balbashov, A. K. Zvezdin, *Physical Review* B **104,** 024419 (2021)**.**
[9] A. Kirilyuk, A.V. Kimel, T. Rasing, *Reviews of Modern Physics* **82**, 2731 (2010).
[10] D. Bossini,M. Pancaldi, L.Soumah, M.Basini, F.Mertens, M.Cinchetti,T.Satoh, O.Gomonay,S.Bonetti, *Physical Review Letters* **127**, 077202(2021)
[11] D. Bossini , D. M. Juraschek, R. M. Geilhufe, N. Nagaosa, A.V. Balatsky, M. Milanović, V.V. Srdić, P. Senjug, E. Topic, D. Barisic, M. Rubčić D. Pajić, T.Arima, M. Savoini, S. L. Johnson, C. S. Davies, A. Kirilyuk, *Journal of Physics* D: *Applied Physics* **56**, 273001 (2023)

* Acknowledgement(s) : This work was supported by the Deutsche Forschungsgemeinschaft (DFG) through the SFB1432 (425217212, Project B07). D.B. acknowledges the support of the DFG program BO 5074/1- D.B. thanks Alexey Kimel, Joe Barker, Andrea Cavalleri and Steve Johnson for useful discussions. The authors thank Stephan Eggert, Christian Beschle and Alessandro Baserga for technical support.

From visible to mid-infrared ultrafast fluoride fiber lasers

M. Bernier, M.-P, Lord, M. Olivier, R. Vallée
Université Laval, Québec, G1V 0A6 Canada

Ultrafast lasers, particularly those operating in the femtosecond regime, are currently revolutionizing many fields of science by providing access to record optical intensities, enabling many nonlinear processes that are not possible in long-pulse regime. Femtosecond pulses were traditionally generated in crystalline materials using mirror-based bulk cavities. Over the last two decades or so, fiber lasers have attracted a great deal of interest for their operation in the ultrafast regime, taking advantage of distributed gain and balancing the fiber's dispersion and nonlinearity. Fibers are excellent hosts for lasers, the heat can be well distributed over long fiber lengths, allowing for their power scaling. In addition, by using fiber-based photonic components, it is possible to make them all-fiber which significantly improve their robustness. Ultrafast fiber lasers were first developed in silica fibers at near infrared wavelengths. Hosting fiber lasers in silica offers great advantages, as this material is easily available and fairly robust, with favorable thermo-mechanical properties. Unfortunately silica's relatively high maximum phonon energy, combined with its limited transparency at wavelengths above 2200 nm, has limited ultrafast fiber lasers to the wavelength range of about 900nm to 2100nm. Recently, thanks to the availability of excellent quality fluoride optical fibers doped with rare earths, ultrafast fiber lasers were reported at mid-infrared (mid-IR) wavelengths ranging from 2800 to 3500 nm [1-4], using the nonlinear polarization evolution as modelocking mechanism. In this report, we will review these fiber laser systems based on erbium, dysprosium and praseodymium in fluoride fibers, modelocked by the nonlinear polarization evolution in fiber as shown in Fig.1.

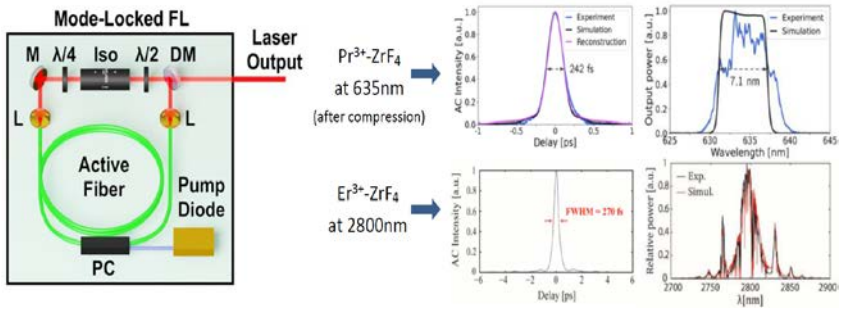

***Fig. 1 (left) Experimental setup** implementing the nonlinear polarization evolution in fluoride fibers. M: Mirror, λ/2: half-wave plate, λ/4: quarter-wave plate, **L**: lens, **PC**: pump combiner, **ISO**: isolator, **DM**: dichroic mirror. **(right)** Output characteristics (pulse width and output spectrum) of femtosecond fiber lasers operating at 635nm as reported in [5] (top) and at 2800nm as reported in [4]. Figures from [4, 5].*

Very recently, we have also extended the operation of ultrafast fiber lasers at visible wavelengths [5] by taking advantage of the low maximum phonon energy of fluoride glasses combined with newly available GaN-based blue laser diodes as a pump source.

References

[1] S. Duval, M. Bernier, V. Fortin, J. Genest, M. Piché, R. Vallée, *Optica* **2**, 623 (2015).
[2] Y. Wang, F. Jobin, S. Duval, V. Fortin, P. Laporta, M. Bernier, G. Galzerano, R. Vallée, *Optics Letters* **44**, 395 (2019).
[3] N. Bawden, O. Henderson-Sapir, S.D. Jackson, D.J. Ottaway, *Optics Letters* **46**, 1636 (2021).
[4] S. Duval, M. Olivier, V. Fortin, M. Bernier, M. Piché, R. Vallée, *Proceedings SPIE* **9728,** 972802 (2016).
[5] M.-P. Lord, M.Olivier, M. Bernier, R. Vallée, *Optics Letters* **48**, 3709 (2023).

Intense femtosecond mid-infrared sources at 4-micron

Z. Chang
University of Ottawa, Ottawa, ON K1N 6N5, Canada

Many physical phenomena in strong-field benefit from longer laser wavelengths. Yet, most of our experience with intense light fields has been restricted to a very limited near infrared (NIR) range of 0.8 to 1 μm, provided by the popular Ti:Sapphire and neodymium/ytterbium based solid-state lasers. Attosecond extreme ultraviolet sources driven by Ti:Sapphire lasers centered at 800 nm have been the workhorse for studying electron dynamics since 2001. However, the photon energy range with sufficient flux for time-resolved experiments is limited <200 eV. In recently years, significant progress has been made in developing few-cycle, carrier-envelope phase stabilized, high peak-power lasers in the 1.6 to 2 μm that has laid the foundation for attosecond X-ray sources in the water window (282 – 533 eV), which covers the atomic K-shell excitation of carbon and oxygen [1]. Even longer wave-length high-peak-power lasers are becoming available, which are suitable to study light filamentation, high harmonic

generation, and laser-plasma interaction in the relativistic regime [2]. We first review the recent progress on Chirped Pulse Amplification (CPA) lasers centered at 2.5 μm and 4.1 μm based on the Cr:ZnSe [3] and Fe:ZnSe gain media [4], which are able to output mJ-level femtosecond pulses at >100 Hz repetition rate. We then describe recent breakthroughs in Chirped Pulsed Optical Parametric Amplifiers (OPCPA) based on the $ZnGeP_2$ (ZGP) nonlinear crystals pumped by Ho:YLF CPA lasers at 2 μm. Sub-100 fs pulses with mJ energy can be generated at 1 kHz [5]. The Fe:ZnSe gain medium features a unique combination of spectroscopic, optical, and technological characteristics enabling power-scalable mid-infrared (MIR) sources: a long upper-level lifetime (55 μs over 77-140K) suitable for energy storage of light from commercial, high-energy free running Er:YAG pump lasers; high ($>10^{-18}$ cm^2) emission cross-section at 4 μm allowing a straightforward high-efficiency amplifier design; and large emission bandwidth supporting femtosecond pulses [6]. We have developed a chirped pulse amplifier based on cryogenically cooled Fe:ZnSe, as shown in Fig.2.

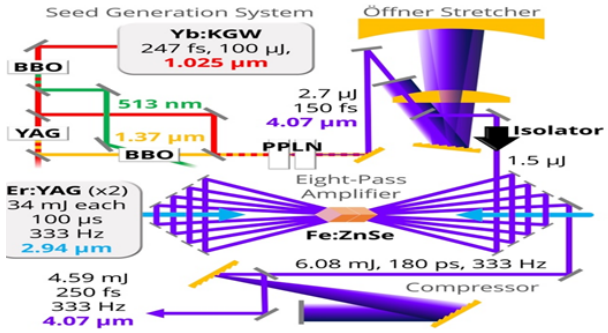

***Fig. 1. A high-repetition - rate M I R chirped pulse** aplification laser based cryogenically cooled Fe:ZnSe pumped by free-running ErYAG lasers[4] .*

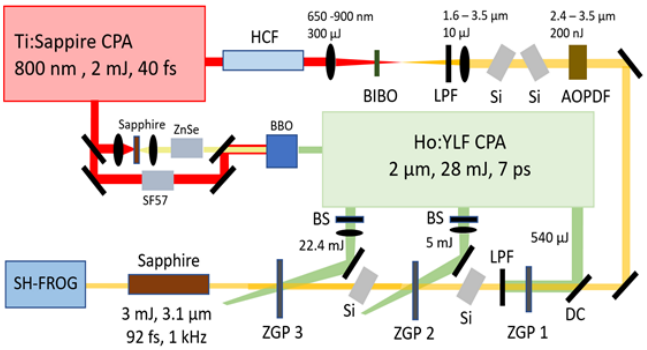

***Fig. 2. Ahigh-efficiency MIR optical parametric chirped pulse amplifier** based $ZnGeP_2$ pumped by Ho:YLF lasers at 2 mm [5]*

The seed pulses were produced by a two-stage optical parametric amplifier using BBO and PPNL nonlinear crystals pumped by a 1.03-□m YbKGW CPA laser. The broadband mJ-level MIR seed pulses were then chirped by an aberration-free Öffner-triplet grating stretcher. The Fe^{2+}:ZnSe crystals were pumped by two 100-μs, 2.94-μm Er:YAG lasers. The gain medium is cooled to 77 K to take advantage of the long florescence life time of the Fe:ZnSe at cryogenic temperature, which permits the usage of the commercially available diode-pumped free-running Er:YAG lasers. The output pulses are 247-fs at 333 Hz and 4.6 mJ with a center wavelength of 4.07 μm. Few-cycle pulses were generated by passing the beam, at a repetition rate of 400 Hz, through a large-diameter gas-filled hollow core fiber followed by dispersion compensating bulk CaF_2. A krypton-filled fiber at 53 psi yielded 1.14-mJ, 42-fs pulses centered at 4.07-μm [7]. $ZnGeP_2$ is a unique MIR nonlinear crystal. It is attractive for OPA applications due to a very high nonlinearity, d_{36}=75 pm/V. Its specific thermal conductivity, 36 W/(m·K) is 20 times larger than that of KTA that is critical for high repetition rate operation. The laser-induced damage threshold at 2.05 □m is large that favors high energy operation. Advances in the fabrication haveled to high quality ZGP products with 30×30 mm^2 clear apertures. 60-mm diameter crystals have been grown in research labs. We have developed a tabletop optical parametric chirped pulse amplification system based on ZGP crystals as illustrated in Fig.2. 3.2-mJ, 92-fs pulses centered at 3.1 μm were generated. Pumped by a 2-μm chirped pulse amplifier with a flat-top beam profile, the amplifier achieves a 16.5% overall efficiency, which, to the best of our knowledge, is the highest efficiency achieved by OPCPA at this wavelength. By focusing the GW-level MIR beams from the Fe:ZnSe CPA and ZGP OPCPA in air, non-perturbative harmonics were observed. The peak power and repetition rate will be increased for strong-field physics applications that include attosecond keV X-ray sources, laser plasma wavefield electron acceleration and intense terahertz pulse generation.

References

[1] N. Saito, H. Sannohe, N. Ishii, T. Kanai, N. Kosugi, Y. Wu, A.Chew, S. Han, Z. Chang, J. Itatani, *Optica* **6**, 1542 (2019).
[2] Z. Chang, L. Fang, V. Fedorov, C. Geiger, S.Ghimire, C. Heide, N. Ishii, J. Itatani, C. Joshi, Y. Kobayashi, P Kumar, A. Marra, S. Mirov, I. Petrushina M. Polyanskiy, D. A Reis, S. Tochitsky, S. Vasilyev, L. Wang, Y. Wu, F. Zhou, *Advances in Optics & Photonics* **14**, 652 (2022).
[3] Y. Wu, F Zhou, E. W. Larsen, F. Zhuang, Y.Yin, Z. Chang, *Scientific Reports* **10**, 7775 (2020).
[4] Z. A. Marra, Y. Wu, F. Zhou, Z. Chang, *Optics Express* **31**, 13447 (2023).
[5] F. Zhou, Y. Wu, A. Marra, Z. Chang, *Optics Letters* **47**, 6057 (2022).
[6] S. B Mirov, V.V. Fedorov, D. Martyshkin, I.S. Moskalev, M. Mirov, S. Vasilyev, *IEEE Journal of selected topics in QE* **21**, 292 (2014).
[7] Z. Alphonse Marra (*in print*) (2024).

* Acknowledgements: The author acknowledge support from the US Air Force OSR (FA9550-20-1-0295), NSF (2207674), and Canada ERC program.

Bimolecular and extraordinarily large Auger recombination processes in hexagonal boron nitride

A. I. Chatzakis
Texas Tech University, Lubbock, TX 79409, USA

Hexagonal boron nitride (hBN) is a wide, indirect bandgap semiconductor that holds great promise for optoelectronic devices in the ultraviolet and mid-infrared spectral regimes. The efficiency of optoelectronic devices is dominated by the dynamic behavior of photogenerated carriers. Here, we report on the dynamics of photoexcited free carriers in exfoliated ^{10}B-enriched (99%) hBN at room temperature. By using ultrafast ultraviolet-pump near infrared-probe transient transmission spectroscopy, we can analyze the response of materials over very short time scales. We identify three characteristic recombination rates described by the so-called ABC model [1]. A slow recombination mechanism which is independent of the excitation fluence at a rate of A~3.9 $\times 10^{9}$s^{-1} was assigned to Shockley-Read-Hall (SRH) term that is due to the impurities and defects in the lattice. At free carrier densities in the order of 10^{16}cm^{-3}, induced by the excitation pulse, we found that the dominant recombination mechanism is bimolecular with a characteristic rate constant B as of ~2.0 $\times 10^{-7}$ cm^{3}s^{-1}. At higher excitation densities $\geq 10^{17}$cm^{3}*cm*"%, the Auger recombination takes place. Auger recombination is one of the three mechanisms that determine the kinetics of photoexcited carriers, and it strongly contributes to losses in quantum efficiency known as the *droop effect* and has a strong dependence on the excitation fluence. The characteristic constant rate C we deduced here is in the range 10^{24} to 10^{-26} cm^{3}s^{-1} [2]. The recombination coefficients for the SRH and bimolecular mechanisms are consistent with earlier reported measurements on other semiconductors [3,4].

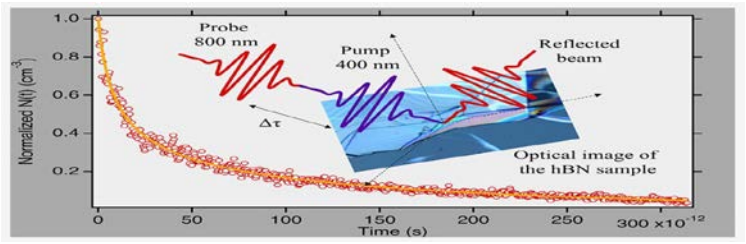

Fig.1. The graph displays the normalized differential transients *plotted as a function of the time delay between the pump and probe pulses. The* ***yellow solid*** *line represents the fit of the data. The* ***inset*** *shows the sample and illustrates the pump-probe principle.*

The Auger rate we found here is significantly larger than that in other nitride-based semiconductors [5] and sufficient to reduce the internal quantum efficiency of hBN-based devices at high operating charge densities. The larger values of the Auger coefficient deduced here can potentially be attributed to the localization of the charges by defects and impurities, as well as to the build-in polarization field caused by the strain. The strain value is about -1.8%, induced by lattice mismatch between the sapphire and hBN layers, and found to be as large as ~5.9% and close to the theoretical calculation, which is 5.2%.

References

[1] E. Kioupakis, Q. Yan , D. Steiauf, C. G van de Walle, *New Journal of Physics* **15,** 125006 (2013).
[2] S. Sharma, **S.** Liu, J.H. Edgar, I. Chatzakis, *ACS Photonics* **10,** 3586 (2023).
[3] M. Brendel, A. Kruse, H. Jönen, L. Hoffmann, H. Bremers, U. Rossow; A. Hangleiter , *Applied Physics Letters* **99**, 031106 (2011).
[4] X. Li, K. Zhang, J. Treu, L. Stampfer, G. Koblmueller, F. Toor, J.P. Prineas *Nano Letters* **19,** 990 (2019).
[5] E. Kioupakis, D. Steiauf, P. Rinke, K.T. Delaney, C. G. Van de Walle, *Physical Review* B ***92***, 035207 (2015).

Controlling THz emission in topological materials

E. E. M. Chia
Nanyang Technological University, Singapore 637371, Singapore.

This talk describes follow-up work on the two materials described at the Symposium in 2023 [1]. First, in the ferromagnet-semiconductor Co/MoS_2 heterostructure, by making use of the strongly out-of-equilibrium character of the injected spins, we demonstrate a highly-efficient spin injection from a ferromagnet into a semiconductor, thus overcoming the crippling problem of impedance mismatch. Surprisingly, we measure a giant spin current that is orders of magnitude larger than typical injected spin current densities using currently available techniques Fig.1 [2].

Fig. 1 (a) (THz peak)/(absorbed fluence) *of Co/MoS_2 under different pump wavelengths. The* ***red, white and purple*** *regions represent different spin injection processes illustrated in panels* ***(b), (c)*** *and* ***(d),*** *respectively [2].*

A follow-up question is: can this spintronic THz emitter architecture be integrated with silicon? Our data shows the formation of silicide layer at the Co/Si interface that also shows large spin-to-charge conversion - see Fig.2, [3].

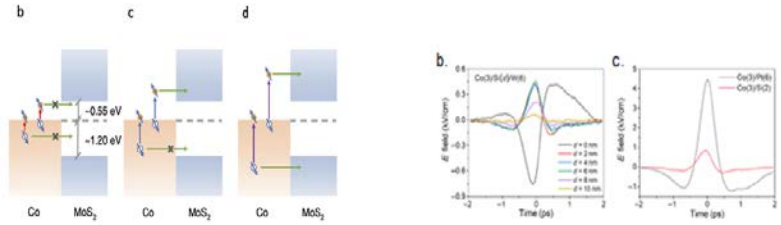

Fig. 2 (a) Schematic of THz emission setup *for SiO_2/Co/Si/quartz heterostructure. Emitted THz waveforms for* ***(b)*** *Co(3 nm)/Si (d)/W(6 nm), and* ***(c)*** *Co(3 nm)/Pt (6 nm) and Co(3 nm)/Si(2 nm) [3].*

Second, in thin polycrystalline films of the centrosymmetric Dirac semimetal $PtSe_2$ we observe a giant and highly tunable THz emission that is (a) rapidly turned on at oblique incidence, (b) locked to both the in-plane photon momentum and polarization state of the incident pump beam, and (c) whose polarization-state-locked THz emission is strong evidence of the central role played by quantum geometry-see Fig.3 [4].

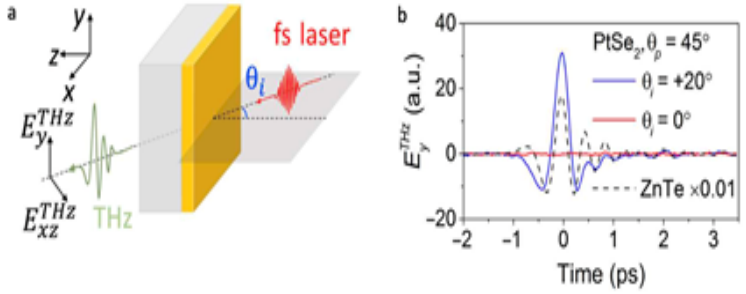

Fig. 3. (a) Schematic of THz emission setup *for Dirac semimetal $PtSe_2$.*
(b) *THz emission amplitude for different incident pump angle [4].*

A follow-up of this work would be: can we tune the THz emission of this material, by electrical means, via the control its quantum geometry? The answer is yes.

References

[1] E.E.M Chia, *Ultrafast Dynamics, Metastability and Ultrafast Bandgap Photonics* ***X***, 28, (2023).
[2] L. Cheng, X. Wang, W. Yang, J. Chai, M. Yang, M. Chen, Y. Wu, X. Chen, D. Chi, K. E. Johnson Goh, J.-X. Zhu, H. Sun, S. Wang, J. C. W. Song M. Battiato, H. Yang, E. E. M. Chia, *Nature Physics*, DOI:10.1038/s41567-018-0406-3 (2019).
[3] J. Liu, Y. Yang, K. Lee, R. Sharma, H. Yang, M. Battiato, E. E. M. Chia, *Physical Review Applied* **18,** 034056 (2022).
[4] L. Cheng, Y. Xiong, L. Kang, Q. Chang, M. Chen, J. Qi, H. Yang, Z. Liu, J.C. W. Song, E. E. M. Chia. *Science Advances* **9,** eadd7856 (2023).

Elucidating the pairing symmetry of infinite-layered nikelate superconductors

E. E. M. Chia
Nanyang Technological University, Singapore 637371, Singapore

The superconducting infinite-layer nickelate family has risen as a promising platform for revealing the mechanism of high-temperature superconductivity. However, its challenging material synthesis has obscured effort in understanding the nature of its ground state and low-lying excitations, which is a prerequisite for identifying the origin of the Cooper pairing in high-temperature superconductors. In particular, the superconducting gap symmetry of nickelates has hardly been investigated and remains controversial. Here, we report the pairing symmetry of the infinite-layer nickelates in neodymium-based (Nd,Sr)NiO2 and lanthanide-based (La,Ca)NiO2 thin films of high crystallinity, using a tunnel-diode-based penetration depth technique in the MHz frequency range. Our microscopic analysis reveal that a complex order parameter is able to explain the temperature dependence of both samples. In contrast to the cuprates, our results suggest that the superconducting order parameter in the nickelates is beyond a single d-wave gap.

Ultrafast control of optical Kerr rotation in bulk transition Metal dichalcogenides

E. Cappelluti[1], H. Rostami[2], F. Cilento[3]
[1] *Istituto di Struttura della Materia, 34149 Trieste, Italy*
[2] *University of Bath, Bath BA2 7AY, UK*
[3] *Elettra-Sincrotrone Trieste,34149 Basovizza, Italy*

The present semiconductor technology largely exploits the manipulation of the electronic charge through its entanglement with other degrees of freedom, including spin, lattice, or coupling with photons. Transition-metal dichalcogenides (TMDs) of the type MX_2 (M =Mo, W; X = S, Se) are among the best materials for employing such scenario [1]. Obeying to their layered hexagonal structure and to the sizeable spin-orbit coupling, their electronic structure is dominated by two inequivalent valleys that, when exfoliated or grown at the monolayer limit, because of the broken symmetry inversion, show a complementary spin/orbital content and an opposite optical response. This scenario enables the possibility of tailoring the optical, electronic and magnetic properties of the compounds by a selected spin/valley population controlled by the circular polarization of the incoming light [2]. However, the possibility of exploiting such physics in materials with even number of layers, where the inversion symmetry is restored and no control of the valleys is feasible, hampers straightforward applications to bulk materials. We perform broadband time-resolved optical spectroscopy [3] on bulk WSe_2 and, by using a circularly polarized pump pulse tuned at the A-excitonic resonance, we show that a large room temperature transient optical rotation of the reflected polarization (Kerr effect) is obtained. We observe a Kerr signal in the energy range of all the three main optical features associated with the A, B and C excitons. The time-resolved dynamics of the pump-induced Kerr signal reveals a common timescale for all the three features, with a remarkably long lifetime of ≈1.8 ps. An additional exponential faster decay, with characteristic timescale of ≈300 fs is further observed only for the Kerr signal at the A-exciton resonance.

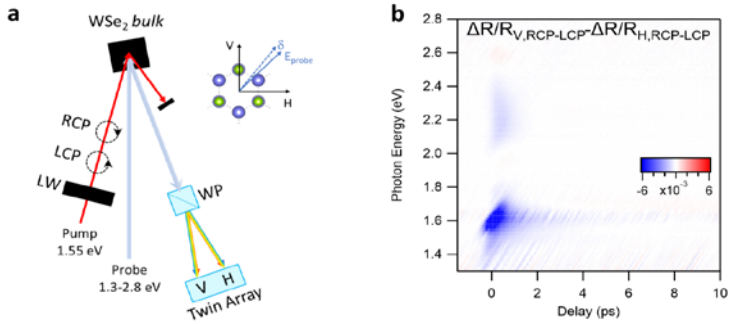

Fig. 1. a*. Sketch of the experimental apparatus, consisting in a pump-probe setup capable of measuring simultaneously two orthogonal polarizations, matching theprincipal axes of the crystalline sample. The probe is a broadband supercontinuum, while the polarization of the pump at 800 nm can be quickly switched between right and left circular.*
b. *Difference of the time-resolved reflectivity as a function of pump-probe delay and probe photon energy, obtained as a difference between the two probe polarizations* ***(V-vertical and Hhorizontal****) and the two pump pulse helicities. A Kerr signal, indicative of polarization rotation, is observed at the three exciton energies and lasts for a few hundreds of femtoseconds.*

Based on a comprehensive theoretical analysis [4], we show that the origin of a finite Kerr rotation in centrosymmetric bulk TMDs is due to the intrinsic quantum entanglement between the spin, layer, valley and orbital degrees of freedom, encoded in the proper optical selection rules. The present results pave the way for the exploitation of bulk transition-metal dichalcogenide materials for future feasible opto-magnetic manipulations, circumventing the limitations of exploiting single-layer compounds.

References

[1] S. Manzeli , D. Ovchinnikov, D. Pasquier, O. V. Yazyev, A. Kis, *Naure Reviews Materials* **2**, 17033 (2017).
[2] W. Yao, D. Xiao, O. Niu, *Physical Review* B **77**, 235406 (2008).
[3] M. Perlangeli, S. Peli, D. Soranzio, D. Puntel, F. Parmigiani, F. Cilento, *Optics Express* **28**, 8819 (2020).
[4] H. Rostami, *(to be published)* (2024).

Coherent THz lattice dynamics coupled to spins in 2D antiferromagnetic Semiconductors: a combined magneto-optical and ARPES study

M. Cinchetti
Technische Universität Dortmund, 44221 Dortmund, Germany

Two-dimensional (2D) materials have attracted a huge interest from the physics, chemistry and engineering community as extremely promising candidates for future emerging technologies. A prominent example is the demand for miniaturized, ultrahigh-speed electronic devices that currently drives the electronic industry, where van der Waals antiferromagnetic semiconductors could provide systems with intrinsic magnetic stability and THz dynamics, scalable down to the monolayer limit. In my talk I will discuss our recent studies on $FePS_3$, that we have chosen as a promising van der Waals antiferromagnetic semiconductor that can be scaled down to the 2D limit without losing its magnetic order. We have studied this material using two complementary experimental methods. First, we performed pump-probe magneto-optical measurements to access the laser-driven lattice and spin dynamics. When pumping in resonance with a d-d transition of the Fe^{2+} multiplet, we

generated a coherent phonon mode oscillating at 3.2 THz. This mode can be excited in a regime of low optical absorption that prevents damage even of single antiferromagnetic layers [1]. The amplitude of this mode decreases as the sample is heated up to the Néel temperature and eventually vanishes as the phase transition to the paramagnetic phase occurs, thus revealing its connection to the long-range magnetic order. In the presence of an external magnetic field, the optically triggered 3.2 THz phonon hybridizes with a magnon mode, which we utilize to excite the hybridized phonon-magnon mode optically. Second, we utilized angle-resolved photoelectron spectroscopy (ARPES) to probe the electronic structure of $FePS_3$ in its ground state [2] and employed time-resolved ARPES to capture the ultrafast dynamics of selected spin-allowed and spin-forbidden d-d transitions in $FePS_3$ [3]. The insights from magneto-optical experiments, juxtaposed with ARPES findings, shed light on the intricate quasiparticle dynamics underpinning the observed THz dynamics in $FePS_3$, offering a deeper understanding of the role of resonant excitation of d-d transitions in quantum material behaviour. To conclude, I will underline how our findings pioneer the application of time-resolved ARPES in exploring the dynamics of d-d transitions across a broad spectrum of solid-state systems, and their interplay with other quasiparticles such as phonons, excitons and magnons.

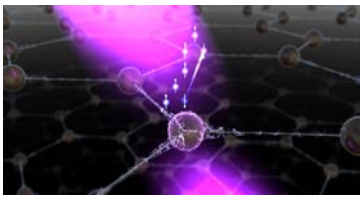

References

[1] F. Mertens, D. Mönkebüscher, U. Parlak, C. Boix-Constant, S. Mañas-Valero, M. Matzer, R. Adhikari, A. Bonanni, E. Coronado ,A.M. Kalashnikova, D. Bossini M.Cinchetti.. *Advanced Materials* **35**, 2208355 (2023).

[2] J. E. Nitschke, D. L. Esteras, M. Gutnikov, K. Schiller, S. Mañas-Valero, E. Coronado, M. Stupar, G. Zamborlini, S. Ponzoni, J. J. Baldovi, M. Cinchetti *Materials Today Electronics* **6,** 100061 (2023).

[3] J. E. Nitschke, M. Gutnikov, K. Schiller, E. Coronado, A. Omar, G. Zamborlini, C. Saraceno, M. Stupar, A.M. Ruiz, D. L. Esteras, J. J. Baldoví, F. Anders M. Cinchetti, *arXiv:2402.03018* (2024).

THz emitting magnetic hybrid nanostructures in spintronic devices

O. Crisan[1], E. Th. Papaioannou[2]

[1] *National Institute for Materials Physics, 077125 Magurele, Romania*

[2] *Aristotle University of Thessaloniki, Thessaloniki, Greece*

The formation of hybrid nanostructures in spintronic devices has been investigated as a response to specific needs especially in nanoelectronics or adjacent fields where combined optical and magnetic response to various excitations is required for various types of sensing. With the advent of high accuracy and high resolution fabrication technologies such as lithography, coupling phenomena at the nanoscale may become accessible. The integration of the magnetic and semi-conductor components adds new capabilities to the electronic devices. While spin phenomena have long been investigated within the context of conventional ferromagnetic materials, the study of spin generation, relaxation, and spin-orbit coupling in non-magnetic materials took off only recently with the advent of hybrid spintronics and it is here many novel materials and architectures can find their greatest potentials in both science and technology [1]. Here we present initial approach to nanostructuring of hybrid patterned structures based on magnetic FePt-based bilayers, as well as their response to the optical excitation of magnetization, in view of potential applications as THz spintronic emitters. Indeed, spintronic THz emitters made of $L1_0$ phase ferromagnetic/non-magnetic bilayers, can exhibit spin-to-charge current transition, resulting in controlled and tunable THz pulse emission. We have synthesized magnetic bilayers made of Si(001) / Fe(2 nm) / Pt(3 nm) and by appropriate annealing we have engineered at the Fe / Pt interface an area of alloying made of $L1_0$ phase FePt (Fig. 1).

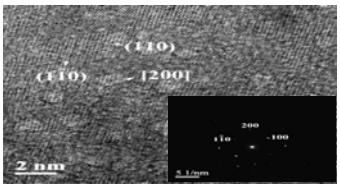

Fig. 1: *The HREM proof*

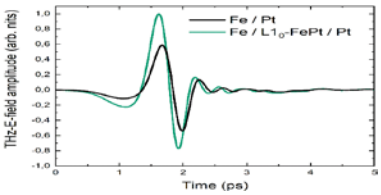

Fig. 2: The THz electric field of Fe / Pt bilayer *as well as the emission in the presence of $L1_0$ phase at the bilayer's interface*

Upon optical pumping with a femtosecond laser pulse, we have found that the THz signal emitted from the heterostructure is highly enhanced in the presence of the $L1_0$ interfacial area, compared with the case where the alloying at the interface is not manifested (Fig. 2).This is interpreted in terms of spin dynamics simulated by the spin lattice in the face centred tetragonal $L1_0$ interfacial region. It is inferred that the presence of $L1_0$ alloyed interlayer enhances the spin asymmetry between the Pt 5d band and the Fe 3d band.
This leads to an increased THz emission, stimulated by the interfacial alloyed region.

References

[1] O. Crisan, A.D. Crisan, G. Schinteie, V. Kuncser, *Coatings* **13**, 2068 (2023).

[2] L. Scheuer, M. Ruhwedel, D. Karfaridis, I. G. Vasileiadis, D. Sokoluk, G. Torosyan, G. Vourlias, G.P.Dimitrakopoulos, M. Rahm, B.Hillebrands, T. Kehagias R.Beigang, E. Th. Papaioannou, *iScience* **25**, 104319, (2022) .

* Acknowledgement(s): This work is funded through grant PN- III -P4-PCE-2021-0573 contract PCE 79 / 2022, from Romanian Ministry of Research, Innovation and Digitalization. Also, this work acknowledges the support from EU funded Romanian National Plan for Resilience and Redress, I 9 Pillar, Project 760085/23.05.2023.

Resilience of the Mott insulating state of La_2CuO_4 against Photodoping

A. R. Pokharel[1], M. Beyer[2], M. Obergfell[1], S. Y. Agustsson[1], T. Dong[1], G. Logvenov[4], I. Bozovic[3]
K. Warawa[5], M.D. Thomson[5], H.G. Roskos[5], Z. Lenarčič[6], P. Prelovšek[6]
J. Demsar[1]

[1]*Johannes Gutenberg University Mainz, 55128 Mainz, Germany*
[2]*University of Konstanz, 78457 Konstanz, Germany*
[3]*Brookhaven National Laboratory, Upton, NY 11973, USA*
[4]*Max Planck Institute for Solid State Research, 70569 Stuttgart, Germany*
[5]*Universität Frankfurt, 60438 Frankfurt, Germany*
[6]*Jozef Stefan Institute, 1000 Ljubljana, Slovenia*

The parent compounds of high-T_c cuprate superconductors are Mott insulators with antiferromagnetic (AFM) order, where strong correlations between Cu 3d-electrons split the half-filled Cu 3d-band into the upper (UHB) and lower (LHB) Hubbard band, resulting in an antiferromagnetic insulating ground state [1]. The insulating parent (undoped) compounds are characterized by a charge-transfer (CT) gap of about 2 eV between the oxygen-derived p-band, located within the Mott gap, and the upper Hubbard band (UHB). The nature of doping induced changes in the low energy electronic structure by introducing electrons or holes into the CuO_2 planes is, like the problem of high-T_c cuprates itself, still under intense discussion [1-4]. Introducing a few percent of holes (or electrons) into the CuO_2 planes, results in a transfer of spectral weight to lower energies, with the appearance of excitations in the mid-infrared (MIR) range [2]. Upon further doping the MIR peak eventually merges into the Drude-like free carrier peak as doping approaches optimal doping [2]. While numerous models have been put forward to account for the doping evolution of free carrier and MIR response, the consensus is still lacking [5]. Photodoping, i.e., generating electron- and hole-like carriers by absorption of light with frequency exceeding the CT gap, was shown to induce similar changes in low energy excitation spectrum to chemical doping, both by using quasi-continuous [6] or pulsed excitation [7-9], where studies on thick films and single crystals suggest photoinduced metallic state [7-9]. Here, we investigate transient photo-doping phenomena in La_2CuO_4, an archetypal antiferromagnetic Mott insulating parent compound of the cuprate high-T_c superconductor. We capture the dynamics of the transient state by tracking the time-evolution of THz photoconductivity [8] and the changes in the complex dielectric function e(w,t) [10] in the 0.5 – 2.6 eV range in optically-thin films, following optical excitation across the charge transfer (CT) gap. We cover a large range of excitation densities from 0.001 to ~0.12 absorbed photons [electron-hole (e-h) pairs] per Cu. Analysis of De(w,t) demonstrates a pronounced photoinduced reduction of the CT gap, consistent with recent transient X-ray absorption study [11], concomitant with the appearance of mid-infrared absorption and a weak free carrier response, all simultaneously relaxing on a (sub)picosecond scale. Up to the highest excitation densities, where at comparable chemical-doping levels a metallic state is realized, the free carrier contribution remains negligible, underscoring the robustness of the underlying electronic correlations. Recovery dynamics proceeds on the ps timescale and is density-independent up to 0.01 e-h pairs per Cu. The low free-carrier spectral weight and the overall fast recombination suggest that relaxation proceeds via pair-wise recombination of nearly bound e-h pairs through multi-magnon emission [12]. Only at densities beyond 0.01 e-h pairs per Cu the relaxation rate starts to increase with increasing excitation density, which we attribute to partial melting of the antiferromagnetic background and many-body recombination processes. Comparison of the excitation density dependence of the Drude-like and MIR spectral weights suggests the two are intimately related, providing constraints for theories of low-energy excitations in weakly doped cuprates.

References

[1] P. A. Lee, N. Nagaosa, X.G. Wen, *Reviews of Modern Physics* **78**, 17 (2006).
[2] S. Uchida, S Uchida, T Ido, H Takagi, T Arima, Y Tokura, S Tajima, *Physical Review* B **43**, 7942 (1991).
[3] A. S. Mishchenko, N. Nagaosa, Z.-X. Shen, G. De Filippis, V. Cataudella, T. P. Devereaux, C. Bernhard, K. W. Kim , J. Zaanen, *Physical Review Letters* **100**, 166401 (2008).
[4] S. Zhou, Y. Wang, Z. Wang, *Physical Review* B **89**, 195119 (2014).
[5] A. J. Leggett, *Proceedings of National Academy of Science USA* **96**, 8365 (1999).
[6] Y. H. Kim, S.-W. Cheong, Z. Fisk, *Physical Review Letters* **67**, 2227 (1991).
[7] H. Okamoto, T. Miyagoe, K. Kobayashi, H. Uemura, H. Nishioka, H. Matsuzaki, A. Sawa, Y. Tokura, *Physical Review* B **83**, 125102 (2011).
[8] J. C. Petersen, A. Farahani, D.G. Sahota, R. Liang J.S. Dodge, *Physical Review* B **96**, 115133 (2017).
[9] E. Baldini, M. A. Sentef, S. Acharya, T. Brumme, E. Sheveleva, F. Lyzwa, E. Pomjakushina, C. Bernhard, M. van Schilfgaarde, F. Carbone A. Rubio, C. Weber, *Proceedings of National Academy of Science USA* **117**, 6409 (2020).
[10] M. Obergfell, J. Demsar, *Physical Review Letters* **124,** 037401 (2020).
[11] D. R. Baykusheva, H. Jang, A. A. Husain, S. Lee, S. F. R. Ten Huisen, P. Zhou, S. Park, H.Kim, J.-K. Kim, H.D. Kim , M. Kim, S.-Y. Park P. Abbamonte, B. J. Kim, G. D. Gu,Y. Wang, M. Mitrano, *Physical Review* X **12**, 011013 (2022).
[12] Z. Lenarcic, P. Prelovsek, *Physical Review Letters* **112,** 087402 (2014).

Optical control of superconductivity probed with ultrafast optical magnetometry

G. De Vecchi[1], S. Fava[1], G. Jotzu[1], M. Buzzi[1], Y. Liu[2], S. Nakata[2], B. Keimer[2]
A. Cavalleri[3]
[1] *Max Planck Institute for the Structure and Dynamics of Matter, 22761 Hamburg, Germany*
[2] *Max Planck Institute for Solid State Research, 70569 Stuttgart, Germany*
[3] *University of Oxford, Oxford OX1 3PU, UK*

A number of recent experiments have made use of ultrashort pulses to dynamically reduce or enhance signatures of superconductivity. Irradiation with visible or ultraviolet pulses has been used to study the disruption and recovery of the superconducting state [1]. In a series of more recent experiments, mid infrared optical pulses were used to drive $YBa_2Cu_3O_{6+x}$ along the insulating c-axis direction, coupling to apical oxygen vibrations, to coherently modulate their electronic properties. A transient state with superconducting-like optical properties was observed up to temperatures far in excess of equilibrium T_c [2-4]. Whether these out-of-equilibrium superconducting-like states also show a dynamical diamagnetic response, beyond the documented transient optical conductivities, remains an open question. Here, we make use of an ultrafast optical magnetometry technique to measure changes in the magnetic field in the vicinity of a $YBa_2Cu_3O_{6.48}$ sample with $\sim 1\ \mu T$ sensitivity and sub-picosecond time resolution (Figure 1). We provide evidence that, under the same excitation conditions that generate a transient superconducting-like state in this material, a prompt expulsion of a statically applied magnetic field ensues, a response indicative of the appearance of an ultrafast Meissner effect [5]. I will then discuss how disruption of superconductivity in $YBa_2Cu_3O_7$ thin films can be used to generate ultrafast magnetic field transients that allow for ultrafast magnetization control. We create a device based on a lithographically defined $YBa_2Cu_3O_7$ disk and photo-excite it with ultraviolet ~100fs pulses. After photo-excitation, the magnetic shielding currents in the $YBa_2Cu_3O_7$ disk are quenched and the magnetic field rapidly increases on picosecond timescales. We use these ultrafast magnetic field ramps to study the magnetization dynamics of a $Bi:Y_3Fe_5O_{12}$ sample included in this device and show that the ultrafast magnetic field transient launches coherent oscillations of the ferromagnetic resonance mode in $Bi:Y_3Fe_5O_{12}$ [6].

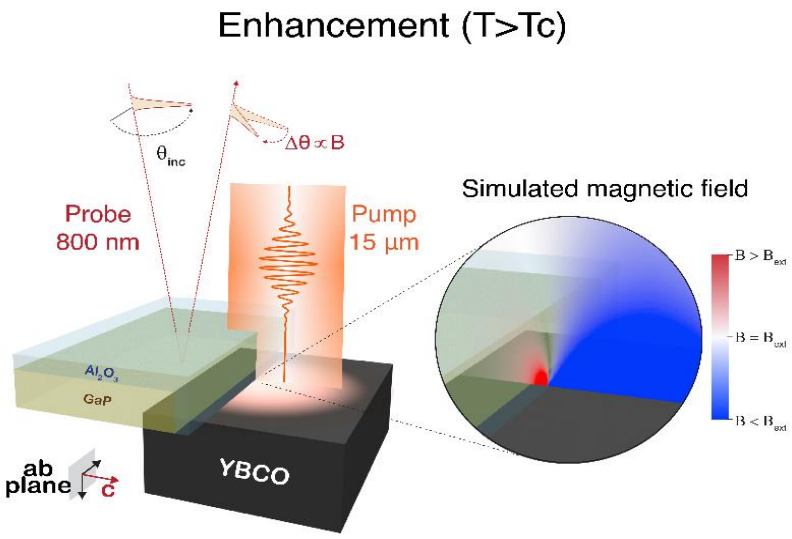

Fig, 1 Magnetic field expulsion after phonon excitation in $YBa_2Cu_3O_{6.48}$. *Schematic of theexperiment. **A** thin Al_2O_3 crystal is placed on top and next to the exposed side of the GaP (100) detectioncrystal to completely reflect the 15 μm pump and prevent it from generating a spurious non-linear optical response in the GaP (100) crystal. The thin Al_2O_3 crystal also creates a well-defined edge in the mid infrared pump beam, shaping the photo-excited region into a half disc of ~ 375 μm diameter. The expected changes due to magnetic field expulsion upon photo-excitation are shown in the magnified area on the right. The time dependent magnetic field is sampled positioning the probe beam in the vicinity of the edge of the photo-excited region.*

We use these ultrafast magnetic field ramps to study the magnetization dynamics of a $Bi:Y_3Fe_5O_{12}$ sample included in this device and show that the ultrafast magnetic field transient launches coherent oscillations of the ferromagnetic resonance mode in $Bi:Y_3Fe_5O_{12}$ [6].

References

[1] J. Demsar, *Journal of Low Temperature Physics* **201**, 676 (2020).
[2] W. Hu, S. Kaiser, D. Nicoletti, C.R.Hunt, I.Gierz, M.C.Hoffmann, M.Le Tacon, T. Loew, B. Keimer, A.Cavalleri, Nature Materials 13, 705(2014).
[3] B. Liu, M. Först, M. Fechner, D. Nicoletti, J. Porras, T. Loew, B. Keimer, A. Cavalleri, Physical Review X **10**, 011053 (2020).
[4] A. von Hoegen, M . Fechner, M. Först, N. Taherian, E. Rowe, A. Ribak, J. Porras, B. Keimer, M. Michael, E. Demler, A. Cavalleri, *Physical Review* X **12**, 031008 (2022).
[5] S. Fava, G. De Vecchi, G. Jotzu, M. Buzzi, T. Gebert, Y. Liu, B. Keimer, A. Cavalleri, *in print* (2024).
[6] G. De Vecchi, S. Fava, G. Jotzu, M. Buzzi, T. Gebert, A. Cavalleri, *in print* (2024).

Magnetism and spin dynamics in low-dimensional materials

A. Delin
KTH Royal Institute of Technology, 10691 Stockholm, Sweden

The conventional wisdom for a long time was that fluctuations would kill any long-range magnetic order in materials of lower dimensions than three since continuous symmetries cannot be spontaneously broken at finite temperature in systems with sufficiently short-range interactions in dimensions lower or equal to two. It was also thought that two-dimensional materials themselves could not be realized, since they would inevitably spontaneously roll up into a three-dimensional configuration with lower energy. However, by introducing sufficiently high energy barriers, such low-dimensional states can indeed be created. As we all now know, the structure of two-dimensional materials like graphene can be stabilized with the help of thermal undulations, and in low-dimensional magnetic systems, the spin-orbit coupling is an important origin of barriers protecting the long-range ordered magnetic state. This leads to a range fascinating phenomena. In this talk, I will give an overview of our recent theoretical work on spin textures and spin dynamics in low-dimensional systems and our recent efforts to develop methods to identify both local and global minima in highly convoluted spin-Hamiltonian potential energy surfaces. We have, for example, discovered complex magnetic textures in the vanadium stibnites [1], a class of Kagome systems, and large spin-lattice couplings, i.e, how the magnetic interactions depend on atomic displacement, in CrI3 [2,3]. Employing fully relativistic first-principles calculations, we extract an effective measure of the spin-lattice coupling in the prototypical two-dimensional magnet CrI3, finding that they are up to ten times larger than what is found for bcc Fe. The magnetic exchange interactions, including Heisenberg and relativistic Dzyaloshinskii-Moriya interactions in this system are found to e sensitive both to the in-plane motion of Cr atoms and out-of-plane motion of ligand atoms. Furthermore, we have identified a large number of metastable topologically nontrivial spin textures in two-dimensional systems with frustrated exchange, using our newly developed metaheuristic conditional neural-network-based method (see Fig. 1) [4].

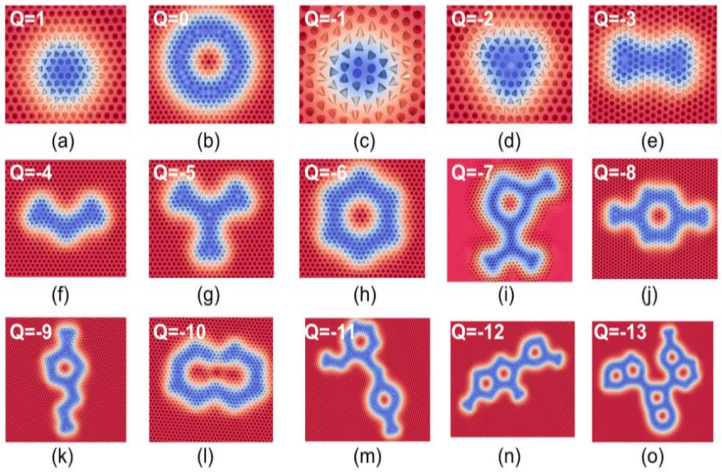

Fig. 1. A subset of identified topological metastable spin textures *in the Pd/Fe/Ir(111) system with an external magnetic field of 3.5 T.* ***(a) Skyrmion****,* ***(b skyrmionium****,* ***(c)antiskyrmion****,* ***(d)–(o)*** *isolated magnetic textures, with higher-order topological charge varying between Q = −2 and Q −13. The distance between neighboring* ***Blue*** *and* ***red*** *colors indicate opposite spin directions.*

We have also developed an efficient genetic-tunneling based algorithm to identify skyrmionic ground states, which in contrast to simulated annealing correctly converges to the correct topological charge state as a function of magnetic field [5].

References

[1] M. N. Hasan, R. Bharati, J. Hellsvik, A. Delin, S. K. Pal, A. Bergman, S. Sharma, I. Di Marco, M. Pereiro, P. Thunström, P. M. Oppeneer O. Eriksson, D. Karmakar, *Physical Review Letters* **131**, 196702 (2023).
[2] J. Hellsvik, D. Thonig, K. Modin, D. Iuşan, A. Bergman, O. Eriksson, L. Bergqvist, A. Delin, *Physical Review* B **99**, 104302 (2019).
[3] B. Sadhukhan, A. Bergman, Y. O. Kvashnin, J. Hellsvik, A. Delin, *Physical Review* B **105**, 104418 (2022).
[4] Q. Xu, I. P. Miranda, M. Pereiro, F. N. Rybakov, D. Thonig, E. Sjöqvist, P. F. Bessarab, A. Bergman, O. Eriksson, P. Herman, A. Delin *Physical Review Research* **5**, 043199 (2023).
[5] Q. Xu, Z. Shen, M. Pereiro, E. Sjöqvist, P. Herman, O. Eriksson, A. Delin, *Communications Physics* **6**, 239 (2023).

* Acknowledgements: this work was supported by the K&A. Wallenberg Foundation (Grants No. 2018.0060, 2021.0246, 2022.0108) Vetenskapsrådet (No. 2017-03832, 2019-03666, 2016-05980, 2019-05304, 2020-05110), the Icelandic Research Fund (No. 217750) University of Iceland Research Fund (15673), the European Research Council (854843-FASTCORR), the foundation for Strategic Research SSF, and CSC Grant No. 201906920083. Support from STandUP, Digital Fu- tures, SeRC, ER (project FASTCORR-Grant No. 854843), and eSSENCE is also acknowledged. Computations/data handling were enabled by resources provided by KAW (Berzelius-2022-259) and the Swedish National Infrastructure for Computing (SNIC), partially funded by the Swedish Re- search Council through Grant No. 2018-05973.

Transferable optical enhancement nanostructures by Gapless stencil lithography

A. K. Demir, J. Li, T. Zhang, C. Occhialini, L. Nessi, Q. Song, J.Kong, R. Comin
Massachusetts Institute of Technology, Cambridge, MA 02139, USA

Optical spectroscopy is one of the prime tools for unveiling the electronic properties and symmetries of materials in the atomically thin limit. However, the vanishing thickness of two-dimensional (2D) materials often results in a cross section too low for conventional optical methods to produce measurable signals. In this work, we developed a scheme based on the stencil lithography technique to fabricate transferable high-resolution optical enhancement nanostructures for Raman and photoluminescence (PL) spectroscopy [Fig. 1]. We also demonstrate that the method is particularly effective for optical studies of air-sensitive materials, as the fabrication and the transfer can be performed in situ. The fabrication technique can be easily generalized to enable a high degree of flexibility for functional photonic devices and surfaces.

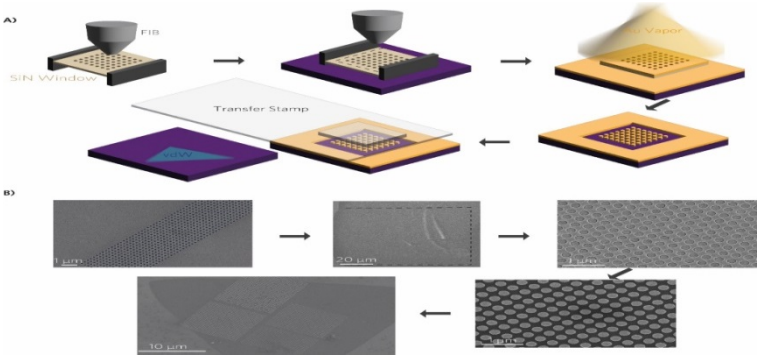

Fig. 1. An illustration of the fabrication steps with the corresponding SEM/FIB images. A, *A commercial SiN_x membrane is milled, flipped, and lowered to contact the substrate. The window is removed, and the material of choice is evaporated. The membrane is loosely stuck to the surface and can be easily removed with a low-adhesion tape. After the removal, the nanostructures can be transferred onto the sample of interest.* ***B,*** *Clockwise, from* ***top right****: Milled membrane (SEM); the sides are cut with FIB (FIB); before the membrane is removed (SEM); after the membrane is removed (SEM); after the nanostructures are transferred on a single-layer WSe_2 sample (SEM).*

Equipped with this nanofabrication technique, we designed and fabricated plasmonic nanostructures to tailor the interaction of atomically thin materials with light. We demonstrate orders-of-magnitude increase in the Raman intensity of ultrathin flakes of 2D semiconductors and magnets [Fig. 2] as well as selective Purcell enhancement of quenched excitons in WSe_2/MoS_2 heterostructures.

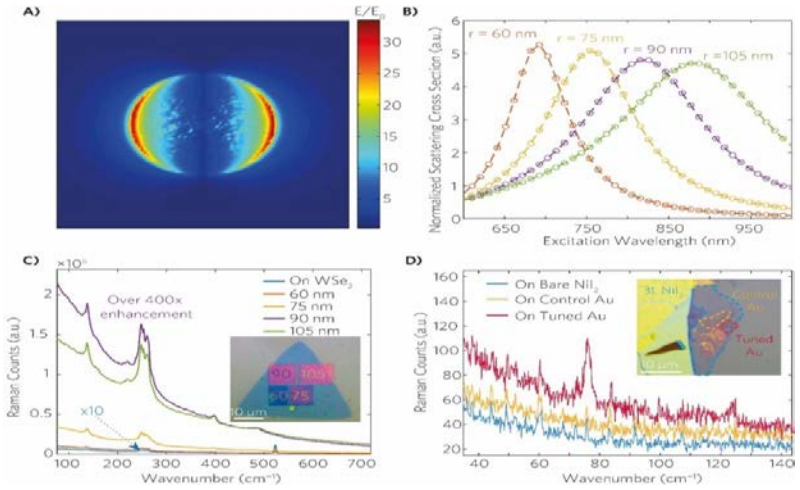

Fig. 2. Raman Enhancement due to Transferred Plasmonic Arrays. A, *Illustration of electric field enhancement due to a single gold nanodisk with radius R = 90 nm and thickness = 20 nm on the plane 0.7 nm under the nanodisk.* ***B,*** *Wavelength dependent normalised scattering cross sections for various radii, with the same thickness, 20 nm.* ***C,*** *Raw Raman spectra of Wse_2 taken with 785 nm excitation with and without the nanodisks for a gold filling factor of 0.32. The low wavenumber tail is the intralayer exciton of WSe_2. The inset shows the optical micrograph of the structure, with nanodisks radii overlaid on each array.* ***D,*** *Raw Raman spectra of three-layer NiI_2 taken with 785 nm excitation with and without nanodisks. The inset shows the optical micrograph of the structure, with the regions of interest delineated and labelled.*

This approach can be readily implemented with virtually no change of parameters for optical enhancement of spectroscopy methods other than Raman and PL, such as second-harmonic generation and infrared absorption, and can be critical for obtaining statistically significant data due to orders of magnitude increase in signal quality. Combining the highly precise characteristics of the technique with the transferability provided with our method can prove instrumental in fabricating complex metasurfaces and photonic structures and find uses in quantum information/sensing technologies with optical read-outs.

References

[1] A.K. Demir, *to be submitted,* (2024).

* Acknowledgements: this work was supported by the U.S. DoE, office C2QA under contract DE-SC0012704, the support by U.S. DoE Office of Science, Basic Energy Sciences award No. DE-SC0020042 for the WSe2 and MoS2 material synthesis. This work was performed in part on the Raith VELION FIB-SEM in the MIT. nano Characterization Facilities (Award: DMR-2117609), and in Fab.nano and Characterization.nano facilities at MIT.nano. A.K.D. acknowledges support from MathWorks Science Fellowship. Thank Yang Yu for his assistance in FIB use.

Electron-phonon scattering processes in ferromagnets observed in real time

H. A. Dürr
Uppsala University, 75120 Uppsala, Sweden

The non-equilibrium energy exchange mechanism between electronic and lattice degrees of freedom is of central importance for understanding ultrafast phenomena such as manipulating magnetism on the femtosecond timescale. We show for ferromagnetic Ni, where ultrafast demagnetization was first discovered, how scattering processes between transient phonons and valence electrons take place in real time [1]. The observed momentum-dependent filling of electronic states provides a new avenue to understand and ultimately tailor materials properties far from equilibrium. Fig. 1 illustrates the central idea behind observing electron-phonon scattering processes in real time. Following fs laser excitation transient phonons are excited as observed via ultrafast electron diffraction from the vibrating lattice [2]. Reabsorption of transient phonons leads to characteristic electron scattering processes that can be detected with time-resolved photoemission spectroscopy as state-dependent state occupations. These electronic scattering events are also spin dependent and affect to spin polarizations of the involved electronic states [1].

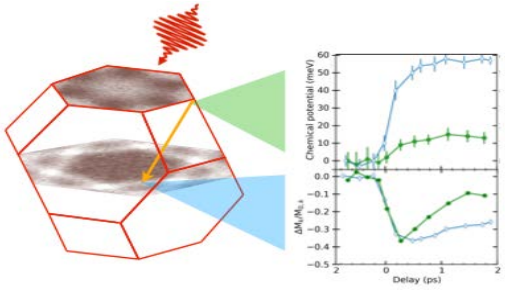

***Fig. 1. Left**: Ni Brillouin zone with electronic states at the Fermi level shown in white on brown background. Following laser excitation electrons are scattered by transient phonons between the k-points marked by the yellow arrow.*
***Right**: This results in different band occupations as quantified by a state-dependent chemical potential **(top panel)** and it also affects the state-resolved magnetic moment changes observed with time-resolved photoemission spectroscopy [1].*

We will show that these processes are also at work in other ferromagnetic materials and can lead to intriguing nanoscale spin dynamics [3].

References

[1] V. Shokeen, M.Heber, D.Kutnyakhov, X.Wang, A.Yaroslavtsev, P.Maldonado, M.Berritta, N. Wind, L.Wenthaus, F. Pressacco, C.- H. Min, M. Nissen S. K.Mahatha, S.Dziarzhytski, P.Oppeneer, K.Rossnagel, H.-J.Elmers, G.Schönhense, H. Dürr, *Science Advances* **10**, eadj2407 (2024).
[2] P. Maldonado, T. Chase, A. Reid, X. Shen, R. Li, K. Carva, T. Payer, M. Horn von Hoegen, K. Sokolowski-Tinten, X. J. Wang, P. M. Oppeneer H. A. Dürr, *Physical Review* B **101**, 100302 (2020).
[3] D. Turenne, A. Yaroslavtsev, X. Wang V. Unikandanuni, I. Vaskivskyi, M. Schneider, E. Jal, G. Mercurio, R. Gort, N. Agarwal, B. V. Kuiken L. Mercadier, J. Schlappa, l. le Guyader, N. Gerasimova, M. Teichmann, D. Lomidze, A. Castoldi, D Potorochin, D. Mukkattukavil, J. Brock N. Z. Hagström, A. H. Reid, X. Shen, X. J. Wang, P. Maldonado, Y. Kvashnin, K. Carva, J. Wang, Y. K. Takahashi, E. E. Fullerton, S. Eisebitt P. M. Oppeneer, S. Molodtsov, A. Scherz, S. Bonetti, E. Iacocca, H. A. Dürr, *Science Advances* **8**, eabn0523 (2022).

Resonant inelastic x-ray scattering investigations of Excitons in and out of equilibrium

M. P. M. Dean
Brookhaven National Laboratory, Upton, NY 11973, USA

Excitons are quasiparticles that emerge when a valence electron is promoted in energy to the conduction states, leaving behind a hole that interacts with the electron. Many aspects of exciton physics in traditional insulators are well understood. However, in correlated quantum materials, the situation becomes richer and more complex due to the emergence of many-body excitons, which involve strong electron-electron and electron-spin interactions. In this talk I will explain the technique of resonant inelastic x-ray scattering [1], which we have recently been applying to several aspects of exciton physics. The first part of the talk will address $NiPS_3$, which has received intense interest since it hosts an excitonic quasiparticle whose properties appear to be intimately linked to the magnetic state of the lattice. Despite ex- tensive studies, the electronic character, mobility, and magnetic interactions of the exciton remain unresolved. Fig. 1 shows RIXS map measurements and calculations. We find that exciton formation is primarily a spin rearrangement of the Ni d^8 electrons and that on-site Ni inter-orbital exchange interactions are primarily responsible for the energy of formation of the exciton. This quasiparticle is therefore best thought of as Hund's exciton. Fig. 2 plots the momentum dependence of the Hund's exciton, which reveals that it propagates in a way that is analogous to the double-magnon excitation. .

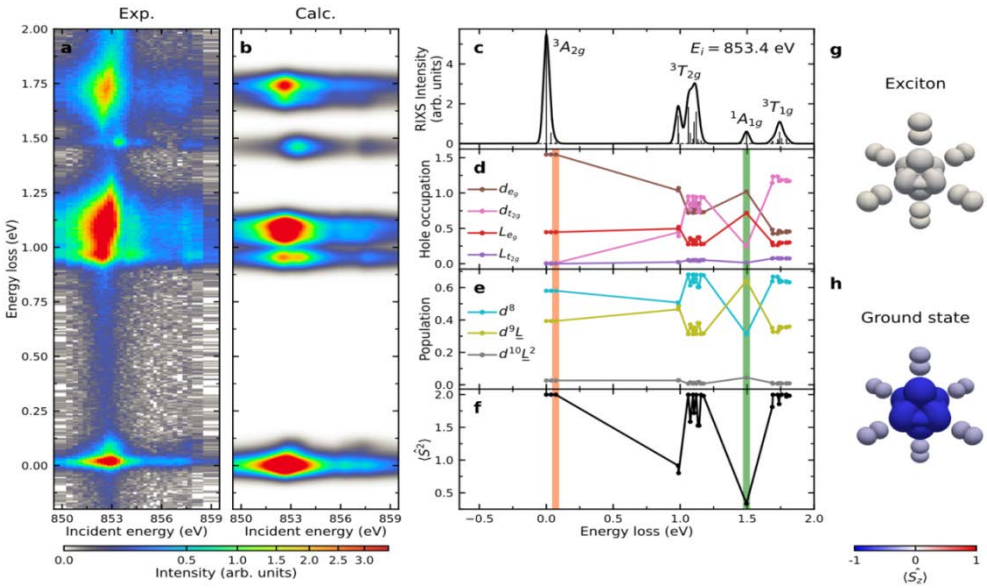

***Fig. 1. a**, **RIXS intensity map as a function of incident photon energy** through the Ni L_3 resonance. The exciton is visible at an energy loss of 1.47 e. **b**, RIXS calculations for $NiPS_3$ that capture the energy and resonant profile of the dd-transitions and exciton in the material. **c**, Calculated unbroadened RIXS intensity (**vertical lines**) and broadened RIXS spectra (**solid curve**) at the main resonant incident energy of the exciton peak. **d–f**, Description of the ground and excited states in $NiPS_3$. **d** shows the hole occupations of Ni 3d (**denoted by d**) and ligand (**denoted by L**) orbitals. **e** displays probabilities of having d^8, $d^9\underline{L}$, and $d^{10}\underline{L}^2$ configurations. **f** gives the expectation value of the total spin operator squared $\langle \hat{S}^2 \rangle$. The **orange (green) vertical** lines in **d–f** indicate the energy for the double-magnons (excitons). **g**, **h**, Wavefunction illustrations extracted from **b** for **g** the exciton and **h** the ground state. The size of each orbital (3d for the central Ni site and 3p for the six neighboring S sites) is proportional to its hole occupation. The color represents the expectation value of the spin operator along the z axis $\langle \hat{S}^2 \rangle$, again calculated separately for the Ni and S states. Therefore, the change in spin state and the partial transfer of holes involved in the exciton transition is encoded in the change in color and size of orbitals, respectively. We represent the ground state by only the down-spin configuration, omitting the up-spinand spin-zero elements of the triplet.*

We trace this unique behavior to fundamental similarities between the $NiPS_3$ exciton hopping and spin exchange processes, underlining the unique magnetic characteristics of this novel quasiparticle [2].

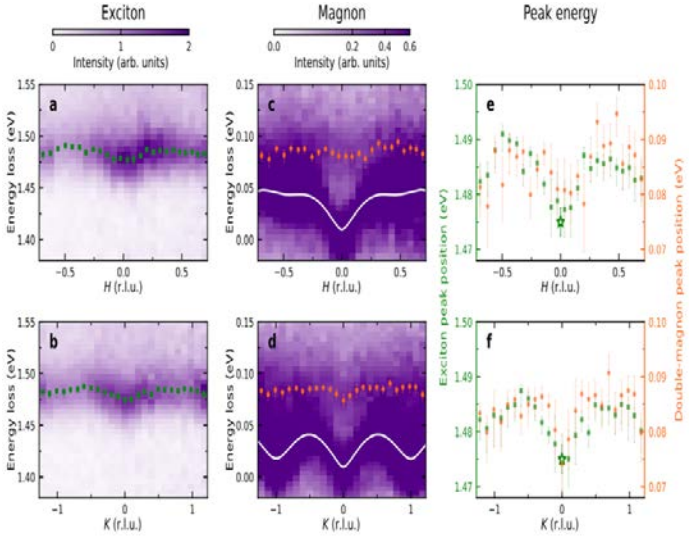

***Fig. 2. a. Exciton dispersion and comparison with double-magnons**. **a**, **b**, RIXS intensity maps as a function of the H and K in-plane momentum transfer, respectively, with an energy window chosen to isolate the exciton dispersion. The overlaid green squares mark the peak positions of the exciton. **c** and **d** show the low energy dispersion at equivalent momenta with the observed inelastic feature, including magnons (**white lines**) and double-magnons (**orange circles**). Panels **e** and **f**, show that both the exciton and double-magnon have similar dispersion with an energy offset of ~ 1.4 eV. The **asterisks** in panels e and f denote the reported exciton energy from previously reported optical measurements.*

In the latter part of the talk, I will discuss ultrafast pump-probe RIXS measurements of a charge-transfer exciton in cuprate $La_{2-x}Sr_xCuO_4$, which reveal a novel Floquet renormaliztion of the Cu-O hybridization.

References

[1] M. Mitrano, S. Johnston, Y.-J. Kim, M. P. M. Dean, (*to be published*) (2024).
[2] W. He, Y. Shen, K. Wohlfeld, J. Sears, J. Li, J. Pelliciari, M. Walicki, S. Johnston, E. Baldini, V. Bisogni, M. Mitrano, M. P. M. Dean, *Nature Communications* (in print) (2024).

* Work performed at Brookhaven National Laboratory was supported by the U.S. DOE, under the Contract No. DE-SC0012704.

On-chip testing of the transient metallization of dielectrics

P. Dombi
Wigner Research Centre for Physics, 1121 Budapest, Hungary

Control over the carrier-envelope phase (CEP) of laser pulses provides a powerful knob to steer interactions of laser light with matter in the strong-field regime, as evidenced by numerous studies of electric-field-controlled ultrafast electron dynamics in atomic, molecular and solid-state media. In the future, CEP-controlled few-cycle laser pulses could be the carrier of digital information in petahertz technology. For example, petahertz multiplexing could be achieved by encoding information into CEP spatial maps. Moreover, characterizing and controlling CEP in space could enable the scaling up of attosecond experiments [1] and the investigation of the collective behavior of extensive systems [2]. In this paper, we present the development of a compact on-air optical chip that is capable of measuring 3D CEP maps of laser pulses without the need for a vacuum equipment. The operation of the device is based on the transient metallization of dielectrics [3] induced by a few-cycle laser pulse of sufficient intensity. The probe detects CEP using ultrafast current generation in dielectrics [3]. Using a spatial light modulator, we could also sculpt CEP distributions and implement a mechanism that enables a feedback loop for CEP sculpting [4]. The ability to sculpt CEP in 3D will enable CEP control of light-phase-sensitive systems of sizes comparable to that of a laser beam. Remarkably, our device can operate using a fraction of the full pulse energy of an off-the-shelf few-cycle Ti:sapphire oscillator, as low as 1 nJ. The spatial CEP distribution of few-cycle laser beams is neither uniform nor trivial. Due to volume smearing effects, experiments exploring the CEP sensitivity of laser-matter interactions are usually limited to small systems with sizes that are far below the volume of the laser focal volume. With our probe we can localize volumes of uniform CEP and determine their size. Fig.1 shows an example of a measured CEP(x,y,z) distribution visualized as a colored cloud. We identified that it contains 18.4 μm^3 of uniform phase settled between 15° and 25° (the pink-colored volume). Fig.1 also provides a preview of the measurement setup.

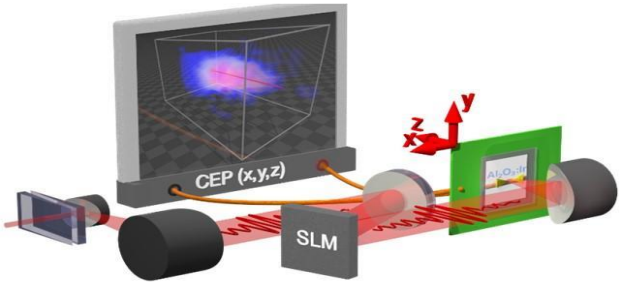

***Fig. 1. Sketch of the optical chip setup with a cloud** representing measured values of 3D CEP(x,y,z) distribution. **Pink, white** and **blue** color show positive, zero and negative CEP values respectively.*

In summary, we constructed an optical chip device to test the transient metallization of different dielectric and semiconductor media. We found a clear correlation between the bandgap and the generated current and the intensity dependence of the current enables us to draw conclusions about the current generation mechanism, as well. Our on-chip probe also allows to provide a 3D scan of the CEP of ultrashort laser pulses around the focus of the beam.

References

[1] H. Y. Kim, M. Garg, S. Mandal, L. Seiffert,T. Fennel, E. Goulielmakis, *Nature* **613**, 662 (2023).
[2] K. Jana, K. R. Herperger , F. Kong, Y. Mi , C. Zhang, P. B. Corkum, S. Sederberg, *Nature Photonics* **15**, 622 (2021).
[3] V. Hanus, V. Csajbók, Zs. Pápa, J. Budai, Zs. Márton, G. Zs. Kiss, P. Sándor, P. Paul, A. Szeghalmi, Z.Wang, B.Bergues, M. F. Kling, Gy. Molnár J. Volk, P. Dombi, *Optica* **8**, 570 (2021).
[4] V. Hanus, B. Fehér, V. Csajbók, P. Sándor, Zs. Pápa, J. Budai, Z. Wang, P.Paul, A.Szeghalmi, P.Dombi, *Nature Communications* **14**, 5068 (2023).
* Acknowledgements: Support from the National Office for Research, Development and Innovation of Hungary is gratefully acknowledged (Projects KKP137373 and TKP2021-NVA-04).

Ultrashort pulse propagation in suspensions

K. Pistsova[1], O. Fedotova[1], O. Khsanov[1], R. Rusetsky[1], T. Smirnova[2], A. Bugay[3], A. Kovačević [4]
[1] *Scientific- Practical Material Research Centre, 220072 Minsk Belarus*
[2] *Belarus State University, 220070 Minsk, Belarus*
[3] *Joint Institute for Nuclear Research, Dubna 141980, Russia*
[4] *Belgrade University, 11000 Belgrade, Serbia*

The problems of laser pulse deep penetration into biological tissues and suspensions are challenges because these media are turbid and laser radiation is subject to multiple scattering. Solution of these

problems allow to elaborate reliable techniques of deep tissue imaging and noninvasive diagnostics. The issues of laser pulse stable propagations in such media have not yet been resolved, but the first steps towards their solution have been undertaken [1, 2]. As is known, laser radiation acts on microparticles with a gradient force directed along the gradient of the field intensity and moving them into the high intensity area. As a result, they are concentrated along the optical axis of laser beam and provide nonlinear laser beam-suspension interaction. A rise in particle concentration in this region causes a nonlinear change in the bio-suspension's effective refractive index, which in turn creates an effective waveguide that allows laser light to self-channel inside it. Particle diffusion and optical pressure forces compete to bring about dynamic equilibrium. Furthermore, forward scattering force impact is another factor that provides self-trapping radiation in suspensions, as demonstrated in work [1]. The findings of our research on laser beam propagation in suspensions containing red blood cells, in particular, are shown below. The bioparticles have diameters significantly bigger than the wavelength of the radiation. Theoretical analysis of possible scenarios of laser beam propagation in bio-suspension reduces to solution of self-consistent equation system, namely modified nonlinear Schrödinger equation taking into account the concentration nonlinearity of the medium and possible dissipation of radiation due to scattering and absorption, as well as the convection-diffusion equation. In the last equation we consider the movement of microparticles under the combined action of the gradient force of light pressure associated with polarizability and the forward scattering force. To ensure correctness of analysis, we consider the WKB approximation of light scattering. In order to solve the self-consistent equation system, we employed numerical methods, as well as a variational approach. The calculations assumed that the polarizability of particles can be a complex quantity due to absorption. It is shown that the optical nonlinearity of the suspension, caused by the movement of particles in a field of gradient forces, acts similar to Kerr nonlinearity, leading to self-focusing of radiation in the medium, if the input power of laser radiation is above the threshold value. Regarding the Kerr medium, the threshold power has an inverse relationship with the square of the particle size and a direct relationship with the square of the wavelength. In a steady state, when the effect of diffusion is offset by the action of gradient forces, soliton radiation propagation in a bio-suspension is achievable. The shape of the soliton is determined by the polarizability of the particles, the diffusion coefficient, the mobility and size of the particles, their concentration in the suspension and the effective refractive index of the medium.

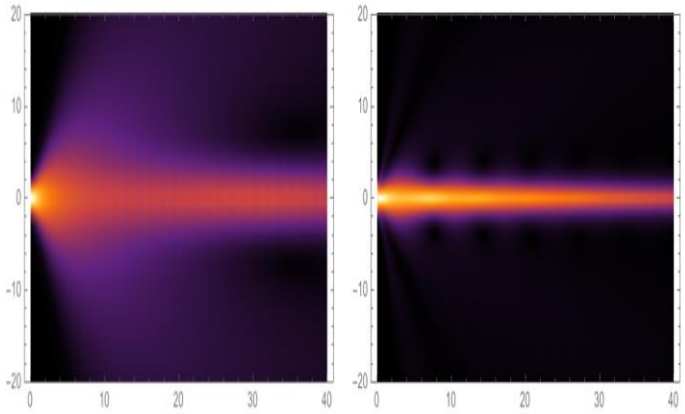

Fig. 1. Modeling of laser radiation propagation *bio-suspension in (x,z) plane at different initial field amplitudes :**Left**: initial field amplitude is less than threshold for self-channeling regime;*
***Right**: initial field amplitudes is more than threshold for self-channeling regime.*

The regimes of laser beam propagation in the bio-suspension with concentration nonlinearity are analyzed, taking into account the diffraction divergence of the beam, forward scattering, and dissipative losses. The possibility of deep penetration of laser radiation into a bio-suspension is substantiated if forward scattering compensates for the dissipative loss of radiation energy. Under conditions of complete compensation of losses due to beam amplification as a result of forward scattering of radiation, its self-channeling in the medium is achievable.

References

[1] A. Bezryadina, T.Hansson, R.Gautam, B.Wetzel, G.Siggins, A. Kalmbach, J.Lamstein, D.Gallardo, E.J. Carpenter, A.Ichimura, R. Morandotti Z. Chen *Physical Review Letters* **119**, 058101 (2017).
[2] R. Gautam, Y. Xiang, J. Lamstein, Y. Liang, A. Bezryadina, G.Liang, T.Hansson, B.Wetzel, D. Preece, A.White, M. Silverman, S.Kazarian, J. Xu R. Morandott, Z. Chen,. *Light: Science and applications* **8,** 31 (2019).

Advances in ultrafast optical parametric oscillators

M. Ebrahim-Zadeh
The Barcelona Institute of Science and Technology, 08860 Castelldefels, Spain

A novel approach for frequency comb generation based on bulk degenerate $\chi^{(2)}$ OPOs presented. Driven by a continuous-wave laser and using intracavity dispersion control, coherent broadband spectral output with corresponding to transform-limited femtosecond pulses in the time domain is obtained. Optical frequency combs have had a remarkable impact on photonics, paving the way for many new applications from frequency metrology and spectroscopy to remote sensing and astronomy. The established techniques for comb generation are based on the direct use of mode-locked femtosecond laser oscillators such as Ti:sapphire and fiber lasers [1,2], their combination with photonic fibers [3], or the use of $\chi^{(3)}$ Kerr microcavities pumped by mode-locked or continuous-wave (cw) lasers [4]. These approaches have resulted in tremendous advances in frequency combs, enabling remarkable progress in photonics. Nevertheless, it remains the case that these techniques rely on relatively complex and costly femtosecond lasers, or sophisticated fabrication methods for advanced microstructures. It would be desirable to explore potential alternative approaches to frequency comb generation offering reduced complexity and cost, increased flexibility, practical powers, and wider accessibility for continually evolving applications. Optical parametric oscillators (OPOs) based on bulk $\chi^{(2)}$ nonlinear materials are now widely established as flexible sources of tunable radiation across broad spectral regions from the UV to mid-IR. Using ultrafast femtosecond laser oscillators, in combination with synchronous pumping, femtosecond OPOs can provide broadband radiation in non-degenerate [5,6] or degenerate [7,8] operation, offering another approach to comb generation. However, the need for a mode-locked pump laser (to provide the input comb), together with synchronous pumping, similarly result in high complexity and cost. Broadband generation can also be achieved using cw OPOs in *singly resonant oscillator* (*SRO*) configuration by exploiting large parametric gain bandwidth [9] or cascaded $\chi^{(2)}$ nonlinearity [10]. However, both these techniques are strictly limited to specific phase-matching conditions and do not generally provide a coherent phase-locked output spectrum characteristic of a frequency comb. An alternative approach to optical frequency comb generation is active phase modulation based on $\chi^{(2)}$ cw OPOs in degenerate *doubly resonant oscillator* (*DRO*) configuration. This technique has been previously demonstrated in MgO:$LiNbO_3$ pumped at 532 nm, generating an output spectrum over a bandwidth of 20 nm (5.4 THz) centered at ~1064 nm [11]. In the time domain, operation of such a degenerate phase-modulated cw OPO corresponds to mode-locked output pulses, where using a degenerate cw OPO based on MgO:sPPLT pumped at 532 nm, we demonstrated the generation of ~500 ps output pulses [12]. In a recent report, we further theoretically investigated the process of spectral formation and pulse generation in degenerate cw OPO based on MgO:PPLN pumped at 532 nm subjected to intracavity phase modulation [13]. Using an intracavity electro-optic modulator synchronized to the free-spectral-range of the cavity, in combination with spectral filtering, we showed that a stable, uniform, and periodic train of picosecond pulses of <5 ps with FWHM spectral bandwidth of 0.4 THz could be generated (Fig. 1).

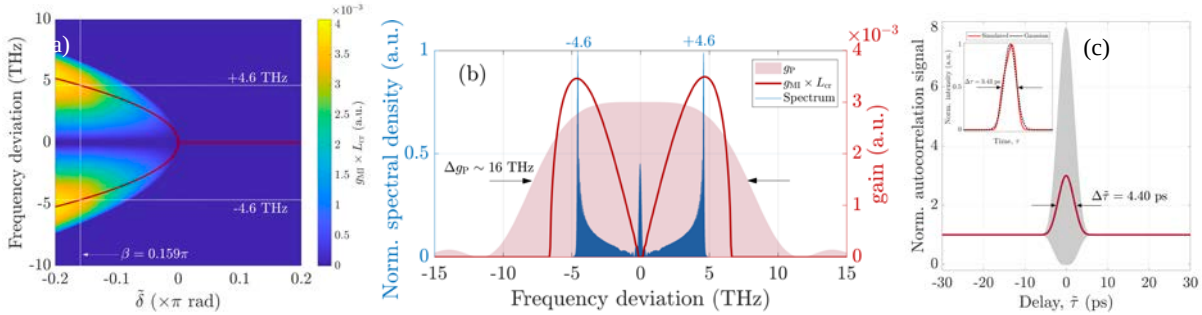

Fig. 1. (a) Modulation instability (MI) gain profile (g_{MI}). *The **red** curve corresponds to the spectral peak for net cavity detuning (**d**), while for positive detuning degeneracy is maintained, as shown by the single **red** line. The **red** curve is well-matched with the g_{MI} maxima. (**b**) Output spectrum and the corresponding parametric and MI gain profiles. The spectrum exhibiting two peaks at the position of g_{MI} maxima at $\pm$4.6 THz. (**c**) Normalized interferometric and intensity autocorrelations (grey and red curves, respectively). Inset: the last pulses (red solid) in the final round-trip with a Gaussian fit (black dashed) showing a pulse FWHM=3.43 ps.*

Our simulations confirmed that the intracavity phase modulator enables spectral broadening accompanied by uniform period pulse train formation at degeneracy. On the other hand, in the context of

frequency comb generation, the spectral and temporal coherence of phase-modulated cw OPOs are strictly limited due to the dispersion characteristics of the DRO configuration. In normal operation, cw DROs are over-constrained by the requirements of phase-matching ($k_p=k_s+k_i$), energy conservation ($\omega_p=\omega_s+\omega_i$), and simultaneous cavity resonance at both signal and idler frequencies ($m_s\omega_s=c/2n_sL$; $m_i\omega_i=c/2n_iL$, L is the optical cavity length). In conventional schemes widely deployed to date, cw DROs can only be reliably operated at a single (or very few) signal-idler frequency pairs nearest the peak of parametric gain [14]. This is an intrinsic property of DRO due to the *Vernier* effect arising from cavity dispersion. As such, the generation of broadband multi-axial-mode radiation is fundamentally precluded in cw DROs at any wavelength. To overcome this fundamental limitation and thus enable broadband generation from degenerate cw OPOs, a parameter of critical importance is thus the control of cavity dispersion. We previously demonstrated the generation of broadband radiation from a degenerate cw OPO based on MgO:sPPLT pumped at 532 nm [15]. By deploying chirped mirrors for dispersion compensation of the cavity, we generated broadband radiation over 34 nm (9 THz) about ~1064 nm, limited by unoptimized dispersion characteristics of the mirror coatings. Under this condition, we also observed signature of the frequency comb generation by recording the RF spectrum of the output spectrum under passive conditions. At the same time, we have also recently theoretically studied the feasibility of broadband frequency comb generation in degenerate cw OPOs using active phase modulation in combination with full dispersion control of the cavity [16]. Our simulations show that under this condition, it is possible to achieve coherent broadband phase-locked output spectrum characteristic of a frequency comb, with a temporal output corresponding to transform-limited femtosecond pulses, irrespective dispersion regime (normal or anomalous). Using a degenerate cw OPO based on MgO:PPLN pumped at 532 nm, in the presence of intracavity dispersion compensation, we confirm spectral generation with a FWHM bandwidth of $\Delta\nu \approx 6.9$ THz centred at 1064 nm, with stable pulses of duration as short as $\Delta\tau \approx 65$ fs in the normal dispersion regime, corresponding to a transform-limited time-bandwidth product of $\Delta\tau\Delta\nu \approx 0.45$, can be achieved (Fig. 2).

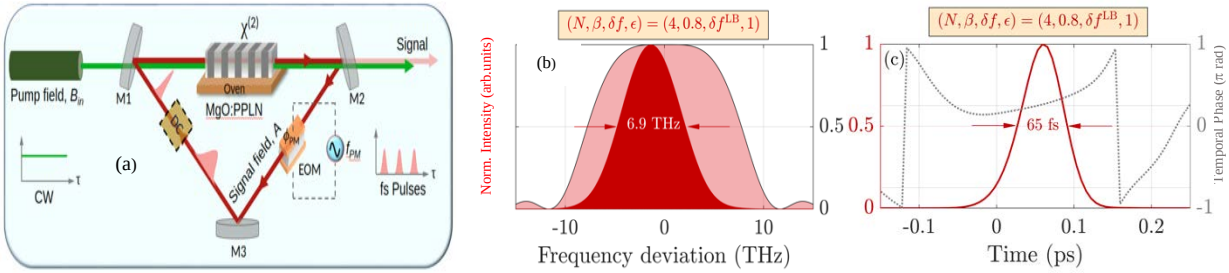

Fig. 2. (a) Generic design of the phase-locked degenerate cw OPO with intracavity dispersion control. *In the normal dispersion regime, optimum detuning together with dispersion compensation result in* ***(b)*** *spectral output with a FWHM bandwidth of 6.9 THz, and* ***(c)*** *transform-limited pulses of 65 fs duration with flat temporal phase.*

Our calculations point to the feasibility of generating coherent broadband frequency combs using bulk degenerated cw OPOs under optimum compensation of cavity dispersion. The approach could pave the way for the realization of a new class of coherent broadband femtosecond light sources in different spectral regions based on bulk $\chi^{(2)}$ OPOs driven by cw pump lasers.

References

[1] T. Udem, R. Holzwarth, T. W. Hänsch, *Nature* **416**, 233 (2002).
[2] S. A. Diddams, *Journal of Optical Society of America* B **17**, 51 (2010).
[3] S. A. Diddams, D. J. Jones, J. Ye, S. T. Cundiff, J. L. Hall, J. K. Ranka, R. S. Windeler, R. Holzwarth, T. Udem, T. W. Hänsch, *Physical Review Letters* **84**, 5102 (2000).
[4] P. Del'Haye, A. Schliesser, O. Arcizet, T. Wilken, R. Holzwarth, T. J. Kippenberg, *Nature* **450**, 1214 (2007).
[5] F. Adler, K. C. Cossel, M. J. Thorpe, I. Hartl, M. E. Fermann, J. Ye, *Optics Letters* **34**, 1330 (2009).
[6] S. Chaitanya Kumar, A. Esteban-Martin, T. Ideguchi, M. `Yan, S. Holzner, T. W. Hänsch, N. Picqué, M. Ebrahim-Zadeh, *Laser & Photonics Review* **8** L86 (2014).
[7] T. Wong, T. Plettner, K. L. Vodopyanov, K. Urbanek, M. Digonnet, R. L. Byer, *Optics Letters* **33**, 1896 (2008);
[8] V. R. Badarla, A. Esteban-Martin, M. Ebrahim-Zadeh, *Laser & Photonics Review* **7**, L55 (2013).
[9] R. Das, S. Chaitanya Kumar, G. K. Samanta, M. Ebrahim-Zadeh, *Optics Letters* **34**, 3836 (2009).
[10] V. Ulvila, C. R. Phillips, L. Halonen, M. Vainio, *Optics Letters* **38**, 4281 (2013).
[11] S. A. Diddams L. S. Ma, J. Ye, J. L. Hall, *Optics Letters* **24**, 1747 (1999).
[12] K. Devi, S. Chaitanya Kumar, M. Ebrahim-Zadeh, *Optics Express* **21**, 23365 (2013).
[13] A. D. Sanchez, S. Chaitanya Kumar, M. Ebrahim-Zadeh, *IEEE Journal of Selective Topics in Quantum Electronics* **29**, 1 (2023).
[14] R. C. Eckardt, C. D. Nabors, W. J. Kozlovsky, R. L. Byer, *Journal of Optical Society of America* B **8**, 646 (1991).
[15] K. Devi, S. Chaitanya Kumar, M. Ebrahim-Zadeh, *Advanced Solid-State Lasers*, JTu6A.2, Nagova, Japan (2017).
[16] A. D. Sanchez, S. Chaitanya Kumar, M. Ebrahim-Zadeh, *Physical Review Research* **6**, 013263 (2024).

Measuring ultrafast electron correlations with core X-ray photoemission and X-ray absorption spectroscopies

J. Freericks[1], O.Matveev[1], A. Shvaika[2], N. Sirica[3], S. Kwon[4], S.H. Park[4], A. Katoch[5]
[1]*Georgetown University, Washington, DC 20057, USA*
[2]*Institute for Condensed Matter Physics, 79011 Lviv, Ukraine*
[3]*U.S. Naval Research Laboratory, Washington, DC 20375 USA*
[4]*Pohang Accelerator Laboratory, Pohang 37673, Korea*
[5]*Yonsei University, Seoul 03722, Korea*

The relaxation dynamics of nonequilibrium electrons have been extensively studied via many different pump-probe spectroscopies. But the estimation of how far the excited system is from a thermal state is often indirect, especially at short times, usually requiring fits to thermal distribution functions to estimate effective temperatures. Here, we show how time-resolved x-ray photoemission spectroscopy and time-resolved x-ray absorption spectroscopy can be employed as ultrafast thermometers that measure the effective energy content in the electronic subsystem. The scheme uses a correlation between the integrated weights of the spectral peaks as a function of time, with the thermal correlation functions of the appropriate many-body states of electrons near the initial Fermi level. When the spectral peaks are well separated, these integrated weights serve as an ultrafast probe of the energy (and ultimately the effective temperature) of the excited electrons. With sufficiently short time resolution, one can go beyond thermometry, to directly probing electron correlation functions, which provide time-averaged dynamics of the electron correlations. Pump-probe experiments excite electrons out of equilibrium and then probe how they relax back to a steady state (which usually is back to an equilibrium state). This is a new frontier, which allows us to examine different relaxation mechanisms and, in some cases, to discover novel nonequilibrium phases that cannot be reached in equilibrium. When studying relaxation processes, it is critical to have a way to determine how close one is to equilibrium and what is the average energy as a function of time. The hot-electron model assumes that the electronic system rapidly thermalizes to an effective hot temperature, which then slowly relaxes with the phonon bath until it reaches its final equilibrium temperature [1]. The true relaxation process is more complex than that, but even in this simplified picture, it is important to be able to monitor how the energy content of the electrons changes on an ultrafast time scale. Yet there is no known thermometer that can be used to monitor this process on these ultrafast time scales. In earlier work, we showed how a combination of time-resolved photoelectron spectroscopy and Raman scattering could be employed to show how close a system is to thermal equilibrium [2]. This methodology does not allow us to easily monitor the energy content of the system at short times, because it also requires fitting with thermal distribution functions. Here, we show how such an ultrafast analysis can be performed with time-resolved core x-ray photoemission spectroscopy (tr-XPS) and time-resolved core x-ray absorption spectroscopy (tr-XAS) in strongly correlated quantum materials even if the system has not yet thermalized. The energy content is inferred from the effective energy of an equilibrium system that has the same integrated weights for the spectral peaks. In earlier thermometry work on x-ray probes, the strategy has been to focus on the shape of the spectral function and fit it with the appropriate convolution with a Fermi-Dirac distribution. But when one wants to work with shorter and shorter time scales, such an approach becomes difficult, because the short-time pulses distort the shape of the spectra due to the energy-time uncertainty relation [3.4], making such an analysis increasingly more difficult as the time-scale is decreased. Instead, when we have strongly correlated systems, the weights in the spectral peaks depend on correlation functions of the local electron density for conduction and localized electrons. Technically, the way to see why this should be the case is to think in terms of partial spectral moment sum rules. The integrated weight of the core-hole spectral function is equal to 1---but the partial weights, integrated under each of the separated peaks, is instead equal to correlation functions of electron densities of electrons that lie near the original Fermi level of the system. This observation takes a total sum rule, which cannot be used for thermometry, because it is independent of temperature, into partial sum rules that can be used for thermometry, because they depend on the correlation functions that are modified by the pump pulse. Similar arguments show that this approach will also work for XAS. This observation then allows us to correlate the integrated weight of different spectral peaks with the effective energy content of the system after the pump has been applied. Because the integrated weights are not subject to the energy-time uncertainty relation, they are much more robust for use at ultrafast time scales (although, even here, at some point peaks will be broadened so much so that we cannot separate them and determine the partial spectral weights). What is most remarkable about this approach is that it works on ultrafast time scales currently accessible to experiments on X-ray free-electron lasers. This approach provides a novel high-precision tool to monitor the energy content without requiring any fitting protocols (although it does require calibration). We want to be clear that when we use the general term thermometry, we do not imply that this means the system is in thermal equilibrium, or even can be described by a hot-electron model. Instead, it is just a shorthand way to describe how

we are measuring energy content via a mapping to an effective thermodynamic temperature by comparing the values of different correlation functions. Examples of how this works are shown in *Fig.1 and 2.*

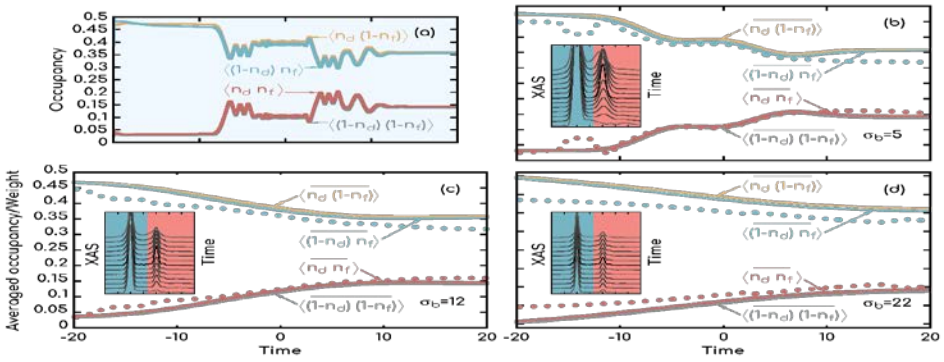

Fig. 1: XAS results for a Mott insulator.
Panel ***(a)****: time-dependent correlations of the four states with respect to presence or absence of d− or f −electrons on the site. Panels* ***(b)****,* ***(c)****,* ***(d)****: correlations averaged over the probe-pulse window* ***(solid lines)*** *for increasingly broader probe widths.*

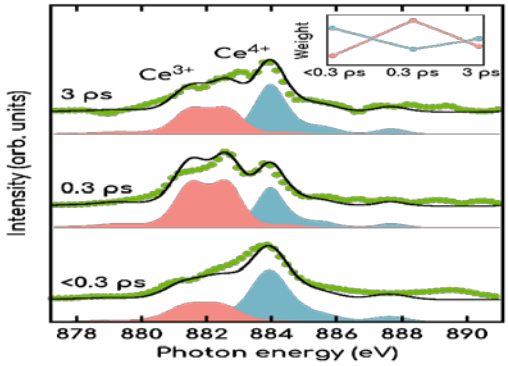

Fig. 2: Experimental data for CeO_2 *illustrating this behavior. In this system, the peaks do not fully separate, because the difference in the core-hole-electron interactions is not large enough to create a splitting. So, we need to fit the peaks to identify which charge state on the Ce ion corresponds to which spectral weight. By integrating these weights, as shown in the inset, we can see the ultrafast transfer of spectral weight corresponding to the change in the electron correlations mediated by the pump pulse. This shows that these correlation effects take place on the ultrafast time scales. Future experiments will hopefully show more details by performing probes more densely spaced in time.*

It is important to keep in mind that we are not assuming anything about thermal equilibrium, but instead are focused on learning about the nonequilibrium state during and after the pump is applied by using equilibrium values of measurements as a way to quantitatively summarize the nonequilibrium behavior.

References

[1] A. F. Kemper, O. Abdurazakov, J. K. Freericks, *Physical Review* X **8**, 041009 (2018).
[2] O. P. Matveev, A. M. Shvaika, T. P. Devereaux, J. K. Freericks, *Physical Review Letters* **122**, 247402 (2019).
[3] D. Randi, M. Fausti, M. Eckstein, *Physical Review* B **95**, 115132 (2017).
[4] M. Shvaika, O. P. Matveev, T. P. Devereaux, J. K. Freericks, *Condensed Matter Physics* **21**,33707 (2018).

Time-dependent scattering approach to non-equilibrium and Core-hole spectroscopies

A. E. Feiguin
[1]*Northeastern University, Boston, MA 02115, USA*

The conventional calculation of scattering cross sections relies on a treatment based on time-dependent perturbation theory that provides formulation in terms of Green's functions in the frequency domain. In equilibrium, it boils down to evaluating a simple spectral function equivalent to Fermi's golden rule, which can be solved efficiently by a number of numerical methods. However, away from equilibrium, the resulting expressions –similar to a Kramer-Heisenberg formula-- require a full knowledge of the excitation spectrum and eigenvectors to account for all the possible allowed transitions and intermediate states, a seemingly unsurmountable complication. Similar problems arise when the quantity of interest originates from higher order processes, such as in Auger, or resonant inelastic X-ray scattering (RIXS) spectroscopies. We have recently presented a new paradigm to overcome these hurdles[1-4] by formulating the problem in the time-domain, without relying on Green's functions: we explicitly introduce the scattering particles (neutron, electron, photon, positron) and simulate the full scattering event by solving the time-dependent Schrödinger equation. The spectrum is recovered by measuring the momentum and energy lost by the scattered particles, akin an actual energy-loss experiment. These ideas can be generalized to study photoemission beyond the sudden approximation, milti-photon processes, two-electron ARPES, and the interplay between radiative and non-radiative recombination channels in

X-ray spectroscopies, to mention a few examples.

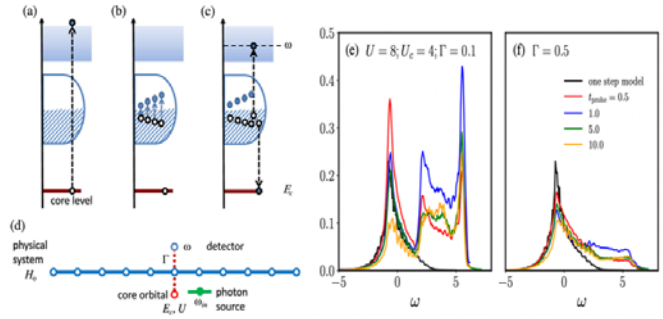

***Fig. 1. Left**: Schematic representation of the regimes involved in the core-hole creation and non-radiative Auger recombination: (**a**) core-hole creation; (**b**) transient regime in which the core hole is screened creating a polarizarion cloud; (**b**) an electron recombines with the core-hole while a second one is ejected into the continuum. (**d**) Geometry used in the calculations.*
***Right:** Comparison between perturbative results (**black curve**) and non-perturbative results obtained with our time-dependent scattering approach. The core-hole is created by a pulse of light; and different curves correspond to pulses of different duration.*

In addition, by not relying on perturbation theory, the results offer a window into higher-order contributions that are not accounted for by other formulations.

References
[1] K. Zawadzki, A. Nocera, A. E. Feiguin, *SciPost Physics*. **15**, 166 (2023).
[2] K. Zawadzki, L. Yang, A. E. Feiguin, *Physical Review* B **102**, 235141 92020).
[3] K. Zawadzki, A. E. Feiguin, *Physical Review* B **100**, 195124 (2019).
[4] A. Nocera, A. E. Feiguin, *European Physical Journal Plus* **138**, 1106 (2024).

* Acknowledgment: this Project is supported by the U.S. Department of Energy, Office of Basic Energy Sciences, under grant DE-SC0014407.

Ultrafast hidden spin polarization dynamics of bright and dark Excitons in 2H-WSe_2

M. Fanciulli[1,], D. Bresteau[1], J. Gaudin[2], S. Dong[3], R. Géneaux[1], T. Ruchon[1], O. Tcherbakoff[1]
J. Minár[4], O. Heckmann[1,], M. C. Richter[1], K. Hricovini[1], S. Beaulieu[2]
[1] *Université Paris-Saclay, 91191 Gif-sur-Yvette, France*
[2] *Université de Bordeaux, 33405 Talence, France*
[3] *Beijing National Laboratory for Condensed Matter Physics, 100190 Beijing, China*
[4] *University of West Bohemia, 30100 Plzen, Czech Republic*

Combining a high harmonic generation extreme ultraviolet (XUV) beamline [1] with a hemispherical analyzer equipped with a spin polarimeter, we performed *spin-*, *time-* and *angle-resolved* photoemission spectroscopy (STAR-PES) of excitons prepared by photoexcitation of inversion-symmetric 2H-WSe_2 with circularly polarized light. The very short probing depth of XUV photoemission permits selective measurement of photoelectrons originating from the top-most WSe_2 layer (Fig. 1), allowing for direct measurement of hidden spin polarization of bright and momentum-forbidden dark excitons.

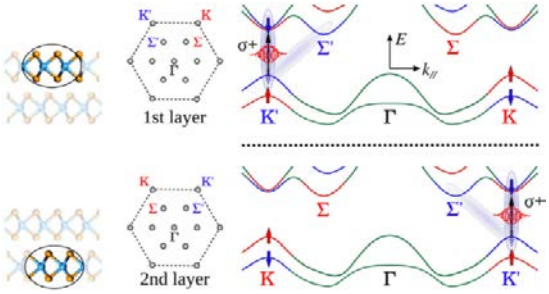

***Fig. 1. Schematic of crystal structure, associated Brillouinzone, and band structure for two adjacent layers in 2H-WSe2.** Valley-dependent chiroptical selection rules within each layer are visualized by a black arrow, bright and dark excitons are represented as **shaded** areas, and the spin-orbit texture is shown with **red** and **blue** color code.*

Our results [2] reveal efficient chiroptical control of bright excitons' hidden spin polarization. Following optical photoexcitation, intervalley scattering between nonequivalent K-K' valleys leads to a decay of bright excitons' hidden spin polarization. Conversely, the ultrafast formation of momentum-forbidden dark excitons acts as a local spin polarization reservoir, which could be used for spin injection in van der Waals heterostructures involving multilayer transition metal dichalcogenides.

References
[1] D.Bresteau, C. Spezzani, O. Tcherbakoff, J.-F. Hergott, F. Lepetit, P. D'Oliveira, P. Salières, R. Géneaux, M. Luttmann, I. Vadillo-Torre J. Lenfant, S. J. Weber, M. Dehlinger, E. Meltchakov, F. Delmotte, C. Bourassin-Bouchet, J. Im, Z. Chen, J. Caillaux, J. Zhang, M. Marsi L.Barreau, L. Poisson, D. Dowek, M. Fanciulli, O. Heckmann, M. C.Richter, K. Hricovini, M. Sebdaoui, D. Dennetiere, F. Polack, T. Ruchon, *European Physical Journal Special Topics* **1** (2023).
[2] M.Fanciulli, D . Bresteau, J. Gaudin, S. Dong, R. Géneaux, T. Ruchon, O. Tcherbakoff, J. Minár, O. Heckmann, M. C. Richter, K. Hricovini S. Beaulieu, *Physical Review Letters* **131**, 066402 (2023).

* Acknowledgements: French ANR No. 11-EQPX0005-ATTOLAB and No. 11-EQPX0034-PATRIMEX

What is the role of disorder in the nonequilibrium dynamics of Correlated quantum systems?

H.F. Fotso
University at Buffalo SUNY, Buffalo. NY 14260

The interplay of interaction and disorder gives rise in equilibrium to a vast array of intriguing properties and has thus rightfully received a great deal of attention. Away from equilibrium however, the transient dynamics of many-particle correlated systems that feature both interaction and disorder is rather challenging. To enable the investigation of the nonequilibrium dynamics of interacting systems in the presence of disorder, we recently introduced the nonequilibrium DMFT+CPA method [1]. An embedding scheme that combines the nonequilibrium extensions of both the dynamical mean field theory (DMFT) [2,3] and the coherent potential approximation (CPA) [4,5]. This framework opens up the possibility for detailed exploration of the effects of disorder on the dynamics away from equilibrium of correlated quantum systems with connections to various fundamental questions and practical applications. The approach was previously benchmarked on the equilibrium solution of the Anderson-Hubbard model describing itinerant electrons with local electron-electron interaction as well as a site dependent random on-site energy. The analysis reveals among other features the disorder-induced insulator-to-metallic phase transition that occurs when the Mott gap due to strong interaction is filled when the disorder strength is increased. In recent efforts, we have analyzed the effect of disorder on the nonequilibrium dynamics of this correlated system, described by the Anderson-Hubbard model, under an interaction quench. The system, initially in equilibrium at a given temperature, $T_{initial} = 1/\beta_{initial}$, has the interaction abruptly switched from zero to a finite value at a given time.

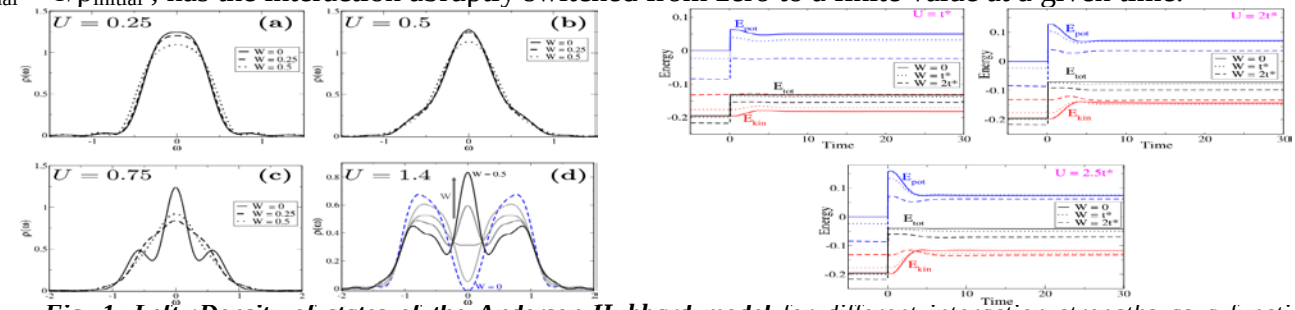

Fig. 1. Left :Density of states of the Anderson-Hubbard model *for different interaction strengths as a function of disorder strength, Observe on panel (**d**) the insulator to metal transition that occurs when the disorder strength is finite near the critical value of the interaction [1].* ***Right****: Relaxation of the kinetic, potential and total energy of the system across the interaction quench [7].*

To investigate the role of disorder on the nonequilibrium dynamics of a correlated many-particle system, we use our effective medium approach to calculate, through the nonequilibrium Green's functions, for different values of the final interaction and varying disorder strengths, different observables of the system as it evolves in time. We are also able to determine the effective steady state temperature after the quench and to analyze the effects of disorder on the thermalization for various interaction strengths. The analysis shows that disorder can tune the final temperature of the system across a broad range of values [6]. Very importantly this analysis also reveals that for a quench from a non-interacting system to a weakly interacting one, the steady state temperature is increased with increasing disorder strength whereas this trend is reversed for moderate final interaction strengths. Within our nonequilibrium DMFT+CPA framework, we consider various types of disorder and analyze the thermalization of the system under an interaction quench. Figure 1 shows the density of states of the Anderson-Hubbard model for different interaction strengths as a function of disorder strength, Observe on panel (d) the insulator to metal transition that occurs when the disorder strength is finite near the critical value of the interaction [1]. The figure also shows the relaxation of the kinetic, potential and total energy across an interaction quench for and interaction quench occurring at time $t = 0$ from $U_1 = 0$ to $U_2 = t^*$, $2t^*$, and $2.5t^*$ for different values of disorder. It shows that for for weak final interaction, the final kinetic energy following the nontrivial transient immediately after the quench is increased with increased disorder strength and that this trend is reversed when the final interaction is increased [7].

References

[1] E. Dohner, H. Terletska, K.-M. Tam, J. Moreno, H. F. Fotso, Physical Review B **106,** 195156 (2022).
[2] E. Dohner, H. Terletska, H. F. Fotso, *Physical Review* B **108**, 144202 (2023).
[3] J. K. Freericks, Physical Review B **77**, 075109 (2008).
[4] H. F. Fotso, J. K. Freericks, *Frontiers in Physics* **8**, 324 (2020).
[5] Y. Zhu, L. Liu, H. Guo, Physical Review B **88**, 205415 (2013).
[6] A. V. Kalitsov, M. G. Chshiev, J. P. Velev, Physical Review B **85**, 235111 (2012).
[7] E. Dohner, K.-M. Tam, H. Terletska, H. F. Fotso, *(to be submitted)*.

* Acknowledgment: we acknowledge support from the Department of Energy under grant number DE-SC0024139.

Quenched lattice fluctuations in optically driven $SrTiO_3$

M. Fechner[1], M. Först[1], G. Orenstein[2], V. Krapivin[2], A.S. Disa[3], M. Buzzi[1], A.von Hoegen[1], G. de la Pena Munoz[2]
Q. L Nguyen[2], R. Mankowsky[2], M. Sander[4], H. Lemke[4], Y. Deng[4], M. Trigo[2] A. Cavalleri[5]
[1]*Max Planck Institute for the Structure and Dynamics of Matter, 22761 Hamburg, Germany*
[2] *SLAC National Accelerator Laboratory, Menlo Park, CA94025, USA*
[3]*Cornell University, Ithaca, NY14853, USA*
[4]*Paul Scherrer Institut, 5232 Villigen, Switzerland*
[5] *University of Oxford, Oxford OX1 3PU, United Kingdom*

Crystal lattice fluctuations, which are known to influence phase transitions of quantum materials in equilibrium, are also expected to determine the dynamics of light-induced phase changes. However, they have only rarely been explored in these dynamical settings. Here, we study the time evolution of lattice fluctuations in the quantum paraelectric SrTiO3, in which mid-infrared drives have been shown to induce a metastable ferroelectric state. Crucial in these physics is the competition between polar instabilities and antiferrodistortive rotations, which in equilibrium frustrate the formation of long-range ferroelectricity. We make use of high intensity mid-infrared optical pulses to resonantly drive the Ti-O stretching mode at 17 THz, and we measure the resulting change in lattice fluctuations using time-resolved x-ray diffuse scattering at a free electron laser. After a prompt increase, we observe a long-lived quench in R-point antiferrodistortive lattice fluctuations. Their enhancement and reduction are explained theoretically by considering fourth-order nonlinear phononic interactions to the driven optical phonon and third-order coupling to lattice strain, respectively.

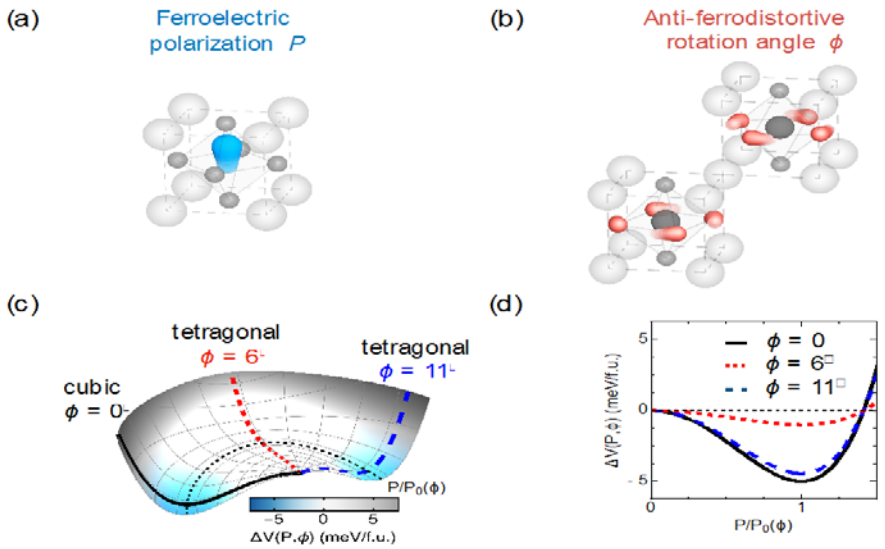

Fig. 1. The fundamental distortions of $SrTiO_3$. ***(a)*** *The polar distortion, creating the symmetry-broken ferroelectric state with polarization , involves the displacement of the center Ti atom along the c-axis;*
(b) *The antiferrodistortive distortion involves the rotation of the oxygen octahedra around the c axis by an angle ϕ, with a (½ ½ ½) wave vector;*
(c) *Illustration of the change in potential energy $\Delta V(P,\phi) = V_{TOT}(P,\phi) - V_{TOT}(0,\phi)$ along the ferroelectric coordinate P for a range of antiferrodistortive rotation angles ϕ , with $V_{TOT}(P,\phi)$ being the DFT total energy, which is not the same for all the ϕ-dependent $P = 0$ states. As $\Delta V(P,\phi)$ measures the difference between two states, it is zero for all angles at the origin with $P = 0$ although the structures are different. Starting from $\phi = 0°$, the depth of the potential energy ΔV along P reduces with the onset of antiferrodistortive rotations. At $\phi = 6°$, the rotation angle of the equilibrium tetragonal state, the gain in potential energy $\Delta V(P_0, 6°)$ is reduced by a factor of five compared to $\Delta V(P_0, 0°)$. Rotations beyond this angle revive the deeper instability of the ferroelectric state.*
(d)*Selected cuts of potential energy $\Delta V(P,\phi)$ along the ferroelectric coordinate P for selected rotation angles ϕ. Fig.1 adapted from Ref. [1]*

These observations provide a number of testable hypotheses for the physics of light-induced ferroelectricity.

References

[1] M. Fechner, M. Först, G. Orenstein, V. Krapivin, A.S.Disa, M. Buzzi, A. von Hoegen, G. de la Pena, Q.L. Nguyen, R .Mankowsky, M. Sander H. Lemke, Y. Deng, M. Trigo, A. Cavalleri, *Nature Materials* **23**, 363 (2024).

Observation of Floquet-Bloch states in Dirac materials

N. Gedik
Massachusetts Institute of Technology, 02139 Cambridge, MA USA

Floquet engineering is a novel method of manipulating quantum phases of matter via periodic driving [1, 2]. It has successfully been utilized in different platforms ranging from photonic systems [3] to optical lattice of ultracold atoms [4, 5]. In solids, light can be used as the periodic drive via coherent light-matter interaction. This leads to hybridization of Bloch electrons with photons resulting in replica bands known as Floquet-Bloch states. In this talk, I will discuss direct observation of Floquet-Bloch states in topological insulators and graphene. I will first review the original discovery of Floquet-Bloch states in a topological insulator [6]. Since then, their manifestations have been seen in a number of other experiments [7-14]. By engineering the electronic band structure using Floquet-Bloch states, various exotic phase transitions have been predicted [15-22] to occur. To realize these phases, it is necessary to better understand the nature of Floquet-Bloch states in different materials. However, direct energy and momentum resolved observation of these states is still limited to only few material systems [6, 10, 14, 23, 24]. I will then report the recent direct observation of Floquet-Bloch states in monolayer epitaxial graphene which was the first proposed material platform [15] for Floquet engineering. By using time- and angle-resolved photoemission spectroscopy (trARPES) with mid-infrared (mid-IR) pump excitation, we detected replicas of the Dirac cone. Pump polarization dependence of these replica bands unequivocally shows that they originate from the scattering between Floquet-Bloch states and photon-dressed free-electron-like photoemission final states, called Volkov states. Beyond graphene, our method can potentially be used to directly observe Floquet-Bloch states in other systems paving the way for Floquet engineering in a wide range of quantum materials.

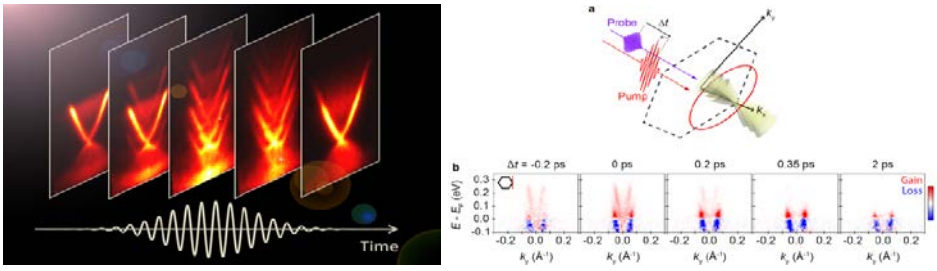

***Fig. 1**. **Left**: **Emergence and decay of Floquet-Bloch states** in Bi_2Se_3 [23]. **Right**: **a**- conceptual schematic of pump-probe experiments on graphene and the generation of replica bands. The **red** circle corresponds to the measurement window of our experiments. **b**- emergence and decay of a replica band in graphene via 5 μm pump excitation.*

Beyond graphene, our method can potentially be used to directly observe Floquet-Bloch states in other systems paving the way for Floquet engineering in a wide range of quantum materials.

References

[1] A. de la Torre, D. M. Kennes, M. Claassen, S. Gerber, J. W. McIver, M. A. Sentef, *Review of Modern Physics* **93**, 041002 (2021).
[2] C. Bao, P. Tang, D. Sun, S. Zhou, *Nature Review Physics* **4**, 33-48, (2022).
[3] M. C. Rechtsman, J. M. Zeuner, Y. Plotnik, Y. Lumer, D. Podolsky, F. Dreisow, S. Nolte, M. Segev, A. Szameit, *Nature* **496**, 196 (2013).
[4] G. Jotzu, M. Messer, R. Desbuquois, M. Lebrat, T. Uehlinger, D. Greif, T. Esslinger, *Nature* **515**, 237 (2014).
[5] A. Eckardt, *Review of Modern Physics* **89**, 011004, (2017).
[6] Y. H. Wang, H. Steinberg, P. Jarillo-Herrero, N. Gedik, *Science* **342**, 453 (2013).
[7] E. J. Sie, J. W. McIver, Y.-H. Lee, L. Fu, J. Kong and N. Gedik, *Nature Materials* **14**, 290 (2014).
[8] E. J. Sie, C. H. Lui, Y.-H. Lee, L. Fu, J. Kong, N. Gedik, *Science* **355**, 1066 (2017).
[9] J. W. McIver, B. Schulte, F.-U. Stein, T. Matsuyama, G. Jotzu, G. Meier, A. Cavalleri, *Nature Physics* **16**, 38 (2020).
[10] S. Aeschlimann, S. A. Sato, R. Krause, M. Chávez - Cervantes, U. De Giovannini, H. Hübener, S. Forti, C. Coletti, K. Hanff, K. Rossnagel A. Rubio, I. Gierz, *Nano Letters* **21**, 5028–5035, (2021).
[11] J. Kim, X. Hong, C. Jin, S.-F. Shi, C.-Y. S. Chang, M.-H. Chiu, L.-J. Li, F. Wang, *Science* **346**, 1205–1208, (2014).
[12] J.-Y. Shan, M. Ye, H. Chu, S. Lee, J.-G. Park, L. Balents, D. Hsieh, *Nature* **600**, 235–239, (2021).
[13] S. Park, W. Lee, S. Jang, Y.-B. Choi, J. Park, W. Jung, K. Watanabe, T. Taniguchi, G. Y. Cho, G.-H. Lee, *Nature* **603**, 421–426, (2022).
[14] S. Zhou, C. Bao, B. Fan, H. Zhou, Q. Gao, H. Zhong, T. Lin, H. Liu, P. Yu, P. Tang, S. Meng, W. Duan, S. Zhou, *Nature* **614**, 75–80, (2023).
[15] T. Oka, H. Aoki, *Physical Review B* **79**, 081406(R), (2009).
[16] N. H. Lindner, G. Refael, V. Galitski, *Nature Physics* **7**, 490 (2011).
[17] N. H. Lindner, D. L. Bergman, G. Refael, V. Galitski, *Physical Review B* **87**, 235131 (2013).
[18] R. Wang, B. Wang, R. Shen, L. Sheng, D. Y. Xing, *Europhysics Letters* **105**, 17004 (2014).
[19] J. H. Mentink, K. Balzer, M. Eckstein, *Nature Communications* **6**, 6708 (2015).
[20] S. Ebihara, K. Fukushima, T. Oka, *Physical Review B* **93**, 155107 (2016).
[21] C.-K. Chan, Y.-T. Oh, J. H. Han, P. A. Lee, *Physical Review B* **94**, 121106 (2016).
[22] H. H¨ubener, M. A. Sentef, U. De Giovannini, A. F. Kemper, A. Rubio, *Nature Communications* **8**, 13940 (2017).
[23] F. Mahmood, C.-K. Chan, Z. Alpichshev, D. Gardner, Y. Lee, P. A. Lee, N. Gedik, *Nature Physics* **12**, 306 (2016).
[24] S. Ito, M. Schüler, M. Meierhofer, S. Schlauderer, J. Freudenstein, J.Reimann, D. Afanasiev, K. A.Kokh, O. E.Tereshchenko, J. Güdde,M. A. Sentef U. Höfer, R. Huber, *Nature* **616**, 696 (2023).

* Acknowledgement(s) : The work at MIT was supported by the US Department of Energy, BES DMSE and Gordon and Betty Moore Foundation's EPiQS Initiative grant GBMF9459.

Ultrafast electron dynamics in 2D materials and heterostructures

I.Gierz
University of Regensburg, 93040 Regensburg, Germany

2D materials exhibit exotic electronic properties that differ from their bulk counterparts due to confinement and reduced screening. Since the discovery of graphene in 2004 a whole zoo of 2D materials has become available. 2D materials can be stacked as desired to form heterostructures. In this way, new artificial materials with customized properties can be created [1]. Despite the weak van der Waals coupling between the individual layers, hybridization effects usually occur, so that the electronic properties of the heterostructure clearly exceed those of the sum of the individual layers. Understanding and tailoring the non-equilibrium carrier dynamics of these ultimately thin high-tech materials is an essential step towards the design of future devices.In my talk I will introduce confinement heteroepitaxy [2] as a new approach for the large-scale production of van der Waals heterostructures with clean interfaces. As an example, I will discuss heterostructures consisting of graphene and 2D Sn, where the Sn layer can be either metallic or Mott insulating depending on its atomic structure [3,4]. We drive these heterostructures out-of-equilibrium with a visible pump pulse and trace the ultrafast carrier and band structure dynamics with time- and angle-resolved photoemission spectroscopy. We find that the dynamics of the graphene π-band sensitively depends on the properties of the 2D Sn layer. We tentatively interpret our results in terms of ultrafast charge transfer and transient changes in screening.

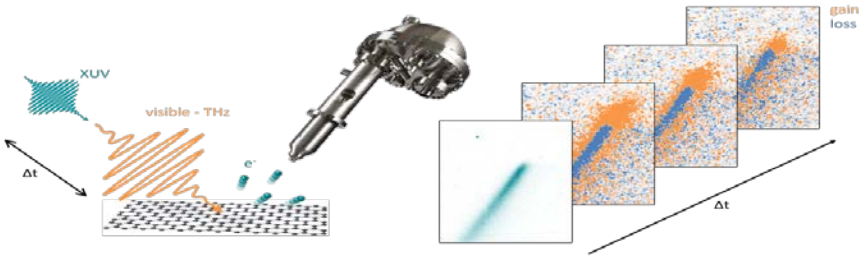

Fig. 1. Time- and angle-resolved photoemission spectroscopy *(trARPES) revealing the transient electronic properties of 2D solids and heterostructures.*

We find that the dynamics of the graphene π-band sensitively depends on the properties of the 2D Sn layer. We tentatively interpret our results in terms of ultrafast charge transfer and transient changes in screening.

References

[1] A. K. Geim, I. V. Grigorieva, *Nature* **499**, 419 (2013).
[2] N. Briggs, B. Bersch, Y. Wang, J. Jiang , R. J. Koch, N. Nayir, K. Wang , M. Kolmer, W.Ko , A. De La Fuente Duran, S. Subramanian, C. Dong J. Shallenberger, M. Fu, Q. Zou, Y.-W. Chuang, Z. Gai, A.-P. Li , A. Bostwick, C. Jozwiak, C.-Z. Chang, E. Rotenberg, J. Zhu, A. C. T. van Duin V.Crespi, J. A. Robinson, *Nature Materials* **19**, 637 (2020).
[3] H. Kim, O.Dugerjav, A.Lkhagvasuren, J.M. Seo, *Journal of Physics D: Applied Physics* **49**, 135307 (2016).
[4] S. Glass, G. Li, F. Adler, J.Aulbach, A. Fleszar, R Thimale, W Hanke, R Claessen, J Schafer, *Physical Review Letters* **114**, 247602 (2015).

Toward multimodal momentum-microscopy studies of novel materials and Interfaces - time, spin, and depth resolution

A. X. Gray
Temple University, Philadelphia, PA 19122, USA

Rational design and efficient ultrafast control of new electronic, magnetic, and topological phases of matter in quantum-material systems are considered to be one of the most promising avenues toward realizing new generations of energy-efficient spintronic devices. Material platforms based on two-dimensional van der Waals crystals are particularly appealing from this perspective because they are both incredibly versatile and sensitive to ultrafast external stimuli.However, a key requirement for the realization of viable devices based on such materials is a clear understanding of the layer-resolved electronic and magnetic structure, which can vary dramatically as a function of depth and proximity to other materials. Equally important, for topologically nontrivial two-dimensional materials, is the ability to resolve the spin and orbital characters of the bands as well as the local Berry curvature. This resolution is crucial for forming a complete picture of the interactions responsible for new physical phenomena and functionalities. Recent theoretical [1,2] and experimental [3] demonstrations of probing local Berry curvature in 2D materials using a combination of spin-resolved ARPES and circular dichroism open up new avenues for ultrafast spectroscopic detection of transient topological states. In this talk, I will discuss our recent proof-of-principle experiments demonstrating momentum-resolved

mapping of the local Berry curvature in strongly-correlated van der Waals ferromagnets using momentum microscopy combined with magnetic circular dichroism and spin resolution (Fig, 1a). I will also talk about our recent standing-wave studies demonstrating the capability to extract depth-resolved electronic structural information from single monolayers of transition-metal dichalcogenides and their heterostructures (Fig.1b).

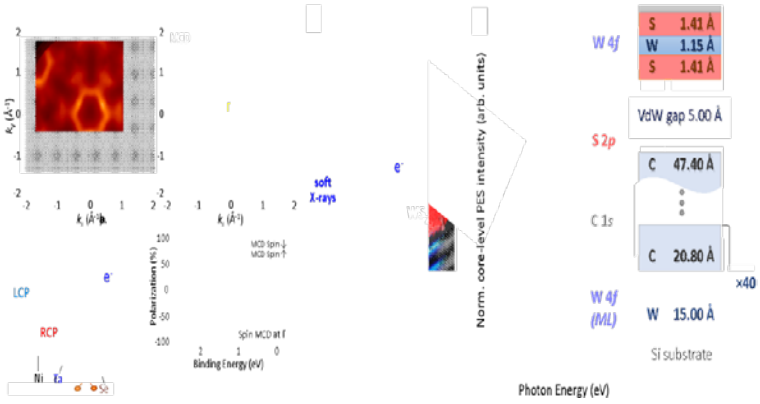

Fig. 1. a. Schematics of the local Berry curvature mapping technique *and the polarization-dependent momentum microscopy images of the Fermi surface (**left**) and magnetic circular dichroism (MCD) (**right**). Bottom right plot shows a combination of MCD and spin resolution, which isolates the Berry curvature, revealing a 'hidden' MCD signal;* ***b.Standing-wave photoemission microscopy measurement*** *of a WS_2 monolayer with the standing-wave modulations of the W, S, and C core-level peaks containing depth-resolved information about the chemical profile of the monolayer.*

These insights are essential for harnessing the unique capabilities of two-dimensional van der Waals crystals in real-world applications, such as ultrafast electronic and spintronic devices, where the ability to manipulate and control these properties rapidly and precisely is key to their functionality and efficiency.

References
[1] M. Schüler, U. De Giovannini, H. Hübener, A. Rubio, M. A. Sentef, and Philipp Werner, *Science Advances* **6**, eaay2730 (2020).
[2] M. Schüler, U. De Giovannini, H. Hübener, A. Rubio, M. A. Sentef, T. P. Devereaux, P. Werner, *Physical Review* X **10**, 041013 (2020).
[3] D. Di Sante, C. Bigi, P. Eck, S. Enzner, A. Consiglio, G. Pokharel, P. Carrara, P. Orgiani, V. Polewczyk, J. Fujii, P. D. C. King, I. Vobornik,G.Rossi I. Zeljkovic, S. D. Wilson, R.Thomale, G. Sangiovanni, G.Panaccione, F.Mazzola, *Nature Physics* **19**, 1135 (2023).
* Acknowledgements: A.X.G. acknowledges support from DOE, (grant DE-SC0024132).

Attosecond field emission

E.Goulielmakis
University of Rostock, 18059 Rostock, Germany

Field emission of electrons underlies great advances in science and technology, ranging from signal processing at ever higher frequencies to imaging of the atomic-scale structure of matter. The advancing of electron microscopy techniques to enable the complete visualization of matter on the native spatial (picometre) and temporal (attosecond) scales of electron dynamics calls for techniques that can confine and examine the field emission on sub-femtosecond time intervals. Here we introduce Homochromatic Attosecond Streaking (HAS) to characterize the temporal structure of the strong-field emission from metallic nanotips. In our approach an intense single cycle [1,2] laser pulse shone to a tungsten nanotip generates electron pulses by optical field emission, while its weak replica is used to probe the dynamics of the released electron pulses in real time (Fig. 1a). We record electron spectra as a function of the delay between the two pulses to compose a streaking spectrogram (Fig. 1b) whose reconstruction (Fig. 1c) allows the direct imaping of the emission dynamics.

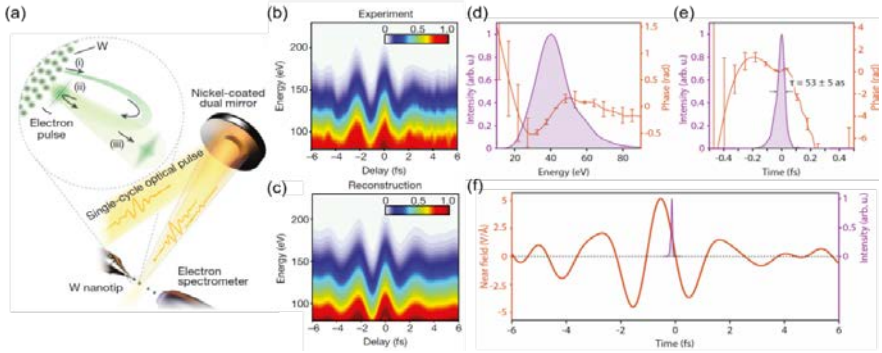

Fig. 1, Illustration of photoemission from a tungsten nanotip *under intense laser pulses (**a**). Measured (**b**) and reconstructed (**c**) streaking spectrogram of photoelectrons. Temporal structure of photoemission is revealed by reconstruction of the spectrogram, as shown in (**d** and **e**). (**f**) Near field and its timing with respect to the attosecond electron pulse.*

Access to the temporal properties of the electron pulses, including the duration $\tau = (53\ \text{as} \pm 5\ \text{as})$ and chirp, and the direct exploration of nanoscale near fields open new prospects for research and applications at the interface of attosecond physics and nano-optics [3].

References

[1] A. Wirth, M. Th. Hassan, I. Grguraš, J. Gagnon, A. Moulet, T. T. Luu, S. Pabst, R. Santra, Z. A. Alahmed, A.M. Azzeer, V.S.Yakovlev, V. Pervak ,F. Krausz, E. Goulielmakis, *Science* **334**, 195 (2011).

[2] M. Th. Hassan, T. T. Luu, A. Moulet , O. Raskazovskaya , P. Zhokhov, M. Garg, N. Karpowicz , A. M. Zheltikov, V. Pervak , F. Krausz E. Goulielmakis, *Nature* **530**, 66 (2016).

[3] H Y Kim, M Garg, S Mandal, L Seiffert, T Fennel, E. Gouleilmakis, *Nature* **613**, 662 (2023).

Metastable phases in photo-doped Mott insulators

D. Golež

Jozef Stefan Institute, 1000 Ljubljana, Slovenia

Chemically doped Mott insulators have long intrigued condensed matter physicists due to their display of intriguing phenomena, such as high-temperature superconductivity and metal-insulator transitions. Can photoexcitation across the charge gap induce similar phenomena and new (metastable) phases? We present a recent study on Ca_2RuO_4 under epitaxial strain, where optical spectroscopy and X-ray diffraction identified a transition into a metastable metallic phase. The driving force behind this nonthermal transition is a strong coupling between lattice and orbital orders, altered by photoexcitation, and the proximity of first-order phase transition. While the equilibrium Landau-Ginzburg landscape provides useful guidance, microscopic time-dependent Dynamical mean-field theory shows unconventional trajectories from equilibrium insulating to metastable metallic states due to strong electronic correlations, see Fig.1.

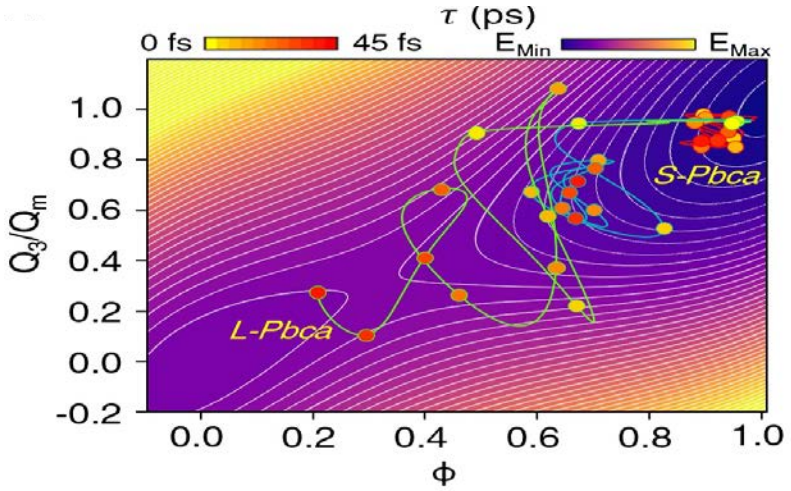

Fig. 1. *Dynamics of the microscopic trajectories for the lattice distortion Q_3 and the electronic order ϕ from different excitation strengths embedded in the equilibrium free-energy landscape. S-PBca marks the equilibrium insulating state and L-Pbca the metastable metallic state.*

In the second part, we demonstrate long-lived states in the paradigmatic Mott insulator NiO after above gap excitations, comparing time-resolved X-ray absorption spectroscopy with microscopic simulations based on Dynamical Mean-Field Theory-DMTF. The X-ray absorption signal reveals bandgap renormalisation on different orbitals due to photo-induced changes in screening. Furthermore, additional spectral features appear, and the comparison with the nonthermal extension of multiplet ligand field theory shows that these correspond to d-d excitation activated by photo-doped charge carriers. These works open perspective on how developing time-resolved experimental probes based on free-electron laser allows for a systematic analysis of photo-induced changes in Mott insulators and opens a perspective for a systematic search of metastable phase in Mott insulators in particular due to the interplay of strong electron-electron and electron-lattice coupling.

References

[1] A. Verma, D. Golež, O. Y. Gorobtsov, K. Kaj, R. Russell, J. Z Kaaret, E. Lamb, G. Khalsa, H. P Nair, Y. Sun, R. Bouck, N. Schreiber, J. P Ruf V, Ramaprasad, Y. Kubota, T. Togashi, V. A Stoica, H. Padmanabhan, J. W Freeland, N. A Benedek, O. G. Shpyrko, J. W Harter, R. D Averitt D. G Schlom, K. M Shen, A.J Millis, A. Singer, *Nature Physics*, 1 (2024).

[2] T. Lojewski, D. Golez, K. Ollefs, L. Le Guyader, L. Spieker, N. Rothenbach, R. Y. Engel, P. S. Miedema, M. Beye, G. S. Chiuzbaian, R. Carley R. Gort, B. E. Van Kuiken, G. Mercurio, J. Schlappa, A. Yaroslavtsev, A. Scherz, F.Doring, C. David, H. Wende, U. Bovensiepen, M. Eckstein P. Werner, A. Eschenlohr1, *arXiv:2305*.10145 (2023). Under referee report in *Physical Review Letters*.

* Acknowledgement(s) : Denis Golež acknowledge support of Slovenian Research Agency (from programs No. P1-0044 and No. J1-2455).

Quantum photonics with rare-earth materials

D. R. Pearson, Jr., P. Barya, A. Prabhu, J. D'Amelio, D. P. Shoemaker, E. A. Goldschmidt
University of Illinois Urbana-Champaign, Urbana, IL61801,USA

Optically active and highly coherent emitters in solids are a promising platform for a wide variety of quantum information applications, particularly quantum memory and other quantum networking tasks. Rare-earth emitters in solid-state hosts at cryogenic temperatures are particularly well-suited for quantum memory and similar operations due to their unique combination of properties that flow from the relative insensitivity of shielded rare-earth electronic states to the environment [1, 2]. This shielding leads to extremely long coherence times (which set the fundamental limit on quantum light storage) that can reach milliseconds on the optical transitions and hours on the spin transitions. Rare-earth emitters are also not restricted to a particular host material, or even to a particular class of host materials. The best properties are typically found when the rare-earth species is a substitutional dopant in an optically transparent crystalline material, but this encompasses an enormous range of possibilities. This flexibility is useful as a knob to tune the properties of the emitters and to enable integration in larger photonic devices and systems. Finally, rare-earth emitters retain their atom-like properties up to extremely high densities and small separations, far beyond other atoms or solid-state emitters. This "frozen gas" state where we can consider local electronic excitations at individual emitters interacting with externally applied electromagnetic fields continues to inter-emitter spacings well below 1 nm [3]. This feature enables both extremely high optical densities to aid in efficient quantum light storage and opens the potential for blockade-type interactions between coherent and controllable emitters for deterministic entangling gates. We will discuss two different emerging materials systems for rare-earth based quantum optics that take advantage of the flexibility of these emitters to target application-specific functionalities. First, I will show progress in our efforts to identify and grow new materials with rare-earth atoms at stoichiometric concentrations in order to reduce disorder-induced inhomogeneous broadening and increase spectral density to extreme levels [4]. This includes measures of the inhomogeneous linewidth of several promising materials as well as initial characterization of their coherence properties.

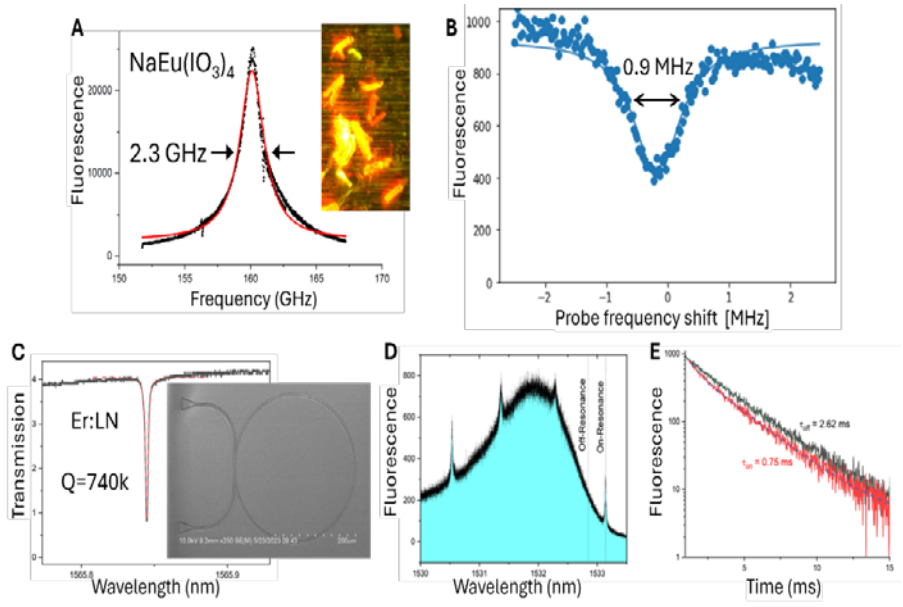

Fig. 1. A. Photoluminescence excitation (PLE) spectrum and optical image of in-house grown stoichiometric material *$NaEu(IO_3)_4$ showing an inhomogeneous linewidth below 3 GHz.* ***B.*** *Spectral hole burned in $NaEu(IO_3)_4$ and probed by PLE showing a sub-MHz width.* ***C.*** *Resonance spectrum and SEM image of a ring resonator fabricated in thin-film lithium niobate doped with erbium atoms showing a quality factor approaching 10^6.* ***D.*** *PLE across the erbium absorption line with cavity peaks visible.* ***E.*** *Lifetime of erbium dopants is shortened on thecavity resonance with a Purcell factor of 3.5.*

I will also show recent results on integration of rare-earth emitters in nanofabricated photonic devices for on-chip quantum light storage [5, 6]. This includes demonstrating Purcell enhanced emission from erbium dopants coupled to a ring resonator.

References

[1] N. Kunkel, P. Goldner, *Zeitschrift für anorganische und allgemeine Chemie* **644**, 66 (2018).
[2] T. Zhong, P. Goldner, *Nanophotonics* **8**, 2003 (2019).
[3] R. L. Ahlefeldt, M. R. Hush, M. J. Sellars, *Physical Review Letters* **117**, 250504 (2016).
[4] Z. W. Riedel, D. R. Pearson, M. H. Karigerasi, J. A. Soares, E. A. Goldschmidt, D. P. Shoemaker, *Journal of Luminescence* **249**, 119006 (2022).
[5] S. Dutta, E. A. Goldschmidt, S. Barik, U. Saha, E. Waks, *Nano letters* **20**, 741 (2019).
[6] S. Dutta, Y. Zhao, U. Saha, D. Farfurnik, E. A. Goldschmidt, E. Waks, *ACS Photonics* **10**, 1104 (2023).

Ultrafast spectroscopic studies of topological quantum matter

M. Z. Hasan, I. Belopolski, B. Kim, S.-Y. Xu, M. Neupane, T. A. Cochrane
Princeton University, Princeton, NJ 08544, USA

Over the last decade, ultrafast techniques have been crucial to gain fundamental insights into the topological properties of quantum materials. We employed ultrafast time- resolved angle-resolved photoemission spectroscopy to probe and elucidate surface electronic structure and electron dynamics of Z_2 topological insulators, Dirac-Weyl semimetals, knotted quantum matter and exotic spin-orbit superconductors [1, 2, 3]. In this talk, I plan to present a few recent examples where ultrafast techniques have been crucial to discover the topological behavior: *Weyl conductors and Chern physics*: (1) It was long been speculated that $Mo_xW_{1-x}Te_2$ materials may realize Lorentz violating topological Weyl fermions. In order to explore its topology, we first showed theoretically that it is crucial to access the full electron dynamics to reveal a non-Lorentz electronic Weyl state in $Mo_xW_{1-x}Te_2$. Then, we experimentally explored $Mo_xW_{1-x}Te_2$ materials by a suite of pump-probe time-resolved ARPES techniques. By comparing our pump-probe results with *ab initio* simulations, we concluded that the materials indeed features topological states associated with non-trivial Berry curvature field which is the generator of the non-Lorentz Weyl topology and non-trivial Chern quantized numbers [4].
(2) In candidate topological semimetal class TaIr(Te/Se)$_4$, the Weyl points and Fermi arcs live entirely above the chemical potential level, making them inaccessible to conventional ARPES. We utilized ultrafast ARPES to directly access the electronic states above the Fermi level in $TaIrTe_4$. We observe signatures of Berry curvature singularity nodes and correspondingly coupled spin textured Fermi arcs states. A full map reveals, for the first time, that $TaIrTe_4$ is a topological metal (doped semimetal) with the minimum number of four Weyl nodes allowed by time-reversal symmetry [3].
Intrinsic Topological Insulators: The third example would be on the possibility of novel phenomena induced by light. Here, we used pump-probe photoemission spectroscopy to explore the optically excited Dirac surface states in the bulk-insulating topological insulator Bi_2Te_2Se. Our results revealed optical and ultrafast properties that are in sharp contrast to those of bulk- metallic (self-doped) topological insulators. We observed a gigantic optical lifetime exceeding 4 μs (1 μs=10^{-6} s) for the surface states in Bi_2Te_2Se, whereas the lifetime in most topological insulators, such as Bi_2Se_3, has been limited to a few picoseconds (1 ps=10^{-12} s). Moreover, we discovered a surface photovoltage, a shift of the chemical potential of the topological surface states, as large as 100 mV. Our results demonstrate a rare quantum platform to explore charge excitation and relaxation in energy and momentum space in two-dimensional systems [5]. Finally, (time permitting) I will talk about electronic structure and relaxation dynamics in a superconducting topological material. Topological superconductors host new states of quantum matter which show a pairing gap in the bulk and gapless surface states providing a platform to realize Majorana zero modes. Recently, alkaline-earth metal Sr intercalated Bi_2Se_3 has been reported to show superconductivity with a T_c ~ 3 K and a large shielding fraction. We report systematic electronic structure studies of $Sr_{0.06}Bi_2Se_3$ (T_c ~ 2.5 K). Using ARPES, we observed a quantum well confined two-dimensional state coexisting with a topological surface state in $Sr_{0.06}Bi_2Se_3$. Furthermore, our time-resolved ultrafast ARPES reveals the relaxation dynamics showing different decay mechanism between the excited topological surface states and the two-dimensional states. Our experimental observation is understood by considering the intra-band scattering for topological surface states and an additional electron phonon scattering for the 2D states, which is likely responsible for the superconductivity and topological phenomena [6-8]. These ultrafast studies and their future extensions (that we plan to carry out) will be helpful in understanding low temperature superconducting states realized in these topological materials [8].

References

[1] M. Z. Hasan, C. L. Kane, *Review of Modern Physics* **82**, 3045 (2010).
[2] D. N. Basov, R. D. Averitt, D. Hsieh, *Nature Materials* 16, 1077 (2017).
[3] I. Belopolski,P. Yu, D. S. Sanchez, Y. Ishida, T.-R. Chang, S. S. Zhang, S.-Y. Xu, H.Zheng, G. Chang,G. Bian, H.-T. Jeng, T. Kondo, H. Lin, Z. Liu S. Shin, M. Zahid Hasan, *Nature Communications* **8,** 942 (2017).
[4] I. Belopolski I, S.-Y. Xu, Y. Ishida, X. Pan, P. Yu, D. S. Sanchez, H. Zheng, M. Neupane, N. Alidoust, G. Chang, T.-R. Chang, Y. Wu, G. Bian S.- M. Huang, C .- C. Lee, D. Mou, L. Huang, Y. Song, B. Wang, G. Wang, Y.-W. Yeh, N.Yao, J.E. Rault, P.Le Fèvre, F.Bertran, H. Jeng, T. Kondo A. Kamiski, H. Lin, Z Liu, F. Song, S. Shin, M. Z.Hasan, *Physical Review* B **94**, 085127 (2016).
[5] M. Neupane, S.-Y. Xu, Y. Ishida, S. Jia, B. M. Fregoso, C. Liu, I. Belopolski, G. Bian, N. Alidoust, T. Durakiewicz, V. Galitski, S.Shin, R. J. Cava M. Zahid Hasan, *Physical Review Letters* **115**, 116801 (2015).
[6] M. Neupane,*in preparation*, (2024).
[7] J. Han, P.Mao, J.Han, P. Mao, H.Chen, J.-X. Yin, M.Wang, D.Chen, Y.Li1, J. Zheng, X. Zhang D.Ma, Q. Ma, Z.-M. Yu, J. Zhou, C.-C. Liu, Y.Wang S. Jia, Y. Weng, Z. Hasan, W. Xiao, Y. Yao, *Science Bulletin* **68**, 417 (2023).
[8] M. Z. Hasan, *Proceedings of SPIE* **PC12419**, https://doi.org/10.1117/12.2652024 2 (2023)**.**

Clocking the subcycle dynamics of atomically confined tunnelling currents

J. Hayes, T. Siday, F. Schiegl, F. Sandner, P. Menden, V. Bergbauer, M. Zizlsperger, S. Nerreter, S. Lingl, J. Repp, J. Wilhelm, M. A. Huber, Y. A. Gerasimenko, R. Huber
University of Regensburg, 93040 Regensburg, Germany

In condensed matter physics, there has been a persistent pursuit to sample light-matter interaction at the shortest length and time scales conceivable. Scanning near-field optical microscopy (SNOM), which utilizes evanescent fields confined to nanoscale metallic objects, offers insights into this interaction but the spatial resolution is limited by the probe apex size (~10 nm) [1]. On the other hand, lightwave-driven scanning tunnelling microscopy (LW-STM) has provided glimpses into atomic-scale dynamics [2,3]. Yet, there the rapid motion of electrons within a single cycle of light cannot be resolved, as only the time-integrated electronic response in the form of rectified currents is collected. Here, we present a novel optical microscopy paradigm, leveraging strong-field nonlinearities to achieve atomic-scale spatial resolution with subcycle time resolution [4].

We use qPlus sensors with atomically sharp tungsten tips in ultrahigh vacuum and cryogenic conditions and illuminate the tip apex with phase-locked terahertz pulses (Fig. 1a), detecting the scattered light with electro-optic sampling (EOS). Intriguingly, when approaching the tip to atomic-scale tip-sample separation, a significant signal increase with a distinct phase delay $\Delta\varphi$ occurs (Fig. 1b). This hallmark phase shift indicates the origin of the signal: a transient dipole induced by the AC tunnelling currents flowing in response to the THz field (Fig. 1c,d). Owing to the atomic confinement of this novel near-field optical tunnelling emission (NOTE) signal (Fig. 1e), we can image single packing defects on an Au(111) surface (Fig. 1f). Moreover, with NOTE we can clock the subcycle electron tunnelling dynamics in WSe_2 trilayers (Fig. 1g).

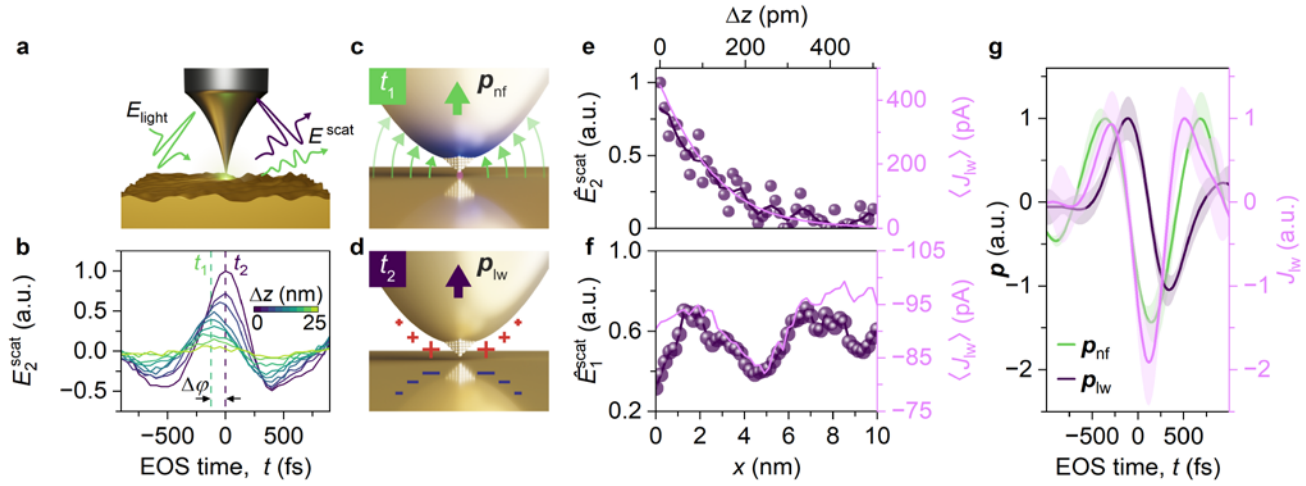

Fig. 1. NOTE microscopy. ***(a)*** *We couple a THz light pulse (E_{light}) to a tungsten tip tapping above an Au(111) surface and detect scattered near fields demodulated at the* n*-th harmonic of the tapping frequency (E_n^{scat}) via EOS.* ***(b)*** *Scattered THz transients (E_2^{scat}) for varying tip-sample distance Δz (tapping amplitude $A = 25$ nm). At minimal Δz, the transient transforms accruing a phase shift $\Delta\varphi$, and significant amplitude increase relative to conventional near fields.* ***(c)*** *Formation of a mesoscopic near-field dipole $\boldsymbol{p}_{nf}$ at the tip apex, driven by E_{light} at time t_1, causing a tunnelling current J_{lw}* ***(d)*** *At time t_2, $\boldsymbol{p}_{nf} = 0$ as E_{light} crosses zero, but the NOTE dipole $\boldsymbol{p}_{lw}$ induced by the tunnelling current is maximal.* ***(e)*** *Peak of the NOTE signal $\hat{E}_2^{scat}$ for $A = 200$ pm, plotted together with the time-integrated lightwave tunnelling current $\langle J_{lw}\rangle$ measured for increasing Δz.* ***(f)*** *Quasi- constant height LW-STM and NOTE line scans across a single packing defect on an Au(111) surface.* ***(g)*** *Real- time subcycle sampling of ultrafast tunnelling currents on trilayer WSe_2, showing $\boldsymbol{p}_{nf}$ at the tip apex (**green**), the NOTE dipole $\boldsymbol{p}_{lw}$ (**dark purple**), and retrieved ultrafast tunnelling currents (**pink**).*

This all-optical approach provides first ever experimental access to subcycle atomic-scale electron dynamics in various quantum materials, promising strong-field control over light-matter interaction at atomic lengthscales.

References

[1] M. Eisele, T. L. Cocker, M. A. Huber, M. Plankl, L. Viti, D. Ercolani, L. Sorba, M. S. Vitiello, R. Huber, *Nature Photonics* **8,** 841 (2014).
[2] T. L. Cocker, D. Peller, P. Yu, J. Repp, R. Huber, *Nature* **539,** 263 (2016).
[3] D. Peller, L. Z. Kastner, T. Buchner, C. Roelcke, F. Albrecht, N. Moll, R. Huber, J. Repp, *Nature* **585,** 58 (2020).
[4] T. Siday, R.Huber, *in review* (2024).

* Acknowledgements: The authors acknowledge support from DFG (Project-ID 314695032, SFB 1277 (Subprojects A05 and B02), major instrumentation grant INST 89/505-1, and research grants HU1598/8, HU1598/9 and WI5664/3-1).

Spin- and momentum-resolved valleytronic dynamics in Atomically thin semiconductors

L. Münster[1], S. Zajusch[1], J. Güdde[1], R. Wallauer[1], Y. Gerasimenko[2], R. Huber[2], U. Höfer[1]
[1]*Philipps-University of Marburg, 35032 Marburg, Germany*
[2]*University of Regensburg, 93053 Regensburg, Germany*

In two-dimensional transition metal dichalcogenides (TMDCs), strong spin-orbit coupling and Coulomb interactions result in a variety of bright and dark excitonic states, distributed over the whole Brillouin zone. Time-resolved momentum microscopy, a variant of time- and angle-resolved photoemission spectroscopy, allows for the detailed spectroscopical characterization of these excitons in two-dimensional momentum space and to investigate their dynamics in the time domain. While momentum-dark excitons as well as interlayer excitons formation have been observed in several previous experiments [1-5], the spin state has remained elusive. However, due to the valley degree of freedom in TMDcs, the spin plays an important role for charge transfer processes in these materials and for future device applications. Here, we report a time-resolved momentum microscopy experiment which makes this spin information accessible. In a complete experiment, we succeeded in tracing electrons every time step after optical excitation. The centerpiece of our experimental setup is an optical pumping scheme which makes excitation under near-normal incident with circularly polarized light possible. This allows for the preparation of a well-defined initial state with a single spin- and valley polarization (Fig. 1). Precisely titled pulse fronts of the pump beam match the pulse fronts of the XUV probe beam incident on the sample under an angle of 70°. In this way, we disentangle the scattering rates between the bright and the various momentum- and spin-forbidden dark excitons of the K, K', Σ, and Σ' valleys with 10-fs time resolution.

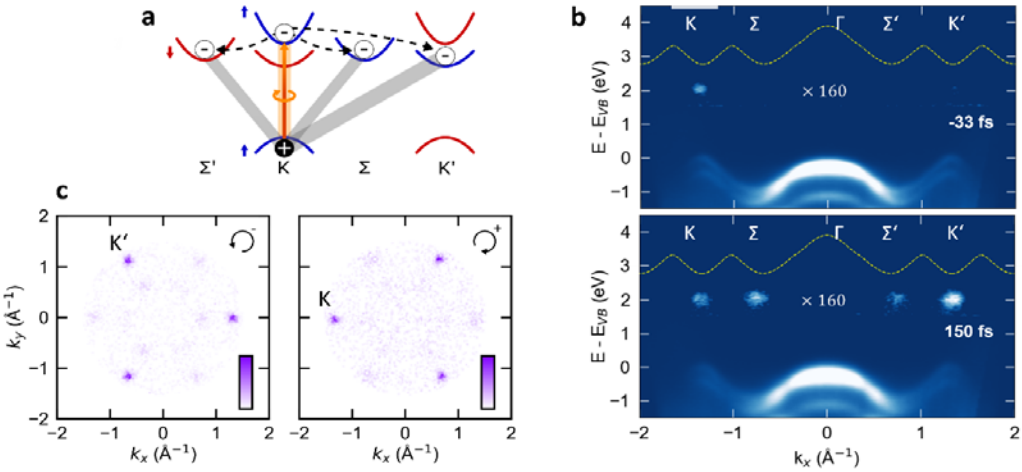

***Fig. 1. a:** Energy scheme of WS_2 with bright and momentum-dark excitons.*

***b**: E(k) photoemission intensity distribution in the K-Γ-K' direction for right circular pump two delays of the XUV probe.*

***c**: Photoemission momentum maps an energy of E=2 eV above the valence band maximum E_{VB} for left and right circular pump and zero pump-probe delay.*

The build-up of the momentum-dark KK' exciton is found to proceed within 40 fs, similarly fast as the formation of the previously investigated KΣ exciton [2]. In contrast, we find at least six times longer scattering times for processes involving a spin flip of the electron and leading to spin-dark KK as well as spin- and momentum-dark KΣ' excitons. While the fast relaxation of the bright into momentum-dark excitons is clearly related to the strong exciton phonon scattering in TMDCs [2,5], different mechanisms for spin-flip scattering have been discussed. One of them is intervalley electron-hole exchange interaction between the K and K' valleys. Another one is the phonon-mediated Elliot-Yafet mechanism. We will discuss the relative importance of these different spin-relaxation channels in light of the valley-resolved exciton dynamics of our experiment.

References

[1] J. Madeo, M. K. L. Man, C. Sahoo, M. Campbell, V. Pareek, E. L. Wong, A. Al-Mahboob, N. S. Chan, A. Karmakar, B. M. K. Mariserla, X. Li, T. F. Heinz, T. Cao, K. M. Dani, *Science* **370**, 1199 (2020).
[2] S. Dong, M. Puppin, T. Pincelli, S. Beaulieu, D. Christiansen, H. Hübener, C. W. Nicholson, R. P. Xian, M. Dendzik, Y. Deng, Y. W. Windsor, M. Selig, E. Malic, A. Rubio, A. Knorr, M. Wolf, L. Rettig, R. Ernstorfer, , *Natural Sciences* **1**, e10010 (2021).
[3] R. Wallauer, R. Perea-Causin, L. Münster, S. Zajusch, S. Brem, J. Güdde, K. Tanimura, K.-Q. Lin, R. Huber, E. Malic, U. Höfer,, *Nano Letters* **21**, 5867 (2021).
[4] O. Karni, E. Barré, V. Pareek, J. D. Georgaras, M. K. L. Man, C. Sahoo, D. R. Bacon, X. Zhu, H. B. Ribeiro, A. L. O'Beirne, J. Hu, A. Al-Mahboob, M. M. M. Abdelrasoul, N. S. Chan, A. Karmakar, A. J. Winchester, B. Kim, K. Watanabe, T. Taniguchi, K. Barmak, J. Madéo, F. H. da Jornada, T. F. Heinz, K. M. Dani, *Nature* **603**, 247 (2022).
[5] D. Schmitt, J. P. Bange, W. Bennecke, A. A. AlMutairi, G. Meneghini, K. Watanabe, T. Taniguchi, D. Steil, D. R. Luke, R. T. Weitz, S. Steil, G. S. M. Jansen, S. Brem, E. Malic, S. Hofmann, M. Reutzel, S. Mathias, *Nature* **608**, 499 (2022).

* Acknowledgment:supported by the Deutsche Forschungsgemeinschaft (DFG) through SFB 1083 "Structure and Dynamics of Internal Interfaces."

Ultrafast light-induced Lifshitz transition in High Tc superconductor Bi2212

L. Hellbrück[1], J. Dai[1], M. Puppin[1], F. Barantani[2], A. Crepaldi[1], T. LaGrange[1], A. Magrez[1], L. Forró[1]
E. Martino[2], M. Grioni[1], H. M. Rønnow[1], F. Carbone[1], S. Benhabib[3]
[1] *École Polytechnique Fédérale de Lausanne, 1015 Lausanne, Switzerland*
[2] *University of Texas, Austin, TX 78712, USA*
[3] *Université Paris-Saclay, 91191 Gif-sur-Yvette, France*

Cuprates as a class of high Tc superconductors host multiple unconventional phases that require further studies to fully understand. Studying the time-dependent response of these materials can enhance our understanding of excitations, light-matter interaction, electron-phonon coupling, and the electronic response in different phases. Here we focus on the relationship between the pseudogap and superconducting phases. To study this, we employ time and angle-resolved photoemission spectroscopy (trARPES). We directly probe the Fermi surface and electron dispersion, giving us access to the spectral function at different momenta and the dynamics of quasi-particles. Relating this information about the quasi-particles to the pseudogap and superconducting phase respectively can help us understand the underlying mechanism of superconductivity in these compounds.

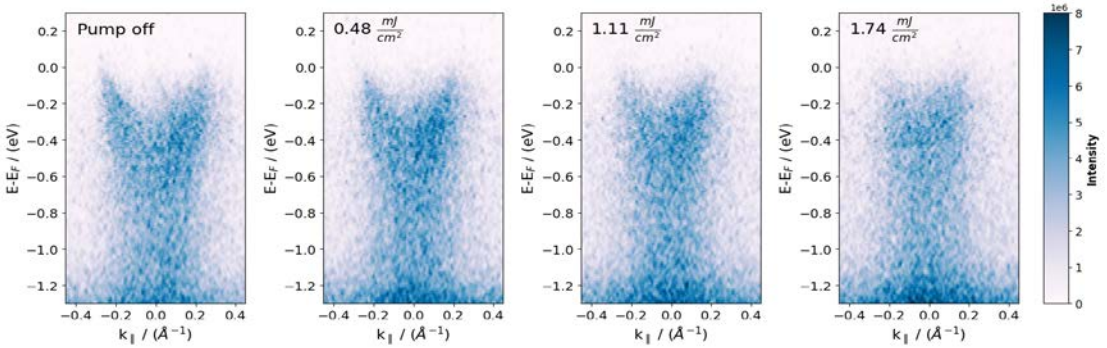

Fig. 1. Series of band maps measured on Bi2212 *for* $k_{\parallel} = 0.39 A^{-1}$ *at different pump fluencies. A shift in* k_F *as well as* μ *is observed*

The pseudogap phase is characterized by a low density of states (DOS) at the Fermi level, a loss of states in the Fermi surface compared to the superconducting phase, and the loss of one hole contributing to the charge transport. Doping-dependent studies on the bi-layer high Tc superconductor Bi2212 reveal a change in the topology of its Fermi surface [1,2,3].

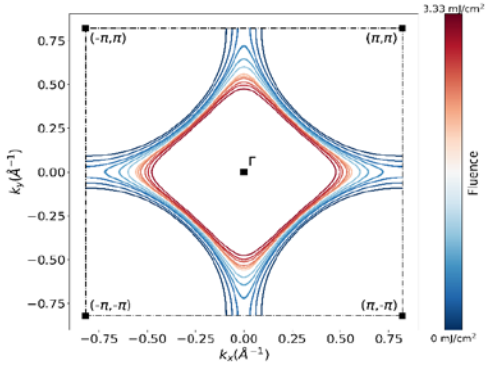

Fig. 2. Fluence-dependent Fermi-Surface evolution*. Fermi-Surface is reconstructed from* k_F *points in a Tight-Binding approach*

At a hole doping of 22%, the topology changes from a hole- to an electron-like Fermi surface, which is usually called a Lifshitz transition. We find that for the optimally doped Bi2212 (16% hole doping), we are able to induce this Lifshiftz transition by irradiating the sample with high fluence femtosecond laser excitation. The induced transition persists for multiple microseconds and is of reversible nature. Exploiting this effect could allow for controlled manipulation of the phase diagram through the use of laser radiation.

References

[1] A. Kaminski, S. Rosenkranz, H. M. Fretwell, M. R. Norman, M. Randeria, J. C. Campuzano, J-M. Park, Z. Li, H. Raffy, *Physical Review* B **73** 174511 (2006).
[2] S. Benhabib, A. Sacuto, M. Civelli, I. Paul, M. Cazayous, Y. Gallais, .A. Measson, R. D. Zhong, J. Schneeloch, G. D. Gu, D. Colson A. Forget, *Physical Review Letters* **114**, 147001 (2015).
[3] N. Doiron-Leyraud, O. Cyr-Choinière, S. Badoux, A. Ataei, C. Collignon, A. Gourgout, S. Dufour-Beauséjour, F. F. Tafti, F. Laliberté M.-E.Boulanger, M.Matusiak, D.Graf, M.Kim, J.-S.Zhou, N.Momono, T.Kurosawa, H.Takagi,L.Taillefer, *Nature Communications* **8**, 2044(2017).

Phonon-induced chirality and multiferroicity

C. Paiva,[1] C. Romao,[2] M. Fechner,[3] D. M. Juraschek[1]
[1] *Tel Aviv University, Tel Aviv,6997801 Israel*
[2] *ETH Zürich, 8092 Zürich, Switzerland*
[3] *Max Planck Institute for the Structure and Dynamics of Matter,22761 Hamburg, Germany*

Chiral phononics is emerging as a new field that utilizes the angular momentum of circularly polarized lattice vibrations to manipulate the properties of quantum materials. Phonon angular momentum naturally couples to the angular momentum of light, to electronic spin, orbital, and valley angular momentum, and further serves as a fundamental quantized physical observable in its own right. Some of the most prominent discoveries in recent years include the observation of chiral phonons in 2D and chiral materials [1,2], chiral-phonon transport phenomena such as the phonon Hall and spin Seebeck effects [3,4], and ultrafast phonon angular momentum coupling upon demagnetization of magnetic materials [5].When driven resonantly with an ultrashort circularly polarized laser pulse, light makes the ions in the material behave like microscopic electromagnetic coils, by producing circular motions of the atoms around their respective equilibrium positions in the crystal [6]. This induces real and effective magnetic fields that have been predicted and measured to yield up to the tesla-scale [7-13], unlocking an unprecedented means for the control of magnetic order.Here, I present our recent theoretical predictions of novel phenomena arising from chiral phonon driving. In particular, I will focus on two mechanisms, (1) the chirality-dependent generation of multiferroic polarization [14] and (2) the dynamical generation of chiral crystal structures with geometric chiral phonons [15]. *1. Dynamically induced multiferroic polarization*. We develop a methodology to simultaneously create a ferroelectric polarization and a magnetization in the nonpolar, nonmagnetic material $LiBO_2$, see Fig. 1(a). The ferroelectric polarization is generated by resonantly driving linearly polarized phonon modes that couple to and rectify a polar optical phonon mode. The magnetization in turn is generated by the magnetic moment of resonantly driven circularly polarized phonon modes. When driven elliptically, the material accordingly will yield both, effectively generating multiferroic polarization that can be reversed by changing the chirality of the laser pulse. *2. Phonon-induced geometric chirality*. We describe a mechanism by which achiral crystal structures can be turned into chiral ones upon ultrafast phonon excitation, see Fig.1(b).

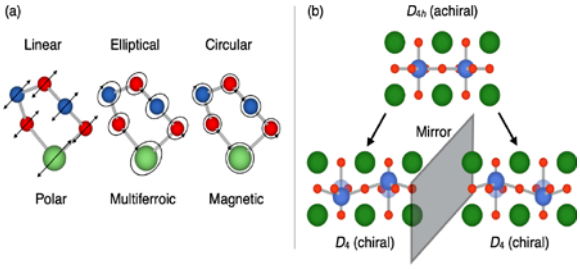

Fig. 1: Effects of dynamical and geometric phonon chirality. (a) *Chirality-dependent generation of multiple ferroic polarizations in $LiBO_2$ [14]. Linear, elliptical, or circular excitation of phonons induces a ferroelectric polarization, ferroelectric polarization and magnetization, or a magnetization, respectively.* ***(b)*** *Phonon-induced chirality in various materials [15]. The displacement of the atoms along the eigenvectors of geometric chiral phonons brings the material from an achiral to a chiral crystal structure. Example shown here for a generic tetragonal perovskite oxide.*

We show that materials in every achiral point group contain phonon modes, whose displacement pattern changes the symmetry of the system into a chiral point group. This distinguishes them from conventional chiral phonons, in which the circular motion, not the displacement, induces chirality. These *geometric chiral phonons* can be rectified through nonlinearly light-driven phonons and further switched between two enantiomeric states upon reorientation of the laser pulse. This method enables the creation of chirality on demand, with likely implications for chiral electronic and optical properties.

References

[1] H. Zhu, J.Yi, M.-Y.Li, J.Xiao, L.Zhang, C.-W.Yang, R. A.Kaindl, L.-J. Li, Y. Wang, X. Zhang, *Science* **359**, 579 (2018).
[2] H. Ueda,M.García-Fernández, S.Agrestini, C.Romao, J.Brink, N.A.Spaldin, K.-J.Zhou, U.Staub, *Nature* **618,** 946 (2023).
[3] G. Grissonnanche, S. Thériault, A. Gourgout, M.- E. Boulanger, E. Lefrançois, A. Ataei, F. Laliberté, M. Dion, J.- S. Zhou, S. Pyon, T. Takayama H. Takagi, N. Doiron-Leyraud, L. Taillefer, *Nature Physics* **16**, 1108 (2020).
[4] K. Kim,E.Vetter, LYan, C.Yang, Z.Wang, R.Sun,Y.Yang, A. Comstock, X.Li, J.Zhou, L.Zhang, W.You, D. Sun, J.Liu,*Nature Materials***22**, 322 (2023).
[5] S. R. Tauchert, M. Volkov, D. Ehberger, D. Kazenwadel, M. Evers, H. Lange, A. Donges, A. Book, W. Kreuzpaintner, U. Nowak, P. Baum *Nature* **602**, 73 (2022).
[6] C. P. Romao, D. M. Juraschek, *Nature* **628**, 505 (2024).
[7] D. M. Juraschek, M. Fechner, A. V. Balatsky, N. A. Spaldin, *Physical Review Materials* **1**, 014401 (2017).
[8] D. M. Juraschek, T. Neuman, P. Narang, *Physical Review Research* **4**, 013129 (2022).
[9] S. Chaudhary, D. M. Juraschek, M. Rodriguez-Vega, G. A. Fiete, *arXiv:2306.11630* (2023).
[10]T. F. Nova, A. Cartella, A. Cantaluppi, M. Först, D. Bossini, R. V. Mikhaylovskiy, A. V.Kimel, R.Merlin, A.Cavalleri,*Nature Physics* **13**,132 (2017)
[11] J. Luo, T. Lin, J. Zhang, X. Chen, E. R. Blackert, R. Xu, B. I. Yakobson, H. Zhu, *Science* **382**, 698 (2023).
[12] M. Basini, M.Pancaldi, B.Wehinger, M. Udina, T. Tadano, M. Hoffmann, A.V.Balatsky, S.Bonetti, *Nature* **628**,534 (2024)
[13] C. S. Davies, N. Fennema, A. Tsukamoto, I. Razdolski, A. V. Kimel, A. Kirilyuk, *Nature* **628**, 540 (2024).
[14] C. P. Romao, D. M. Juraschek, *arXiv:2311.00824* (2023).
[15] C. Paiva, M. Fechner, D. M. Juraschek, *arXiv:2404.16234* (2024).

Ultrafast simultaneous manipulation of multiple ferroic orders through Nonlinear phonon excitation

D.A. Bustamante Lopez[1], D. M. Juraschek[2], M. Fechner[3], X. Xu[4], S.-W.Cheong[4], W. Hu[1]
[1]*Boston University, Boston, MA 02215, USA*
[2]*Tel Aviv University, Tel Aviv 6997801 , Israel*
[3] *Max Planck Institute for the Structure and Dynamics of Matter, 22761 Hamburg, Germany*
[4]*Rutgers University, Piscataway, NJ 08854, USA*

Magnetoelectric multiferroics exhibit ferroelectric and magnetic order that are intrinsically coupled to each other within a single phase. All-optical control of the magnetoelectric phase using femtosecond laser pulses is appealing for low-energy consumption spintronics. It has remained unexplored whether light can control multiple ferroic order parameters simultaneously in a single domain. We report the observation of ultrafast enhanced second-harmonic generation (SHG) in multiferroic $BiFeO_3$ by resonant excitation of a high-energy A_1 phonon with strong-field mid-infrared laser pulses. Interestingly, we find that both the ferroelectric and antiferromagnetic contributions to the SHG signal are enhanced on a sub-picosecond timescale. We perform phonon dynamics simulations by density functional theory calculations, which confirms the enhanced ferroelectric SHG signal. We conclude that coherent phonon excitation with ultrashort laser pulses concurrently controls ferroelectricity and antiferromagnetic order.

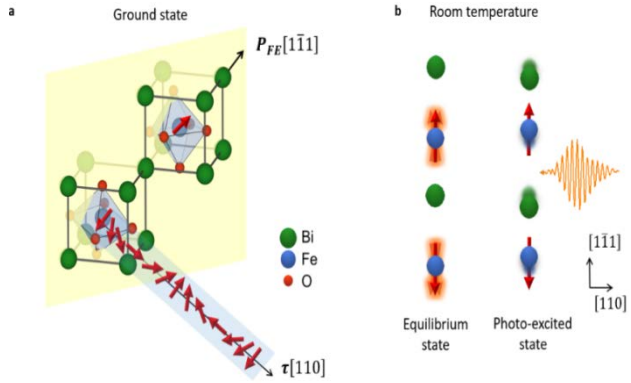

***Fig. 1. Control of multiferroic order through nonlinear phonon dynamics. Left** : Rhombohedral crystal structure of $BiFeO_3$. The ferroelectric polarization (P_{FE}) is along the stretched body-diagonal of the pseudocubic unit cell. The spins between nearest-neighbor iron ions are antiferromagnetically aligned (**red arrows**) and form a spin cycloid with a wavelength of 62 nm along the normal vector τ of the mirror plane (**yellow**). In a single-magnetic domain crystal, the spin cycloid breaks the three-fold rotation symmetry around P_{FE}. **Right**: **(Left)** Initial state with the equilibrium ferroelectricpolarization and a thermal broadening of the iron-spin alignment. (**Right**) The lattice distortion following the resonant excitation of a A_1 phonon leads to a change in polarization and to an improved alignment of the iron spins [1].*

Our findings demonstrate that nonlinear phonon driving may serve as a compelling technique for manipulating multiple ferroic order parameters in a single shot, which we expect to be applicable generically to a broad category of materials exhibiting magnetoelectric coupling, providing a route towards information processing using cross-coupled orders on ultrashort timescales [1].

References

[1] D. A. Bustamante Lopez, D. M. Juraschek, M. Fechner, X. Xu, S.-W. Cheong, W.Hu Xiv: 2305.08250 92023).

* Acknowledgement(s): D.A.B.L. and W.H acknowledge support from the U.S. Department of Energy, Office of Science, Office of Basic Energy Sciences Early Career Research Program under Award Number DE-SC-0021305. The work at Rutgers was supported by the W.M. Keck Foundation. D.M.J. was supported by Tel Aviv University.

Real-time ab initio study of chiral spin dynamics in laser-induced demagnetization

J. He
Charles University, Prague 12843, Czech Republic

Two-dimensional (2D) magnets and van der Walls (vdW) heterostructures open unprecedented opportunities for discovering emergent phenomena and implementing device structures in all-2D spintronics. Although light is the fastest means to manipulate the magnetism, the spin dynamics of light driven 2D magnetic materials and vdW heterostructures remains mostly untapped. Using real-time density functional theory (rt-TDDFT) and ab initio non-adiabatic molecular dynamics (NAMD), we systematically investigate the ultrafast laser pulses induced spin transfer and relaxation dynamics of 2D antiferromagnetic-ferromagnetic (AFM/FM) van der Waals heterostructures. Laser pulses can induce a ferrimagnetic (FiM) state in the AFM layer within tens of femtoseconds and maintain it for subpicosecond time scale before reverting to the AFM state. We identify the unequal electron–phonon coupling of spin-up and spin-down channels of AFM spin sublattice causes an inequivalent spin relaxation, in turn extending the time scale of the FiM state. On the other hand, we further to unveil significant x and y components of spin (SAM) and orbital (OAM) angular momentum SAM and OAM

induced by circularly left (σ+) and right (σ–) polarized laser pulses in 2D ferromagnets and ferromagnetic Fe, Co, and Ni. Our results show that the magnitude of the OAM is an order of magnitude larger than that of the SAM, highlighting a stronger optical response from the orbital degrees of freedom of electrons. Intriguingly, σ+ and σ– pulses induce chirality in the precession of SAM and OAM, respectively, with clear associations with laser frequency and duration. Finally, we identify the chiral SAM and OAM related the generation of chiral phonon during the demagnetization process.

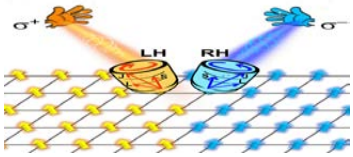

Fig. 1. Circularly left (σ+) and right (σ–) polarized laser pulses *induced chiral dynamics in 2D ferromagnets.*

These insights offer a comprehensive understanding of SAM and OAM dynamics, along with lattice rotation, during and shortly after a polarized laser pulse.

References

[1] B. Huang, G. Clark, E. Navarro-Moratalla, D. R. Klein, R.Cheng, K. L. Seyler, D.Zhong, E.Schmidgall , M.A. McGuire, D. H. Cobden, W.Yao D. Xiao, P. Jarillo-Herrero, X, Xu, *Nature* **546**, 270 (2017).

[2] C. Gong, L. Li, Z. Li, H. Ji, A. Stern, Y. Xia, T. Cao, W. Bao, C. Wang, Y. Wang, Z. Q. Qiu, R. J. Cava, S.G. Louie, J. Xia, X. Zhang, *Nature* **546**, 265 (2017).

[3] J. He, S. Li, T. Frauenheim, Z. Zhou, *Nano Letters* **23**, 8348 (2023).

[4] J. He, T. Fruenheim, S. Li, *The Journal of Physical Chemistry Letters*, 15, 2493 (2024).

[5] S. Li, R. Wang, T. Fruenheim, J. He, *arXiv preprint arXiv:2401.04038* (2024).

* Acknowledgement(s): authors (JH) acknowledged the support from MSCA Fellowships CZ–UK with CZ.02.01.01/00/22_010/0002902.

All-optical sampling of optical waveforms in solids using Photoionization-induced currents

A. Husakou[1], V. S. Yakovlev[2], N. Karpowicz[,4], D. A. Zimin[,3]

[1] *Max Born Institute, 12489 Berlin, Germany*

[2] *Max-Planck-Institut für Quantenoptik, 85748 Garching, Germany*

[3] *Ludwig-Maximilians-Universität, 85748 Garching, Germany*

[4] *CNR NANOTEC Institute of Nanotechnology, 73100 Lecce, Italy*

Direct access to the temporal profile of the electric field is of key importance for many applications and research areas, such as nonlinear optics, investigations of ultrafast electron and molecular dynamics, metrology and so on. Several methods were developed to address this challenging problem, many of them relying on the generation of free electrons either by a weak extreme ultraviolet pulse or a strong optical pulse. Another possibility is all-optical methods, where the nonlinear wave mixing is used. This class of techniques includes electro-optic sampling (EOS) [1,2] and air-biased coherent detection. In this contribution we start by reviewing the existing methods of the all-optical sampling. The well-known scheme of EOS is shown in Fig. 1.

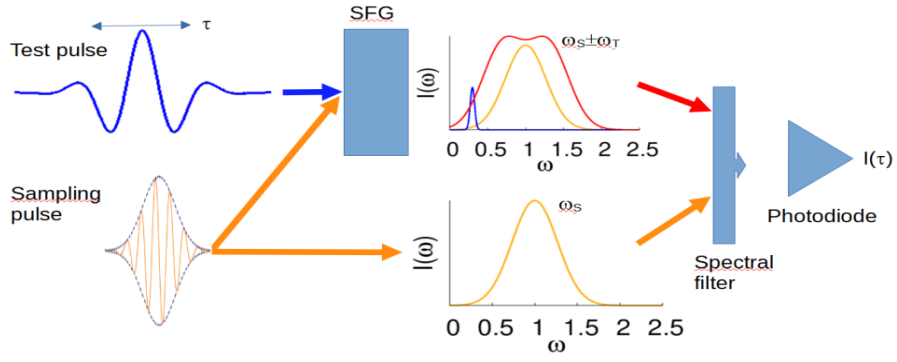

Fig. 1. The scheme of the EOS approach*. Terahertz or infrared pulse (**blue curve**), which can be delayed by the time τ, is sent into a nonlinear crystal which provides sum-frequency generation (**SFG**) signal together with a sampling pulse (**orange curve**). As a result of SFG, sidebands are generated in the spectrum (**red curve**) which is made to interfere with the unperturbed sampling pulse at a photodiode. The delay-dependentintensity at the photodiode characterizes the temporal profile of the test pulse.*

Narrow-band, weak, low-frequency test pulse propagates together with a shorter sampling pulse in a nonlinear crystal which is characterized by a second-order optical nonlinearity. As a result, sidebands at sum and difference frequencies (signal) are generated. These sidebands interfere with the unperturbed sampling pulse in the lower arm, called the local oscillator (LO), at a photodiode. The measured dependence of the photodiode signal on the delay provides direct information about the temporal profile of the test pulse. This scheme has an advantage of being independent on the carrier-envelope offset (CEO) of the sampling pulse, with a very significant trade-off: the bandwidth of the test pulse must be

the input pulse and the post-compressed pulse, i.e., with ZnSe sample in the beam path. Like the Gaussian-shaped input pulse, the post-compressed pulse also shows an almost undisturbed beam shape, indicating a regime below the onset of filamentation. After passing through the ZnSe sample, the beam profile exhibits a Townes profile, which corresponds to the formation of a self-similar spatial soliton and indicates spectral homogenization of the beam profile. The spectral homogeneity of the beam profile is confirmed by measuring the V-parameter [6]. The intensity-weighted V-parameter is larger than 85% within the $1/e^2$ intensity range of the beam profile. The temporal characterization of the pulses is performed using the SHG-FROG technique and provides the temporal pulse shapes before and after post-compression in ZnSe (Fig. 1b). The input pulses with a duration of 95 fs are compressed to 53 fs. Only 5 % of the pulse energy is contained in the visible satellite structures. Using ZnS the self-compression regime is realized, benefiting from the shorter ZDW and hence larger negative GVD compared to ZnSe. In this process, 75 fs input pulses are compressed to 35 fs, which corresponds to only two optical cycles. The resulting peak power reaches almost 50 GW, that is, a record value for wavelengths above 4 µm.

References

[1] Z. Chang, L. Fang, V. Fedorov, C. Geiger, S. Ghimire, C. Heide, N. Ishii, J. Itatani, C. Joshi, Y. Kobayashi, P. Kumar, A. Marra, S. Mirov I Petrushina, M. Polyanskiy, D. A.Reis, S.Tochitsky, S.Vasilyev, L.Wang, Y.Wu, Fangjie Zhou, *Advances in Optics and Photonics* **14**, 652 (2022).
[2] A. Hildenbrand, C. Kieleck, A. Tyazhev, G. Marchev, G. Stöppler, M. Eichhorn, P. G. Schunemann, V. L. Panyutin, V. Petrov, *Optical Engineering* **53**, 122511 (2014).
[3] A. Dubietis, G. Tamošauskas, R. Šuminas, V. Jukna, A. Couairon, *Lithuanian Journal of Physics* **57**, 3 (2017).
[4] L. von Grafenstein, M. Bock, D. Ueberschaer, E. Escoto, A. Koç, K. Zawilski, P. Schunemann, U. Griebner, T.Elsaesser, *Optics Letters* **45**, 5998(2022).
[5] T. Kawamori, P. G. Schunemann, V. Gruzdev, K. L. Vodopyanov, *APL Photonics* **7**, 086101 (2022).
[6] J. Weitenberg, A. Vernaleken, J. Schulte, A. Ozawa, T. Sartorius, V. Pervak, H.-D. Hoffmann, T. Udem, P.Russbuldt, T. W.Hänsch, *Optics Express* **25**, 20502 (2017).

Room temperature superfluorescence in Lead Halide Perovskites

K. Gundogdu

North Carolina State University, Raleigh, NC 27606, USA

The formation of coherent macroscopic states and the manipulation of their entanglement using external stimuli are essential for emerging quantum applications. However, the observation of collective quantum phenomena such as Bose–Einstein condensation, superconductivity, superfluidity and superradiance has been limited to extremely low temperatures to suppress dephasing due to random thermal agitations. In this presentation we will talk about room-temperature superfluorescence (SF) in hybrid perovskite thin films [1,2]. In SF an optically excited population of incoherent dipoles develops collective coherence spontaneously. This emergent collective state forms a giant dipole and radiates a burst of photons [Fig. 1]. Because electronic transitions dephase extremely fast, observation of SF in semiconductors is extremely rare and under high magnetic fields and at very low temperatures [3]. Therefore, the discovery of room temperature SF in perovskites is very surprising and shows that in this material platform, there exists an extremely strong immunity to electronic dephasing due to thermal processes. To explain this observation, we propose that the formation of large polarons in hybrid perovskites provides a quantum analogue of vibration isolation to electronic excitation and protects it against dephasing even at room temperature.

Fig. 1 An incoherent ensemble of dipoles *is shown on the left. Arrows indicate the randomly distributed phases of individual dipoles. The red waves resemble vacuum fluctuations, which lead to spontaneous synchronization. After a time delay, the phases of the excited dipoles are locked, forming a macroscopic quantum coherent state: a 'giant atom' (**on the right**). This macroscopic state interacts with the radiationfield collectively. The system isthen described as a single wavefunction of indistinguishable particles. The collective emission of the macroscopic coherent system leads to a superfluorescent burst.*

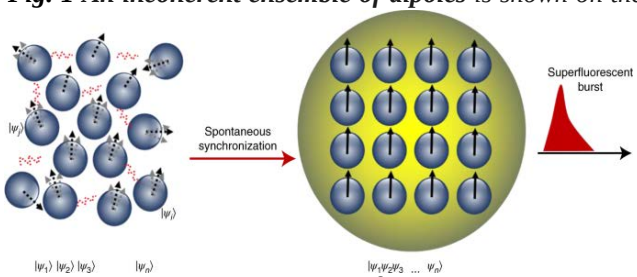

Understanding the origins of sustained quantum coherence and the superfluorescence phase transition at high temperatures can provide guidance to design systems for emerging quantum information technologies and to realize similar high-temperature macroscopic quantum phenomena in tailored materials.

References

[1] M. Biliroglu, G. Findik, J. Mendes D. Seyitliyev, L. Lei,Q. Dong,Y. Mehta,V.V. Temnov,F. So, K. Gundogdu, *Nature Photonics* **16,** 324 (2022).
[2] M. Findik, M. Biliroglu, D.Seyitliyev, J.Mendes, A. Barrette, H. Ardekani, L. Lei,Q. Dong, F. So, K.Gundogdu, *Nature Photonics* **15,** 676 (2021).
[3] G. T. Noe II , J.-H. Kim, J. Lee, Y. Wang, A. K. Wójcik, S. A. McGill, D.H. Reitze, A. A. Belyanin, J. Kono, *Nature Physics* **8**, 219 (2012).

* Acknowledgement(s) : authors acknowledge support from DOE DE-SC0024396

Post-compression of few-cycle millijoule pulses beyond 4 µm wavelength

M.Bock, G.Steinmeyer, U.Griebner
Max Born Institute for Nonlinear Optics and Short Pulse Spectroscopy, 12489 Berlin, Germany

Coherent high-intensity sources in the mid-infrared spectral range are of great interest for driving a wide range of secondary light sources, e.g., for applications in strong-field and attosecond physics [1]. In the wavelength range beyond 4 µm, only a very limited number of such sources are available. One of the main reasons is the limited availability of suitable nonlinear crystals, which, typically, also possess a rather low damage threshold [2]. The established method for generating even shorter optical pulses is spectral broadening by means of self-phase modulation (SPM) in nonlinear media and subsequent compression. To this end, in the spectral range beyond 4 µm, only dielectric bulk media have been used so far [3].Here we present the nonlinear compression of sub-100 fs multi-mJ pulses at 5 µm wavelength using polycrystalline ZnSe and ZnS. The post-compression provides shortest pulses with two optical cycles and energies >1.5 mJ at 1 kHz repetition rate.A simple post-compression scheme is set up, comprising a two-lens telescope and the nonlinear medium under study. The input pulses are provided by a ZGP-based midwave-IR (MWIR) OPCPA operating at 1 kHz repetition rate [4]. In the following, the idler pulses at 4.9 µm are used, which have an energy of 2.2 mJ and sub-100 fs duration. The compression of the idler pulses in the MWIR OPCPA is realized by CaF_2 plates, which enable adjustable GDD for post-compression experiments.ZnSe or ZnS in polycrystalline form is used as medium for spectral broadening via SPM, as these materials exhibit a rather high nonlinear refractive index. Both samples exhibit an anti-reflective coating. ZnSe and ZnS have different band gaps (2.7 eV and 3.54 eV, respectively) and zero dispersion wavelengths (ZDW) (4.8 µm and 3.6 µm, respectively). Using ZnS one can therefore exploit the self-compression regime. In the case of ZnSe, the positive dispersion resulting from SPM must be subsequently compressed, since the ZDW almost coincides with the center wavelength of the input pulse.

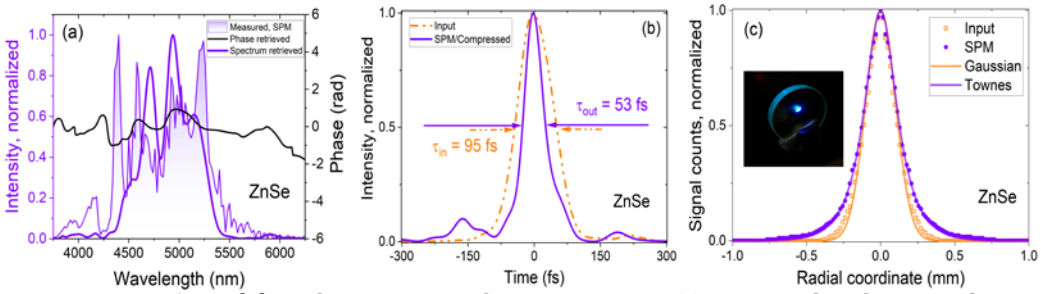

Fig. 1. Post-compression of fs *multi-mJ 5-µm pulses using ZnSe.* ***(a)*** *Measured and retrieved normalized spectral amplitudes after spectral broadening in ZnSe and related spectral phase.* ***(b)*** *Retrieved temporal pulse shape before and after spectral broadening with subsequent post-compression.* ***(c)*** *Far-field intensity distribution with and without ZnSe in the beam path; Inset: Interband photoluminescence from ZnSe (SPM:self-phase modulation).*

The intensity at the sample entrance surface is adjusted by the telescope consisting of two CaF_2 lenses in such a way that no signs of filamentation can be observed, and an optimum in terms of spectral broadening and beam profile is achieved. The corresponding intensity for both samples is ~170 GW/cm^2. Even at this intensity, a bright glow can be observed in the visible spectral range, which we attribute to the generation of higher harmonics. For ZnSe, the dominant visible emission is bluish (Inset Fig. 1c), which corresponds to its band gap energy. The latter is due to the recombination of generated free charge carriers by multiphoton absorption (MPA) [5]. The ZnS sample appears orange, which corresponds to the eighth harmonic. The spectrum of the 4.9 µm input pulse with a bandwidth of 0.7 µm (1/e^2 level) is broadened by SPM in the nonlinear media. In the case of ZnSe, whose group velocity dispersion (GVD) at 5 µm is only -10 fs^2/mm, the resulting positive dispersion must be compensated after passing through the sample, which is realized by a CaF_2 lens. The pulse input spectrum is broadened to 1.3 µm in the ZnSe sample with a thickness of 5 mm (Fig. 1a), which supports a FTL pulse duration of 40 fs. The loss in the post-compression process is only 15%, resulting in final pulse energy of 1.9 mJ. After passing the ZnSe sample, the measured spectrum shows a fine structure (Fig. 1a), which is attributed to MPA. Simulations of the propagation of the 4.9 µm pulse in the ZnSe sample were carried out using the non-linear Schrödinger equation (NLSE). The result of this simulation shows a good agreement with the measured spectrum as well as with the spectral phase. The reduction in intensity, especially in the central region of the spectrum due to MPA, is clearly visible (Fig. 1a).Fig. 1c shows the far-field intensity distributions of

much shorter than that of the sampling pulse, fundamentally limiting the application of EOS. Recently, an important progress was made in removing this limitation and extending the detection bandwidth of optical methods to the petahertz domain [3]. Instead of an unperturbed sampling pulse in the lower arm, third-harmonic generation of the sampling pulse was used as a LO. While requiring a locked CEO of the sampling pulse, this approach no longer limits the bandwidth of the test pulse to a fraction of the sampling bandwidth. In addition, it offers an advantage in terms of sensitivity and signal-to-noise ratio. Further development of these ideas into the several-PHz range relies on higher-order nonlinear processes, which yield several-octave spectra suitable for characterization of ultrashort and/or high-frequency test pulses. We propose a scheme for such a method, as shown in Fig. 2. As explained in the caption, in this case, due to several nonlinear processes which affect the generation of both the signal and the LO, the resulting spectra are very broad, allowing in principle characterization of the test pulses down to and below of 1 femtosecond. However, three key requirements must be met for the scheme to function properly: first, high-order nonlinear processes must be efficient enough to provide a broad spectrum, second, generation of the signal and of the LO must happen in the same crystal, thus a careful separation of the two arms must happen by considering the corresponding polarization, and third, CEO of the sampling pulse must be locked. We have experimentally implemented the above scheme based on the cascaded third-harmonic generation in a SiO_2 crystal in the signal (upper) arm. We were able to characterize test pulses with a duration around one cycle, using 2.8-fs sampling pulse with a field strength of $1.5x10^{10}$ V/m, which is sufficient to provide a broad spectrum. In addition, we have developed a numerical model, based on the unidirectional propagation equation, which describes both signal and LO generation as a function of delay τ.

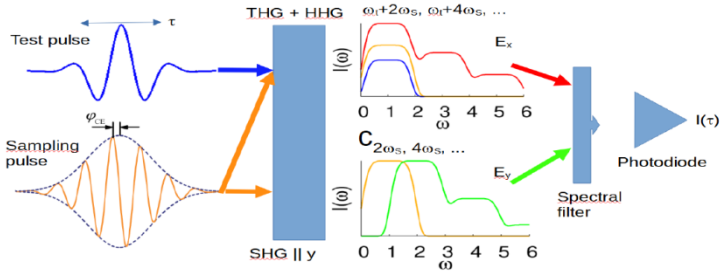

Fig. 2. The scheme of the approach proposed in this contribution*. Weak test pulse (**blue curve**) is sent into a nonlinear medium together with a sampling pulse (**orange curve**), resulting in a broad signal spectrum (**red curve**) due to third- and higher-order nonlinear processes. Simultaneously, second-harmonic generation provides a broad LO spectrum (green curve). The two arms can be separated by considering different polarization of the test pulse and LO. The delay-dependent intensity at the photodiode characterizes the temporal profile of the test pulse.*

The excellent agreement of the experimentally characterized (green curve) and simulated (red curve) pulse is observed, as shown in Fig. 3(a).

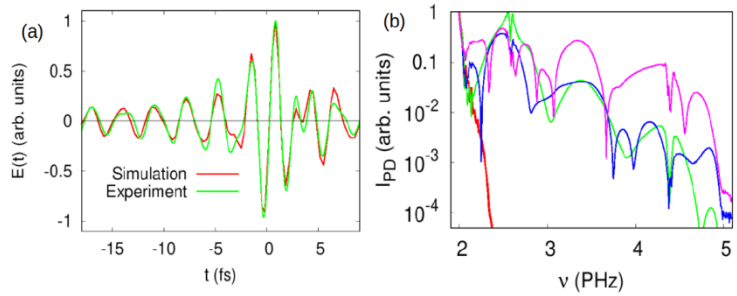

Fig. 3. The simulated and experimental test pulses (**a**) and the contribution of different nonlinearity mechanisms to the Fourier transform of the photodiode signal (**b**). The sampling pulse strength is $1.5x10^{10}$ V/m (**a**) and $5x10^{10}$ V/m (**b**). In(**b**), the contributions of non-cascaded third harmonic generation (**red curve**), cascaded third-harmonic generation (**green curve**), third-harmonic generation plus Brunel radiation (**blue curve**), and third-harmonic generation plus Brunel radiation plus injection current (**magenta curve**) are shown.

To access the capabilities of the all-optical methods to characterize even shorter/short-wavelength pulses, a role and strength of other nonlinear mechanisms, such as transition from the valence zone and the conduction zone, must be investigated. In Fig. 3(b) we show the contributions of the different mechanisms, such as the third harmonic generation, cascaded generation during propagation, as well as Brunel radiation and injection current, which are associated with time-dependent conduction-zone electron density and polarization at the instant of the electron injection to the conduction zone, correspondingly. One can see that cascaded third-harmonic generation is the key mechanism for extending the response above 2 PHz, while Brunel radiation does not increase response significantly. On the other hand, injection current is critical for extending the response even further, up to 4.8 PHz. Thus the all-optical sampling based on injection current in solids has a significant potential for the characterization of ultrashort sub-fs pulses.

References

[1] A. Leitenstorfer, S. Hunsche, J. Shah, M. C. Nuss, W. H. Knox, *Applied Physics Letters* **74**, 1516 (1999).
[2] S. Keiber, S. Sederberg, A. Schwarz, M. Trubetskov, V. Pervak, F. Krausz, N. Karpowicz, *Nature Photonics* **10**, 159 (2016).
[3] D. A. Zimin, V. Yakovlev, N. Karpovicz, *Science Advances* **8**, eade1029 (2022).

Understanding control and modulation of color center defects

V. Ivanov
Virginia Tech, Blacksburg, VA24061, USA

Color centers are molecule-like defects in semiconductor materials that emit photons of a particular frequency and can host single electron spins. This spin-photon interface has made them a promising platform for realizing a variety of quantum technologies relevant for defense applications, including quantum networking, positioning, and sensing. In particular, for quantum networking, it is desirable to have defects that are optically bright, emit at telecommunications wavelengths with narrow linewidth, have an optically addressable spin degree of freedom, and can be easily integrated with existing wafer-scale fabrication processes for electronics and photonics. Color centers in silicon satisfy all of these requirements, and as a result have recently been the focus of intensive research efforts to characterize known defects and engineer new defects with optimal characteristics [1-7]. A key aspect for developing these technologies is understanding how the electrical and optical properties are affected both by local changes in defect bond structure [2], and non-local effects like strain [3-4] and disorder [5]. Another aspect is scalability; the random nature of defect synthesis by ion-beam implantation lacks the necessary control in both the density and position of defects. With regard to this, recent work has demonstrated how local laser processing can be used to write and erase defects on demand by changing local chemistry [6].

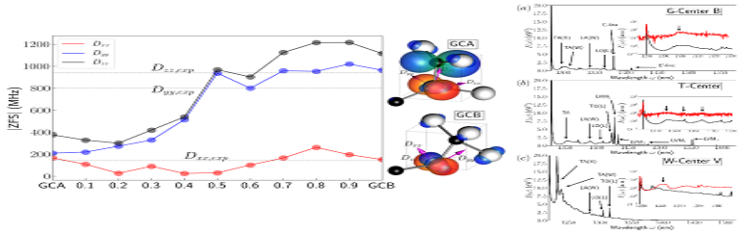

***Fig. 1. Left**: **Components of the zero field splitting tensor**, D_{zz} (black), D_{yy} (blue), and D_{xx} (red), of the silicon G-center for defect configurations that linearly interpolate between GCA and GCB (shown on the side) in steps of 0.1 (10%). Dashed lines indicate the experimentally measured ZFS values.*
***Right**: **Computed photoluminescence spectra** of common color center defects in silicon.*

This increased level of control over defect formation, has motivated recent high-throughput calculations seeking to identify defect candidates, and the creation of publicly-accessible databases of defects and their properties [7]. These vast amounts of computed data are uncovering novel correlations between defect chemistry and electro-optical properties. This also forms the basis for machine learning approaches used to predict defect characteristics directly from their structures, accelerating computational screening and revealing rules-of-thumb for engineering defects optimally suited for quantum applications.

***Fig. 2. Distribution of silicon defects** identified by the quantumdefects.com database [7]. The squared transition dipole moment is plotted against defect zero-phonon-line. Marker shape indicates if the defect has two midgap states (**Midgap**), no midgap levels (**Buried**), or midgap state and level within the conduction band (**CB Buried**)/valence band (**VB Buried**). Marker color denotes the number of unpaired spins in the groundstate – 0 (**yellow**), 1 (**blue**), 2 (**green**), 3 (**magenta**), or 4 (**orange**). The extend of the telecom band (**dark grey**) is marked, with an 0.1 eV error (**light grey**). High quality predicted and known defects are indicated by arrows.*

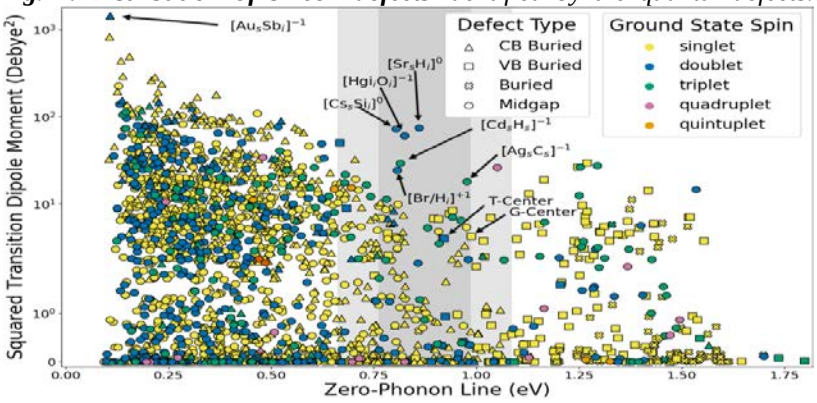

This also forms the basis for machine learning approaches used to predict defect characteristics directly from their structures, accelerating computational screening and revealing rules-of-thumb for engineering defects optimally suited for quantum applications.

References

[1] W. Redjem, A. J. Amsellem, F. I. Allen, G. Benndorf, J. Bin, S. Bulanov, E. Esarey, L.C.Feldman, J.F.Fernandez, J.G.Lopez, L. Geulig, C.R. Geddes H. Hijazi, Q. Ji, V. Ivanov, B. Kanté, A. Gonsalves, J. Meijer, K. Nakamura, A. Persaud, I. Pong, L.Obst-Huebl, P.A. Seidl, J. Simoni, C. Schroeder S. Steinke, L.Z. Tan, R. Wunderlich, B. Wynne, T. Schenkel, *Communications Materials* **4**, 22 (2023).
[2] V. Ivanov, J. Simoni, Y. Lee, W. Liu, K. Jhuria, W. Redjem, Y. Zhiyenbayev, C. Papapanos, W. Qarony, B. Kanté, A. Persaud, T. Schenkel L.Z. Tan, *Physical Review* B **106**, 134107 (2022).
[3] Y. Zhiyenbayev, W. Redjem, V Ivanov, W. Qarony, C. Papapanos, J. Simoni, W. Liu, K. Jhuria, L.Z. Tan, T. Schenkel, B. Kanté, *Optics Express* **31** 8352 (2023).
[4] W. Redjem, Y. Zhiyenbayev, W.Qarony, V.Ivanov, C.Papapanos, W.Liu, K.Jhuria, Z.Y.A. Balushi, S. Dhuey, A. Schwartzberg, L. Z. Tan, T. Schenkel B. Kanté, *Nature Communications* **14**, 3321 (2023).
[5] W. Liu, V. Ivanov, K. Jhuria, Q. Ji, A. Persaud, W. Redjem, J. Simoni, Y. Zhiyenbayev, B. Kanté, J.G. Lopez, L. Z. Tan, T. Schenkel, *Physical Review Applied* **20**, 014058 (2023).
[6] K. Jhuria, V. Ivanov, D. Polley, W. Liu, A. Persaud, Y. Zhiyenbayev, W. Redjem, W Qarony, P. Parajuli, Q. Ji, A. J. Gonsalves, J. Bokor, L. Z. Tan B. Kanté, T. Schenkel, *Nature Communications*, (2023).
[7] V. Ivanov, A. Ivanov, J. Simoni, P. Parajuli, B. Kanté, T. Schenkel, L.Z. Tan, *arxiv:2303.16283* (2023).
* Acknowledgements: This research used resources of the National Energy Research Scientific Computing Center, a DOE Office of Science User Facility supported by the Office of Science of the U.S. Department of Energy under Contract No. DE-AC02-05CH11231.

Efficient first Stokes generation in methane-filled anti-resonant fibers

R. Avrahamy[1], D. Belker[1], M. H. Frosz[2], A. A. Ishaaya[1]
[1] *Ben-Gurion University of the Negev, Beer-Sheva 8410501, Israel*
[2] *Max Planck Institute for the Science of Light,91058 Erlangen, Germany*

In the last two decades, wavelength conversion using stimulated Raman scattering (SRS) in gas-filled hollow-core fibers (HCF) has been an active area of research. These fibers offer several advantages, including tight light confinement, long interaction length, and the ability to guide very high peak powers, making them an ideal platform for nonlinear light-matter interactions. Photonic band-gap and Kagomé photonic crystal fibers (PCF) were the first to show efficient SRS conversions in gas-filled HCFs [1]. However, anti-resonant fibers (ARFs) with circular tubes in the cladding were later found to offer broader transmission windows and recently surpassed the gold standard of standard telecom fibers in terms of lower transmission losses [2]. ARFs enable low-loss single-mode guidance across a broad spectrum with minimal light-glass overlap, allowing for sustained high-power delivery. Additionally, their attenuation outside the designed transmission windows can increase drastically, inhibiting undesired conversions (e.g., to the second Stokes), which makes them a superior apparatus for efficient first Stokes generation. Lasers centered at ~1470 nm find applications in both medical and defense fields. In medicine, they are used for skin rejuvenation, treating enlarged prostate (BPH), and addressing varicose veins. Their eye-safe properties also make them valuable for military purposes, including range finding, illumination, and covert operations. In addition, in-band pumping of Erbium-doped glasses used both for bulk and fiber lasers and amplifiers can also benefit from lasers emitting at ~1.45 μm. Methane (CH_4) gas has a large vibrational Raman shift of ~2916 cm^{-1} and a Raman gain that is second largest only to hydrogen, but favorably, due to its isotropic polarizability, it is **not rotationally** Raman active. A CH_4-filled ARF can convert a technologically mature 1030 nm Ytterbium-doped fiber laser pump to the first Stokes (S_1) around 1470 nm while preserving the pump beam properties, such as single mode propagation. However, CH_4 weakly absorbs radiation at both the pump (~1030 nm) and first Stokes (1470 nm) wavelengths. In contrast, a 1065 nm pump converts to S_1 ~1545 nm, which is also a highly applicable wavelength, and in this case, the CH_4 absorption is negligible. Plausibly, as a result, most experimental studies with methane-filled ARFs converted a ~1060 nm pump laser [3], and some used the converted S_1 ~ 1545 nm as a pump for an additional conversion to ~2.8 μm [4,5]. Most reported conversions achieved sub-1 W average powers, but only very recently did two reports reach a few watts levels with a picosecond laser pump. The first report used a pump centered at ~1064 nm with a repetition rate of 100 kHz [6], and the second report used a pump centered at 1030 nm and a repetition rate of 200 kHz [7]. These two reports also differ in the laser and fiber types used for conversions.

Here, we focus on efficient conversion to the first Stokes of ns duration pulses and study and compare the conversion process when pumping at λ_{p1}=1029.5 nm and λ_{p2}=1065.1 nm. The HCF is a custom-designed ARF (Fig. 1a) with ~29 μm mode field diameter, 400 μm cladding, and dual transmission bands that are qualitatively plotted in Fig. 1b. The pump source is a high peak power Q-switched ytterbium-doped PCF laser with an interchangeable central wavelength λ_{p1} or λ_{p2} using different volume Bragg grating mirrors, and a linewidth of ~ 0.15 nm (Fig. 1c). The pulse duration can also vary from ~8 ns to over 60 ns, depending on the Q-switch repetition rate and the power of the 976 nm pump diode. The linearly polarized pump beam is attenuated via a half-wave plate and a linear polarizer. The beam is focused with an aspherical lens into the bare end of the ARF through an antireflection-coated glass window, which seals the input gas cell. The opposite end of the ARF is mounted inside an output gas cell, pointing at another antireflection-coated window. The cells are first vacuum-pumped and then pressurized to variable CH_4 pressures. The output beam, comprising both the pump and the converted Stokes signal, is collimated after the cell window and reflected off a dichroic mirror to separate the first Stokes signal from the pump. The pump and Stokes beams are measured at the dichroic mirror's reflection and transmission, respectively. Selected conversion experiment results with an ARF length of ~9 meters are plotted in Figs. 1d-1f. An example of the first Stokes spectrum centered at ~ 1471.8 nm is shown in Figs. 1d. The output quantum efficiency for conversion from λ_{p2} (CH_4 pressure 9 bars) and λ_{p1} (CH_4 pressure 5 bar) are graphed in Fig.1e and 1f, respectively. The difference in the magnitude of the methane absorption between the two conversions significantly affects the results. The conversion efficiency saturates much faster in terms of gas pressure and peak powers when pumping at $\lambda_{p1.}$ Still, comprehensive experimental characterizations allowed us to reach over 2 W average power at ~1471 nm. In addition,at ~1545nm, we reached over 2.5W average power with almost 50% input to first Stokes

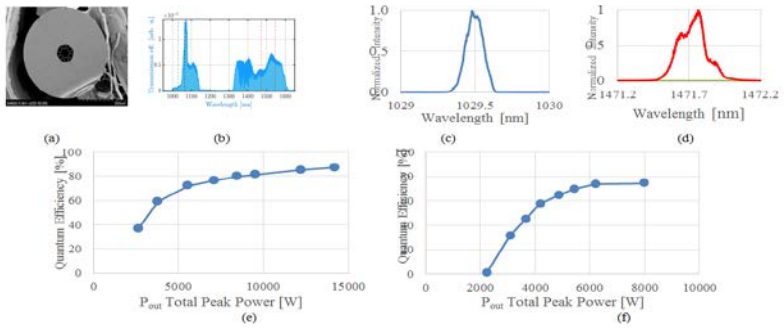

***Fig. 1. The ARF a**- scanning electron micrograph; **b**- qualitative dual band transmission efficiency.The measured spectrum of **c**- the pump laser at λ_{p1} and **d**- the converted first Stokes. Quantum efficiency experimental measurements for pumping at **e**- λ_{p1}=1029.5 nm, and **f**- λ_{p2}=1065.1 nm.*

We believe these results are promising, especially for conversions of the discussed longer pulse lengths.

References

[1] F. Benabid, J. C. Knight, G. Antonopoulos, P. St. J. Russell, *Science* **298**, 399 (2002).
[2] Y. Chen, M. N.Petrovich, E.Numkam Fokoua, A. I.Adamu, M.R.A. Hassan, H. Sakr, R. Slavík, S. Bakhtiari Gorajoobi, M. Alonso, R. Fatobene Ando A. Papadimopoulos, T. Varghese, D. Wu, M. Fatobene Ando, K. Wisniowski, S. R. Sandoghchi, G.T. Jasion, D.J. Richardson, F. Poletti, *Optical Fiber Communication Conference (OFC)*, Th4A.8 (2024).
[3] Z. Li, W. Huang, Y. Cui, Z. Wang, W. Wu, , *Optics Express* **26,** 12522 (2018).
[4] Z. Li, W. Huang, Y. Cui, Z. Wang, *Optics Letters* **43**, 4671 (2018).
[5] W. Huang, Y. Cui, Z. Li, Z. Zhou, Y. Chen, Z. Wang,, *Laser Physics Letters* **16**, 085107 (2019).
[6] X. Zhang, Z. Peng, Z. Dong, P. Yao, Y. Hou, P. Wang,, *IEEE Photonics Technology Letters* **34**, 1007 (2022).
[7] A. M. Lanari, H.C.H. Mulvad, I.A. Davidson, Q. Fu, P. Horak, D.J. Richardson, F. Poletti, *Optics Express* **31**, 41191(2023).

Decoupled few-femtosecond electronic and structural transitions in VO_2: Bad metal, a semi-metal, and structural revivals

C.Brahms[1], L.Zhang[2], X Shen[3], U.Bhattacharya[4], M.Recasens[2], J.Osmond[2], T.Grass[5], W. Chhajlany[6], K Hallman[7] R. F. Haglund[7], S. T. Pantelides[7], M. Lewenstein[2], J.C. Travers[1], A. S. Johnson[8]

[1]*Heriot-Watt University, Edinburgh EH14 4AS, UK*
[2]*The Barcelona Institute of Science and Technology, 08860 Castelldefels, Spain*
[3]*University of Memphis, Memphis, Tennessee 38152, USA*
[4]*ETH Zurich, 8093 Zurich, Switzerland*
[5]*DIPC - Donostia International Physics Center, 20018 San Sebastian, Spain*
[6]*Adam Mickiewicz University, 61-614 Poznań, Poland*
[7]*Vanderbilt University, Nashville, Tennessee 37235, USA*
[8]*IMDEA Nanoscience, Calle Faraday 9, 28049, Madrid, Spain*

Ultrafast spectroscopy has long promised to reveal the key degrees of freedom which drive phase transitions in quantum materials by decoupling the electronic, lattice, spin and orbital degrees of freedom in the time-domain. A classic example is the application of ultrafast spectroscopy to the insulator to metal phase transition in vanadium dioxide (VO_2), where a more than 50 year old debate continues over whether the transition is electronically driven (Mott-like) or structurally driven (Peirls-like) [1,2] (Fig. 1a).

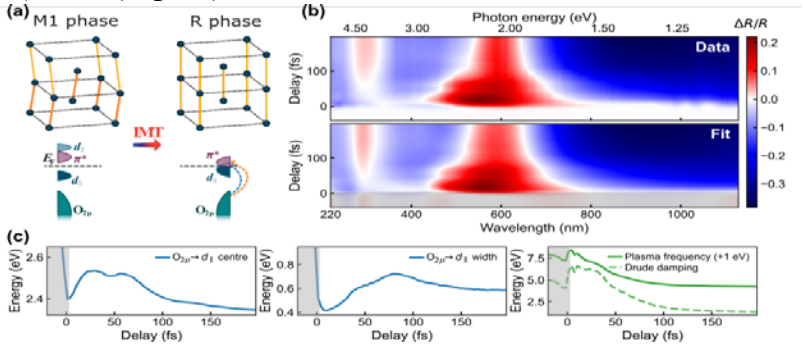

***Fig. 1. Ultrafast dynamics of the light-induced phase transition in VO_2.** **(a)** Structural and electronic changes in the insulator to metal phase transition in VO_2. **(b)** Experimental and modelled changes in the broadband reflectivity as a function of time-delay following photoexcitation. **(c)** Dynamics of the four most relevant optical components of the phase transition, tracking the motion of the $d_{\parallel}$ band and Drude plasma.*

Ultrafast X-ray diffraction measurements have shown that the lattice can transform from the insulating monoclinic structure to the metallic rutile in less than 100 fs [3,4], while various types of optical measurements show the associated reflectivity changes occurring in as little as 25 fs [5-6], suggesting the electronic transition proceeds the structural one. However, to date these measurements have only shown direct sensitivity to *either* the electronic or structural degrees of freedom, and so a comprehensive picture of the full dynamics at sub-100 fs timescales is still lacking.Here we present such a comprehensive picture. Using ultrabroadband pulses spanning the entire deep ultraviolet to infrared (220-2500 nm) which we generate by high-energy soliton self-compression [7,8], we map the evolution of the electronic structure in VO_2 following photoexcitation with 5 fs resolution. Fits to the ultrabroadband optical response (Fig. 1b) allow us to track the energies and bandwidths of the key $d_{\parallel}$

and π^* bands along with the Drude plasma response (Fig 1c). We find the overall electronic structure changes from the insulator to metal in less than 10 fs, with the associated collapse of the $d_\parallel$ band splitting and emergence of a Drude plasma term, in agreement with the Mott picture. However, instead of a simple monotonic switching process [3–6], we observe that the transition follows a complex pathway. We find that at short times the $d_\parallel$ band is narrower than in equilibrium and that the Drude term shows highly enhanced electronic scattering of around 100 attoseconds, making VO_2 at short times the "worst bad" metal yet observed. Surprisingly, given the rapid scattering rate, this non-equilibrium state persists for over 100 fs, suggesting a barrier to electron-hole recombination. This barrier to relaxation can be explained by the motion of the $d_\parallel$ band, where complex, 20 fs-scale oscillations in energy and bandwidth shift the band 0.2 eV upward in energy, which is consistent with a partial re-opening of the insulating gap and a transient semi-metallic phase. Thus, even though intraband collisions are extremely frequent, this bottleneck prevents full relaxation until the $d_\parallel$ band finishes its evolution at around 100 fs. We assign this transient gap opening to the competition between the structural crystal-field splitting and Mott-band, and the oscillations in the $d_\parallel$ band to the coherent motion of the vanadium dimers launched by the ultrafast transition. We support these observations, which come directly from the experimental data, with advanced DFT calculations [9] and novel tensor-network calculations which comprehensively treat the electronic correlations in a simplified 1D model [10]. Our work not only resolves the nature of the phase transition in VO_2 at ultrafast timescales, but reveals an unexpected complexity which may be present in many other light-induced phase transitions at their earliest time scales, and suggests that ultrabroadband few-femtosecond pump-probe spectroscopy enabled by soliton-based light sources may prove a powerful technique in unravelling the dynamics of quantum materials [11].

References

[1] J. B. Goodenough, *Journal of Solid State Chemistry* **3**, 490 (1971).
[2] A. Zylbersztejn, N. F. Mott, *Physical Review* B **11**, 4383 (1975).
[3] S. Wall, S. Yang, L. Vidas, M. Chollet, M. Glownia , M. Kozina, T. Katayama, T. Henighan, M. J iang, T. A. Miller, D. A.Reis, L. A. Boatner O. Delaire, M. Trigo, *Science* **362**, 572 (2018).
[4] G. De la Peña, A. A. Correa, S.Yang,O.Delaire, Y.Huang, A. S.Johnson, T.Katayama, V.Krapivin, E. Pastor, D.A.Reis, S.Teitelbaum, L.Vidas, S.Wall M. Trigo, *Nature Physics* **19**, 1489 (2023).
[5] M. F. Jager, C.Ott, P.M. Kraus, C.J. Kaplan, W.Pouse, R.E.Marvel, R.F. Haglund, D.M. Neumark, S. R. Leone, *Proceedings of NAS* **114**, 9558 (2017).
[6] M. R. Bionta,V. Wanie, V. Gruson, J.Chaillou, N. Émond, D. Lepage, P.Lassonde, M. Chaker, F. Légaré, *Physical Review* B **97**, 125126 (2018).
[7] J. C. Travers,T. F. Grigorova, C.Brahms, F.Belli, *Nature Photonics* **13**, 547 (2019).
[8] C. Brahms,F.Belli , J. C. Travers, *Physical Review Research* **2**, 043037 (2020).
[9] S. Xu, X.Shen, K. A. Hallman, R.F. Haglund, Jr., S.T. Pantelides, *Physical Review* B **95**, 125105 (2017).
[10] L Zhang, U Bhattacharya, M Recasens, T Grass, RW Chhajlany, M Lewenstein, AS Johnson, *arXiv 402.01247* (2024).
[11] C. Brahms, L.Zhang, X.Shen, U.Bhattacharya, M. Recasens, J.Osmond, T. Grass, R. W. Chhajlany, K. A. Hallman, R. F. Haglund, S. T. Pantelides M. Lewenstein, J. C. Travers ,A.S. Johnson, *arXiv 2402.01266* (2024)

Driving the fluxonium qubit

A. Bista, K. Nie, M. Thibodeau, B. K. Clark, W. Pfaff, A. Kou
University of Illinois at Urbana-Champaign, Urbana, IL 61801, USA

The fluxonium qubit has garnered significant interest recently due to its high gate fidelities and strongly anharmonic spectrum. These valuable features have resulted in the fluxonium being proposed as the basis for a quantum processor, for use in transducing between microwave and optical signals, and as a nonlinear element for manipulating long-lifetime linear cavities. The capabilities of the fluxonium qubit for such schemes can be significantly improved under the application of a microwave drive. Here we discuss our recent experimental efforts demonstrating the benefits of applying a microwave drive for initializing [1] and reading out a fluxonium qubit. We will conclude by discussing prospects for improving multiple-fluxonium devices through the application of a microwave drive [2].

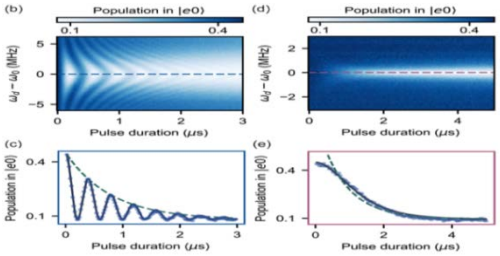

Fig. 1. Parametric control of a fluxonium *coupled to a rapidly- decaying resonator.*

We will conclude by discussing prospects for improving multiple-fluxonium devices through the application of a microwave drive [2].

References

[1] K. Nie, A. Bista, K. Chow, W. Pfaff, A. Kou, *arXiv*2404.11847 (2024)
[2] M. Thibodeau, Angela Kou, Bryan K. Clark, arxiv: 2401.08762 (2024)
[3] A. Kou, W. C Smith, U. Vool, R. T. Brierley, H. Meier, L. Frunzio, S. M. Girvin, L. I.Glazman, M. H. Devoret, *Physical Review* X **7**, 031037(2017)

* Acknowledgement(s) : we acknowledge support from the Air Force Office of Scientific Research under award number FA9550-21-1-032,the Army Research Office under Grant Number W911NF-23-1-0096, and the National Science Foundation under NSF Award 201613.

Ultrafast dynamics of correlated charges in transition metal oxides

Sh. Iwai
Tohoku University, 980-8578 Sendai, Japan

High-Tc superconducting $YBa_2Cu_3O_y$ (T_C~92 K): Since the early 1990s, the relaxation dynamics of superconducting (SC) quasiparticles have been reported enormously [1]. In contrast, the generation processes have not been directly captured (Fig. 1(a)), although this process is not only very important for elucidating the microscopic mechanism of high-T_c superconductivity, but also provides insights into recent studies on the high-harmonic generation [2] and the photoinduced superconductivity [3].

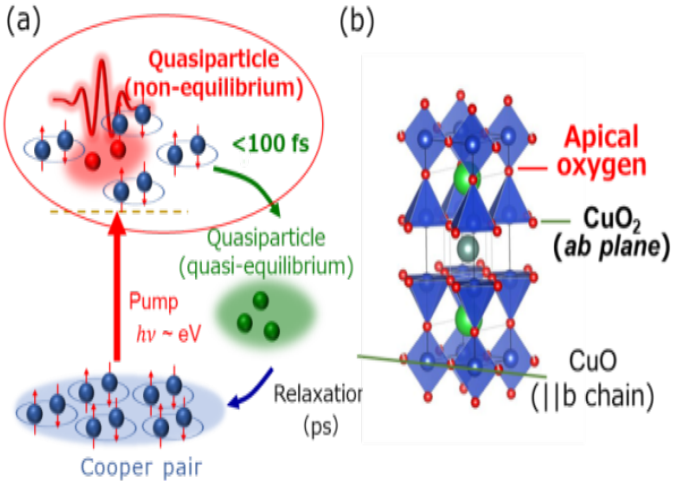

Fig. 1 (a) Quasiparticle generation and relaxation (b) *Crystal structure of YBCO*

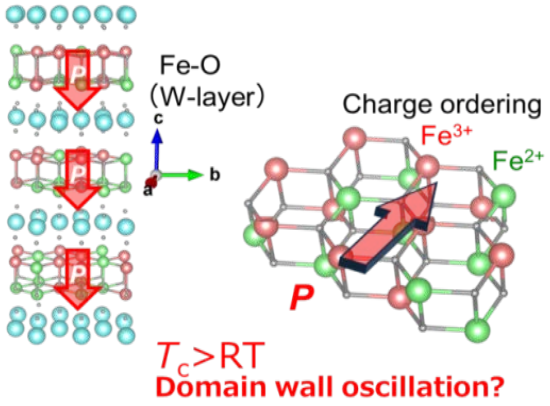

Fig. 2 Crystal structure and ferroelectric CO in $LuFe_2O_4$

In fact, measurements with a time window of <100 fs have not been made at $T<T_c$. Furthermore, ultrafast measurements of the SC state have focused on the THz range near the SC gap of about meV [1]. However, electronic phase transitions in strongly correlated systems should be characterized by a broader spectrum covering the eV scale and the overall spectral changes are still unclear. In view of this situation, we have performed transient reflectivity measurements in optimally-doped SC YBCO ($YBa_2Cu_3O_y$ (T_C~92 K); Fig. 1(b)) with 6 fs near-infrared light and those using conventional 100 fs pulses in the spectral range of 0.1-3 eV. We found 1) quasiparticle generation by near infrared excitation is characterized by a spectral-weight transfer in the broad spectral range. 2) Coherent apical oxygen phonons are produced during the quasiparticle generation. *Electronic ferroelectric* $LuFe_2O_4$:in electronic ferroelectrics, wherein spontaneous polarization ***P*** is realized by charge ordering (CO) arising from inter-site Coulomb repulsion, ultrafast/large electronic responses are expected therein. Layered iron oxides $LuFe_2O_4$ is promising candidates toward practical applications for showing the ferroelectric CO at room temperature [4, 5]. Here we report highly-sensitive nature of the ferroelectric polarization ***P*** at room temperature; the concomitant second harmonic generation (SHG) has been found to show the largest (ca. 150%) increase among bulk ferroelectrics upon applying 100 kV/cm-class THz electric field. Ultrafast modulation of the anisotropy of the ferroelectric polarization is discussed based on the THz-field induced change of the SHG anisotropy. Phase-sensitive responses of 2'd order nonlinear susceptibility (*d*-tensor) show that the sensitivity is increasing during the THz-field application, reflecting the cooperativity.

References

[1] C. Giannetti, M. Capone, D. Faustic , M. Fabriziob , F. Parmigiani, D. Mihailovic, *Advances in Physics* **65**, 58(2016).
[2] J. Alcala, U. Bhattacharya, J. Biegert, M. Ciappina, U. Elu, T. Graß, P.T. Grochowski, M. Lewenstein. A.P. Cidiropoulos, T. Steinle, I. Tyulnevet *Proceedings of National Academy of Sciences* **119**, e2207766119 (2022).
[3] S. Kaiser, D. Nicoletti, C. R. Hunt, W.Hu, I Gierz, H. Y.Liu, M.Le Tacon, T.Loew, D.Haug, B.Keimer, A.Cavalleri, *Physical Review* B **89** 184516 (2014).
[4] N. Ikeda, H. Ohsumi, K. Ohwada, K. Ishii, T. Inami, K. Kakurai, Y. Murakami, K. Yoshii, S. Mori, Y. Horibe, H. Kitô, *Nature* **436**, 1136 (2005).
[5] K. Fujiwara, Y. Fukada, Y. Okuda, R. Seimiya, N. Ikeda, K. Yokoyama, H. Yu, S. Koshihara, Y. Okimoto, *Scientific Reports* **11**, 4277 (2021).

Many-body effects of excited carriers in atomically thin TMDC semiconductors

A. Steinhoff, D. Erben, T. Schulz, M. Lorke, F. Jahnke
University of Bremen, 28334 Bremen, Germany

Atomically thin layers of transition metal dichalcogenides (TMDCs) are structures similar to graphene with an optical bandgap in the visible spectral region and promising optical properties for applications in optoelectronic devices. We study many-body effects of photoexcited carriers and their ultrafast dynamics. For low and intermediate excited carrier densities, excitons are present even at room temperature with large binding energies due to the two-dimensional nature of the system and reduced dielectric screening of the Coulomb interaction. At large excited carrier densities, the excitonic Mott transition takes place [1], leading to an interacting electron-hole-plasma in which many-body effects shape the optical properties of the TMDC system. For the regime, in which excitons are present, we study Auger-like exciton-exciton annihilation (EEA). As a result of the Coulomb interaction, one bound electron-hole-pair recombines nonradiatively while transferring its excess energy to another bound electron-hole-pair. The EAA is often considered to be among the most important fundamental constraints on quantum yield in devices based on excitons in two-dimensional materials. A range of EEA coefficients from several 10^{-3} cm^2 s^{-1} to about 0.1 cm^2 s^{-1} have been found experimentally for different TMD materials. Since it is challenging to experimentally disentangle EEA from competing processes, guidance of a quantitative theory is highly desirable. The very nature of EEA requires a material-realistic description that was not available so far. We present a many-body theory of EEA based on first-principle band structures and Coulomb interaction matrix elements. The challenge is to combine the large phase space of target states with a theory for exciton-exciton interaction in the second order of the Coulomb potential. Our approach consistently takes into account all electron-hole correlations on a two-particle level and goes beyond an effective bosonic picture. Applying our theory to monolayer MoS_2 encapsulated in hBN, we obtain EEA coefficients on the order of 10^{-3} cm^2 s^{-1} at room temperature [2], suggesting that carrier losses are often dominated by other processes, such as defect-assisted scattering.

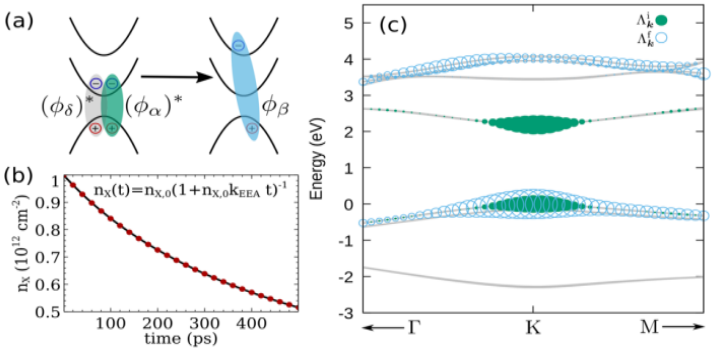

Fig. 1. (a) Fundamental EEA process: *An exciton in state $|\delta\rangle$ is annihilated, while a second exciton is promoted from low-energy state $|\alpha\rangle$ to high-energy state $|\beta\rangle$. (**b**) Time dependence of the total exciton density nX in hBN-encapsulated MoS2 at T = 300 K. (**c**) Contribution of Bloch bands to EEA scattering rates. The symbol size repre- sents the projection of initial (**full green circles**) and final (**open blue circles**) two-particle states onto Bloch states according to the corresponding two-particle wave functions. The single-particle band structure is shown in gray.*

Vertically stacked van der Waals heterobilayers with type-II band alignment host layer-separated, Coulomb-correlated electron-hole pairs forming interlayer excitons (ILX) with binding energies of more than 100 meV and lifetimes that are often drastically increased in comparison to excitons within a single layer [3]. We demonstrate in [3] that dipolar blue shifts are almost perfectly compensated by many-body effects, mainly by screening-induced self-energy corrections. Moreover, we identify a crossover between attractive and repulsive behavior at elevated exciton densities. Theoretical findings are supported by experimental studies of spectrally-narrow interlayer excitons in atomically-reconstructed, hBN-encapsulated $MoSe_2$/WSe_2 heterobilayers. Both theory and experiment show energy renormalization on a scale of a few meV even for high injection densities in the vicinity of the Mott transition. Our results revise the established picture of dipolar repulsion dominating exciton-exciton interactions in van der Waals heterostructures and open up opportunities for their external design (Fig.2). Ultrastrong photoexcitation can generate a high density plasma of unbound electrons and holes. Due to optical nonlinearities, which originate from Pauli blocking and many-body effects of the excited carriers, the generated carrier density will deviate from the estimate using a linear absorption coefficient. We describe nonlinear absorption properties and excited carrier dynamics using a theoretical approach that combines results from ab-initio electronic-state calculations with a many-body treatment of optical excitation [4].

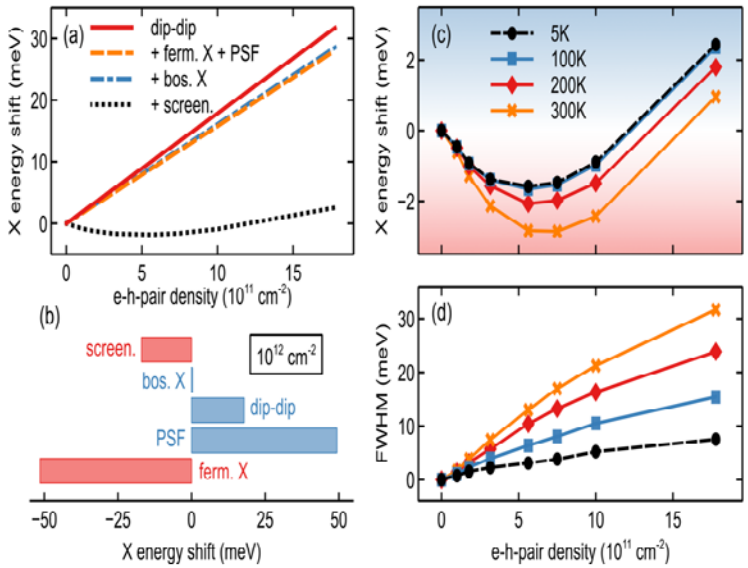

Fig. 2. Exciton energy renormalization induced by exciton-exciton interaction. (a) *Cumulative density-dependent renormalization of the zero-momentum bright 1s-exciton (spin-singlet) energy at a temperature of 100 K, subsequently adding dipole-dipole interaction (**dip-dip**), fermionic exchange interaction and phase-space filling (+ **ferm. X + PSF**), bosonic exchange interaction (+ **bos. X**), and screened bosonic exchange (+ **screen.**). The latter represents the result of the full calculation. (**b**) Individual contributions to the exciton energy renormalization corresponding to the cumulative presentation in panel (**a**) at an electron-hole pair density 10^{12} cm^{-2}. The red shift due to fermionic exchange and the blue shift due to phase-space filling compensate to a large extent. (**c**) Calculated temperature and density dependence of energy renormalization for the zero-momentum bright 1s-exciton. (**d**) Calculated temperature and density dependence of the zero-*momentum bright 1s-exciton broadening.

We determine the excited carrier density vs. pump power and identify the role and magnitude of optical nonlinearities at elevated excitation carrier densities for the frequently used TMDC materials MoS_2, $MoSe_2$, WS_2, and WSe_2 considering various excitation conditions. Our calculations use a DFT-based 6-band Wannier lattice model in connection with solutions of the semiconductor Bloch equations including carrier-carrier and carrier-phonon interactions on a self-consistent GW-level for the non-equilibrium carrier dynamics [4]. For photoexcitation at the bandgap, we find that the use of a linear absorption coefficient of the unexcited system underestimates the achievable carrier density in MoS_2 due to giant band-gap shrinkage and excitation-induced dephasing. The same holds for excitation of the high-energy band continuum in W-based materials. Generally, the excitation-induced shifts of the electronic states lead to dynamically changing absorption during intense photoexcitation depending on the spectral position of the pump laser.

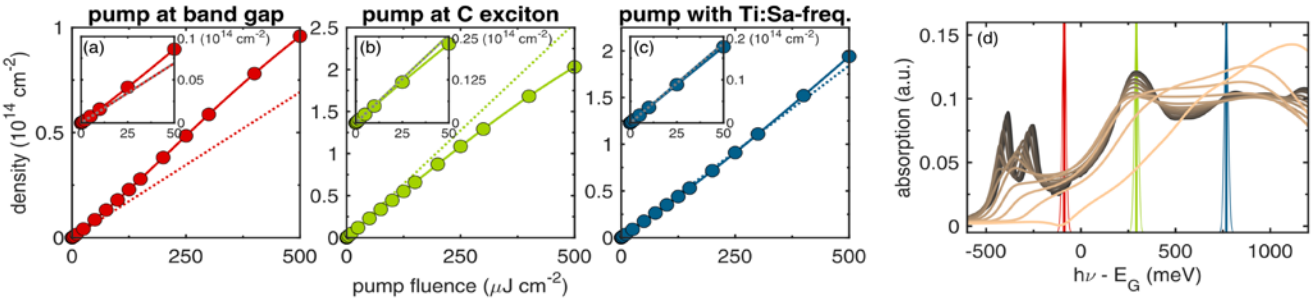

Fig. 3. Photoexcited charge-carrier density vs pump fluence *for excitation of hBN-encapsulated MoS_2 at a lattice temperature of 300 K with a 150-fs laser pulse tuned to the bandgap energy including polaron effects (**a**), at the C exciton (**b**), and well above the bandgap corresponding to the Ti:Sa laser emission wavelength (**c**). Solid lines and symbols represent calculated carrier densities including optical nonlinearities. Dashed lines correspond to an extrapolation of carrier density in the linear regime. Absorption spectra of MoS_2 for different excited carrier densities in thermal equilibrium at 300 K are shown in (**d**) together with the energetic position and spectral width of the pump pulses used in **(a)–(c)**. The carrier density increases from zero (**black line**) to 3 × 10^{14} cm^{-2} (**orange line**). E_G is the bandgap energy in the absence of excited carriers.*

The absorption spectra in Fig. 3 (d) exhibit A and B excitons below the bandgap and the C exciton at the position of the green line for weak excitation densities. The bleaching of the excitonic resonances with increasing excitation density is accompanied by a reduction of the exciton binding energy, which is nearly compensated by the band-gap shrinkage. As a result, the energetic positions of the exciton lines exhibit almost no shift.

References

[1] A. Steinhoff, M. Florian, M. Rösner, G. Schönhoff, T.O. Wehling, F. Jahnke, *Nature Communications* **8**, 1166(2017).
[2] A. Steinhoff, F. Jahnke, M. Florian, *Physical Review* B **104**, 155416(20 21).
[3] A. Steinhoff, E. Wietek,M.Florian, T. Schulz, T. Taniguchi, K. Watanabe, S. Zhao, A. Högele, F. Jahnke, A. Chernikov, *arXiv:2310*. 18328 (2023).
[4] D. Erben, A. Steinhoff, M. Lorke, F. Jahnke, *Physical Review* B **106**, 045409 (2022).

Ultrafast spin-currents mediated by interfacial spin-orbit interactions probed by THz-TDS Spectroscopy

H. Jaffrès[1], E. Rongione[1,2], L. Baringthon[1, 3], A. Pezo[1], S. Fragkos[4], P. Tsipas[4], J. Hawecker[2], T.- H. Dang[1]
E. Xenogiannopoulou[4], P. Lefèvre[3], N. Reyren[1], G. Patriarche[5], A. Lemaître[1], A. Dimoulas[4], R. Lebrun[1]
K. Abdukayumov[5], M. Chschiev[5], F. Ibrahim[5], M. Jamet[5], J.-M. George[1], S. Dhillon[2]
[1]*Université Paris-Saclay, 91767 Palaiseau, France*
[2]*Sorbonne Université, 75005 Paris, France*
[3]*Synchrotron SOLEIL, 91190 Saint-Aubin, France*
[4]*National Center for Scientific Research "Demokritos", 15310 Athens, Greece*
[5]*Université Grenoble Alpes, 38058 Grenoble, France*

Spintronics THz using ultrafast spin-currents generated by an ultrashort femtosecond laser optical pulse is at the heart of a new technology of THz emitters in the 0.1-30 THz window [1]. In those active spintronic structures and devices, the ultrafast spin-current generated from a ferromagnetic reservoir like played by a thin 3*d* transition metal layer under the optical excitation, is known to *i*) accelerate the demagnetization process within the ferromagnet itself and concomitantly *ii*) to relax at the interface with a material of a high-spin orbit coupling (SOC) giving rise to the generation of an ultrafast lateral charge current [1-4]. Such spin-charge conversion (SCC) process required for the observation of such emission in the femtosecond window are ensured either by the inverse spin Hall effect (ISHE) of 5d heavy metals (Pt, W, Ta) and/or by the inverse Rashba-Edelstein effect (IREE) at the interface with specific Rashba materials or three-dimensional topological insulators (TIs) [2-3]. In that prospect, the involvement of large spin-orbit interactions at the interface or at its vicinity are of a prime importance. Conversely, THz emission spectroscopy may then offer a very reliable probe to investigate ultrafast spin and charge currents to probe the spin-injection efficiency in devices. Typical systems either consist in nanometer-thin multilayers composed by a ferromagnetic (FM) layer and a heavy metal (HM) from the 3*d*-5*d* family giving rise to ISHE with well-engineered interfaces possibly integrating NIR optical cavity or Bragg reflector for the exciting laser pulse (650 nm - 2.6 um). Alternative path for THz emission as well as spin-orbit torque technologies now turns to bilayers of FM and topological insulator (TI). TIs present conductive topological surface states (TSS) with enhanced SOC strength which allow very efficient interfacial SCC *via* IREE [2-3]. From application perspective point of view, the THz output power generated from SCC is expected to be one order of magnitude larger than THz wave directly generated from TI surface by optical rectification effects [5].In the first part of the talk, we will demonstrate large ultrafast spin-charge interconversion and subsequent THz emission using the TSS of two type of quantum materials and related interfaces. In particular, we will report on THz emission features from dynamical spin-injection in $Bi_{1-x}Sb_x$ (with variable thickness from 2.5 to 50 nm) [6] and Bi_2SnTe_4 (5SL) [7]. In that systems, $Bi_{1-x}Sb_x$ are grown either by molecular beam epitaxy (MBE) or by sputtering methods. Epitaxial $Bi_{1-x}Sb_x$ ultrathin films and corresponding interface quality have been widely characterized by several complementary methods including XRD, TEM cross-section, transport characterization, Angular [8] and Spin-Resolved Photo-Emission Spectroscopy (ARPES and spin-ARPES) [4]. The latter experiments and data display clear electronic dispersion in both the valence band and within the gap representative of S_1 TSS and S_2 Rashba states. Moreover, spin-resolved ARPES reveals clear spin-momentum locking onto the S_1 and S_2 Fermi surface states, SML favorable to SCC and efficient THz emission [Figs.1 and 2].

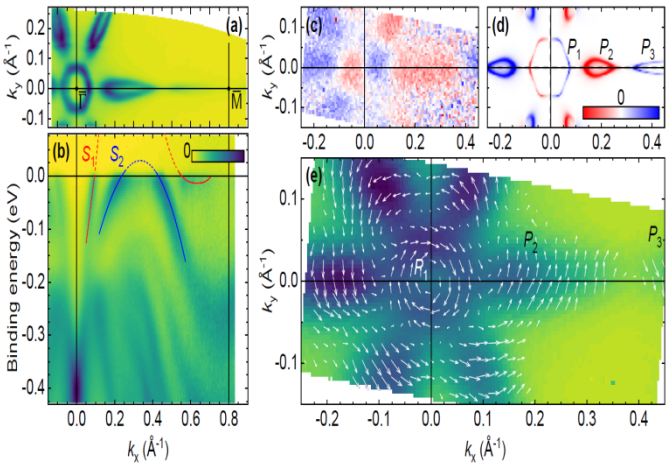

Fig.1. Spin-resolved surface states of a 5-nm $Bi_{0.85}Sb_{0.15}$ on Si (1 1 1). (a) *High-resolution ARPES at the Fermi energy* ***(b)*** *ARPES energy dispersion along the ΓM direction. The color bar represents the density of states in arb. units.* ***(c)*** *σ_y polarization DOS measured at the Fermi level where the color bar is proportional to the spin-polarization with scale extrema of P.S = ±0.1(T=300 K) and* ***(d)*** *corresponding TB modelling of the s-DOS projected on the first bilayer. The color bar indicates the spin polarization σ_y between $-\sigma_{max,y} \simeq -0.7$ and $\sigma_{max,y} \simeq +0.7$. (e) Color map representing the measured ARPES intensity close to Fermi energy integrated on 25 meV with arrows representing the measured spin polarization direction and amplitude (T=300 K). The different electron and hole pockets labeled P1, P2 and P3 in (d) are easily identified in the experimental measurements.*

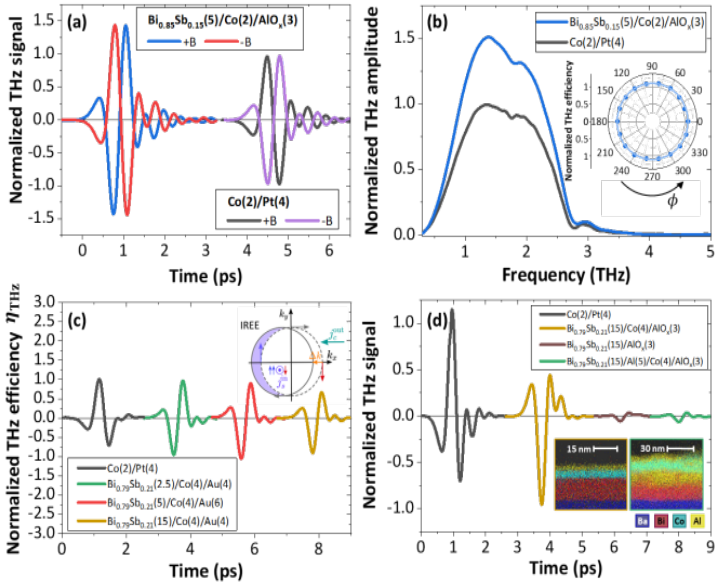

Fig.2. SCC and THz emission from $Bi_{1-x}Sb_x$/Co bilayers acquired at 300 K. (a) *THz time-trace from $Bi_{0.85}Sb_{0.15}$ (5)/Co(2)/AlOx(3) for ±B compared to Co(2)/Pt(4).*
b) *Spectral components of the THz emission from $Bi_{0.85}Sb_{0.15}$ (5)/Co(2)/AlOx(3) and Co(2)/Pt(4) for +B. Inset) Normalized THz efficiency η_{THz} dependence on the azimuthal angle φ.*
(c) *THz efficiency as a function of the $Bi_{0.79}Sb_{0.21}$ layer thickness (2.5, 5 and 15 nm) compared to Co(2)/Pt(4).*
*(**d**)THz signal$Bi_{0.79}Sb_{0.21}$(15)/Al(5)/Co(4)/AlOx(3), $Bi_{0.79}Sb_{0.21}$(15)/AlOx(3), $Bi_{0.79}Sb_{0.21}$(15)/Co(4)/ AlOx(3) on BaF_2 and Co(2)/Pt(4).*
Time traces are shifted in time for clarity. ***Inset)*** *Fluorescence map obtained from a TEM cross-section Bi0.79 $Sb_{0.21}$(15)/Co(4)/AlOx(3)(**brown frame**) $Bi_{0.79}Sb_{0.21}$(15)/Al(5)/Co(4)/AlOx(3)(**green frame**) grown on BaF_2.*

Electronic band structure calculations of $Bi_{1-x}Sb_x$ in the sp^3 tight-binding framework and subsequent SCC calculation response performed within the linear Kubo response theory accounts for the results observed of THz emission vs. $Bi_{1-x}Sb_x$ film thickness. On the other hand, the stoichiometry of Bi_2SnTe_4 explored in that present work has been chosen to minimize the presence of bulk bands at the Fermi crossing contrary to other Bi-based TIs such as Bi_2Se_3. Emission performances of $Bi_{0.79}Sb_{0.21}$ and Bi_2SnTe_4 are about the same order of magnitude as Co/Pt state-of-the-art spintronic THz emitters. Moreover, thickness-independent renormalized emission is demonstrated on Bi_2SnTe_4 is in favor of an interfacial SCC carried by IREE. In the second part of my talk, I will discuss our latest results of THz emission from SCC process generated by IREE occurring at the interface of 2-Dimensional $PtSe_2$ materials [9]. There, 2D materials, such as transition metal dichalcogenides, are ideal platforms as they possess strong SOC, reduced dimensionality and crystal symmetries and tunable electronic band structure compared to metals. Moreover, SCC can be tuned with the number of layers, electric field, or strain. Here, SCC in epitaxially grown 2D $PtSe_2$ and subsequent THz spintronic emission is studied since its 1T crystal allows it by symmetry. High quality of as-grown $PtSe_2$ layers is demonstrated, followed by in situ ferromagnet deposition by sputtering that leaves the $PtSe_2$ unaffected, resulting in well-defined clean interfaces as evidenced with extensive characterizations. Through this atomic growth control and using THz spintronic emission, the unique thickness-dependent electronic structure of PtSe2 allows the control of SCC. Indeed, the transition from IREE in 1–3 monolayers (ML) to the inverse spin Hall effect (ISHE) in multilayers (>3ML) of $PtSe_2$ enabling the extraction of the perpendicular spin diffusion length and relative strength of IREE and ISHE is demonstrated. This band structure flexibility makes PtSe2an ideal candidate to explore the underlying mechanisms and engineering of the SCC as well as for the development of tunable THz spintronic emitters.

References

[1] T. Seifert, S.Jaiswal, U.Martens, J.Hannegan, L. Braun, P. Maldonado, F. Freimuth, A. Kronenberg, J. Henrizi, I. Radu, E. Beaurepaire, Y. Mokrousov P. M.Oppeneer, M. Jourdan, G.Jakob, D.Turchinovich, L.M.Hayden, M.Wolf, M.Münzenberg, M.Kläui, T.Kampfrath, *Nature Photonics* **10**, 483 (2016)
[2] T. H. Dang, J. Hawecker, E. Rongione, G. Baez Flores, D. Q. To, J. C. Rojas-Sanchez, H. Nong, J. Mangeney, J. Tignon, F. Godel, S. Collin, P. Seneor M.Bibes, A. Fert, M. Anane, J.-M. George, L. Vila, M. Cosset-Cheneau, D. Dolfi, R. Lebrun, P. Bortolotti, K. Belashchenko, S. Dhillon, H. Jaffrès *Applied Physics Review* **7**, 041409 (2020).
[3] L. Cheng, Z. Li, D. Zhao, E.E. M. Chia, *APL Materials* **9**, 070902 (2021).
[4] J. Hawecker, T.-H. Dang, E. Rongione, J. Boust, S. Collin, J.-M. George, H.- J.Drouhin, Y. Laplace, R. Grasset, J. Dong, J. Mangeney, J. Tignon H. Jaffrès, L. Perfetti, S. Dhillon, Adv. Opt. Mater.2021,9, 2100412.
[5] S. Yang, L. Cheng, J. Qi, *Ultrafast Science* **3**, 0047 (2023).
[6] L. Baringthon, T.H.Dang, H.Jaffrés, N.Reyren, J.-M.George, M. Morassi, G. Patriarche, A.Lemaitre, F. Bertran, P. Le Févre, *Physical Review Materials* **6**, 074204 (2022).
[7] E. Rongione, L. Baringthon, D. She, G. Patriarche, R. Lebrun, A. Lemaître, M. Morassi, N. Reyren, M. Micica, J. Mangeney, J. Tignon, F. Bertran S. Dhillon, P. Le Févre, H. Jaffrès, J.-M. George, *Advanced Science* **10**, 2301124 (2023).
[8] E. Rongione, S. Fragkos, L. Baringthon, J. Hawecker, E. Xenogiannopoulou, P. Tsipas, C. Song, M. Mi˘cica, J. Mangeney, J.Tignon, T. Boulier N. Reyren, R. Lebrun, J.-M. George, P. Le Fèvre, S. Dhillon, A. Dimoulas, H. Jaffrès, *Advanced Optical Materials* **10**, 2102061 (2022).
[9] K. Abdukayumov, M. Mičica, F Ibrahim, L Vojáček, C. Vergnaud, A. Marty, J. Y. Veuillen, P. Mallet, I. Gomes de Moraes, D. Dosenovic S. Gambarelli, V. Maurel, A. Wright, J. Tignon, J, Mangeney, A. Uerghi, V. Renard, F. Mesple, J. Li, F. Bonell, H. Okuno, M. Chishiev, J.-M. George H. Jaffres, S. Dhillon, M. Jamet, *Advanced Materials*, 2304243 (2024).

Ultrafast magnetic field expulsion from optically driven $YBa_2Cu_3O_{6.48}$

G. Jotzu[2], S. Fava[1], G. De Vecchi[1], M. Buzzi[1], T. Gebert[1], Y. Liu[3], B. Keimer[3]
A. Cavalleri[4]
[1]*Max Planck Institute for the Structure and Dynamics of Matter, 22761 Hamburg, Germany*
[2]*Ecole Polytechnique Federale de Lausanne,1015 Lausanne, Switzerland.*
[3]*Max Planck Institute for Solid State Research, 70569 Stuttgart, Germany*
[4]*University of Oxford, Oxford OX1 3PU, United Kingdom*

Driving certain cuprates and organic materials has been shown to induce terahertz optical properties reminiscent of superconductivity far above the equilibrium transition temperature. So far, nothing is known regarding the magnetic response of these non-equilibrium states. Do they also show features equivalent to a Meissner effect, expelling a static external magnetic field? In this work, an underdoped cuprate sample, $YBa_2Cu_3O_{6.48}$ was placed in a weak static external magnetic field and driven with a phonon-resonant mid-infrared laser pulse. Under the same driving conditions, terahertz time-domain spectroscopy had previously shown superconducting-like optical properties [1-3]. The magnetic response of the material upon driving was probed using Faraday rotation in a magneto-optic material [4], positioned adjacent to the superconducting sample. We observe an ultrafast enhancement of the magnetic field at the edge of the sample, indicating light-induced diamagnetism. The degree magnetic field expulsion was comparable to that expected in an equilibrium type II superconductor of similar shape and size, with a volume susceptibility χ_V of approximately -0.3.

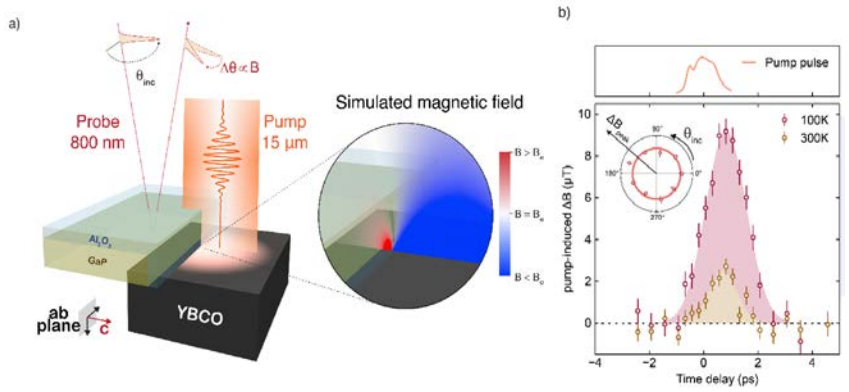

***Fig. 1. a) b)* Magnetic field expulsion after phonon excitation in $YBa_2Cu_3O_{6.48}$. (a)** Schematic of the experiment. A thin sapphire crystal is placed on top and next to the exposed side of the GaP (100) detection crystal to completely reflect the 15 µm pump. This also creates a well-defined edge in the mid infrared pump beam, shaping the photo-excited region into a half disc of ~ 375 µm diameter. The simulated changes due to local (quasi-static) magnetic field expulsion are also shown. The time-dependent magnetic field is sampled by positioning the probe beam in the vicinity of the edge of the photo-excited region.

(b) Pump-induced change in the measured magnetic field ΔB as function of pump-probe delay measured at two different temperatures of 100 K (red) and 300 K (**yellow**). The upper plot shows the cross-correlation of the pump and the probe pulses measured in-situ in a position adjacent to the sample. Its peak defines the time-zero in the delay scan. The inset shows the dependence of the peak value of the pump-induced magnetic field expulsion (ΔB_{peak}), measured via polarization rotation, on the input polarization angle θ_{inc} chosen for the probe pulse, showing a Faraday-type dependence. From [5]

We find that the effect persists up to temperatures of 300K and shows a similar scaling as the superfluid density extrapolated from terahertz conductivity measurements. For the weak magnetic fields (up to about 10mT) studied here, the effect remains linear, and it is an interesting question to examine if and where this state shows a non-linear magnetic field dependence. Terahertz measurements suggest that a light-induced superfluid density appears in a similar temperature and doping regime as the pseudogap state [1] and it will be insightful to investigate to which degree this also applies for light-induced flux expulsion. Furthermore, when studying a sample featuring a topological defect, the magnetic flux therein may be expected to be quantized, which could potentially be probed with the detection method presented here. Beyond superconductivity, ultrafast magnetometry also opens up new avenues in the study of driven magnetic phenomena and potentially of light-induced topologically protected edge currents.

References

[1] S. Kaiser, C. R. Hunt, D. Nicoletti, W. Hu, I. Gierz, H. Y. Liu, M. Le Tacon, T. Loew, D. Haug, B. Keimer, A. Cavalleri, *Physical Review* B **89** 184516 (2014).
[2] W. Hu, S. Kaiser, D.Nicoletti, C.R. Hunt, I.Gierz, M.C. Hoffmann, M.Le Tacon, T.Loew,B. Keimer, A. Cavalleri, *Nature Materials* **13**,705 (2014)
[3] B Liu, M Först, M Fechner, D Nicoletti, J Porras, T Loew, B Keimer, A Cavalleri, *Physical Review* X **10**, 011053 (2020).
[4] J. A. Riordan, X.-C. Zhang, X.-C. *Optical and Quantum Electronics* **32**, 489 (2000).
[5] S. Fava, G. De Vecchi, G. Jotzu, M. Buzzi, T. Gebert, Y. Liu, B. Keimer, A. Cavalleri, *arXiv*:2405.00848, in print *Nature* (2024).

* Acknowledgement(s) : the research leading to these results received funding from the European Research Council under the European Union's Seventh Framework Programme (FP7/2007-2013) / ERC Grant Agreement No. 319286 (QMAC). We acknowledge support from the Deutsche Forschungsgemeinschaft (DFG) via the Cluster of Excellence 'The Hamburg Centre for Ultrafast Imaging' (EXC 1074 – project ID 194651731) and the priority program SFB925 (project ID 170620586).

Quantum algorithms for dynamics and dynamical observables

A. F. Kemper
North Carolina State University, Raleigh, NC 27606, USA

Response functions are a fundamental aspect of physics; they represent the link between experimental observations and the underlying quantum many-body state. In particular, dynamical response functions are part of the toolbox that physicists use to unravel the nature of correlated matter. In this talk, I will discuss some aspects of obtaining response functions on quantum computers. First, I will introduce a new method for measuring response functions by using a linear response framework and making the experiment an inextricable part of the quantum simulation [1]. This method can be frequency- and momentum-selective, avoids limitations on operators that can be directly measured, and is ancilla-free. As prototypical examples of response functions, we demonstrate that both bosonic and fermionic Green's functions can be obtained, and apply these ideas to the study of a charge- density-wave material. The linear response method provides a robust framework for using quantum computers to study systems in physics and chemistry. It also provides new paradigms for computing response functions on classical computers. I will illustrate the use of this idea for equilibrium and non-equilibrium Green's functions. Second, I will discuss some of our recent work that uses a little-known property of Green's functions – and in particular Green's functions – to eliminate a large portion of the noise resulting from NISQ quantum computers. Green's functions are positive definite functions[2,3], a fact that high constrains the relationship between the values of the Green's function at each point in time. We make use of this by insisting that the measured (discretized) Green's function forms a positive semi-definite matrix, and project the noisy data onto the nearest positive function.

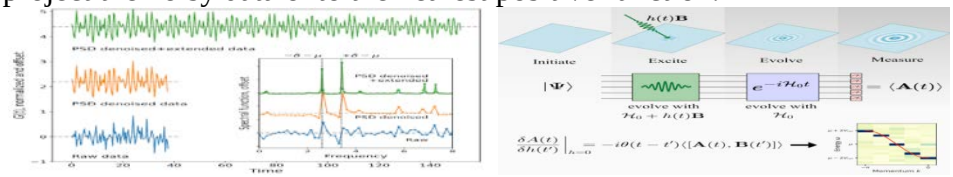

***Fig. 1. Left** :Linear response framework for quantum simulation of correlation functions[1]: **Right**:Denoising quantum simulation data by positive definite projection..*

The overall idea of these works is to get quantum computers to produce quantities that are relevant for condensed matter physics and other natural sciences. Dynamical correlation functions are key in that they provide a direct connection to experiments.

References
[1] E. Kökcü, H.A. Labib, J.K. Freericks, A.F. Kemper, *arXiv:2302.10219* (2024).
[2] A.F. Kemper, C. Yang, E. Gull, *Physical Review Letters* **132**, 160403 (2024)
[3] Y. Yu, A.F. Kemper, C. Yang, E. Gull, *arXiv:2403.12349* (2024).

Enhancing optical clocks and quantum sensors through spatial multiplexing

X. Zheng, J. Dolde, M.C. Cambria, S. Chand, S. Kolkowitz
University of California Berkeley, Berkeley, CA 94720, USA

Quantum sensors offer unique capabilities such as unprecedented spatial resolution or unparalleled accuracy and precision. However, despite their remarkable performance metrics, most quantum sensors today operate by uniformly interrogating a single quantum systesm or ensemble using a standard spectroscopy technique such as Ramsey or Rabi spectroscopy. In this talk I will explain the motivation and operating principles of two novel spatially multiplexed quantum sensors that move beyond this paradigm, enabling novel measurements and enhanced performance. I will first introduce our multiplexed strontium optical lattice clock, which consists of two or more atomic ensembles of trapped, ultra-cold strontium in one vacuum chamber. This miniature clock network enables us to bypass the primary limitations to typical atomic clock comparisons and achieve new levels of precision [1]. I will present on recent experimental results in which we make use of multiple atomic ensembles to perform enhanced phase estimation and demonstrate a reduced absolute instability of an optical lattice clock [2]. I will also briefly present the results of a blinded, laboratory-based precision test of the gravitational redshift at the millimeter to centimeter scale [3].

***Fig. 1**: we demonstrate that by splitting the atoms in an optical lat tice clock up into multiple spatially resolved atomic ensembles, we can more precisely measure the frequency difference between the atomic transition and the clock laser to realize a more stable clock.*

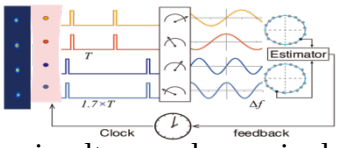

Finally, I will briefly discuss a novel experimental platform we have developed for simultaneously manipulating and independently measuring many single NV centers in parallel[4]. This approach enables parallelization of quantum sensing with nanometer scale spatial resolution while also unlocking the potential of nanoscale covariance magnetometry for the study of complex phases and many-body dynamics in condensed matter systems [5].

References
[1] X. Zheng, J. Dolde, V. Lochab, B.N. Merriman, H. Li, S. Kolkowitz, *Nature* **602**, 425(2022).
[2] X. Zheng, J. Dolde, S. Kolkowitz, *Physical Review X*, **14**, 011006 (2024).
[3] X. Zheng, J. Dolde, M.C. Cambria, H.M. Lim, S. Kolkowitz, *Nature Communications* **14**, 4886 (2023).
[4] M.C. Cambria, S. Chand, S. Kolkowitz, *in preparation for submission* (2024).
[5] J. Rovny, Z. Yuan, M. Fitzpatrick, A.I. Abdalla, L. Futamura, C. Fox, M.C. Cambria, S. Kolkowitz, N.P. de Leon, *Science* **378**, 6626 (2022).

Lightwave electronics and quantum information

M. Kira
University of Michigan, Ann Arbor, MI 48109, USA.

Conventional light–matter interaction processes are driven by absorption where a photon induces an efficient transition between two matter states whose energy difference is resonant with the photon energy. The resulting processes are often relatively slow because they require several field oscillations to match energies of light and matter. But photon energy becomes less relevant when a lightwave is made so strong that already its momentary peak field can efficiently translate electrons on time scales much faster than its half cycle by the force it exerts to electrons. This idea has opened a completely new temporal scope for explorations in condensed matter—lightwave electronics where the carrier wave (not photon energy) drives electronic coherences much faster than electronic scattering occurs. In other words, lightwave electronics operates through intense optical-carrier waves as ultrafast biasing fields that drive the quantum flow of electrons and coherences on timescales faster than an oscillation cycle of light. Consequently, lightwave electronic control may seamlessly convert quantum states between light and matter to create quantum chips that exploit electronics for efficient interactions while optics for speed or long coherence lifetimes. The current repertoire [1] includes quasiparticle colliders that have unveiled the actors behind various quantum phenomena; all-optical band-structure reconstruction that have quantified quantum materials and topology in ambient; attoclocks that have measured electronic interaction dynamics of diverse quantum phenomena; ultrafast electron videography that have followed electronic reactions unfold; efficient light sources and conversion that could create compact chips; and petahertz electronics that could speed up traditional semiconductor electronics million fold. This evolution has been so rapid that lightwave electronics is poised to control and process quantum information via lightwave-driven multi-electron interactions proceeding at unprecedented speeds and precision, as visioned in Fig. 1.

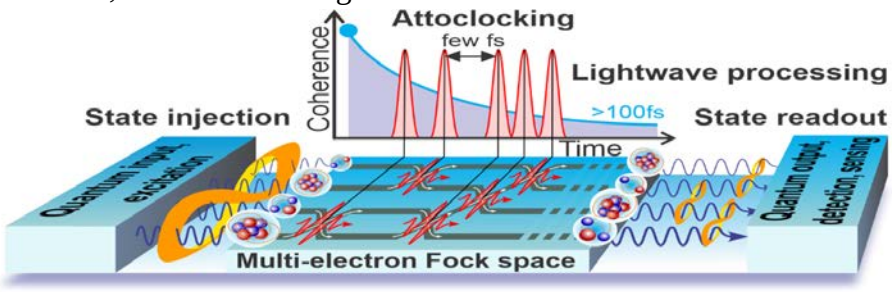

Fig. 1. Vision of lightwave electronic quantum-information processing.

The first steps include flipping a so-called valleytronic electronic quantum state of coherent electrons in less than 5 fs [2], detecting precise electronic state(s) within quantum material's band structure [3], and attoclocking multi-electron interactions [4]. These advancements promise to transform semiconductor technology into a domain a million times faster than present electronic capabilities. With precision control over multi-electron effects, lightwave electronics is carving a path toward integrating, modulating, timing, and characterizing sequences that will not only elucidate emergent quantum correlations but also construct versatile and scalable quantum information technologies, harmoniously integrated with traditional semiconductor systems. Following these ideas, I will present the key opportunities and challenges lightwave electronics could take on to combine, control, (atto)clock, and characterize lightwave sequences to both explore emergent quantum phenomena in semicondoctor quantum materials—also including quantum-functionalized conventional semiconductors[5,6]—and to build both coherent classical and quantum-information technology.

References

[1] M. Borsch, M. Meierhofer, R. Huber, M. Kira, *Nature Review Materials* **8**, 668 (2023).
[2] F. Langer, C. P. Schmid, S. Schlauderer, M. Gmitra, J. Fabian, P. Nagler, C. Schüller, T. Korn, P.G. Hawkins, J.T. Steiner, U. Huttner, S. W. Koch M. Kira, R. Huber, *Nature* **557**, 76 (2018).
[3] M. Borsch, C. P. Schmid, L.Weigl, S. Schlauderer, N. Hofmann, C. Lange, J. T. Steiner, S. W. Koch, R. Huber, M. Kira, *Science* **370**, 1204 (2020).
[4] J. Freudenstein, M. Borsch, M. Meierhofer, D. Afanasiev, C. P. Schmid, F. Sandner, M. Liebich, A. Girnghuber, M. Knorr, M. Kira R. Huber, *Nature* **610**, 290 (2022).
[5] P. Wang, W. Lee, P. Corbett, W. H. Koll, N. M. Vu, D. A. Laleyan, Q. Wen, Y. Wu, A. Pandey, J. Gim, D. Wang, D. Y. Qiu, R. Hovden, M. Kira J. T.Heron, J.A. Gupta, E. Kioupakis, Z. Mi, *Advanced Materials* **34**, 2201387 (2022).
[6] Y. Wu, X. Liu, P. Wang, D. Laleyan, K. Sun, Y. Sun, C. Ahn, M. Kira, E. Kioupakis, Z. Mi, *Applied Physics Letters* **116**, 1013101 (2020).
* Acnoledgment(s):tThe experimental part of this work is performed by Rupert Huber (Univ. Regensburg), Steven Cundiff (Univ. Michigan), and Zetian Mi (Univ. Michigan) groups. This work is supported by ARO through Award W911NF1810299, W.M. Keck Foundation, and NSF through awards No. 2118809 and No. 2235377.

Dark excitons in atomically thin semiconductors and How to make them bright

A.Knorr, M.Katzer, D.Christiansen, L.Greten
Technische Universität Berlin, 10623 Berlin, Germany

Atomically thin semiconductors constitute a remarkable playground for exciton physics in two dimensions. This involves optically accessible (bright) as well as spin- and momentum-forbidden (dark) excitonic states for intra- and interlayer excitations. Momentum-dark excitons outside the optical light cone can typically be excited by momentum transfer resulting from phonon scattering [1], or by spatially structured optical near-fields [2-4] and directly studied by photoelectron spectroscopy [5]. In this talk, we theoretically address the following questions: (a) whether - at increasing densities and under exciton-phonon scattering - dark excitons can be approximated as a weakly interacting boson gas or are possibly dominated by their fermionic substructure [1], (b) how spatially structured near-fields can be induced by nanostructures (such as molecules [3] or metal nanoparticles [4]) to excite dark in-plane excitons, and (c) how dark exciton dynamics can be followed via tr-ARPES [5]

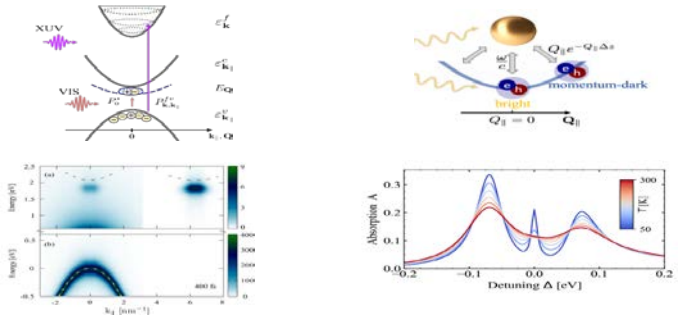

Fig. 1. Left: *Two pulse excitation scheme for tr-ARPES in a three band system involving excitons and the ionization continuum (**top**); calculated ARPES signal at delay time 400fs showing valence band excitations, intravalley and intervalley excitons formed after exciton-phonon scattering (**bottom**).*
Right*: Near-field coupling of gold metal nanoparticle plasmons to dark excitons with Q>0, the coupling for bright excitons vanishes (Q=0) (**top**); Spectral absorption of the coupled exciton – plasmon hybrid, showing peak splitting from strong coupling of dark excitons and plasmons, whereas bright excitons occur undisturbed as a central peak (**bottom**).*

Throughout the talk, a comparison with recent experiments (absorption, luminescence and angle resolved photoemission spectroscopy) will be provided.

References
[1] M. Katzer, M.Selig, L. Sigl, M. Troue, J. Figueiredo, J. Kiemle, F. Sigger, U. Wurstbauer, A. W Holleitner, A. Knorr, *Physical Review* B **108,** 121102 (2023).
[2] M. Katzer, S. Kovalchuk, K.Greben, K. I Bolotin, M. Selig, A. Knorr, *Physical Review* B **107**, 035304 (2023).
[3] R. Salzwedel, L.Greten, S.Schmidt, S.Hughes, A.Knorr, M.Selig, *Physical Review* B **109**, 035309 (2024).
[4] L. Greten, R. Salzwedel, T. Göde, D.Greten, S.Reich, S.Hughes, M.Selig, A. Knorr, *ACS Photonics* **11**, 1396 (2024).
[5] D. Christiansen, M.Selig, E.Malic, R.Ernstorfer, A. Knorr, *Physical Review* B **100**, 205401 (2019).

*Stochastic switching of sub-THz magnon*s in an orthoferrite revealed by Femtosecond spin-noise spectroscopy

T. Kurihara[1], M. A. Weiss[2], A. Herbst[2], J. Schlegel[2], T. Dannegger[2], M. Evers[2], A.Donges[2], M. Nakajima[3]
S. T. B. Goennenwein[2], U. Nowak[2], A. Leitenstorfer[2]
[1]The University of Tokyo, 277-8581, Kashiwa, Japan
[2] University of Konstanz, D-78457 Konstanz, Germany
[3] Osaka University, 565-0871 Osaka, Japan

Observation of antiferromagnetic spin dynamics at ultrafast timescales has conventionally been studied using pump-probe spectroscopy, which in principle is a perturbative technique that measures an excited state of the system induced by pump pulses. In contrast, one of the peculiarities of the sub-THz frequency range is that it lies below the thermal energy at ambient conditions and therefore, incoherent magnon dynamics occurs spontaneously due to thermal excitation. Such a dynamics should have significant contributions to the state of matter, but it is difficult to measure with traditional pump-probe spectroscopy where only the average change of the probed quantity is detected upon photoexcitation. To access spontaneous thermal dynamics in spin systems, we have developed a technique called *femtosecond noise correlation spectroscopy*. The principle is based on real-time statistical processing of the correlated noise encoded in two time-delayed femtosecond probe pulse sequences transmitted through the sample [1]. This approach allows us to visualize the temporal autocorrelation of the magnon dynamics with femtosecond resolution. By this way, we successfully observed the critical enhancement and softening of thermal magnons in the orthoferrite $Sm_{0.7}Er_{0.3}FeO_3$ [2] in the temperature region close to spin reorientation transition [3].

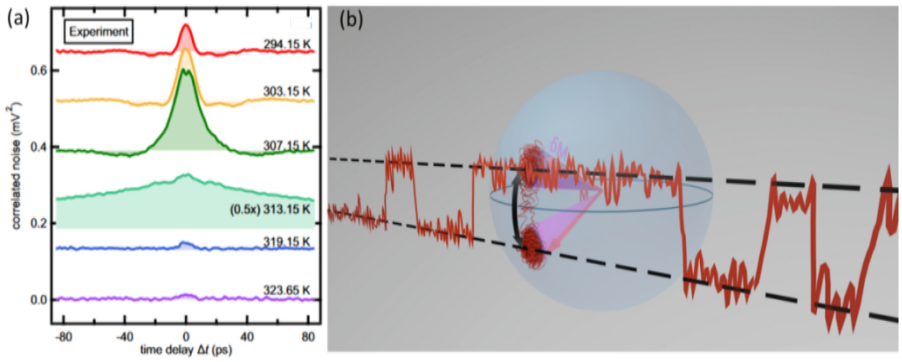

Fig.1. (a) Temporal autocorrelation profile of the magnon noise *in* $Sm_{0.7}Er_{0.3}FeO_3$ *around the spin reorientation transition temperature, as measured by femtosecond noise correlation spectroscopy* [3]. ***(b)Schematic representation of random telegraph noise*** *induced by thermal excitation in a double-well potential.*

Comparison to a stochastic, large-scale Landau-Lifshitz-Gilbert simulation shows that such an enhancement is related to the stochastic switching dynamics of magnetization within a double-well anisotropy potential landscape, often called random telegraph noise (RTN).

References
[1] M. A. Weiss, F. S. Herbst, S. Eggert, M. Nakajima, A. Leitenstorfer, S. T. B. Goennenwein, T. Kurihara, *submitted* (2024).
[2] G. Fitzky, M. Nakajima, Y. Koike, A. Leitenstorfer, T. Kurihara, *Physical Review Letters* **127**, 107401 (2021).
[3] M. A. Weiss, A. Herbst, J. Schlegel, T. Dannegger, M. Evers, A. Donges, M. Nakajima, A. Leitenstorfer, S. T. B. Goennenwein, U. Nowak T. Kurihara, *Nature Communications* **14**, 7651 (2023).

Emission of coherent THz magnons in an antiferromagnetic insulator triggered by Ultrafast spin-phonon interactions

E. Rongione[1], O. Gueckstock[3], M. Mattern[4], O. Gomonay[5], H. Meer[5], C. Schmitt[5], R. Ramos[6], M. Mičica[2]
E. Saitoh[8], J. Sinova[5], S. Massabeau[1], J-M. George[1], H. Jaffrès[1], S. T. B. Goennenwein[7], S. Geprägs[8]
T. Kampfrath[3], M. Kläui[5], M. Bargheer[4], T. S. Seifert[3], S. Dhillon[2], R. Lebrun[1]
[1] *Université Paris-Saclay, 91767 Palaiseau, France*
[2] *Université Paris Cité, 75005 Paris, France*
[3] *Freie Universität Berlin, 14195 Berlin, Germany4*
[4] *Universität Potsdam,14476 Potsdam, Germany*
[5] *Johannes Gutenberg-University Mainz, 55128 Mainz, Germany*
[6] *Tohoku University, Sendai 980-8577, Japan*
[7] *University of Konstanz, 78457 Konstanz, Germany*
[8] *Walther-Meißner-Institut,85748 Garching, Germany*

Antiferromagnets have a strong potential for future spintronic devices due to their insensitivity to perturbative external magnetic fields, absence of stray fields, and for accessing to frequencies from GHz to the terahertz (THz) regime [1–3]. However, their functionalization in thin films remains a challenging task, and requires to access and manipulate their THz resonance modes. In this talk, I will discuss how we can generate coherent THz antiferromagnetic magnons triggered by fs pulses in thin films of NiO capped with platinum [4] and detect them using THz time-domain spectroscopy (Fig. 1a).

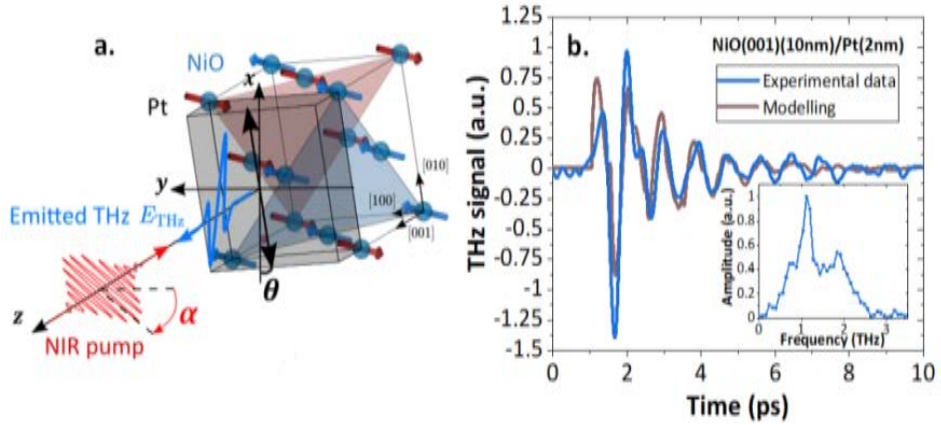

Fig. 1. Laser induced coherent and incoherent THz emission *from NiO/Pt bilayer.* ***(a)*** *Schematic of the setup.* ***(b)*** *THz emission from a low damping NiO(001)(10nm)/Pt(2nm) bilayer showing 1 ps oscillations* ***(exp.: blue, model: brown)****.*

The generated THz signal has two main components as shown in Fig. 1b: i) a broadband contribution (up to 3 THz) alongside ii) a narrowband contribution centred at 1.1 THz. The latter can be associated with the THz radiation of high-frequency AFM mode of NiO. We then evidence that the THz magnon currents can be detected by THz inverse spin Hall effect in the heavy metal layer.
I will then highlight that the THz magnon excitation arises either off-resonant optical spin-torque or from spin-phonon interactions (including ultra-fast strain and spin-Seebeck) depending on the growth orientation. Using ultrafast X-ray diffraction, we thus evidence the presence of an ultra-strain wave that can effectively trigger an out-of-plane precession of the Neel vector in NiO via dynamical magneto-striction in these compounds.Finally, I will discuss how these observations could be extended to other antiferromagnetic systems and how these results opens promising perspectives for the development of narrowband and controllable THz spintronic devices using insulating AFMs.

References

[1] R.Cheng, D. Xiao, A. Brataas, *Physical Review Letters* **116**, 207603 (2016).
[2] J. Li, C. B. Wilson, R. Cheng, M. Lohmann, M. Kavand, W. Yuan, M. Aldosary, N. Agladze, P. Wei, M. S. Sherwin, J. Shi, *Nature* **578**, 70 (2020).
[3] I. Boventer, H. T. Simensen, A. Anane, M. Kläui, A. Brataas, R. Lebrun, *Physical Review Letters* **126**, 187201 (2021).
[4] E.Rongione, O.Gueckstock,M.Mattern, O.Gomonay, H.Meer, C.Schmitt, R.Ramos,T. Kikkawa, M.Mičica, E.Saitoh, J. Sinova, H. Jaffrès, J. Mangeney S.T.B. Goennenwein, S.Geprägs, T.Kampfrath, M. Kläui, M. Bargheer, T. S. Seifert, S. Dhillon, R. Lebrun, *Nature Communications* **14**, 1818 (2023).

Probing quantum materials: nonlinear THz spectroscopy

P. H.M. van Loosdrecht
University of Cologne, 50937 Cologne, Germany

Non-linear THz spectroscopy has developed into a sensitive and effective method to probe electrodynamics and electronic properties of quantum materials. Very efficient THz high-harmonic generation in Dirac materials, such as graphene [1] and the 3D Dirac semimetal Cd_3As_2 [2], has been reported, originating from the linear dispersion in these materials. In superconductors, coupling of the THz field to the Higgs mode also leads to a pronounced non-linear THz response [3], as does the non-Fermi liquid state in CaRuO3 [4], see Fig. 1. Apart from high-harmonic generation, the non-linear THz response can also provide insights into the coupling between for instance magnons and phonons in magnetically ordered materials, as is for instance found in antiferromagnetic CoF_2 [5].

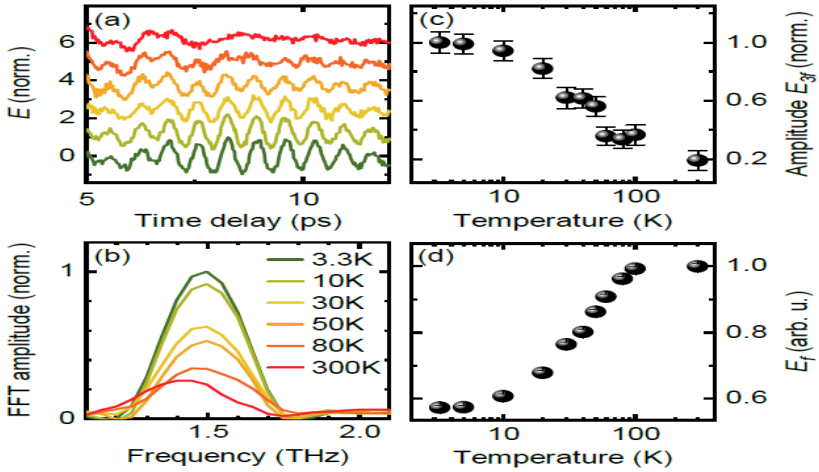

Fig. 1. Non-linear THz response *of $CaRuO_3$ as a function of temperature showing the correlation with the formation of heavy quasi-particles with non-Fermi liquid behavior at low temperatures.* ***(a)*** *Third-harmonic THz signal in time domain at different temperatures.* ***(b)*** *Fourier amplitude of the signal in panel (a).* ***(c)*** *THG amplitude E_{3f} and* ***(d)*** *the transmitted amplitude E_f of the fundamental frequency as a function of temperature. Taken from ref. [4].*

This contribution will present some of the recent achievements in this field, and discuss the underlying mechanisms leading to the non-linear THz response.

References

[1] H. A. Hafez, S. Kovalev, J.-C. Deinert, Z. Mics, B. Green , N. Awari, M. Chen, S. Germanskiy, U. Lehnert, J. Teichert, Z. Wang, K.-J. Tielrooij Z. Liu, Z.Chen, A.Narita, K.Müllen , M. Bonn, M.Gensch, D.Turchinovich, *Nature* **561**, 507 (2070).
[2] S. Kovalev, R. M. A.Dantas, S. Germanskiy, J.- C. Deinert, B. Green, I. Ilyakov, N. Awari, M. Chen, M. Bawatna, J. Ling, F. Xiu P. H. M. van Loosdrecht, P. Surówka, T. Oka, Z. Wan, *Nature Communications* **11**, 2451 (2020).
[3] R. Shimano, N. Tsuji, *Annual Review of Condensed Matter Physics* **11**, 103 (2020).
[4] C. Reinhoffer, S. Esser, S. Esser, *Physical Review Letters*, in print(2024).
[5] T. W.J. Metzger, K.A. Grishunin, C. Reinhoffer, R.M. Dubrovin, A. Arshad, I. Ilyakov, arXiv,org/abs/2308.01052 (2023).

Real-time observations reveal new opportunities on the ultrafast time in Nanostructured quantum materials

E. Janod[1], S. Iwai[2], H. Cailleau[3], C. Mariette[4], S. Ohkoshi[5], H. Tokoro[6], M. Lorenc[3]
[1]*Nantes Université, 44000 Nantes, France*
[2] *Tohoku University, Sendai 980-8578, Japan*
[3]*Universite de Rennes, 35000 Rennes, France*
[4]*European Synchrotron Radiation Facility, 38043 Grenoble, France.*
[5]*The University of Tokyo, Tokyo 113-0033, Japan*
[6]*University of Tsukuba, Tsukuba 305-8577, Japan*

Ultrafast light and electrical pulses can induce new functionality in quantum materials [1] not accessible via the application of conventional thermodynamic parameters like temperature or pressure [2]. The non-equilibrium pathways hold great technological potential [3] and topical examples include insulator to metal transitions (IMT) for optical memories [4] or neural networks for AI [5]. From fundamental standpoint, several degrees of freedom couple during such transformations, which gives rise to multiscale dynamics in time and space. While structural reorganizations often play an important role in the stabilization of the newly formed electronic state, the establishment of a new macroscopic structural order requires long-range crystalline deformations, involving the propagation of acoustic waves. In a recent work, we evidenced a macroscopic transformation pathway from semiconductor to metal in nanocrystals of trititanium pentaoxide (Ti_3O_5) [6],that involved generation and propagation of volumic strain waves. In another example, we studied a prototypical Mott insulator V_2O_3, a widely considered test bed for investigating and benchmarking the out-of-equilibrium models for quantum materials. V_2O_3 is metallic at room temperature and undergoes a first order transition below 150 K towards an insulating phase involving antiferromagnetic and ferroelastic symmetry breakings (AFI). In addition, this transition also involves a non-symmetry-breaking volume expansion (~ +1.4%). Transient reflectivity studies of V_2O_3 in the AFI phase have unveiled a transformation within time consistent with the acoustic propagation of strain waves. Astoundingly, transformation yield of up to 100% at and above a threshold laser fluence (~2 $mJ.cm^{-2}$) can be achieved. Importantly, this observation persisted for low energy of the exciting photon (0.89 eV, just above the Mott-Hubbard gap value of 0.75 eV [7]) and at low temperature down to 10 K, hence precluding trivial heating process. The granular morphology of the V_2O_3 films favors complete transformation to the metallic phase, unlike a single crystal where in-plane clamping takes place and seems to be a hinderance to the photoinduced IMT [8]. The ultrafast x-ray diffraction on thin films revealed volume contraction and confirmed the quasi-complete transformation to metallic phase on the acoustic time-scale of strain waves, as observed in the optical studies. Also, the data indicate symmetry change within each single ferroelastic domain on a faster time scale than the volume change through the film. We suspect triggering a sequence of phase change phenomena: first a non-equilibrium transition towards a high symmetry/high volume insulating phase within ferroelastic domains, then a metallic phase of high symmetry/low volume through the film. In brief, we discuss how structure and morphology can provide with control knobs [6,9] in the fast-growing field of photoinduced phase transitions, and material science at large. The above mentioned findings may stimulate further theoretical developments and guide the assessment of the ultimate performance of ultrafast devices based on Mott insulators and alike.

References

[1] A. de la Torre, D. M. Kennes, M. Claassen, S. Gerber, J.W. McIver, M. A. Sentef, *Review of Modern Physics* **93**, 041002 (2021).
[2] Y. Tokura, M. Kawasaki, N. Nagaosa, *Nature Physics* **13**, 11 (2017).
[3] A. Sood , X. Shen, Y. Shi, S. Kumar, S. J. Park, M. Zajac, Y. Sun, L.-Q. Chen, S. Ramanathan, X. Wang, W. C. Chueh, A. M. Lindenberg *Science* **373**, 352 (2021).
[4] S.- I. Ohkoshi, Y. Tsunobuchi, T. Matsuda, K. Hashimoto, A. Namai, F. Hakoe, H.Tokoro, *Nature Chemistry* **2**, 539 (2010).
[5] V. Guio, L. Cario, E. Janod, B. Corraze, V. Ta Phuoc, M. Rozenberg, P. Stoliar, T. Cren,D. Roditchev, *Nature Communication* **4**, 1 (2013).
[6] C. Mariette, M. Lorenc, H. Cailleau, E. Collet, L. Guérin, A. Volte, E. Trzop, R. Bertoni, X. Dong, B. Lépine, O. Hernandez, E. Janod L. Cario, V. Ta Phuoc, S. Ohkoshi, H. Tokoro, L. Patthey, A. Babic, I. Usov, D. Ozerov, L. Sala, S. Ebner, P. Böhler, A. Keller, A. Oggenfuss T. Zmofing, S. Redford, S. Vetter, R. Follath, P. Juranic, A. Schreiber, P. Beaud, V. Esposito, Y. Deng, G. Ingold, M. Chergui, G. F. Mancini R. Mankowsky,C.Svetina,S.Zerdane,A.Mozzanica,A.Bosak,M.Wulff, M.Levantino, H.Lemke,M.Cammarata, *Nature Communications* **12**, (2021).
[7] G. A. Thomas, D. H. Rapkine, S. A. Carter, A. J. Millis, T. F. Rosenbaum, P. Metcalf, J. M. Honig**,** *Physical Review Letters* **73,** 1529 (1994)
[8] A. von Reppert, L.Willig,J.-E. Pudell,M. Rössle,W.Leitenberger,M.Herzog,F.Ganss,O.Hellwig, M.Bargheer, Applied Physics Letters **113**, (2018)
[9] T. Amano, D. Babich, R. Mandal, J. Guzman-Brambila, A. Volte, E. Trzop, M. Servol, E. Pastor, M. Alashoor, J.Larsson,A.Jurgilaitis,V.-T. Pham D. Kroon,J.C. Ekström, B. Ahn,C,Mariette,M. Levantino,M. Kozhaev, J. Tranchant, B.Corraze, L. Cario, V.T. Phuoc, R. Sopracase, M. Grau, H. Itoh Y. Kawakami, Y. Nakamura, H.Kishida, H.Cailleau, M.Lorenc, S.Iwai, E.Janod, *doi.org/10.21203/rs.3.rs-3239079/v1* (2023).

High-field long wavelength ultrafast laser sources and their applications

G. Dalla-Barda[2], P. Lassonde[1], G. Jargot[1], E. Haddad[1], A. Laramée[1]
A. Leblanc[3], H. Ibrahim[1] E. Cormier[4], F. Légaré[1]
[1] *Institut National de la Recherche Scientifique, Varennes, QC J3X1S2, Canada*
[2] *Université de Bordeaux, 33400 Talence, France*
[3] *Laboratoire d'Optique Appliquée, 91762 Palaiseau, France*
[4] *Institut Universitaire de France 75231Paris, France*

For a decade, a number of ultrafast science applications [1-3] involve high-field coherent radiation in the mid-infrared region, motivating the development of such laser sources. In this context, we have designed an optical setup able to generate few-cycle pulses around 10 µm, with 20 µJ of energy per pulse providing carrier-to-envelop phase (CEP) stability and control [4]. As depicted in figure 1, the laser source is based on a frequency domain optical parametric amplifier (FOPA) [5], coupled with intrapulse difference frequency generation (DFG). From an incident pulse of 45 fs at 800 nm, two spectral bands around 1.8 µm are amplified and shaped in the FOPA before being converted to the mid-infrared by DFG.

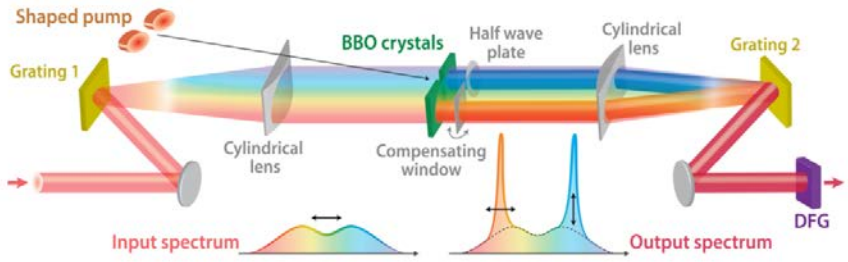

Fig. 1. FOPA used as a dual-band amplifier. *Two spectral bands of an incident pulse are amplified in two independent BBO crystals located in the Fourier plane of a 4f-setup. The polarization of one slice is rotated by a half waveplate and the delay between the two slices can be tuned by tilting a compensating window. A final DFG stage converts the output to the mid-infrared.*

Through this innovative architecture, the wavelength of the resulting mid-infrared pulse can be adjusted by changing the spectral bands amplified in the FOPA. As shown, in the figure 2, we are demonstrating a wavelength tunability from 5.6 µm to 13.5 µm for pulse durations within 50 fs and 120 fs, corresponding to pulse durations ranging from 6.4 to 1.3 optical cycles. The temporal shapes have been characterized by the Frequency Resolved Optical Switching technique (FROSt) [6], a phase-matching free approach insensitive to the wavelength. For this measurement, a near-infrared pump pulse of around 50 µJ and 100 fs induces an ultrafast switch in the transmissivity of a Germanium crystal, while the mid-infrared pulse probes the transmission at different pump-probe delays. A phase retrieval algorithm is then applied to retrieve both temporal amplitude and phase of the probe pulse. To summarize, this work proposes a highly flexible solution for ultrafast science applications including the complete toolbox of generation and also temporal characterization of few-cycles pulses in the mid-infrared spectral range.

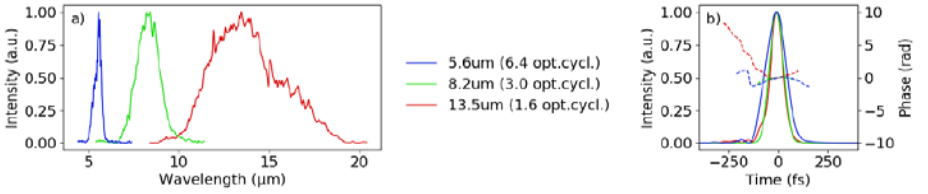

Fig. 2. Left*:**spectrum of the mid-infrared source** at 5.6 µm **(blue)**, 8.2 µm **(green)** and 13.5 µm **(red)** with corresponding.*
Right*: temporal amplitude (solid lines) and phase (**dashed lines**) characterized by FROSt.*

To summarize, this work proposes a highly flexible solution for ultrafast science applications including the complete toolbox of generation and also temporal characterization of few-cycles pulses in the mid-infrared spectral range.

References

[1] J. Li, X .Ren, Y. Yin, K. Zhao, A. Chew, Y. Cheng, E. Cunningham, Y. Wang, S.Hu, Y. Wu, M. Chini, Z,Chang, *Nature Communications* **8,** 1 (2017)
[2] U. Frühling, M. Wieland, M. Gensch, T. Gebert, B. Schütte, M. Krikunova, R. Kalms, F. Budzyn, O. Grimm, J. Rossbach, E. Plönjes, M.Drescher *Nature Photonics* **3**. 523 (2009).
[3] S. Ghimire, A.D. DiChiara, E. Sistrunk, P. Agostini, L.F. DiMauro, D.A. Reis, *Nature Physics* **7**, 138 (2011).
[4] A. Leblanc , G. Dalla-Barba, P.Lassonde, A.Laramée, B.E Schmidt, E.Cormier, H.Ibrahim, F. Légaré, *Optics Letters* **45**, 2267 (2020).
[5] A. B. Schmidt, S. Berner, W. Schimpf, C. Müller, T. Lickert, N. Schwaderlapp, S. Knecht, J. G. Skinner, A. Dost, P. Rovedo, J. Hennig D. von Elverfeldt. J. -B. Hövener. *Nature Communications* **5**. 1 (2014).
[6] A. Leblanc, P. Lassonde, S. Petit, J.-C. Delagnes, E. Haddad, G. Ernotte, M. R. Bionta, V. Gruson, B. E. Schmidt, H. Ibrahim, E. Cormier F. Légaré, *Optics Express* **27**, 28998 (2019).

Towards chemistry simulations on silicon quantum processors

C. K. Long,[1] K. Dalton,[1] Y. S. Yordanov,[1] C. G. Smith, [1] F. Martins[1]
C.H. W. Barnes,[2] N. Mertig,[1] D. R. M. Arvidsson-Shukur[1]
[1] *Hitachi Laboratory, Cambridge, CB3 0HE, United Kingdom*
[2] *University of Cambridge, Cambridge, CB3 0HE, United Kingdom*

Noisy intermediate-scale quantum (NISQ) devices could yield early-stage advantages over classical computers before large-scale fault-tolerant quantum computers emerge. A particularly promising group of NISQ-tailored algorithms are the variational quantum algorithms (VQAs), developed, e.g., for chemistry-simulation purposes. VQAs utilise classical optimisers that guide the operation of shallow-depth quantum circuits. Such quantum-classical symbioses could lead to less-stringent requirements on the coherence times and error rates of the quantum processor. The recent theoretical advances in VQA development have been complimented by rapid improvements of several quantum-processors platforms. Owing to their small size and the potential for rapid industrial scaling, silicon quantum processors constitute a particularly promising platform. Moreover, silicon processors' diverse tunability could endow VAQs with additional degrees of freedom that could improve algorithmic performance. In this talk, I will present numerical results suggesting that current VQAs for quantum computational chemistry are not viable in the presence of realistic noise levels [1]. There are three possible directions for improvement. First, one could rely on error mitigation [1]. Second, one could rely on new noise-robust VQAs [2]. I will argue that neither error mitigation nor algorithmic improvements will be sufficient to perform useful chemical computations on NISQ hardware. However, there is a third option. One can relax the digital gate-based model of quantum computation to a model where the hardware is controlled at the level of the Hamiltonian (experimental pulses) native to the specific platform [3-5]. To explore the prospect of pulse-based VQAs, I will consider the time it takes to variationally prepare molecular ground states on silicon quantum processors. I account for experimental constraints and the effects of pulse filtering such that my model investigates realistic pulse shapes. Finally, I will present an analysis of the effect of noise on these pulse-based computations. I find that silicon quantum processors boast competitive state-preparation times for chemical ground states (Fig. 1 [5]) when compared with superconducting hardware [3, 4]. Further, there is a dramatic reduction in the state-preparation time when going from a digital gate-based model to the silicon pulse-based model. Thus, pulse-based computation with silicon hardware could be a promising route towards chemical simulations on quantum processors.

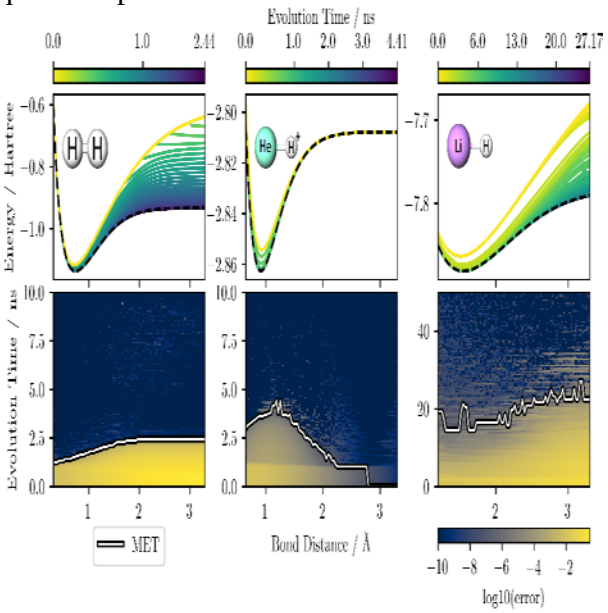

Fig. 1. Estimates of the disassociation curves for H_2 (left), HeH^+ (centre), and +LiH (right). *For each molecule and bond separation the numerically simulated silicon quantum processor is given a fixed amount of evolution time as a resource and prepares the best possible approximation to the ground state in this time. As more time is allowed, the quantum processor can obtain better approximations. The top three panels plot the disassociation curves (energy against bond separation), with the colour of the curve corresponding to the allowed evolution time indicated by the colour bar above each panel. The yellow curve corresponds to zero evolution time. The purple curve corresponds to enough time to reach the full configuration interaction (FCI) energy (**dashed curve**). In the bottom panels, the error from the FCI energy is plotted on a log scale with the evolution time now on the vertical axis. In the bottom panels, we observe a sharp transition: above an evolution time called the minimal evolution time (MET), the ground state can be prepared exactly. We indicate the MET as a function of bond distance by a black-and-white curve. Below the MET, the error is large, and the corresponding colour is yellow, as indicated by the bottom right colour bar. While above the MET, the error is small and fluctuates around the simulation accuracy, and the corresponding colour is blue.*

Further, there is a dramatic reduction in the state-preparation time when going from a digital gate-based model to the silicon pulse-based model. Thus, pulse-based computation with silicon hardware could be a promising route towards chemical simulations on quantum processors.

References

[1] K. Dalton, C. K. Long, Y. S. Yordanov, C. G. Smith, C. H. W. Barnes, N. Mertig, D. R. M. Arvidsson-Shukur, *Quantum Information* **10**, 18 (2024).
[2] C. K. Long, K. Dalton, C. H. W. Barnes, D. R. M. Arvidsson-Shukur, N. Mertig, *arXiv:2308.11708* (2023).
[3] O. R. Meitei, B. T. Gard, G. S. Barron, D. P. Pappas, S. E. Economou, E. Barnes, N. J. Mayhall, *Quantum Information* **7**, 155 (2021).
[4] A. Asthana, C. Liu, O. R. Meitei, S. E. Economou, E. Barnes, N. J. Mayhall, *arXiv:2203.06818* (2022).
[5] C. K. Long, C. H. W. Barnes, N. Mertig, F. Martins, D. R. M. Arvidsson-Shukur, *(to be submitted)* (2024).

Optical multidimensional coherent spectroscopy of Many-body interaction and correlation

H. Li
Florida International University, Miami, FL 33199, USA

Many-body interaction and correlation are fundamental in understanding collective and emergent phenomena that cannot be understood by a simple extrapolation of the microscopic laws of individual particles. Some many-body effects are drastic, such as Dicke superradiance and quantum entanglement in atomic systems. However, some effects of many-body interaction and correlation are subtle and difficult to identify, for example, in semiconductor materials which are intrinsically a complex many-body system of interacting carriers and quasiparticles. In GaAs quantum wells, many-body interaction can be manifested as line shift (excitation induced shift), line broadening (excitation induced dephasing), or FWM signal at negative time delays [1]. Particularly in a 1D spectrum, many aspects of many-body dynamics are indirect and have to be inferred. Optical multidimensional coherent spectroscopy (MDCS) has become a powerful tool for studying couplings and dynamics in complex systems [2], including effects of many-body interaction and correlation. In this presentation, I will give a brief introduction of optical MDCS and how 2D spectra can reveal many-body effects in various systems including atomic systems and 2D materials. In atomic systems, double-quantum MDCS provides an extremely sensitive and background-free detection of dipole-dipole interaction and correlated two-atom states [3, 4]. The technique relies on the detection of double-quantum coherence induced by collective resonances of two correlated atoms. The double-quantum excitation can be extended to multiple-quantum excitation which can excite and probe correlated states of multiple atoms [5, 6]. For example, as shown in Fig. 1(a), 7-atom correlated states are revealed in a multi-quantum 2D spectrum. Optical MDCS has been used extensively to study many-body dynamics in semiconductor quantum wells and dots [2], and more recently carrier and valley dynamics in 2D materials [2]. One advantage of 2D spectra is to clearly separate homogeneous linewidth even in a strongly inhomogeneous system. We have used [7] optical MDCS to measure the homogenous linewidths at different powers and temperatures, which allowed us to extrapolate the intrinsic coherence dephasing time of valley carriers in a monolayer $MoSe_2$.

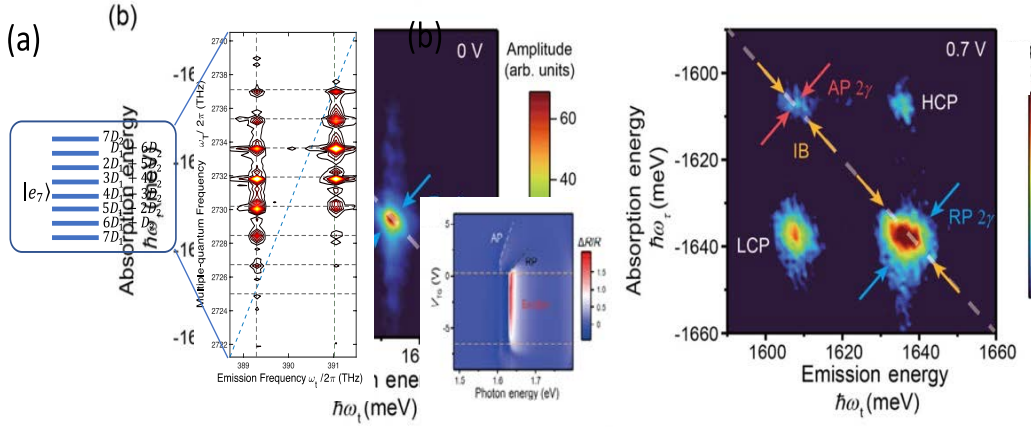

Fig. 1. (a) Energy level diagram and multi-quantum 2D spectrum *showing seven atom quantum coherence.* ***(b)****Reflection spectrum and 2D spectrum showing polaron responses in a doped $MoSe_2$ monolayer.*

Optical MDCS can also be used to explore dynamics of more complex quasiparticles such as polarons [8] which are excitons coherently dressed by a surrounding Fermi sea. As shown in Fig. 1(b), the Fermi-sea dressing results in attractive polaron (AP) and repulsive polaron (RP). These two resonances and their coherent coupling are clearly revealed in a 2D spectrum. The associated polaron dynamics can be quantitative analyzed by fitting the spectra to obtain homogeneous and inhomogeneous linewidths.

References

[1] K. Leo, M. Wegener, J. Shah, D. S. Chemla, E. O. Göbel, T. C. Damen, S. Schmitt-Rink, W. Schäfer, *Physical Review Letters* **65**, 1340 (1990).
[2] H. Li, B. Lomsadze, G. Moody, C. Smallwood, S.T. Cundiff, Oxford University Press, Oxford, UK (2023).
[3] X. Dai, M. Richter, H.Li, A. D. Bristow, C.Falvo, S.Mukamel, S. T. Cundiff, *Physical Review Letters* **108**, 193201 (2012).
[4] F. Gao, S.T. Cundiff, H. Li, *Optics Letters* **41**, 2954 (2016).
[5] S. Yu, M. Titze, Y. Zhu, X. Liu, H. Li, *Optics Letters* **44**, 2795 (2019).
[6] D. Liang, H. Li, *Journal of Chemical Physics* **154**, 214301 (2021).
[7] M.Titze, B. Li, X. Zhang, P.M. Ajayan, H. Li, *Physical Review Materials* **2**, 054001 (2018).
[8] D. Huang, K. Sampson, Y. Ni, Z. Liu, D.Liang, K. Watanabe, T.Taniguchi, H. Li, E.Martin, J. Levinsen, M. M. Parish, E.Tutuc, D.K Efimkin, X. Li *Physical Review* X **13,** 011029 (2023).

Controlling quasi-1D Coulomb correlations by Magnetic order

M. Liebich[1], M.Florian[2], N.Nilforoushan[1], F.Mooshammer[3], K.Mosina[4], Z.Sofer[4], F.Dirnberger[5], M.Kira[2]
R. Huber[1]
[1] *University of Regensburg, 93040 Regensburg, Germany*
[2]*University of Michigan, Ann Arbor, MI 48109, USA*
[3] *Friedrich-Alexander-Universität Erlangen-Nürnberg, 91054 Erlangen, Germany*
[4]*University of Chemistry and Technology Prague, 166 28 Prague, Czech Republic*
[5]*Dresden University of Technology, 01187 Dresden, Germany*

Using phase-locked mid-infrared pulses to probe internal Rydberg-like transitions of excitons in the magnetic semiconductor CrSBr, we reveal their binding energy and a dramatic anisotropy of their quasi-one-dimensional orbitals, which manifests in a strong fine-structure splitting. Further, we switch the internal structure from strongly bound, monolayer-localized to weakly bound, interlayer-delocalized states by pushing the system from the antiferromagnetic to the paramagnetic phase. Our detailed analysis connects this transition to the exciton's spin-controlled effective quantum confinement. This *in situ* control of Coulomb correlations opens a path to future applications where excitons or even condensates may be interfaced with spintronics; extrinsically switchable Coulomb correlations could shape phase transitions on demand. Coulomb correlations define electronic quasiparticles and their interaction chains and therefore have a significant impact on the electronic and optical properties of quantum materials. In van der Waals (vdW) layered crystals, enhanced correlations have been tailored in reduced dimensions giving rise to a variety of fascinating phenomena including strongly bound excitons and exotic electronic and magnetic phases [1]. However, this has mainly been achieved by static structural engineering. In contrast, magnetic vdW materials [2] provide a unique opportunity to control Coulomb correlations *in situ* through magnetic order. In this context, the vdW magnet CrSBr stands out for its magneto-optical properties, which are dictated by quasi-1D excitons coupled to A-type antiferromagnetism. The low-temperature antiferromagnetic coupling of adjacent layers affects the interlayer hybridization and interband resonances observed by interband spectroscopy [3,4]. However, this approach cannot disentangle Coulomb correlation effects from single-particle bandgap renormalization across the magnetic phase transition. Furthermore, the anisotropy-induced fine structure has remained elusive due to the weak oscillator strength for light emission polarized along the crystallographic *a*-axis [4]. Therefore, a precise understanding of the underlying Coulomb correlations in CrSBr has so far remained challenging, even though it is crucial for tailoring novel properties of quantum materials.

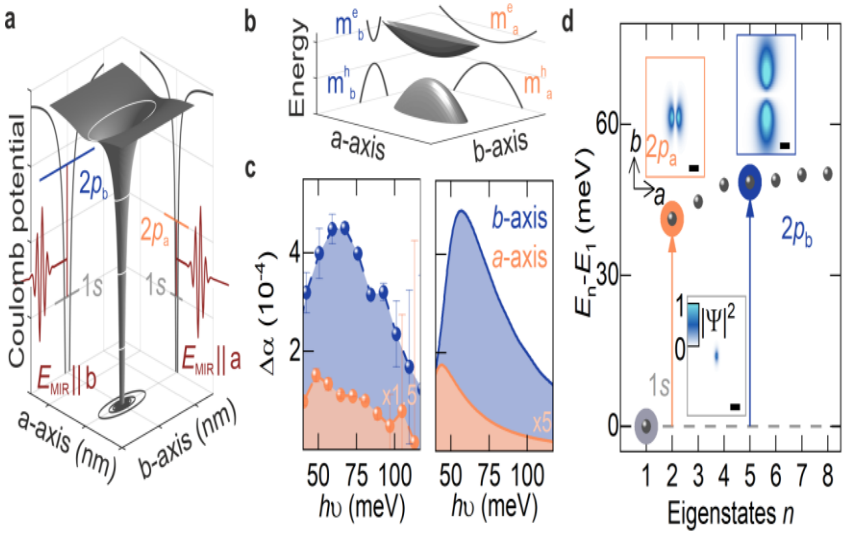

Fig. 1 a, Coulomb potential (grey surface) of the excitons*. The projections emphasise the large in-plane anisotropy. Whereas a- and b-axes share a common 1s level (light grey line), the degeneracy of the 2p states is lifted. The different 1s-2p$_a$ and 1s-2p$_b$ energies (vertical red lines) are interrogated by MIR transients (red waveforms).* ***b,*** *Schematic of the band structure of CrSBr. The projections onto the a- and b-directions highlight the large difference in effective mass of the lowest conduction band (m^e) and the highest valence band (m^h).* ***c,*** *Experimental (left) and theoretical (right) pump-induced changes of the MIR absorption ($\Delta\alpha$) as a function of photon energy at a pump-probe delay time t_{pp} = 500 fs.* ***d,*** *Calculated eigenenergies E_n relative to the ground state energy E_1. The arrows indicate the transition energy from the 1s state (grey) to the 2p$_a$ (orange) and 2p$_b$ (blue) states.* ***Insets:*** *Probability densities $|\Psi|^2$ for 1s, 2p$_a$ and 2p$_b$ orbitals.*

Here, we present a direct measurement of the internal structure of quasi-1D excitons in CrSBr and its evolution across the transition from an antiferromagnetic (AFM) to a paramagnetic (PM) state [5]. To this end, we first excite free electron-hole pairs across the single-particle bandgap using 20-fs near-infrared laser pulses. After a variable delay time t_{pp}, a phase-locked mid-infrared (MIR) light pulse is transmitted through the sample to interrogate internal Rydberg-like transitions of excitons. By simultaneously monitoring the MIR waveform, E_{MIR}, and its pump-induced change, ΔE_{MIR}, using electro-optic sampling,

we extract the full complex-valued dielectric response of the photoexcited electron-hole ensemble in the MIR regime [6] and thus the internal structure and binding energy of excitons [7]. The quantum confinement of the excitons critically depends on the magnetic order [3,4]. At the transition from the AFM to the PM state, the linewidth of the dielectric response increases abruptly together with an apparent blueshift of the resonance (not shown). This strong impact of the magnetic phase on the excitons' internal structure can be directly seen in the raw time domain data (Fig. 2a) as well. Below the Néel temperature T_N, ΔE_{MIR} exhibits an absorptive behavior combined with pronounced trailing oscillations indicative of the excitonic 1*s*-2*p* resonance. Above T_N, these signatures are strongly suppressed while a characteristic time shift of the photoinduced response, t_{shift} (inset, Fig. 2a), occurs suggesting a less-pronounced exciton response. Our state-of-the-art many-body theory reproduces these results and explains the observations as follows (Fig. 2b): The transition to the PM phase results in the delocalization of excitons over several layers, which increases the scattering rate γ and reduces the exciton binding energy (Fig. 2c). The drastic changes of the exciton fine structure demonstrate that Coulomb correlations can be switched from strongly bound, monolayer-localized to weakly bound, interlayer-delocalized states through magnetic order. To put our hypothesis that the magnetic order controls excitonic correlations to the ultimate test, we induce an intermediate ferromagnetic phase close to the AFM-PM phase transition using a static magnetic field. Indeed, the abrupt changes in the dielectric response and in t_{shift} now occur at a substantially lower temperature (Fig. 2b,c, orange symbols and lines). Thus, the magnetic field breaks the out-of-plane quantum confinement and leads to a delocalization of excitons even below T_N. This highlights the potential of the magnetic field as a tuning knob for Coulomb correlations in magnetic vdW materials. The drastic magnetic-phase-dependence of the Coulomb correlations is also reflected in the ultrafast decay dynamics (not shown). In the PM phase, the exciton lifetime is significantly extended, and inter- and intralayer-like species coexist. This corroborates that the magnetic order not only alters the internal exciton structure, but also governs the nature of electron-hole pairs at play.

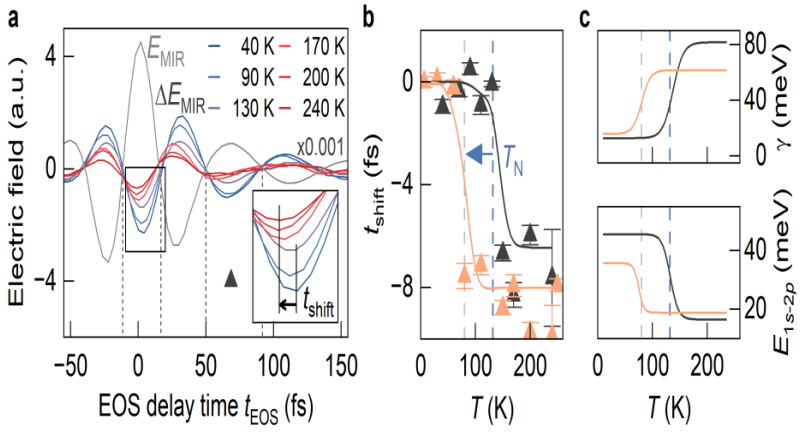

***Fig. 2a, Electric field of the MIR probe transient transmitted through the unexcited CrSBr sample**, E_{MIR}, as a function of the electro-optic sampling time t_{EOS}. The simultaneously acquired pump-induced changes to the electric field ΔE_{MIR} are depicted for different temperatures T. Inset: Close-up view of the data marked by the rectangle. For decreasing temperature, the minimum of ΔE_{MIR} shifts gradually by a time t_{shift} (**arrow**). **b,** experimental (**symbols**) and theoretical (**lines**) time shift t_{shift} of the half-cycle marked by the triangle (compare **a**) without an external magnetic field (**grey color**). The time shift decreases sharply around T_N (blue dashed line). In experiment and theory, an applied magnetic field of ~0.2 T along the b-axis causes the jump in t_{shift} (**orange symbols and line**) to occur at ~80 K (**blue arrow and grey dashed line**). **c,** calculated dephasing constant γ and 1s-2p transition energy E_{1s-2p}.*

In conclusion, we have revealed the fine structure of strongly anisotropic, quasi-1D excitons by intra-excitonic Rydberg spectroscopy. Our quantitative experiment-theory comparisons of the exciton binding energy show how band structure and Coulombic anisotropy jointly lift the degeneracy of the 2*p* states and lead to a strongly polarization-dependent oscillator strength of internal excitonic transitions. By inducing a phase transition from the AFM to the PM state, excitonic correlations can be switched from strongly bound, monolayer-localized to weakly bound, interlayer-delocalized states. Our results demonstrate that the magnetic order is a critical control knob for excitonic correlations, which provides fascinating opportunities for realizing spin-correlated exciton-polaritons [8] and even Bose-Einstein condensates – a captivating perspective for novel solid-state quantum technologies.

References

[1] G. Wang, A. Chernikov, M.M. Glazov, T. F. Heinz, X. Marie, T. Amand, B. Urbaszek, *Review of Modern Physics* **90,** 21001(2018).
[2] B. Huang, G. Clark, E. Navarro-Moratalla, D.R. Klein, R.Cheng, K. L.Seyler, D. Zhong, E.Schmidgall , M.A. McGuire , D. H. Cobden, W.Yao D. Xiao, P.Jarillo-Herrero, X. Xu , *Nature* **546**, 270 (2017).
[3] N. P. Wilson, K. Lee, J. Cenker, K. Xie, A. H. Dismukes, E. J. Telford, J. Fonseca, S. Sivakumar, C. Dean, T.Cao, X. Roy, X. Xu, X. Zhu, *Nature Materials* **20**, 1657 (2021).
[4] J. Klein, B. Pingault, M. Florian, M.-C. Heißenbüttel, A. Steinhoff, Z. Song, K. Torres, F. Dirnberger, J. B. Curtis, M. Weile,A. Penn,T. Deilmann R. Dana, R. Bushati, J. Quan, J. Luxa, Z. Sofer, A. Alù, V. M. Menon, U. Wurstbauer, M. Rohlfing, P. Narang, M. Lončar, F. M. Ross, *ACS Nano* **17** 5316 (2023).
[5] M. Liebich. R. Huber. under review. (2024).
[6] R. Huber, F Tauser, A Brodschelm, M. Bichler, G. Abstreiter, A. Leitenstorfer, Nature **414**, 286 (2001).
[7] C. Poellmann, P. Steinleitner, U. Leierseder, P. Nagler, G. Plechinger, M. Porer, R. Bratschitsch, C. Schüller, T. Korn, R. Huber, *Nature Materials* **14**, 889 (2015).
[8] F. Dirnberger, J. Quan, R. Bushati, G. M. Diederich, M. Florian, J. Klein, K. Mosina, Z. Sofer, X. Xu, A. Kamra, F. J. García-Vidal, A. Alù V. M. Menon, *Nature* **620**, 533 (2023).

Floquet-Bloch bands on subcycle time scales

M. Meierhofer[1], S. Ito[2], M. Schüler[3], S. Schlauderer[1], J. Freudenstein[1], J. Reimann[2], D. Afanasiev[1]
K. A. Kokh[4], O. E. Tereshchenko[4], J. Güdde[2], M. A. Sentef[5], R. Huber[1], U. Höfer[2]
[1]*University of Regensburg, 93040 Regensburg, Germany*
[2]*Philipps-University of Marburg, 35032 Marburg, Germany*
[3]*Condensed Matter Theory Group, Paul Scherrer Institute, 5232 Villigen PSI, Switzerland*
[4]*A.V. Rzhanov Institute of Semiconductor Physics, 630090 Novosibirsk, Russian Federation*
[5]*University of Bremen, 28359 Bremen, Germany*

The discrete translational symmetry of a crystalline solid leads to a band structure of Bloch electrons that is periodic in momentum space. Analogously, when Bloch electrons are exposed to the time-periodic electric field of light with frequency ω, its band structure is periodically repeated in the form of 'Floquet' replicas, which are displaced along the energy axis by multiples of $\hbar\omega$. Quasi-stationary Floquet-Bloch states have been observed in topological insulators [1,2] and black phosphorus [3]. However, the dynamics of Floquet states, including their transient build-up and electron transfer between sidebands, have not yet been accessible experimentally. In a more general context, the relation between Floquet bands and subcycle interband excitations, as well as intraband currents responsible for high-harmonic generation (HHG) in solids (Fig. 1a) has remained mostly elusive despite its crucial role in strong-field light-matter interaction.

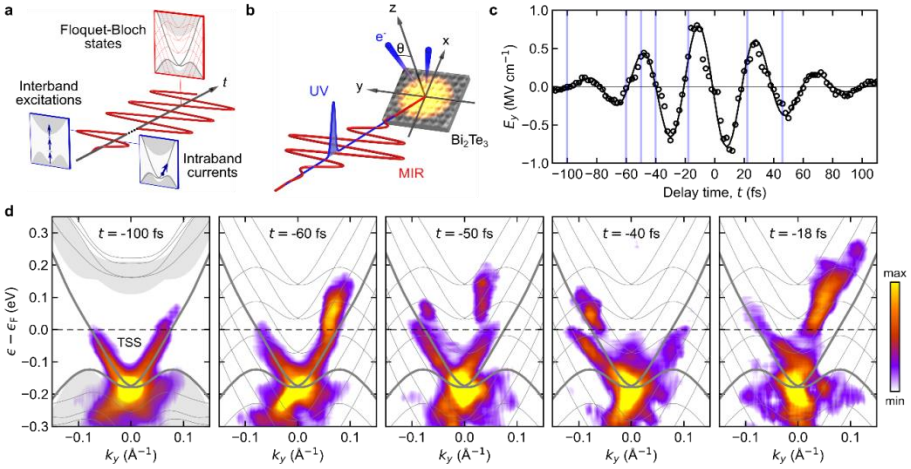

Fig. 1: a) *Transition between subcycle dynamics and quasi-static Floquet-Bloch bands.*
b) *Experimental scheme: an s-polarized, phase-stable MIR pulse* ***(red)*** *drives the topological surface state (TSS) of Bi_2Te_3. An ultraviolet (UV) probe pulse (blue) at variable time delay, t, provides snapshots of the induced dynamics with subcycle temporal resolution.*
c) *Driving electric field* ***(black)*** *and temporal positions* ***(vertical lines)*** *of ARPES maps in d and Fig. 2.*
d) *ARPES maps at selected delay times capturing the build-up of Floquet-Bloch sidebands.*

Here, we study the ultrafast dynamics of Floquet-Bloch bands in the strong-field limit using subcycle angle-resolved photoemission spectroscopy (ARPES) [4]. Figure 1b shows the experimental scheme. We pump the 3D topological insulator Bi_2Te_3 with phase-locked, s-polarized mid-infrared (MIR) pulses with a center frequency of $\omega_{MIR}/2\pi$ = 25 THz. This material exhibits a finite band gap in the bulk and a Dirac-like topological surface state (TSS). Spin-momentum locking protects the electrons in the TSS from scattering [5], which warrants sufficient coherence times for Floquet-Bloch states to form under periodic driving [1,2]. An ultraviolet pulse with a pulse duration of 17 fs, arriving at a variable delay time, *t*, probes the system with subcycle time resolution by two-photon photoemission. The energy and momentum of the released electrons are measured with a hemispherical analyzer. The maximum applied peak field of 0.8 $MVcm^{-1}$ (Fig. 1c) is strong enough for HHG in the TSS [6]. The ARPES maps in Fig. 1d show the initial dynamics of the band structure. Up to 100 fs before the field maximum, the effect of the MIR pulse on the TSS is negligible. 40 fs later (*t* = -60 fs), the electric field has induced a pronounced asymmetry in the electronic distribution along the momentum axis, which is the hallmark of lightwave-driven currents. A clear separation of electronic populations into multiple sidebands becomes apparent only one quarter of an oscillation cycle later. The ARPES maps in Fig. 1d show the initial dynamics of the band structure. Up to 100 fs before the field maximum, the effect of the MIR pulse on the TSS is negligible. 40 fs later (*t* = -60 fs), the electric field has induced a pronounced asymmetry in the electronic distribution along the momentum axis, which is the hallmark of lightwave-driven currents. A clear separation of electronic populations into multiple sidebands becomes apparent only one quarter of an oscillation cycle later, at *t* = -50 fs. Simultaneously, the electron population oscillates back and forth along the momentum axis (*t* = -50 fs and -40 fs). The newly emerging bands clearly follow the ground-state band structure offset by integer multiples of $\hbar\omega_{MIR}$ = 0.1 eV (Fig. 1d, thin grey curves). With increasing field, the band splitting becomes more pronounced, and the electron population shifts

entirely to the upper branch near the field crest (Fig. 1d, t = -18 fs). Thus, Floquet states result from the quantum interference of electrons, which coherently followed the driving field for at least one cycle. Our experiments also clarify the long-standing question of how multi-photon transitions between equilibrium bands proceed in the strong-field regime. In Bi_2Te_3, the direct bulk bandgap at the Γ point exceeds 0.3 eV, thus preventing resonant one-photon interband excitations ($\hbar\omega_{MIR}$ = 0.1 eV). Nevertheless, electrons can overcome the gap via Floquet-Bloch replicas of the TSS. In the second half of the MIR pulse, the electronic distribution deviates strongly from the original dispersion: a substantial fraction of the electrons is transferred to the first and second Floquet-Bloch sidebands, where they are periodically accelerated by the carrier field (Fig. 2a).

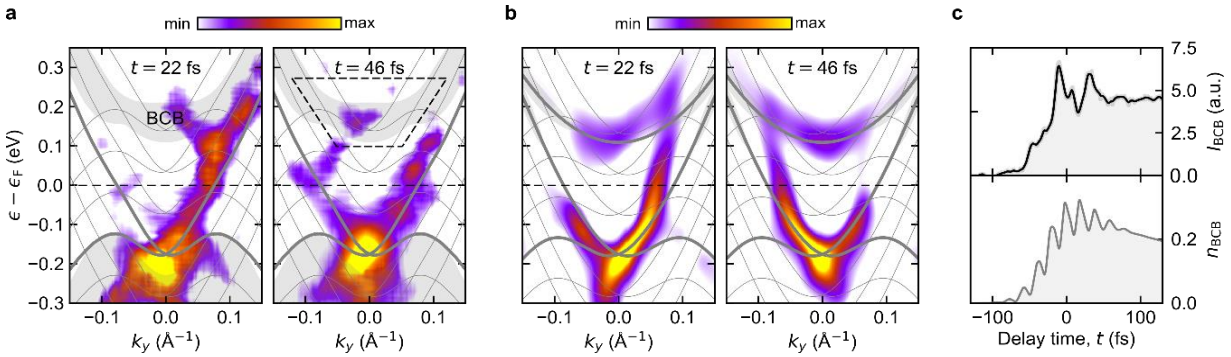

Fig. 2: a) *Experimental and* ***b)*** *theoretical ARPES maps tracking multi-photon excitations via Floquet-Bloch replicas.* ***c)*** *Experimental (upper panel) and theoretical (lower panel) temporal evolution of the photoelectron intensity integrated across the bulk conduction band (dashed trapezoid in a)*

Because the experiment isperformed under conditions sufficient for HHG [6], our measurements capture electron dynamics underlying HHG directly in momentum space. Once the high-energy tail of the Floquet electron distribution reaches the bulk conduction band (BCB; Fig. 2a, t = 22 fs, grey area), the surface states hybridize with the bulk band and populate it. This novel mechanism of transitions between equilibrium bands via Floquet-Bloch states is well reproduced by a nonequilibrium Green's function approach (Fig. 2b). For a more quantitative analysis, we investigate the energy-momentum integral of the recorded photoelectron intensity across the bulk conduction band region (dashed trapezoid; Fig. 2a, t = 46 fs), I_{BCB}, as a function of t (Fig. 2c, upper panel). After a rapid increase during the MIR pulse, I_{BCB} settles to a long-lived plateau, indicating the incoherent electron population scattered into the bulk conduction band. Remarkably, the onset of I_{BCB} is superimposed with pronounced oscillations, which imply coherent coupling of the transiently dressed TSS with the BCB. This behavior is also well reproduced by our simulations (Fig. 2c, lower panel). When the Floquet states reach the conduction band while the surface-bulk coupling is still coherent, the electron population can be transferred into and out of the bulk. Ultimately, scattering creates an incoherent bulk population, which accelerates the collapse of the Floquet band structure while the MIR pulse ends.In summary, we have captured the ultrafast dynamics of Floquet-Bloch bands in a topological insulator with subcycle ARPES. We directly visualize in momentum space how the lightwave-driven surface state of Bi_2Te_3 crosses over from an initial regime of deterministic quantum trajectories to a Floquet band structure. The dynamics unify the particle aspect of electrons describing subcycle acceleration with the wave-like interference of electrons forming light-induced sidebands. Our ability to image Bloch electrons, which are transiently dressed by strong light fields, marks a breakthrough toward a comprehensive understanding of Floquet engineering, HHG, and other strong-field light-matter interaction concepts.

References

[1] Y. H. Wang, H. Steinberg, P. Jarillo-Herrero, N. Gedik, *Science* **342**, 453 (2013).
[2] F. Mahmood, C.-K. Chan, Z. Alpichshev, D. Gardner, Y. Lee, P. A. Lee, N. Gedik, *Nature Physics* **12**, 306 (2016).
[3] S. Zhou, C. Bao, B. Fan, H. Zhou, Q. Gao, H. Zhong, T. Lin, H. Liu, P. Yu, P. Tang, S. Meng, W. Duan, S. Zhou, *Nature* **614**, 75 (2023).
[4] S. Ito, M. Schüler, M. Meierhofer, S. Schlauderer, J. Freudenstein, J. Reimann, D. Afanasiev, K. A. Kokh, O. E. Tereshchenko, J. Güdde. M. A. Sentef, U. Höfer, R. Huber, *Nature* **616**, 696 (2023).
[5] J. Reimann, S. Schlauderer, C. P. Schmid, F. Langer, S. Baierl, K. A. Kokh, O. E. Tereshchenko, A. Kimura, C. Lange, J. Güdde, U. Höfer R. Huber, *Nature* **562**, 396 (2018).
[6] C. P. Schmid, L. Weigl, P. Grössing, V. Junk, C. Gorini, S. Schlauderer, S. Ito, M. Meierhofer, N. Hofmann, D. Afanasiev, J. Crewse, K. A. Kokh O. E Tereshchenko, J. Güdde, F. Evers, J. Wilhelm, K. Richter, U. Höfer, R. Huber, *Nature* **593**, 385 (2021).

Tailoring ultrastrong light-matter coupling through Spatial matter design

J. Mornhinweg[1], L Diebel[1], M. Halbhuber[1], J.Riepl[1], E. Cortese[2], S. De Liberato[3], D. Bougeard[1]
R. Huber[1], C. Lange[4]
[1]*University of Regensburg, 93040 Regensburg, Germany*
[2]*University of Southampton, Southampton, SO17 1BJ, United Kingdom*
[3] *Istituto di Fotonica e Nanotecnologie, 20133 Milan, Italy*
[4] *Technische Universität Dortmund, 44227 Dortmund, Germany*

Light-matter coupling is centered around the coupling of a single optical mode with a single matter excitation, creating the pair of polaritons which define the optical properties of the coupled structure. In the ultrastrong (USC) and deep-strong coupling (DSC) regimes, this has enabled the observation of exciting quantum phenomena of cavity quantum electrodynamics such as cavity quantum chemistry [1], cavity-controlled electronic transport [2] or applications in nanophotonics including novel light sources or squeezed quantum states of light [3]. Precise control of the coupling is pivotal for utilizing the properties of ultrastrong coupling and has enabled e.g., strong custom-tailored nonlinearities [4] or subcycle switch-off of light-matter coupling [5], which is predicted to release the virtual photon population of the exotic vacuum ground state [6]. For USC, the coupling strength Ω_R/ω_c, defined as the ratio of the vacuum Rabi frequency and the carrier frequency of light, approaches unity. For DSC, $\omega_c > 1$ with a recent record of $\Omega_R/\omega_c = 3.19$ accompanied by a ground state populated by more than one virtual photon, on average [7]. Moreover, here, the large spectral bandwidth bridged by the polariton doublet of $2\Omega_R$ may foster further interactions with off-resonant light and matter modes. The resulting multi-mode or very-strong coupling regime [8–11] offers additional degrees of freedom for designing light-matter coupled resonances and the non-trivial vacuum state, beyond the parameters of a two-mode system. However, controlling multiple coupling pathways has remained challenging. Here we experimentally implement a novel strategy to sculpt ultrastrong multi-mode coupling by tailoring the spatial overlap of multiple modes of planar metallic THz resonators and the cyclotron resonances (CR) of Landau-quantized two-dimensional electrons, hosted in quantum wells (QWs), on subwavelength scales [12]. We show that similarly to the selection rules of classical optics, spatial structuring of the matter component allows for suppressing or enhancing certain coupling pathways, thereby enabling control of the number of light-matter coupled modes, their octave-spanning frequency spectra, and their response to magnetic tuning. Our resonators (Fig. 1a) feature a fundamental LC mode with a frequency of ν_1 = 0.8 THz (Fig. 1b), and a second, dipolar mode with a resonance frequency of ν_2 = 1.6 THz (Fig. 1c).

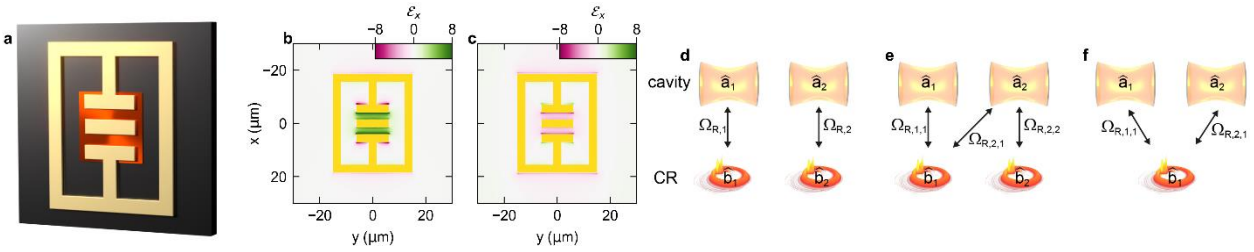

Fig. 1. a. ***Schematic of a THz resonator (gold shape) on top of the GaAs substrate*** *(dark brown), and the cyclotron resonances hosted in spatially confined GaAs quantum well structures (bright orange patch).* ***b****.Simulated x-polarized near-field distribution of the LC mode of the bare resonator, and* ***c****, the dipolar mode.* ***d.****Schematic of the coupling with zero mode overlap,* ***e****, partial overlap and* ***f****, full overlap of the 1st (LC,* $\nu = 1$*) and 2nd (DP,* $\nu = 2$*) cavity modes.*

Their different spatial field profiles allow us to control the coupling pathways by spatially structuring the QWs to tune the overlap of the cavity modes from almost zero to unity (Figs. 2d-f). A reference sample implements a planar QW and is referred to as unstructured, while the QW of the second sample, referred to as structured, is laterally etched to a size of 15 µm by 15 µm to control the overlap with the resonator modes (Fig. 1a). For the unstructured sample the CR couples to both resonator modes without spatial selectivity.Here, each pair of lower (LP) and upper polaritons (UP) of the cavity modes display the typical anti-crossing behavior (Fig. 2a).

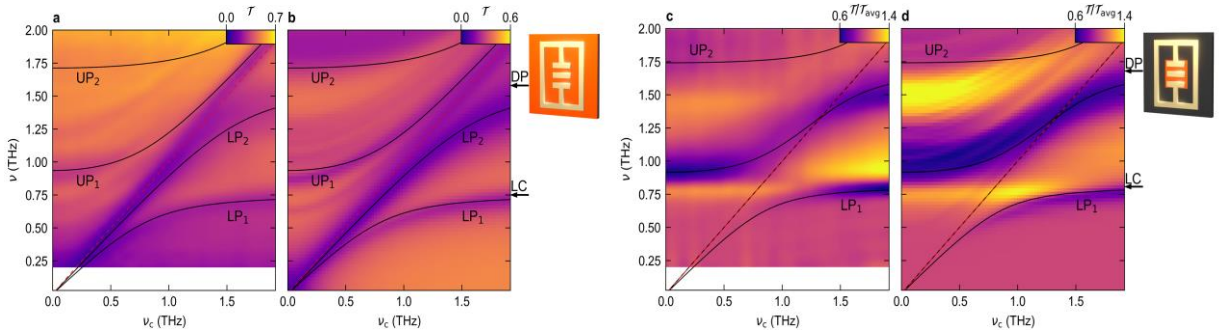

Fig. 2 a. Experimental transmission spectra of the unstructured sample *as a function of the cyclotron frequency ν_c. The curves represent the eigenmodes calculated by theoretical fit.* ***b****, FEFD simulation of the transmission spectra of the structure including the theoretical fit of panel* ***a****. The two arrows indicate the frequencies of the uncoupled LC and DP modes obtained by our fit. Outset: Schematic of the resonator on top of an unstructured QW (****bright orange area****).* ***c****, Experimental transmission spectra of the unstructured sample, each normalized to the average transmission for each frequency ν, as a function of . The curves represent the eigenmodes calculated by theoretical fit.* ***d****, FEFD simulation of the transmission spectra of the structure, each normalized to the average transmission $\mathcal{T}_{avg}$ for each frequency ν as a function of ν_c, including the theoretical fit of panel* ***a****. The two arrows indicate the frequencies of the uncoupled LC and DP modes obtained by our fit. Outset: Schematic of the resonator on top of a structured QW patch (****bright orange patch****).*

In contrast, the spectra of the structured sample (Fig. 2c), where the QW polarization can couple to the near-field only in the central gap area, exhibit a fundamentally different response characterized by three rather than four coupled modes. Here, the resonances associated with UP_1 and LP_2 for the first structure merge into a single coupled resonance resembling an S-shape without an anti-crossing, as theoretically predicted in ref. [11]. These observations are reproduced by our classical electrodynamical finite-element frequency-domain (FEFD) simulations (Fig. 2b,d). The observed differences between both structures are explained by our quantum mechanical formalism which extends the established Hopfield model to non-orthogonal modes and takes the fractional overlap of light and matter modes of our samples into account. This allows us to extract the coupling parameters quantifying the mutual interaction between all partaking modes [11]. For two photonic modes there exists a single overlap parameter $\eta_{2,1}$ based on the electric near-field distribution of the resonator modes. Our formalism allows us to accurately fit the resonances of both sets of data and we obtain an overlap of $\eta_{2,1} = 0.15$ for the unstructured system and $\eta_{2,1} \approx 1$ for the structured sample. We identify the S-shaped spectral signature as a hallmark of nearly full mode overlap, $\eta_{2,1} \approx 1$, accompanied by a change of character of the light-matter coupling mechanism, whereby the number of participating modes is reduced from 4 to 3. Thus, the interaction between the second photon mode and the second electronic mode (orthogonal to and degenerate with the first one), $\Omega_{\mathrm{R},2,2} = 0$, vanishes for $\eta_{2,1} = 1$ and the cross-interaction term proportional to $_{\mathrm{R},2,1}$ becomes dominant, demonstrating the effectiveness of our approach.

In conclusion, the concept of lateral confinement of the quantum wells adds a previously unexplored parameter space for tailoring ultrastrong light-matter coupling by controlling the spatial mode overlap of multiple interacting light and matter modes, across several optical octaves. Our novel design approach increases the flexibility for sculpting polaritonic structures, by selectively boosting or suppressing certain coupling pathways, in similarity to tailoring of selection rules in classical optics. This opens up novel pathways for controlling dissipation, tailoring quantum light sources, nonlinearities, correlations as well as entanglement in quantum information processing.

References

[1] A. D. Dunkelberger, B. S. Simpkins, I. Vurgaftman, J. C. Owrutsky, *Annual Review of Physical Chemistry* **73**, 429 (2022).
[2] G. L. Paravicini-Bagliani, F. Appugliese, E. Richter, F. Valmorra, J. Keller, M. Beck, N.Bartolo, C. Rossler, T. Ihn, K. Ensslin, C.Ciuti, G.Scalari J. Faist, *Nature Physics* **15**, 186 (2019).
[3] S. Fedortchenko, S. Huppert, A.Vasanelli, Y. Todorov, C. Sirtori, C. Ciuti , A. Keller, T. Coudreau ,P.Milman, *Physical* Review A **94**, 13821(2016).
[4] J. Mornhinweg , M. Halbhuber, C. Ciuti, D. Bougeard, R. Huber, C.Lange, *Physical Review Letters* **126**, 177404 (2021).
[5] M.Halbhuber, J. Mornhinweg, V.Zeller, C. Ciuti, D. Bougeard, R. Huber, C. Lange, *Nature Photonics* **14**, 675 (2020).
[6] S. De Liberato, C. Ciuti, I. Carusotto, *Physical Review Letters* **98**, 103602 (2007).
[7] J. Mornhinweg, L. Diebel, M. Halbhuber, M. Prager, J. Riepl, T. Inzenhofer, D. Bougeard, R. Huber, C. Lange,*Nature Communications* **15**,1847(2024)
[8] D. Meiser, P. Meystre, *Physical Review* A **74**, 65801 (2006)
[9] E. Cortese, L. Tran, J.-M. Manceau, A. Bousseksou, I. Carusotto, G. Biasiol, R. Colombelli, S. De Liberato, *Nature Physics* **17**, 31 (2021)
[10] S. Rajabali, E. Cortese, M. Beck, S. De Liberato, J. Faist, G. Scalari, *Nature Photonics* **15**, 690 (2021).
[11] E. Cortese, J. Mornhinweg, R. Huber, C.Lange, S. De Liberato, *Optica* **10**, 11 (2023)
[12] J. Mornhinweg, L. Diebel, M.Halbhuber, J. Riepl, E. Cortese, S. De Liberato, D. Bougeard, R.Huber, C. Lang, *Nanophotonics*, (2024).

Cavity electrodynamics of van der Waals heterostructures

G. Kipp[1], H.M. Bretscher[1], B. Schulte[2], D. Herrmann[1], K. Kusyak[1], M.W. Day[1], S. Kesavan[1], T. Matsuyama[1]
X. Li[1], S.M. Langner[1], J. Hagelstein[1], F. Sturm[2], A.M. Potts[2], C.J. Eckhardt[1], Y. Huang[2], K. Watanabe[3]
T. Taniguchi[3], A. Rubio[1], D.M. Kennes[4], M.A. Sentef[5], E. Baudin[6], G. Meier[1], M.H Michael[1], J.W. McIver[2]
[1] *Max Planck Institute for the Structure and Dynamics of Matter, 22761 Hamburg, Germany*
[2] *Columbia University, New York, NY10027, USA*
[3] *National Institute for Materials Science, Ibaraki 305-0044, Japan*
[4] *Aachen University, 52062 Aachen, Germany*
[5] *University of Bremen, 28334 Bremen, Germany*
[6] *École Normale Supérieure, 75005 Paris, France*

Van der Waals (vdW) heterostructures host many-body quantum phenomena that can be tuned *in situ* using electrostatic gates [1-3]. These gates are often microstructured graphite flakes that naturally form plasmonic cavities, confining light in discrete standing waves of current density due to their finite size. Their resonances typically lie in the GHz - THz range, corresponding to the same μeV - meV energy scale characteristic of many quantum effects in the materials they electrically control. This raises the possibility that built-in cavity modes could be relevant for shaping the low-energy physics of vdW heterostructures. However, capturing this light-matter interaction remains elusive as devices are significantly smaller than the diffraction limit at these wavelengths, hindering far-field spectroscopic tools. Here, we report on the sub-wavelength cavity electrodynamics of graphene embedded in a vdW heterostructure plasmonic microcavity [4]. Using on-chip THz spectroscopy, we observed spectral weight transfer and an avoided crossing between the graphite cavity and graphene plasmon modes as the graphene carrier density was tuned, revealing their ultrastrong coupling-*Fig. 1*

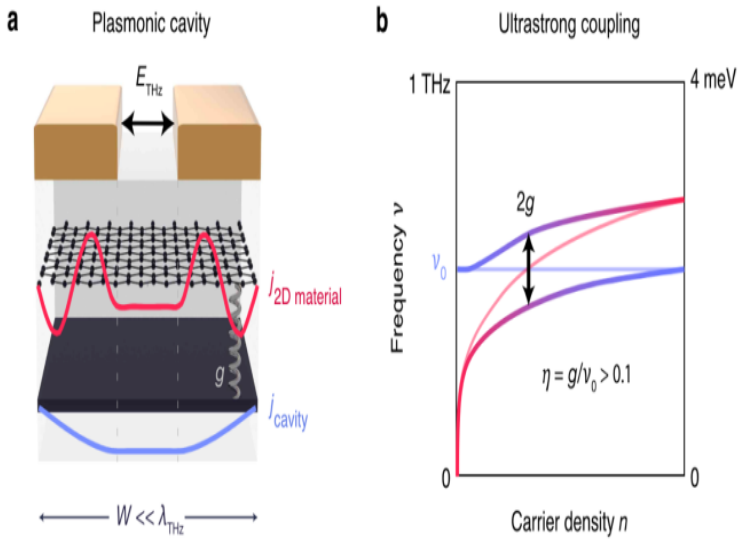

Fig. 1: Plasmonic microcavity setup for ultrastrong coupling of collective modes in 2D materials. *(**a**) Schematic of a 2D material embedded in a sub-wavelength ($W \ll \lambda_{THz}$) plasmonic cavity formed by a few-nm graphite flake and surrounding dielectric environment. A collective mode of a 2D material (**red**), such as a graphene plasmon studied in this work, can hybridize with the plasmonic bare cavity mode (**blue**). (**b**) The frequency of the screened plasmonic mode in the 2D material (**light magenta line**) is tuned with carrier density into resonance with the screened bare cavity mode, ν_0 (**light blue line**). The cavity and plasmon modes hybridize due to coupling mediated by unscreened currents between the metal traces and an avoided crossing appears, with an energy splitting of twice the coupling strength, g. When η, the ratio of g/ν_0, exceeds the value of 0.1, the system is in the ultrastrong interaction regime.*

Our findings show that intrinsic cavity modes of metallic gates can sense and manipulate the low-energy electrodynamics of vdW heterostructures. This opens a pathway for deeper understanding of emergent phases in these materials and new functionality through cavity control [5].

References

[1] E. Y. Andrei, A.H. MacDonald, *Nature Materials* **19**, 1265 (2020).
[2] L. Balents, C. R. Dean, D. K. Efetov, A.F. Young, *Nature Physics* 16, 725 (2020).
[3] K. F. Mak, J. Shan, *Nature Nanotechnology* **17**, 686 (2022).
[4] G. Kipp, H.M. Bretscher, B. Schulte, D. Herrmann, K. Kusyak, M.W Day, S. Kesavan, .Matsuyama, X. Li, S.M. Lagner, J Hagelstein, F.Strum A. M. Potts, C. J. Erckhardt, Y.Huang, K. Watanabe, T. Taniguchi, A. Rubio, D. M. Kennes, M. A. Sentef, E. Baudin, G. Meier, M.H. Michael J. W. McIver, *arXiv:2403.19745* (2024).
[5] F. Schlawin, D. Kennes, M. A. Sentef, *Applied Physics Reviews* **9**, (2022)

Exciton dynamics in two-dimensional quantum materials in space and time

S. Mathias
University of Göttingen, 37077Göttingen, Germany

In 2D semiconducting quantum materials, organic semiconductors and their heterostructures, the energy of absorbed light is stored in Coulomb-bound electron-hole pairs, i.e. excitons. For future technological applications of these classes of materials, for instance in optoelectronics and for energy harvesting, it is crucial to study the initial exciton formation and also the subsequent relaxation and dissipation processes at the fundamental level and on the relevant length and time scales. In our research, we have built a new photoemission-based experiment [1] that is capable studying excitonics at the space-time limit corresponding to nanometers and femtoseconds. In a series of experiments, we identified characteristic signatures in the exciton formation process and the pathways of subsequent energy conversion and thermalization. In addition, the new experiment gives us access to the so-called "dark exciton landscape", where we can follow exciton dynamics with unprecedented temporal and spatial resolution.In my talk, I will present the ultrafast formation dynamics of dark interlayer excitons in twisted WSe_2/MoS_2 heterostructures. In particular, I will report on the identification of a key signature of the moiré superlattice that is imprinted on the momentum-resolved interlayer exciton photoemission signal [2,3].

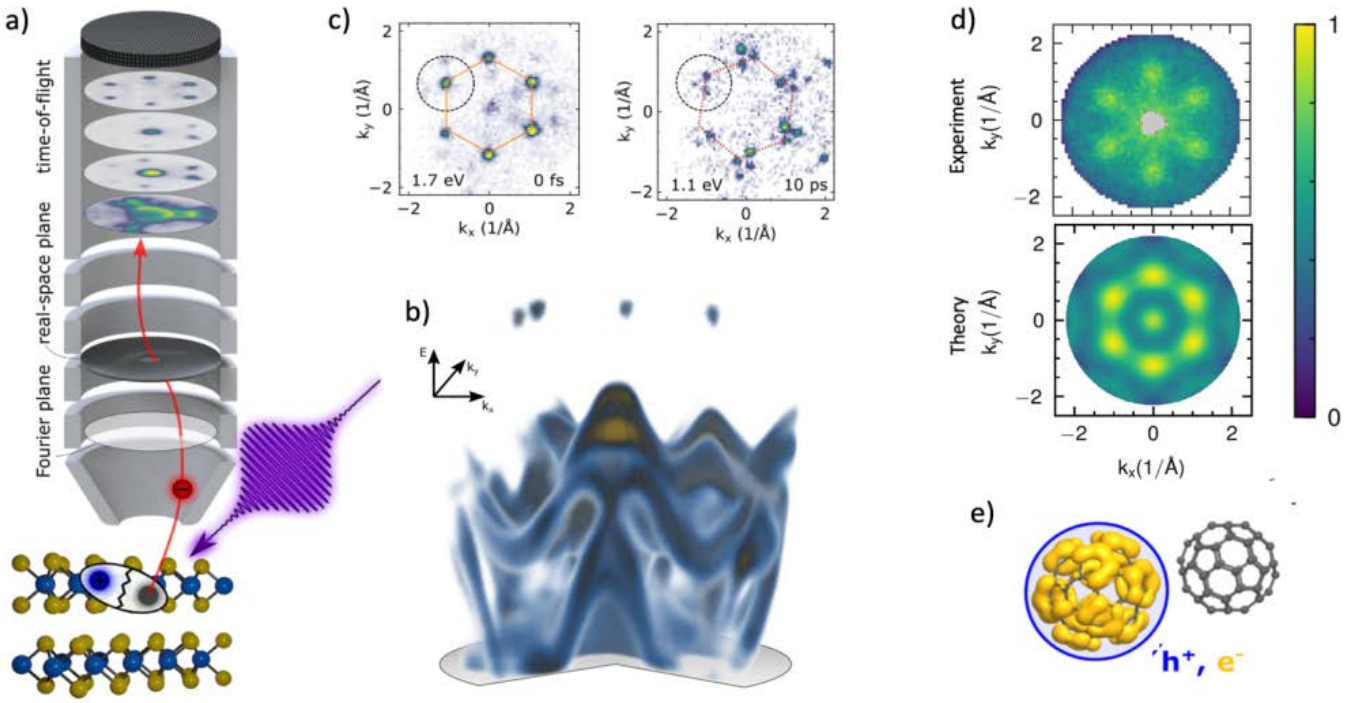

Fig. 1. a) *Scheme of the ultrafast momentum microscopy experiment [1].* ***b)*** *3D electronic structure of WSe_2/MoS_2 with excitonic signals above the valence band maxima [2,3].* ***c)*** *Selected momentum cuts showing the momentum fingerprint of the optically excited A-exciton in WSe_2 (**left**) and an interlayer exciton in WSe_2/MoS_2 [2].* ***d)*** *Exciton photoemission orbital tomography of the 'S1' exciton in C60 [4]. In comparison with theory, the exciton's electron probability density (**yellow**) in comparison to the hole localization (**blue**) can be extracted.*

Furthermore, I will present photoemission exciton tomography [4] that allows us to study ultrafast charge transfer from TMD to organic layers, and to disentangle multiorbital contributions in the exciton formation in the organic semiconductor.

References

[1] M. Keunecke, C. Möller, D. Schmitt, H. Nolte, G. S. Matthijs Jansen, M. Reutzel, M. Gutberlet, G. Halasi, D. Steil, S. Steil, S. Mathias, *Review of Scientific Instruments* **91**, 063905 (2020).
[2] D. Schmitt, J. P. Bange, W. Bennecke, A. A. Al-Mutairi, G. Meneghini, K. Watanabe, T. Taniguchi, D. Steil, D. R. Luke, R. T. Weitz, S. Steil G. S. Matthijs Jansen, S.Brem, E.Malic, S.Hofmann, M. Reutzel, S. Mathias, *Nature* **608**, 499 (2022).
[3] J. P Bange, D. Schmitt, D.S. Wiebke Benenecke , G. Meneghini, A.A. Almutairi, K.K. Watrnabe, T. Taniguchi, D. Steil, S. Steil, R. Thomas Weitz G. S. Matthijs Jansen, S. Hoffmann, S. Brem, E. Malic, M. Reutzel, S. Mathias , *Science Advances* **10**, eadi1323 (2024).
[4] W. Bennecke, A. Windischbacher, D. Schmitt, J. P. Bange, R. Hemm, C. S. Kern, G. D'Avino, X . Blase, D. Steil, S. Steil, M.Aeschlimann B.Stadtmüller, M. Reutzel, P.Puschnig, G. S. Matthijs Jansen, S. Mathias, *Nature Communications* **15**, 1804 (2024).

Light control of coupled electron-lattice ordering

S. Meng
Institute of Physics, Beijing 100190, China

Photoexcitation is a powerful means in distinguishing different interactions and manipulating the states of matter, especially in complex quantum systems. Here we demonstrate photoexcitation-induced ultrafast dynamics in two-dimensional quantum materials, as well as the development of new theoretical tools incorporating both nonadiabatic electron-nuclear couplings and nuclear quantum effects for atomic scale simulations of such ultrafast processes. For instance, we discover a novel mechanism which involves self-amplified exciton-phonon dynamics for the formation of charge density wave (CDW), and we predict a new collective mode induced by photoexcitation which is significantly different from thermally-induced phonon mode [1-6]. We will also discuss photoinduced structural and electronic phases such as controlling the dynamics of Weyl quasiparticles in semimetal WTe_2 (Fig. 1) and the coupled exciton-lattice orders in exciton insulator candidate Ta_2NiSe_7.

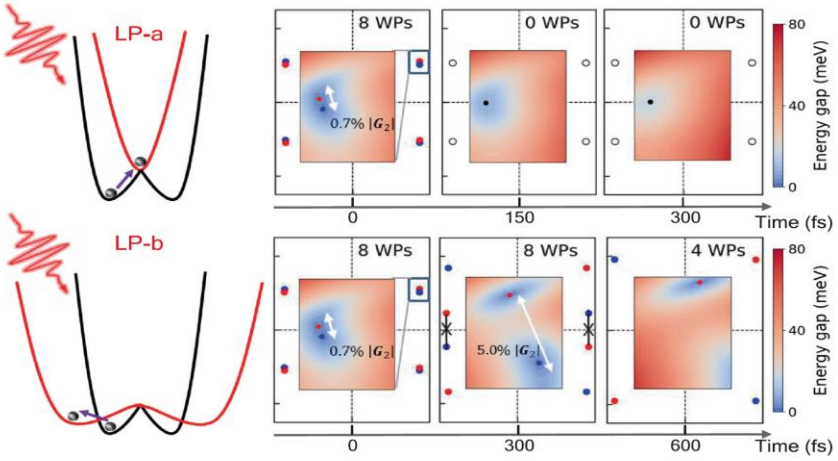

Fig. 1. The dynamics of Weyl points distribution in response to different photoexcitation.

Our results provide insights from a new perspective on the coherent electron and lattice quantum dynamics in materials upon photoexcitation.

References

[1] C. Lian, S.J. Zhang, S.Q. Hu, M.X. Guan, S. Meng, *Nature Communications* **11**, 43(2020).
[2] M. X. Guan, E. Wang, P.W. You, J.T. Sun, S. Meng, *Nature Communications* **12**, 1885(2021).
[3] J. Y. Xu, D.Q. Chen, S. Meng, *Science Advances* **8**, eadd2392 (2022).
[4] M. X. Guan, X.B. Liu, D.Q. Chen, X.Y. Li, Y.P. Qi, Q. Yang, P.W. You, S. Meng, *Physical Review Letters* **128,** 015702 (2022).
[5] R. J. Zhao, P.W. You, S. Meng. *Physical Review Letters* **130**, 166401 (2023).
[6] P. W. You, D.Q. Chen, X.B. Liu, C. Zhang, A. Selloni, S. Meng, *Nature Materials*, in print (2024).

Charge density waves in $ZrTe_3$: the fate of nesting in real 3D materials

N. Mignani[1], N. T. Samani[1], A. Fusinato[1], E. Carpene[1], A. Crepaldi[1], C. Dallera[1], A. Magrez[2], H. Berger[2]
[1] *Politecnico di Milano, 20133 Milano, Italy*
[2] *École Polytechnique Federale de Lausanne, CH-1015 Lausanne, Switzerland*

Among the materials hosting Charge Density Wave (CDW) phases, transition metal tri-chalcogenides have attracted considerable attention thanks to their quasi-one-dimensional (q1D) nature. $ZrTe_3$ is of particular interest because its Fermi surface comprises both a 3D hole like pocket centered at Γ and q1D bands at the zone edges [1,2] (Fig. 1). Extensive angle resolved photoemission spectroscopy (ARPES) studies have shown that the CDW transition, setting in at 63 K [3], is mainly driven by the q1D states, with the opening of a pseudo gap at the D point of the Brillouin zone. For this reason, Fermi Surface Nesting (FSN) between these states was proposed as the driving force of the CDW transition. However, FSN alone does not fully explain the observed changes in the gap and in the 3D band with temperature [4]. We performed time resolved ARPES measurements on $ZrTe_3$ single crystals, probed with 6 eV and 20.9 eV photon energy, revealing a transient photoinduced energy shift of the 3D band and subsequent coherent oscillations of both q1D and 3D bands compatible with the excitation of an A_g phonon mode.

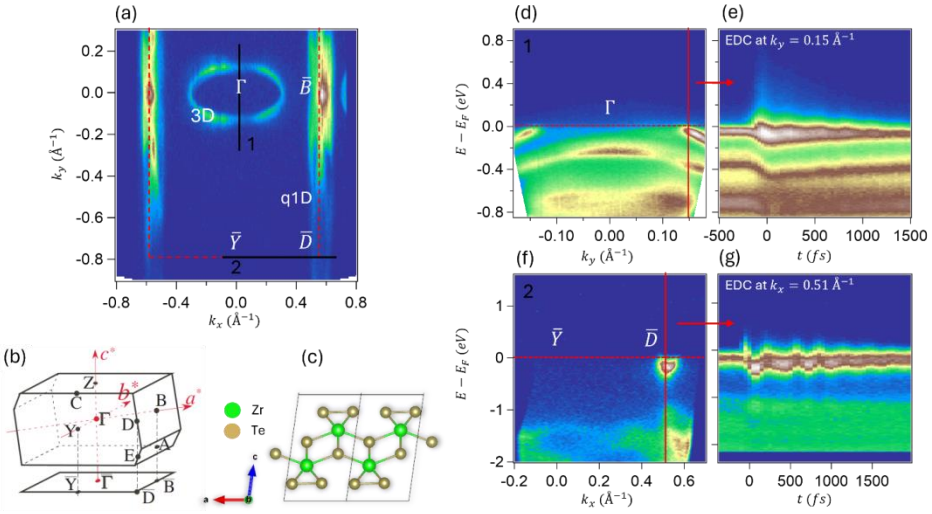

Fig. 1. (a) Fermi surface map of $ZrTe_3$ measured by ARPES *at 15 K. (**b**) Sketch of the Brillouin zone (adapted from [2]). (**c**) $ZrTe_3$ crystal unit cell projected on the [a,c] plane. (d) trARPES data of the 3D band taken along the ΓY direction (vertical black line in (**a**)) at negative pump-probe delay with 6 eV probe energy. (**e**) Energy Distribution Curves (EDC) dynamics taken along the vertical red line in (**d**). (**f**) trARPES data of the q1D band taken along the YD direction (horizontal black line in (**a**)) at negative pump-probe delay with 20.9 eV probe energy.*
*(**g**) EDCs dynamics along the vertical red line in (**f**).*

Hence, our experiment indicates the presence of a strong electron phonon coupling that could be involved in the CDW formation, in agreement with complementary observations [5] and providing an alternative scenario to the nesting mechanism.

References
[1] T. Yokoya, T. Kiss, A. Chainani, S. Shin, K. Yamaya, *Physical Review* B **71**, 140504 (2005).
[2] M. Hoesch, X. Cui, K. Shimada, C. Battaglia, S. I. Fujimori, H. Berger, *Physical Review* B **80**, 075423 (2009).
[3] S. Takahashi. T. Sambongi. S. Okada. *Journal de Physique Colloques* **44.** 1733 (1983).
[4] S.-P. Lyu, L.Yu, J.-W. Huang, C.-T. Lin, Q. Gao, J. Liu, G.-D.Liu, L.Zhao, J.Yuan,C.-T. Chen,Z.-Y.Xu, X.-J.Zhou,*Chinese Physics* B **27**, 087503 (2018)
[5] Y. Hu, F. Zheng, X. Ren, J. Feng, Y. Li, Physical Review B **91**, 14452 (2015).

Structured nonlinear optics in van der Waals crystals

P. Padmanabhan[1], T. Norden[1], L.M. Martinez[1], N.Tarefder[1], K. W. C. Kwock[2], L. M. McClintock[1], N. Olsen[2]
L. N. Holtzman[2], X. Zhu[2], J. C. Hone[2], J.Yoo[1], J.-X. Zhu[1], P. J. Schuck[2], A. J. Taylor[1]
R P. Prasankumar[3], W. J. M. Kort-Kamp[1]
[1] *Los Alamos National Laboratory, Los Alamos, NM 87545, USA*
[2] *Columbia University, New York, NY 10027, USA*
[3] *Deep Science Fund Intellectual Ventures; Bellevue, WA 98005, USA*

Vortex beams possessing helical wavefronts can carry non-zero orbital angular momentum (OAM) equivalent to integer multiples of $\hbar$, indexed by their topological charge (ℓ) [1-2]. Most efforts aimed at exploiting such "twisted" light fields are predicated on an ability to precisely, and independently tune their wavelength and OAM. Conventional nonlinear optical (NLO) approaches used to manipulate these parameters typically rely on birefringent phase matching in bulk crystals with broken inversion symmetry to achieve the requisite energy and momentum conservation [3]. This results in systems that are ill-suited to integrated devices and operational bandwidths that are constrained by material choice and geometry. These challenges have fueled an interest in uncovering NLO processes in low-dimensional materials [4], which offer a high degree of compatibility with emerging two-dimensional (2D) hybrid platforms [5]. In this context, extending van der Waals (vdW) nonlinear optics through the spatial degree of freedom of light would be transformative, dramatically expanding the functionality, while shrinking the length scale, of a wide array of classical and quantum NLO devices. Here, we show that the fundamental properties of optical vortices can be freely and independently tuned via NLO frequency-mixing processes in a 2D vdW crystal. Using monolayer MoS_2, we demonstrate the ad hoc control over wavelength and topological charge through difference frequency generation (DFG), sum frequency generation (SFG), and four-wave mixing (FWM). In our studies, we employ time-resolved structured-light microscopy to drive and interrogate vortex NLO processes in monolayer flakes of MoS_2 exfoliated onto a glass substrate. In all cases, a Gaussian pulse (i.e., $\ell_p = 0$) serves to pump the NLO process. A seed pulse with tunable wavelength supplied by an optical parametric oscillator (OPO) is converted to a Laguerre-Gaussian (LG) vortex beam (i.e., $\ell_s \neq 0$) and is colinearly and spatio-temporally overlapped with the pump on the crystal. The reflected beam is filtered to isolate the generated nonlinear component and its intensity, spectral content, and spatial profile are

simultaneously analyzed.

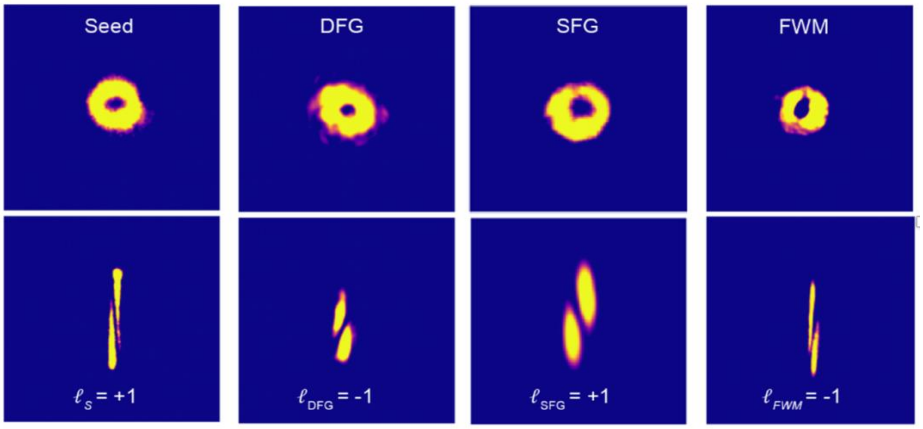

Fig. 1. Real-space images (top panels) *of the donut shaped intensity profile of the vortex seed ($\ell_S = +1$, $\hbar\omega_S = 1.18$ eV) and resulting DFG ($\ell_{DFG} = -1$, $\hbar\omega_{DFG} = 1.92$ eV), SFG ($\ell_{SFG} = +1$, $\hbar\omega_{SFG} = 2.81$ eV) and FWM ($\ell_{FWM} = -1$, $\hbar\omega_{FWM} = 1.92$ eV) outputs. The lower panels show the corresponding momentum space maps imaged at the focal plane of a cylindrical lens. For all data, the pump beam is always Gaussian ($\ell_P = 0$, $\hbar\omega_P^{DFG} = 3.1$ eV, $\hbar\omega_P^{SFG} = 1.63$ eV , $\hbar\omega_P^{FWM} = 1.55$ eV).*

The seed vortex beam is generated using a spatial light modulator (SLM) encoded with a spiral phase mask. For example, a vortex beam with a topological charge of $\ell = +1$ has a 0 to 2π azimuthal phase modulation with a single-phase singularity. This translates to a spatial profile with a characteristic donut-like intensity distribution. The magnitude and sign of the topological charge can be measured by mapping the LG vortex to momentum space using a cylindrical lens [6]. Here, the number of gaps between fringes is equal to the magnitude of the topological charge and the skew corresponds to its sign. To explore vortex DFG, SFG, and FWM, we utilize a Gaussian pump pulse ($l_p = 0$) with various photon energies ($\hbar\omega_p^{DFG} = 3.1$ eV, $\hbar\omega_p^{SFG} = 1.63$ eV, $\hbar\omega_p^{FWM} = 1.55$ eV) and a vortex seed pulse ($\hbar\omega_s = 1.14 - 1.22$ eV, $\ell_s = +1$). The top panels of Fig. 1 show the donut shaped intensity profile of the vortex seed beam ($\ell_s = +1$, $\hbar\omega_s = 1.18$ eV), followed by the resulting DFG ($\hbar\omega_{DFG} = \hbar\omega_p^{DFG} - \hbar\omega_s = 1.92$ eV), SFG ($\hbar\omega_{SFG} = \hbar\omega_p^{SFG} + \hbar\omega_s = 2.81$ eV), and FWM ($\hbar\omega_{FWM} = 2\hbar\omega_p^{FWM} - \hbar\omega_s = 1.92$ eV) outputs, where their respective topological charges should obey OAM conservation laws ($l_{DFG} = \ell_p - \ell_s = -1$, $l_{SFG} = \ell_p + \ell_s = +1$, and $l_{FWM} = 2\ell_p - \ell_s = -1$). Clearly, the DFG, SFG, and FWM outputs inherit the donut-like intensity pattern and are approximately equivalent in diameter to the input seed, indicative of the conservation of the OAM magnitude. Indeed, the lower panels of Fig 1 show the corresponding momentum space maps of the frequency-mixed outputs, each with a single gap between a pair of fringes, confirming that $|\ell_{DFG}| = |\ell_{SFG}| = |\ell_{FWM}| = 1$. The skew direction of the SFG output fringe pattern is the same as that of the seed, reflecting the conservation of the magnitude and sign of the topological charge. In contrast, the skew direction of the DFG and FWM outputs are opposite that of the seed, indicative of an inversion of the topological charge for these two NLO processes, as required by their OAM conservation laws. The ability to realize such multi-beam vortex NLO processes in a monolayer vdW crystal opens a wide range of possibilities to utilize these materials as nanoscale sources of tunable vortex light, applicable to classical and quantum communication nanophotonic devices. Moreover, while we have focused on second-order and third-order processes, we envision that higher-order processes can also be realized, allowing us to extend further into the ultraviolet regime. Moreover, it may allow us to potentially couple the orbital degree of freedom of light to topology-driven light-matter interactions [7], providing us with greater insight into the nature of such material systems.

References

[1] L. Allen, M. W. Beijersbergen, R. J. C. Spreeuw, J. P. Woerdman, *Physical Review* A **45**, 8185 (1992).
[2] K Dholakia, K. Dholakia, N. B. Simpson, M. J. Padgett, L. Allen, *Physical Review* A **54**, 3742 (1996).
[3] S. Araki, K. Ando, K. Miyamoto, T. Omatsu, *Applied Optics* **57**, 620 (2018).
[4] A. Autere, H. Jussila, Y. Dai, Y. Wang, H. Lipsanen, Z. Sun, *Advanced Materials* **30** (2018).
[5] B. Guo, Q. Xiao, S. Wang, H. Zhang, *Laser Photonics Review* **13** (2019).
[6] S. N. Alperin, R.D. Niederriter, J.T. Gopinath, M.E. Siemens, *Optics Letters* **41**, 5019 (2016).
[7] C. Heide, Y. Kobayashi, D. R. Baykusheva, D. Jain, J. A. Sobota, M. Hashimoto, P. S. Kirchmann, S. Oh, T. F. Heinz, D. A. Reis S. Ghimire, *Nature Photonics* **16**, 620 (2022).

* Acknowledgments: T.N., L.M.M., L.M.Mc., W.K.K., and P.P. acknowledge support from the Los Alamos National Laboratory - Laboratory Directed Research and Development Program (20220273ER and 20240037DR). L.M.M. also acknowledges support from the Department of Energy (DOE) National Nuclear Security Administration (NNSA) Minority Serving Institution Partnership Program. K.W.C.K. acknowledges support from the NNSA Laboratory Residency Graduate Fellowship program (DE-NA0003960). Work was primarily performed at the Center for Integrated DOE Nanotechnologies, an Office of Science User Facility operated for the U.S. DOE Office of Science. Los Alamos National Laboratory, an affirmative action equal opportunity employer, is managed by Triad National Security, LLC for the US DOE NNSA, under contract no. 89233218CNA000001.

Ultrafast XUV modulator and ultrafast electronic memory devices based on an Electronic phase transition

Y. Vaskivskyi[1], J. Vodeb[1], I.Vaskivskyi[1], E. Božin[2], D.Mihailovic[1]
[1]*Jozef Stefan Institute, 1000 Ljubljana, Slovenia*
[2]*Brookhaven National Laboratory, Upton, NY 11973, USA*

The discovery of charge-configurable metastable states in charge density wave materials that can be manipulated in time [1,2] and space using ultrafast optical techniques [3], as well as by pulsed direct current injection in diverse device configurations, has led to new applications in important areas of electronics [4–8] and optics [9]. In this talk I will present some of the fundamental principles leading to the emergent metastable quantum state in the prototype material 1T-TaS_2, including some very recent findings on the decay dynamics that elucidate the microscopic origins of the metastable state and the accompanying resistivity switching [10]. These findings may be relevant in the search for similar effects in other quantum materials, such as the recent case of $EuTe_4$ [7]. We pay particular attention to the non-equilibrium phase diagram which reveals different transport mechanisms in different metastable states, ranging from metallic, variable range hopping and simple activated behaviour and the structural deformations caused by the passing current. The second part of the talk will be devoted to a description of new ultrafast memory devices in a superconducting cryo-computing environment [11] and remarkable applications for ultra-efficient XUV and X-ray modulators that promise to revolutionise X-ray beam steering optics shown in Fig. 1 [9] that arise due to completely different manifestations of the metastable state.

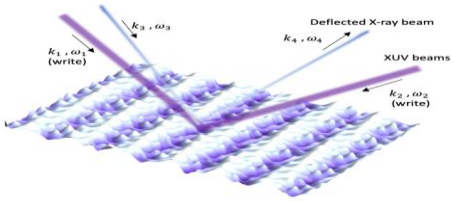

Fig. 1 High-efficiency X-ray modulator based on the spatial modulation of the 1T-TaS2 metastable state*. A buckled surface is formed as a result of a pulsed transient grating. The XUV or X-ray beam is deflected from the grating. The grating can operate as a modulator or as a programmable grating at low temperatures.*

The mechanism for the transition to the metastable state is understood to arise from photodoping of the conduction band with electrons, or by carrier injection with electrical pulses ranging from 1.9 ps to microseconds or more. Similarities between optical excitation and charge injection can be seen in the resulting strain. Charge injection creates domain walls in the electronic crystal order which, after examination of the hidden metastable state by scanning tunneling microscopy are seen to preferrentially run parallel with the direction of the applied current (dark lines in Fig.2). This in turn results in a strain modulation which also runs parallel to the direction of the current (vertical light stripes Fig.2).

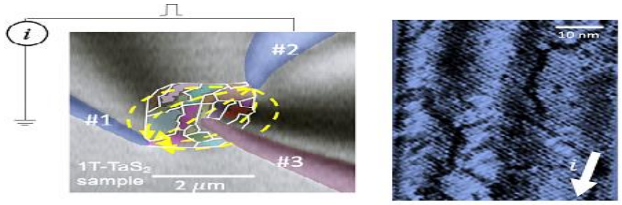

Fig. 2 The strain modulation observed by scanning tunneling microscope *after a short current pulse is applied through STM tips (**left panel**). The direction of the electrical current is indicated by the arrow (**right panel**). Domain walls are also observed as dark lines.*

The remarkably controllable state and experimental accessibility of the microscopic state due to the temperature-tunable lifetime make 1T-TaS_2 an excellent prototype system for detailed investigations of the causes and consequences of the emergent metastable state.

References

[1] D. Mihailovic, D.Dvorsek, V.V.Kabanov, J.Demsar, L.Forro, H.Berger, *Applied Physics Letters* **80**, 871 (2002).
[2] J. Ravnik, I.Vaskivskyi, T.Mertelj, D. Mihailovic, *Physical Review* B **97**, e1400173 (2018).
[3] L. Stoichevska. I. Vaskivskvi1 . T. Merteli . P. Kusar . D. Svetin. S. Brazovskii. D. Mihailovic. *Science* **344**, 177 (2014).
[4] S. Baraghani, Z. Barani, Y. Ghafouri, A. Mohammadzadeh, T,T. Salguero, F. Kargar, A.A. Balandin, *ACS Nano* **16**, 6325 (2022).
[5] A. K. Geremew S. Rumyantsev, B.Debnath,R. K. Lake, A.A. Balandin, *Applied Physics Letters* **116**, 163101 (2020).
[6] A. Khitun, G. Liu, A. A. Balandin, *IEEE Transactions on Nanotechnology* **16**, 860 (2017).
[7] Q. M. Liu, D.Wu, T. Y.Wu, S.S. Han, Y.R. Peng, Z. H. Yuan,Y. H. Cheng, B. H. Li, T. C. Hu, L. Yue, S.X. Xu, R.X. Ding, M. Lu, R.S. Li, S.J. Zhang B. Q. Lv, A. Zong, Y.F. Su, N. Gedik, Z.P. Yin, T. Dong, N.L. Wang, *arXiv 2310.10293v1* (2023).
[8] A. Mraz, R. Venturini, D. Svetin, V. Sever, I. A.Mihailovic, I. Vaskivskyi, B. Ambrozic, G. Dražić, M. D'Antuono, D. Stornaiuolo, F. Tafuri D. Kazazis, J. Ravnik, Y. Ekinci, D.Mihailovic, *Nano Letters* **22**, 4814 (2022).
[9] I. Vaskivskyi, A. Mraz, R. Venturini, G. Jecl, Y. Vaskivskyi, R. Mincigrucci, L. Foglia, D. De Angelis, J.-S. Pelli-Cresi, E. Paltanin, D. Fainozzi F. Bencivenga,C. Masciovecchio, D. Mihailovic, *Nature Photonics* **18**, 458 (2024).
[10] A. Mraz, M. Diego, A. Kranjec, J. Vodeb, P . Karpov, A. Gerasimenko, J. Ravnik, Y. Vaskivskyi, R. Venturini, V. Kabanov, B. Lipovšek M.Topič, I.Vaskivskyi,D.Mihailovic , *Nature Communications* **14**, 8214 (2023).
[11] A. Mraz, V. V. Kabanov, and D. Mihailovic, *arXiv:2203.14586v1* (2022).

Progress in mid-IR ultrafast lasers based on transition metal doped II-VI gain media

S. Mirov
University of Alabama at Birmingham, Birmingham AL 35294, USA

Chromium and iron-doped ZnSe and ZnS lasers have come of age due to advancements in laser design, thermal management, fabrication of low-loss polycrystalline gain media, as well as the availability of effective fiber and hybrid fiber-bulk pump lasers. Arguably, Cr and Fe-doped ZnSe/S lasers currently represent the most effective route for middle-infrared (MIR) lasing over the 1.9–6 μm spectral range in all the known oscillation regimes. Ultrafast MIR lasers based on transition-metal-doped II-VI chalcogenides (TM:II-VI, [3]) attract growing attention because they provide direct access to peak- and average-power scalable few-optical-cycle mid-IR pulses. The progress in TM:II-VI lasers has been further accelerated by the development of new methods of laser material fabrication. Specifically, the technology based on a post-grown thermal diffusion doping of ZnS and ZnSe [1] has enabled large-scale production of large-size polycrystalline gain elements with high optical quality and high dopant concentration (see Fig.1). This, in turn, has dramatically simplified the development of ultrafast amplifiers and enabled the development of fs oscillators with unique output parameters [1-7]. The unique capabilities of polycrystalline Cr:ZnS and Cr:ZnSe for generation, amplification, and nonlinear frequency conversion of ultra-short optical pulses in the MIR range were successfully explored for the development of octave-spanning single optical cycle oscillators [5], full repetition rate MOPAs with average power above 30 W [1], and CPA multipass amplifiers with TW levels of output power [8]. Cr:ZnS is a typical representative of a large TM:II-VI family. It combines superb ultrafast laser capabilities with broad IR transparency and high nonlinearity of wide-bandgap II-VI semiconductors. It supports all mode-locking regimes, from active to passive to Kerr-lens mode-locking. The key advantage of Cr:ZnS Kerr lens-based ultrafast laser and frequency comb technology is high efficiency: 20 – 25% optical-to-optical conversion from low-cost CW EDFL light to 2-cycle MIR pulses and 10 – 12% conversion of 2-cycle pulses at 2.4 μm to single-cycle electromagnetic transients in the longwave IR. Further, the system's complexity is significantly reduced because all the optical signals required for stabilizing the MIR comb with the large lever arm are generated directly inside the polycrystalline Cr:ZnS gain medium of a single-pass amplifier. One can equip the system with an additional optical rectification stage to enhance the optical power in the offset-free longwave IR spectral band. For instance, ZGP crystal allows the record-breaking efficiency of optical rectification. It generates super-octave longwave (4-12 μm) IR combs with Watt-level power [7]. Those advantages allowed the implementation of shoe-box-sized, lightweight fs frequency combs with the brightness exceeding the brightness of a synchrotron by orders of magnitude in a broad spectral range [9]. The developed MIR frequency combs open new avenues in imaging, sensing, and spectroscopy [10]. The combination of effective MIR Cr:II-VI femtosecond oscillators, the high energy storage capabilities of Fe:II-VI, which are unique among MIR gain media, and OPCPA and CO_2 amplifiers will be discussed for the development of TW-class ultrafast MIR systems operating over the 2–10.6 μm spectral range for high energy physics applications.

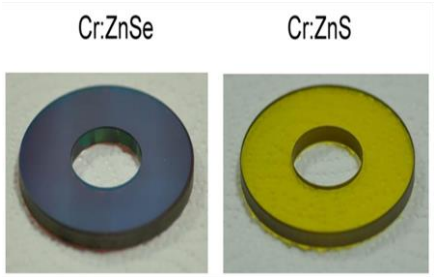

Fig. 1. *Ø50x5mm Cr:ZnSe and Cr:ZnS gain elements with Cr concentration 10^{19}*

References

[1] S. Mirov, I. Moskalev, S. Vasilyev, V. Smolski, V. Fedorov, D. Martyshkin, J. Peppers, M. Mirov, A. Dergachev, V. Gapontsev, *IEEE Journal of Selected Topics in Quantum Electronics* **24**, 1601829 (2018).
[2] S. Vasilyev, I. Moskalev, M. Mirov, S. Mirov, V. Gapontsev, *Optics Express* **24,** 1616 (2016).
[3] S. Vasilyev, M. Y. Sander, J. Gu, V. Smolski, I. Moskalev, M. Mirov, Y. Barnakov, J. Peppers, M. Kolesik, S. Mirov, V. Gapontsev, *JOSA* B **38** 1625(2021).
[4] S. Vasilyev, V. Smolski, J. Peppers, I. Moskalev, M. Mirov, Y. Barnakov, S. Mirov, V. Gapontsev, *Optics Express* **27**, 35079 (2019).
[5] S. Vasilyev, I. Moskalev, V. Smolski, J. Peppers, M. Mirov, Y. Barnakov, V. Fedorov, D. Martyshkin, S. Mirov, V. Gapontsev, *Optics Express* **29** 2458(2021).
[6] S. Vasilyev, I. Moskalev, V. Smolski, J. Peppers, M. Mirov, V. Fedorov, D. Martyshkin, S. Mirov, V. Gapontsev, *Optica* **6**, 126 (2019).
[7] S. Vasilyev, I. S. Moskalev, V. O. Smolski, J. M. Peppers, M. Mirov, A. V. Muraviev, K. Zawilski, P. G. Schunemann, S. B. Mirov K. L. Vodopyanov, V.P. Gapontsev, *Optica* **6**, 111 (2019).
[8] X. Lu, X. Wang, J. Fan, R. Xu, J. Chen, L. Zhang, Y. Leng, *Optica* **10**, 1567 (2023).
[9] S. Vasilyev, M. Mirov, S. Mirov, *Laser Focus World*, 21(2022).
[10] S. Vasilyev, A. Muraviev, D. Konnov, M. Mirov, V. Smolski, I. Moskalev, S. Mirov, K. L. Vodopyanov, *Optics Letters* **48,** 2273 (2023).

* Acknowledgement: S.M. acknowledges support from IPG Photonics Corporation and support from DARPA (grant W31P4Q-15-1-0008), DOE (grant DE-SC0018378), and NIEHS (grant) P42ES027723.

Dark states in silicon

J. M. Nichol, X. X. Cai, H. Y. Walelign
University of Rochester, Rochester, NY 14627 USA

Electron spins in semiconductor quantum dots typically interact with many nuclear spins in their semiconductor environments, realizing a manifestation of the central spin problem. The central spin problem is a widely studied model of decoherence and is predicted to exhibit a rich variety of interesting and useful phenomena, only some of which have been observed. In this talk, I will discuss a series of experiments exploring these dynamics in silicon quantum dots. We report evidence for the formation of a nuclear dark state, which occurs when the nuclei are driven into a state that does not interact with the electrons [1-7]. We show evidence that this dark state depends on the synchronized precession of the nuclear spins, and that driving the nuclear spins into the dark state promotes increased lifetimes of electronic spin states. We also discuss the relationship between the dark state and the coherence time of electronic spin states.

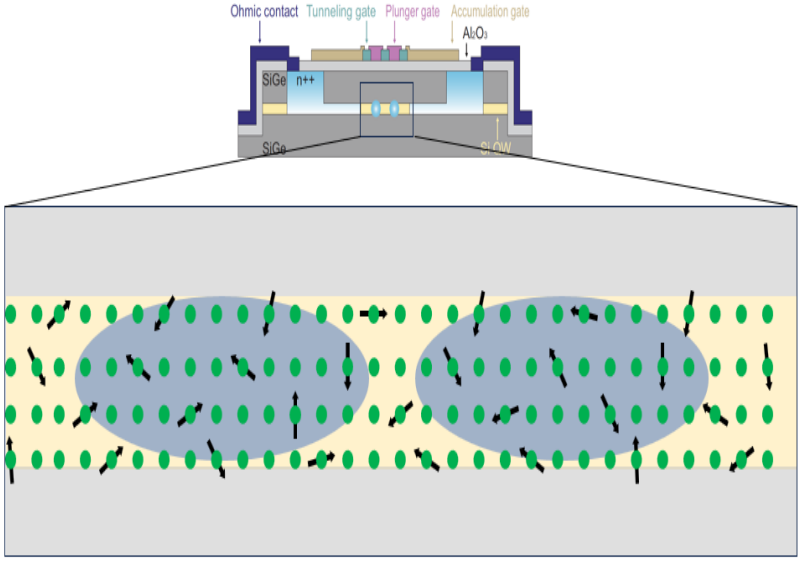

Fig. 1. Schematic of a silicon gate-defined quantum dot (top) *and the electronic wavefunctions interacting with silicon-29 nuclear spins (**bottom**).*

In this work, we prepare and detect nonequilibrium nuclear spin states in Si quantum dots using a two-electron-spin qubit. The electrons in the qubit interact with silicon-29 atoms in the semiconductor. In this system, the transverse hyperfine field from the nuclei mediates dynamic nuclear polarization, which occurs through repeated Landau-Zener sweeps of the electronic spins states. After repeated Landau-Zener sweeps, we find evidence for the suppression of transverse hyperfine fluctuations, indicative of the formation of a nuclear dark state. Together with numerical simulations, we show that this dark state is associated with synchronized precession of the nuclear spins, and without driving, it persists for more than 1 millisecond as determined by the nuclear spin dephasing time. We further show that driving the nuclear spins into the dark state increases the lifetime of the electronic spin states by at least an order of magnitude.Our results open new possibilities for investigations on decoherence-mitigation strategies and inter-particle correlations in central spin systems. Future directions include exploring the effects of spin-orbit coupling, quantum correlations between nuclear spins, uses of the nuclear dark state as a quantum memory, and how the dark state limits the maximum achievable nuclear polarization in silicon quantum dots.

References

[1] A. Immamoglu, E. Knill, L. Tian, P. Zoller , *Physical Review Letters* **91**, 017402 (2003).
[2] J. M. Taylor , A. Imamoglu, M. D. Lukin, Physical Review Letters **91**, 246802 (2003).
[3] M. S. Rudner, L.S. Levitov, *Physical Review Letters* **102**, 065703 (2009)
[4] M. Gullans, J. Kirch, J. Taylor, H. Bluhm, B. Halperin, C. Marcus, M. Stopa, A. Yacoby, M. D Lukin, *Physical Review Letters* **104**, 226807 (2010).
[5] A. Brataas, E.I. Rashba, *Physical Review* B **84**, 045301 (2011)
[6] D. Gangloff, L. Zaporski, J. H. Bodey, C. Bachorz, D. M. Jackson, G. Éthier-Majcher, C .Lang, E. Clarke, M. Hugues, C. Le Gall, M.Atatüre *Nature Physics* **17** 1247(2021).
[7] E. Kirstein, D. S. Smirnov, E. A. Zhukov, D. R. Yakovlev, N. E. Kopteva, D. N. Dirin, O. Hordiichuk, M. V. Kovalenko, M. Bayer, *Nature Communications* **14**, 6683 (2023)

* Acknowledgement(s): The authors acknowledge support NSF Grant No. DMR-1941673 and Army Research Office Grant. No W911NF-23-1-0115

Theory of Higgs spectroscopy for Superconductors in non-equilibrium: latest results

D. Manske
Max Planck Institute for Solid State Research, 70569 Stuttgart, Germany

Higgs spectroscopy is a new and emergent field [1-3] that allows to classify and to determine the superconducting order parameter by means of ultra-fast optical spectroscopy. There are two ways to activate the Higgs mode in superconductors, namely a single-cycle 'quench' or an adiabatic, multicycle 'drive' pulse, both illustrated in Figure 1. In the talk I will review and report on the latest progress on Higgs spectroscopy, in particular on the role of the third-harmonic-generation (THG) [4-6] and the possible IR-activation of the Higgs mode by impurities or external dc current [7,8]. I also provide new predictions for time-resolved ARPES experiments in which, after a quench, a continuum of Higgs mode is observable and a phase information of the superconducting gap function would be possible to extract [9].

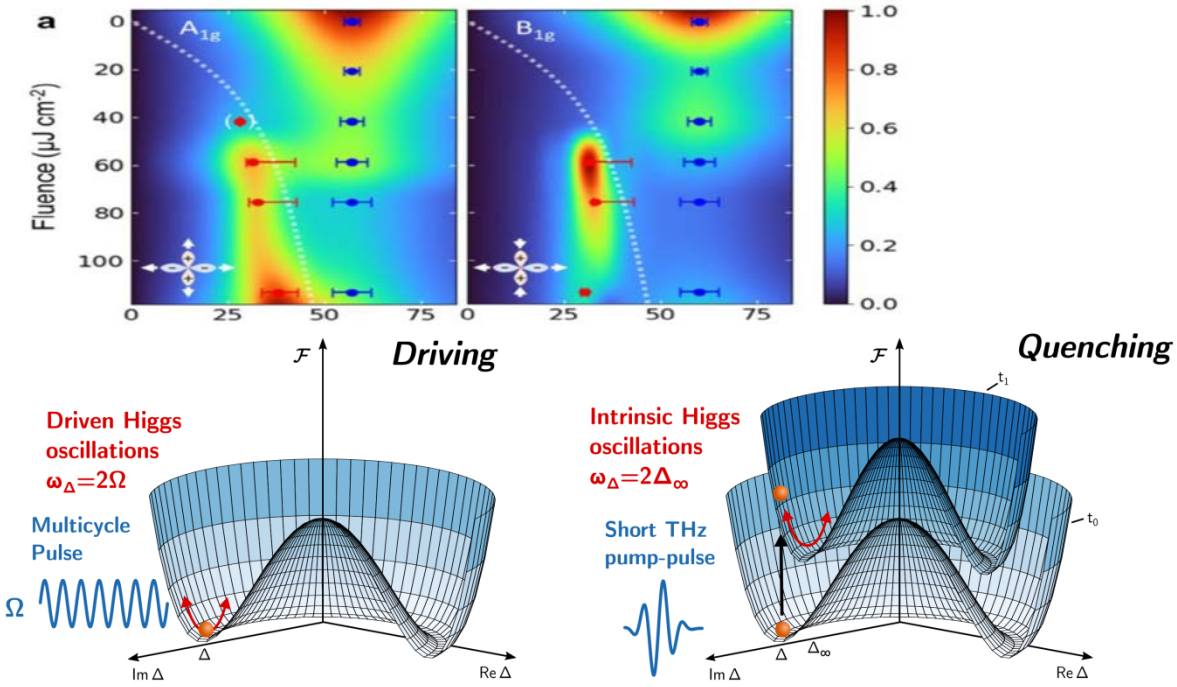

Fig. 1. Top panel *Higgs mode in the NEARS spectrum of optimally doped BISSCO for A_{1g} and B_{1g} polarization, respectively. Taken from Ref. [10.]* ***Bottom panel:*** *2 ways for activation of the Higgs mode by light* ***(left)*** *Illustration of multi-cycle driving the Higgs mode:* ***(right)****: Illustration of single-cycle quenching of the free energy potential.*

Finally, I discuss recent results on Non-Equilibrium Anti-Stokes Raman Scattering (NEARS) [10] and on two-dimensional coherent spectroscopy [11,12] where the Higgs mode has been observed experimentally.

References

[1] L. Schwarz, B. Fauseweh, N. Tsuji, N. Cheng, N. Bittner, H. Krull, M. Berciu, G. S. Uhrig, A. P. Schnyder, S. Kaiser, D. Manske, *Nature Communications* **11**, 287 (2020).
[2] L. Schwarz, D. Manske, *Physical Review* B **101**, 184519 (2020).
[3] H. Chu, M.-J. Kim, K. Katsumi, S. Kovalev, R. D. Dawson, L. Schwarz, N. Yoshikawa, G. Kim, D. Putzky, Z .Z. Li, H. Raffy, S. Germanskiy J.- C. Deinert, N.Awari, I. Ilyakov, B. Green, M. Chen, M. Bawatna, G. Cristiani, G. Logvenov, Y. Gallais, A.V. Boris, B. Keimer, A.P. Schnyder D. Manske, M. Gensch, Z. Wang, R. Shimano, S. Kaiser, *Nature Communications* **11**, 1793 (2020).
[4] L. Schwarz. R. Haenel, D. Manske, *Physical Review* B **104**, 174508 (2021).
[5] H. Chu, S. Kovalev, Z. X. Wang , L. Schwarz, T. Dong, L. Feng, R. Haenel, M.-J. Kim, P. Shabestari, L. P. Hoang, K. Honasoge, R. D. Dawson D. Putzky, G. Kim, M. Puviani, M. Chen, N. Awari, A. N. Ponomaryov, I. Ilyakov, M. Bluschke, F. Boschini, M. Zonno, S. Zhdanovich, M. Na G. Christiani, G. Logvenov, D. J. Jones, A. Damascelli, M. Minola , B. Keimer, D. Manske, N. Wang, J.- C. Deinert, S. Kaiser, *Nature Communications* **14**, 1343 (2023).
[6] M.- J. Kim, S. Kaiser, D. Manske, *Science Advances* **10**, 3adi7598 (2024).
[7] M. Puviani, L. Schwarz, X.-X. Zhang, S. Kaiser, D. Manske, *Physical Review* B **101**, 220507 (2020).
[8] R. Haenel, P. Froese, D. Manske, L. Schwarz, *Physical Review* B **104**, 134504 (2021).
[9] L. Schwarz, B. Fauseweh, D. Manske, *Physical Review* B **101**, 224510 (2020).
[10] T. E. Glier, M. Rerrer, L. Westphal, G. Lullau, L. Feng, S. Tian, J. Dolgner, R. Haenel, M. Zonno, H. Eisaki, M. Greven, A. Damascelli, S. Kaiser M. Rubhausen, *arXiv 2310.08162*. submitted to Nature (2024).
[11] K.Katsumi, J. Fiore, M. Udina, R. Romero III, D. Barbalas, J .Jesudasan, P. Raychaudhuri, G. Seibold, L. Benfatto, N. P. Armitage, arXiv 2311.16449, *in print Physical Review Letters* (2024).
[12] M.Puviani, R. Haenel, D. Manske, *Physical Review* B **107**, 094501 (2023).

Recent advances in the optical control of superconductivity in High-T_C cuprates

D. Nicoletti[1], M. Buzzi[1], A. Ribak[1], R. Singla[1], N. Taherian[1], M. Först[1], A. Liu[1], M. Fechner[1], D. Pavicevic[1] A. von Hoegen[1], E. Rowe[1], Y. Liu[2], S. Nakata[2], B. Keimer[2], E. Demler[3], M. H. Michael[1], A. Cavalleri[4]
[1] *Max Planck Institute for the Structure and Dynamics of Matter, 22761 Hamburg, Germany*
[2] *Max Planck Institute for Solid State Research, 70569 Stuttgart, Germany*
[3] *ETH Zurich, 8092 Zurich, Switzerland*
[4] *University of Oxford, Oxford OX1 3PU, United Kingdom*

Tailored optical excitation in certain high-T_C cuprates has been shown to induce superconducting-like interlayer coherence at temperatures far above T_C, as evidenced by the terahertz-frequency optical properties in the nonequilibrium state [1, 2]. In $YBa_2Cu_3O_{6+x}$, this phenomenon was initially attributed to the nonlinear excitation of certain lattice modes in the mid infrared and the creation of new crystal structures [3]. More recent work, however, has associated this phenomenon to a parametric excitation and amplification of Josephson plasma polaritons, which are overdamped above T_C but are made coherent by the phonon drive [4]. Here, we discuss our latest experiments in the field of optical control of superconductivity in $YBa_2Cu_3O_{6+x}$, which have led to considerable advances both in optimizing the nonequilibrium state and understanding the underlying mechanism behind its formation. First, we investigated both the enhancement of the "superfluid density", $\omega\sigma_2(\omega)$, and the dissipative response of quasiparticles, $\sigma_1(\omega)$, by systematically tuning the duration and energy of the mid-infrared excitation pulse while keeping the peak field fixed [5]. We found that the photoinduced $\omega\sigma_2(\omega)$ saturates to the zero-temperature equilibrium value for pulses made longer than the phonon dephasing time, while the dissipative component continues to grow with increasing pulse duration (see Fig. 1). Therefore, superfluid and dissipation remain uncoupled as long as the drive is on, enabling the identification of an optimal regime of pump pulse durations for which the superconducting-like response is maximum and dissipation is minimized.

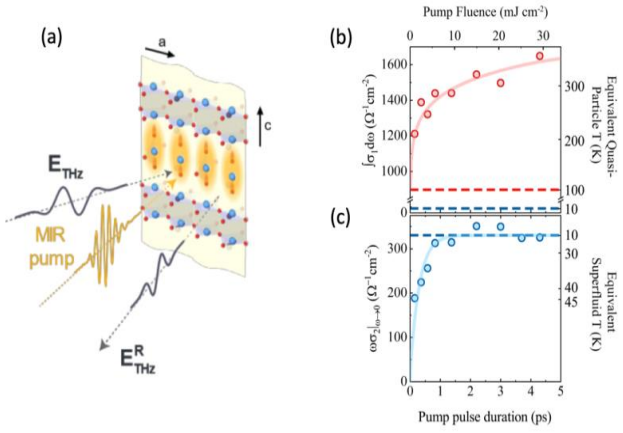

Fig. 1. a- Schematic of the mid-infrared (MIR) pump–THz probe experiment *in $YBa_2Cu_3O_{6.48}$. The sample is excited by a MIR pump pulse (**yellow**) polarized along the crystal c-axis, resonantly driving apical oxygen phonon modes as indicated inside the yellow shading. The subsequent changes in the low-frequency optical properties are sampled by a broadband, also c-polarized THz probe pulse (**grey**). **b-** Evolution of the transient spectral weight and (**c**) of the coherent superconducting-like response measured at the time delay corresponding to the peak of the light-induced response, as a function pump pulse duration. The top horizontal axis indicates the pump fluence which increases linearly with the pump pulse duration to keep the peak electric field constant. The red and blue horizontal dashed lines in (**b**) indicate the equilibrium spectral weight values at T = 100 K and T = 10 K, respectively, while that in (**c**) refers to the equilibrium superfluid density at T = 10 K. Equivalent temperatures are reported on the right axes.*

Second, in another recent experiment we went beyond conventional pump-probe schemes and acquired two-dimensional frequency maps using pairs of mutually delayed, carrier envelope phase stable mid-infrared pump pulses, combined with measurements of the time-modulated second-order nonlinear optical susceptibility [6]. We found that the driven zone-center phonons amplify coherent pairs of opposite-momentum Josephson plasma polaritons, generating a squeezed state of interlayer phase fluctuations. This squeezed state is a potentially important ingredient in the microscopic physics of photo-induced superconductivity in $YBa_2Cu_3O_{6+x}$ as well as in other materials.

References

[1] W. Hu, S.Kaiser, D. Nicoletti, C. R. Hunt, I. Gierz, M. C. Hoffmann, M. Le Tacon, T. Loew, B. Keimer, A. Cavalleri, *Nature Materials* **13,** 705 (2014)
[2] B. Liu, M. Först, M. Fechner, D. Nicoletti, J. Porras, B. Keimer, A. Cavalleri, *Physical Review X* **10,** 011053, (2020).
[3] R. Mankowsky, A. Subedi, M. Först, S. O. Mariager, M. Chollet, H. Lemke, J. Robinson, J. Glownia, M. Minitti, A. Frano, M. Fechner N. A. Spaldin, T. Loew, B. Keimer, A. Georges, A. Cavalleri, *Nature* **516,** 71 (2014).
[4] A. von Hoegen, M.Fechner, M. Först, N.Taherian, E. Rowe, A. Ribak, J. Porras, B. Keimer, M. Michael, E. Demler, A. Cavalleri, *Physical Review* X **13** 031008, (2022).
[5] A. Ribak, M. Buzzi, D. Nicoletti, R. Singla, Y. Liu, S. Nakata, B. Keimer, A. Cavalleri, *Physical Review B* **107,** 104508, (2023).
[6] N. Taherian, M. Först, A. Liu, M. Fechner, D. Pavicevic, A. von Hoegen, E. Rowe, Y. Liu, S. Nakata, B. Keimer, E. Demler, M. H. Michael A. Cavalleri, *arXiv:2401.01115* (2024).

* Acknowledgement(s): The research leading to these results received funding from the European Research Council under the EU's Seventh Framework Programme (FP7/2007- 2013)/ERC Grant Agreement No. 319286 (QMAC). Support from the Deutsche Forschungsge- meinschaft (DFG; German Research Foundation) via the excellence cluster "CUI: Advanced Imaging of Matter" (EXC 2056, project ID 390715994) and the priority program SFB925 (Project ID 170620586).

Attosecond currents in solids

M. Ossiander[2], K. Golyari[3], K. Scharl[3], I. Floss[4], V. Smejkal[4], C. Lemell[4]
F. Krausz[3], M. Schultze[1]
[1]*Graz University of Technology, 8010 Graz, Austria*
[2]*Harvard University, Cambridge, MA 02138, USA*
[3]*Max-Planck-Institute of Quantum Optics, 85748 Garching, Germany*
[4]*Vienna University of Technology, 1040 Vienna, Austria*

Achieving solid-state coherent electronics requires controlling light-induced carrier generation and motion on the one-femtosecond-scale to beat incoherence via equilibration. Because the durations of carrier and photon wavepackets are dictated by their spectral bandwidth, observing sub-femtosecond dynamics requires exploiting extreme ultraviolet laser pulses or nonlinear optical effects.

Carriers created via multi-photon absorption or strong-field injection are spectrally broad, and their energy spread in the conduction band is hard to predict. We avoid these complicated initial states by implementing extreme ultraviolet-inject and visible-drive photoconductive sampling (Fig. 1a) [1]: First, we single-photon-excite carriers from the valence to the conduction band of lithium fluoride (LiF, $_{\text{ap}} = 13.6$ eV) using a ~1-fs long extreme ultraviolet light pulse generated via high-harmonic generation. Then, using the electric field of a delayed, carrier-envelope-stable, visible laser pulse, we drive the crystal momentum of the photocarriers and generate a macroscopic current that we detect using electrodes on the sample surface (Fig. 1b). At low drive intensities, we find that the current is linear to vector potential of the driving laser field at the instant of carrier injection.

At increased driving field, the delay-dependent current deviates from the vector potential (Fig. 1b). We identify two contributions to the deviations (Fig. 1c): at the maxima of the observed current, the driving laser field can move carriers into non-parabolic regions of the band structure. This effect crops such maxima locally and is fully reversible after the maximum. When further increasing the driving field, the carriers are pushed near the Brillouin zone edge, where the distance to the second conduction band decreases. Here, the drive laser can non-adiabatically excite them to the second conduction band, a non-reversible transition that inverts the group velocity of the involved carriers. Because these transitions only occur after carriers have been propelled to the Brillouin zone edge, they modify the current signal before the driving laser pulse maximum and can be recognized by their timing.

This observation highlights that populating multiple adjacent conduction bands diminishes light-driven currents, allowing us to formulate a Fourier-type upper limit for the speed of efficient optoelectronics: carriers in an optoelectronic device made from a material possessing a conduction band with bandwidth ΔE_{CB} can most efficiently generate light wave-driven currents if the duration of the carrier wavepacket exceeds $\Delta\tau_{\text{FWHM}}$:

$$\Delta\tau_{\text{FWHM}}\,\frac{\Delta E_{\text{CB}}}{2} > 3.66\ \text{eV fs}$$

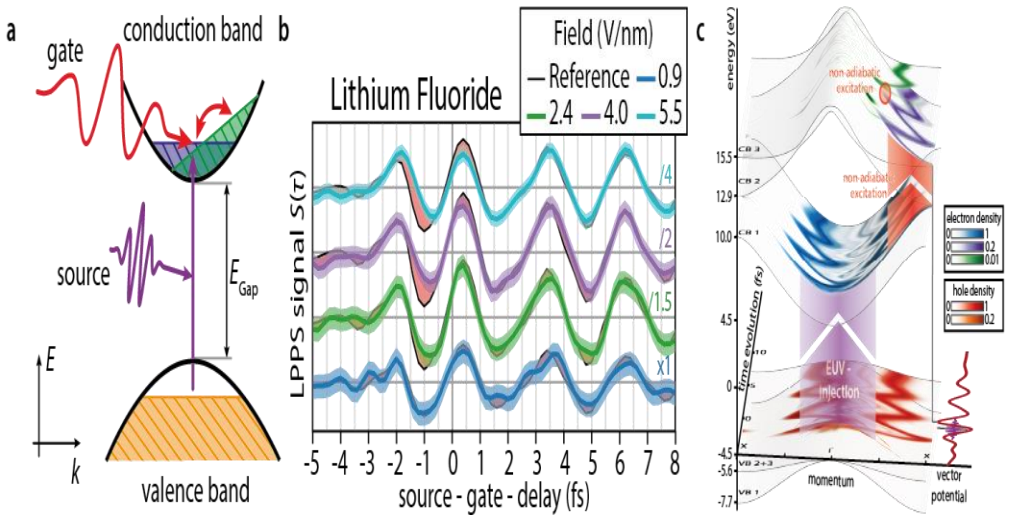

Fig. 1: a) Experiment: an extreme-ultraviolet laser pulse excites carriers from the valence to the conduction bands of LiF. *The electric field of a visible few-cycle laser pulse modulates their momentum. This accelerates the carriers and creates a macroscopic current.* ***b)*** *the measured current versus the delay between the extreme ultraviolet and the visible light pulses at different driving field strengths.* ***c)*** *semiconductor-Bloch-equation-modeled carrier dynamics in LiF. From [1].*

References

[1] M. Ossiander, K. Golyari, K. Scharl, L. Lehnert, F. Siegrist, J. P. Bürger, D. Zimin, J. A. Gessner, M. Weidman, I. Floss, V. Smejkal, S. Donsa C. Lemell, F. Libisch, N. Karpowicz, J. Burgdörfer, F. Krausz, M. Schultze, *Nature Communications* **13**, 1620 (2022).

Materials engineering of THz emission from spintronic emitters

E. Th. Papaioannou[1], O. Crisan [2], L. Scheuer[3], G. Torosyan[3], R. Beigang[3]
[1]*Aristotle University of Thessaloniki, 54124 Thessaloniki, Greece*
[2] *National Institute of Materials Physics, 077125 Magurele, Romania*
[3]*Technische Universität Kaiserslautern-Landau, 67663 Kaiserslautern, Germany*

The fascinating field of ultrafast spin physics has recently opened a new research direction in THz physics [1]. The main concept relates the generation/transport of ultrafast spin current to the emission of THz radiation. Such effect takes place after femtosecond laser pulse excitation of nanostructures which are composed of magnetic (FM) and non-magnetic (NM) ultra-thin layers [2]. The spin current is converted to an ultrafast charge current that is able to emit THz radiation. The key factor that defines the strength of the THz emission is the transfer of the spin current across the FM/NM interface. Such FM/NM nanostructures, the so-called spintronic THz emitters (STEs), hold the promise for the next generation of THz technologies, since they are able to provide high field strengths [3], spatiotemporal modulation of the THz beam [4] and a very wide spectrum reaching up to 30 THz [1,2]. Future applications of the effect on THz devices need the better understanding of ultrafast spin physics and reliable control of spin current generation and transport. Furthermore, the subsequent charge current dynamics need to be taken into account in terms of shaping the THz bandwidth and signal strength [5].In this work, we are addressing the need for controllable spin and charge current properties by investigating material aspects of the spintronic emitters. Although many materials have been so far studied as potential STEs [6], still the goal for a better functional THz emitter has not been fulfilled. We will present results from 'unconventional' STEs such as alloys of FePt, antiferromagnetic layers and emitters with different structural and magnetic anisotropies.We first refer to the need of finding the best material combination of ferromagnetic (FM) and nonmagnetic (NM) layer. We show how we can drastically modify the THz emission by inducing alloyed FM/NM phases. We use Fe/Pt bilayers as a model system to induce different alloyed phases in the layers [7]. We show that a graded structure of Fe/$L1_0$-FePt/Pt can boost the THz emission. We also reveal the role of other phases like the Fe_3Pt and $FePt_3$ which can also modify the strength of the spin current and the interface transmission. Next, we probe the role of very thin antiferromagnetic interlayers like NiO and CoO in Ni(Co)/NiO(CoO)/Pt heterostructures in transporting ultrafast spin current and subsequently emitting THz radiation [8]. We show that antiferromagnetic layers are able to transport spin current and modify the THz spectrum. Furthermore, we focus on different crystallographic phases of the non-magnetic layers where the spin-to-charge conversion is taking place. We present the cases of Pt and Ta where the layers exhibit different crystallographic growth modes in the spintronic heterostructure.

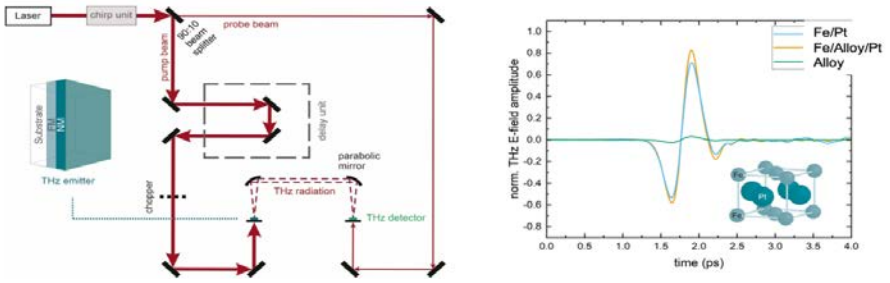

***Fig. 1. Left**: **Schematic of THz-Time Domain Spectroscopy** (THz-TDS) system used for our measurements. [7] **Right**: Large THz emission signals from modified Fe/Pt structures. The tetragonal alloyed phase (**shown as an inset**) induces the strongest signal compared to Fe/Pt bilayers and other Fe_xPt_{1-x} alloys.*

We show that a phase transition of Ta and a polycrystalline to epitaxial transition of Pt are able to reconstruct the THz emission and bandwidth. Our results show that materials engineering have a great influence in THz spintronic heterostructures and it can be of highly importance topic for the future applications of THz spintronics.

References

[1] T. Seifert, S.Jaiswal, U.Martens, J.Hannegan, L.Braun, P.Maldonado, F.Freimuth, A.Kronenberg, J.Henrizi, I. Radu, *Nature Photonics* **10**, 483(2016).
[2] E. Th. Papaioannou, R. Beigang, *Nanophotonics* **10**, 1243 (2021).
[3] R. Rouzegar, A. Chekhov, Y. Behovits, B. Serrano, M. Syskaki, C. Lambert, D. Engel, U. Martens, M. Münzenberg, M. Wolf, *Physical Review Applied*, **19**, 034018, (2023).
[4] H. Niwa, N. Yoshikawa, M. Kawaguchi, M. Hayashi, R. Shimano, *Optics Express* **29**, 13331 (2021).
[5] G. Schmidt, B. Das-Mohapatra, E. Th. Papaioannou, *Physical Review Applied* **19**, L041001 (2023).
[6] C. Bull, S.M. Hewett, R. Ji, C.H. Lin, T. Thomson, D.M. Graham, P.W. Nutter, *APL Materials* **9**, 090701 (2021).
[7] L. Scheuer, M. Ruhwedel, D. Karfaridis, I.G. Vasileiadis, D. Sokoluk, G. Torosyan, G. Vourlias, G.P. Dimitrakopoulos, M. Rahm, B. Hillebrands *iScience* **25**, 104319 (2022).
[8] N. Kanistras, L.Scheuer, D.Anyfantis, A.Barnasas, G.Torosyan, R.Beigang, O.Crisan, P.Poulopoulos, E. Papaioannou, *Nanomaterials* **14**, 215 (2024).
* Acknowledgement(s): authors E. Th. Papaioannou, O. Crisan acknowledge support from Romanian Recovery and Resilience Plan PNRR, Pillar III, Component C9-I8, contract 760085/23.05.2023.

Electron dynamics in tunable Dirac states

E. Papalazarou[1], J. Zhang[1], N. Nilforoushan[1], M. Casula[2], Z. Chen[1], A. Amaricci[3], L. Perfetti[4]
D. Santos-Cottin[5], Y. Klein[2], A. Gauzzi[2], M. Marsi[1]
[1] *Université Paris-Saclay, 91405 Orsay, France*
[2] *Sorbonne Université, 75252 Paris, France*
[3] *Istituto Officina dei Materiali, 34136 Trieste, Italy*
[4] *Institut Polytechnique de Paris,91128 Palaiseau, France*
[5] *University of Fribourg, 1700 Fribourg, Switzerland*

We investigate $BaNiS_2$, a prototype of correlated Dirac semimetal with Dirac states positioned along the Γ−M symmetry line. Our interest lies in understanding how the band inversion mechanism and the formation of Dirac cones are influenced by *p*−*d* hybridization and charge transfer gap within this system. A recently published work indicate that substituting Ni for Co can alter both properties, thereby allowing for the movement of the cones along the aforementioned symmetry line [1]. Specifically, as the Ni concentration increases in $BaCo_{1-x}Ni_xS_2$, the cones shift away from Γ and decrease in energy. Notably, x also serves as a control parameter affecting the strength of electronic correlations, leading to a notable Mott metal−insulator transition and influencing spin−orbit coupling. These observations underscore the efficacy of chemical substitution as a means to manipulate Dirac states in $BaCo_{1-x}Ni_xS_2$, with charge transfer serving as a crucial control parameter [2]. Furthermore, an alternative method for manipulating the Dirac states of $BaNiS_2$ is using alkali-metal deposition on its surface [3]. Through a combination of conventional angle-resolved photoemission spectroscopy (ARPES) and time-resolved (trARPES) techniques (Fig. 1a), coupled with first-principles calculations, we have successfully probed and theoretically elucidated the effects of surface doping on the electronic structure of $BaNiS_2$ in situ (Fig. 1b and 1c).

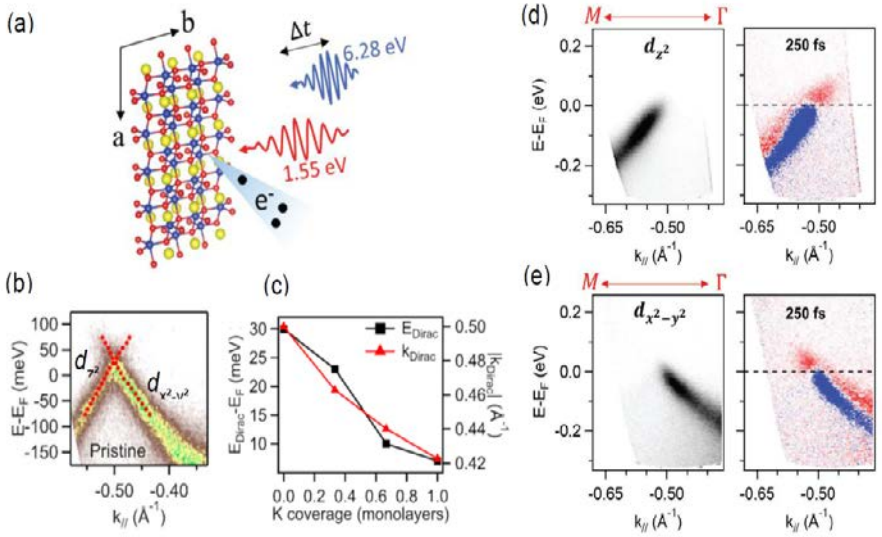

Fig.1. a) Experimental geometry of the trARPES setup. b) *ARPES images for the d_{z2} and d_{x2-y2} bands forming a Dirac linear dispersion.* ***c)*** *Curves extracted from the experimental Dirac states in* ***b)*** *for different alkali metal (here K) dosing time.* ***d)*** *ARPES images for the d_{z2} band and* ***e)*** *for the d_{x2-y2} bands, and their respected difference trARPES images (after photo-excitation minus before photoexcitation):* ***red*** *and* ***blue*** *in the color scale indicate gain and loss of photoemission yield, respectively*

Moreover, we illustrate that ultrafast light pulses have the profound ability to substantially modify the Dirac states and transport characteristics of this Dirac semimetal [4]. Utilizing trARPES, we reveal that photoexcitation induces a significant decrease in the Fermi velocities of Dirac electrons (Fig. 1d and 1e). This striking phenomenon is complemented by non-rigid, orbital-dependent band shifts occurring at the center of the Brillouin zone. These findings are corroborated by dynamic alterations in the screening length of non-local interactions.

References

[1] D. Santos - Cottin, M. Casula, G. Lantz, Y. Klein, L. Petaccia, P. Le Fèvre, F. Bertran, E. Papalazarou, M. Marsi, A Gauzzi, *Nature Communications* **7**, 11258 (2016).
[2] N. Nilforoushan, M. Casula, A. Amariccic, M. Caputo, J. Caillaux, L. Khalil, E. Papalazarou, P. Simon , L. Perfetti, I. Vobornik , P. Kumar Das J. Fuji, A. Barinov, D. Santos-Cottin, Y. Klein, M. Fabrizio, A. Gauzzi, M. Marsi, *arXiv:1905.12210* (2020).
[3] J. Zhang, T. D. Pierre Sohier, M. Casula, Z. Chen, J. Caillaux, E. Papalazarou, L. Perfetti, L. Petaccia, A. Bendounan, A. Taleb-Ibrahimi D. Santos-Cottin, Y. Klein, A. Gauzzi, M. Marsi, *Nano Letters* **23**, 1830 (2023).
[4] N. Nilforoushan, M. Casula, M. Caputo, E. Papalazarou, J. Caillaux, Z. Chen, L. Perfetti, A. Amaricci, D. Santos-Cottin, Y. Klein, A. Gauzzi M. Marsi, *Physical Review Research* **2**, 043397 (2020)

* Acknowledgments: authors E. P., M. M. and L. P. gratefully acknowledge financial support from the Region Ile-de-France (DIM OxyMORE), the EU/FP7 under the contract Go Fast (Grant No. 280555, the "Investissement d'avenir Labex Palm" (Grant No. ANR-10-LABX-0039-PALM) and by the ANR "Iridoti" (Grant ANR-13-IS04-0001). J. Z. thanks the China Scholarship Council (CSC).

Laser-induced carrier dynamics in metal-metal vs. metal-insulator Heterostructures from real-time time-dependent DFT

E. Shomali, M. E. Gruner, R. Pentcheva
, University of Duisburg-Essen, 47057 Duisburg, Germany

Using RT-TDDFT calculations with the ELK code, we compare the excitation pattern and nonequilibrium dynamics in metal-metal vs. metal-insulator heterostructures. As an example for the latter we investigated $Fe_n/(MgO)_m(001)$ with a varying number of layers of both constituents (n=1-5, m=3-7) [1-3] and found a strong anisotropy of response depending on the orientation of the electric field and laser frequency. The metal part is excited most efficiently by in-plane laser pulses with frequencies below the band gap of the insulator, whereas a strong excitation of MgO occurs predominantly for out-of-plane orientation of the electric field and frequencies above the band gap of MgO. From the analysis of the spin- and layer resolved changes of the density of states (Fig. 1, left) a concerted mechanism of excitation was identified, that comprises a transfer of carriers from the top of the valence band of MgO to states above the Fermi level in Fe and - simultaneously - from states in Fe just below the Fermi level to the conduction band of MgO, mediated by hybridized states at the interface. This effective bidirectional transfer of hot carriers between the *d*-states of the transition metal part and the valence and conduction band states of the insulating subsystem may be applicable to a broader class of metal/insulator heterostructures. $Fe_5/Au_5(001)$ serves as a model system for a metal-metal heterostructure [4]. From the layer-resolved changes in occupation numbers at 20.2 fs after the excitation with a 2 eV pulse, also here we observe a much richer behavior in the heterostructure as compared to the corresponding bulk constituents. Both for bulk Fe and the Fe layers in the heterostructure, a significantly enhanced number of excited electrons appears around 1 eV and 1.7 eV in the minority channel due to the availability of unoccupied 3*d* states above E_F in contrast to the majority 3*d* states, that are largely occupied. While excitations below ~0.6 eV are nearly absent in bulk Fe, they are pronounced in bulk Au, stemming from the localized occupied Au 4d band at ~-2 eV and appear also in the $Fe_5/Au_5(001)$ heterostructure, as a result of hybridization effects at the interface.

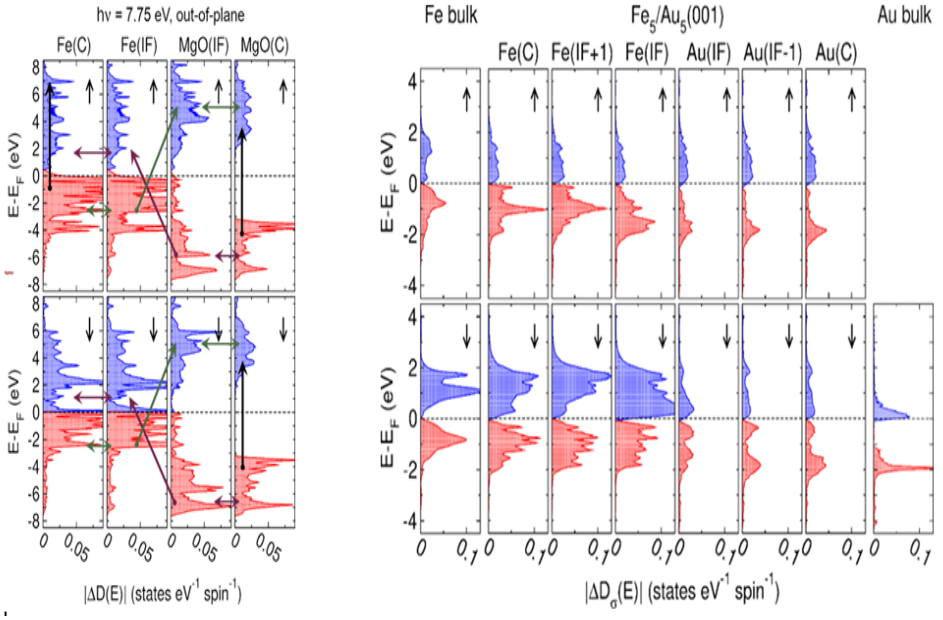

***Fig. 1. Spin- and layer-resolved changes** in the density of states $\Delta D(E) = D_\sigma(E,20fs) - D_\sigma(E, 0)$ **Left**: of the central and interface layers of Fe and MgO in $Fe_5/(MgO)_7(001)$, excited with an out-of-plane laser pulse with hν = 7.75 eV. **Purple** and **green arrows** indicate concerted transfer and excitation of carriers. Adapted from Ref. [3]; **Right**: in a $Fe_5/Au_5(001)$ heterostructure and bulk Fe and Au. Adapted from Ref. [4].**Blue**: positive sign, accumulation; **Red**: negative sign, depletion of occupation. The **upper** panels refer to the majority spin channel and the lower panels to the minority spin channel.*

Since mainly minority spin carriers from Fe are transferred through the interface, this generates a noticeable spin-polarization in the interface Au region.

References

[1] M. E. Gruner, R. Pentcheva, *Physical Review* B **99**, 195104 (2019).
[2] E. Shomali, M. E. Gruner, R. Pentcheva, *Physical Review* B **105**, 245103 (2022).
[3] E. Shomali, M. E. Gruner, R. Pentcheva, *Advanced Theory and Simulations* **6**, 2300319 (2024).
[4] M. Heckschen, Y. Beyazit, E. Shomali, F. Kühne, J. Jayabalan, P. Zhou, D. Diesing, M. E. Gruner, R. Pentcheva, A. Lorke, B. Sothmann U. Bovensiepen, *PRX Energy* **2**, 043009 (2023).

* Acknowledgement: funding by the German Research Foundation (DFG) within CRC 1242, project C02, and computational time at the MagnitUDE supercomputer at UDE are gratefully acknowledged.

Multi-dimensional coherent spectroscopy of superconductors: Discovery of unconventional quantum echoes and soliton states

M. Mootz[1], J. Wang[2], I.E. Perakis[3]
[1]*Ames National Laboratory, Ames, IA 50011, USA*
[2]*Iowa State University, Ames, IA 50011, USA*
[3]*University of Alabama at Birmingham, Birmingham, AL 35294, USA*

Multi-dimensional Coherent Terahertz Spectroscopy (THz-MDCS) is a new tool for studying with unprecedented resolution and controlling quantum materials by using a pair of phase-locked, intense Terahertz (THz) laser pulses [1]. Establishing this experimental technique in superconductors and topological materials requires solving a non-equilibrium many-body problem [2-5] that spans across several fields of current interest, including light-induced superconductivity, parametric driving of metastable phases, and quantum entanglement of supercurrent qubits. In this talk, we will discuss two examples of how THz-MDCS can be used to control and characterize strong nonlinearity and quantum interference not achieved so far in superconductors. The first example, observation of *quantum echo* signals (Fig. 1), demonstrates constructive and destructive interference of time-delayed Higgs and quasi-particle coherences, along with preservation and retrieval of the phase coherence amid multiple such excitations [6].

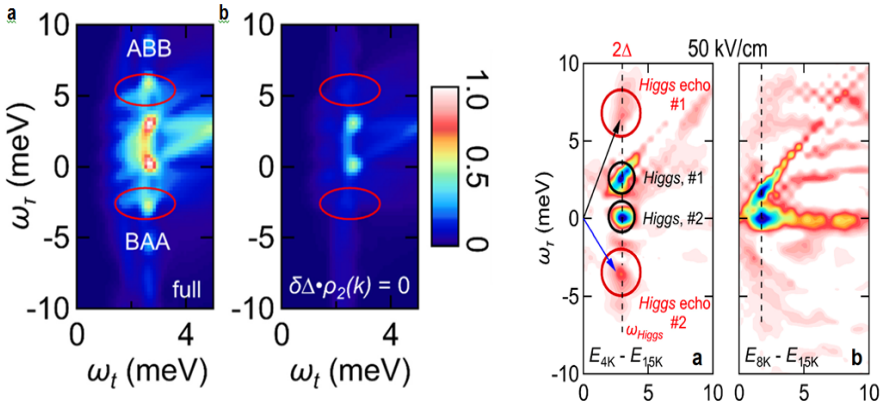

***Fig.1.Left*:*(a)* Theoretical prediction of *Higgs echo** nonlinear peaks centered at the symmetry-forbidden Higgs frequency and displaced along the vertical axis that measures the phase coherence between two time-delayed excitations.
***(b)* Demonstration of quantum echo** arising from temporal modulation, $\delta\Delta$, of the superconductor order parameter.
Right*: *(a) *Experimental observation of quantum echo peaks in the THz-MDCS spectra of Nb at 4K.* ***(b)*** *Higgs echo signals diminish by increasing the temperature from 4K to 8K*

We discuss the unconventional quantum echo signal arising from Higgs coherence in a niobium superconductor, and identify distinct experimental signatures attributed to anharmonicity. In particular, a THz pulse-pair time modulation of the superconducting gap generates a "time grating" of coherent Higgs population, analogous to exciton discrete states in semiconductors, which scatters echo signals distinct from conventional spin- and photon-echoes in atom and semiconductor continua. Notable differences from conventional behaviors include Higgs echo satellite peaks occurring at frequencies forbidden by equilibrium particle-hole symmetry, an asymmetric time delay in the echo formation, and negative time signals attributed to Higgs-quasiparticle anharmonic coupling absent for two-level system continua. As a second example, we discuss a dynamical transition to a *soliton state that is periodically driven by intense multi-cycle THz excitation* of the continuum states of an iron-based superconductor with strong inter-band couplings [7]. The delayed transition to such THz-driven state during the pulse, Fig. 2, is marked by the emergence, above excitation threshold leading to quasi-particle population inversion, of Floquet-like spectral sidebands centered well below the superconductor energy gap. These protected low-frequency peaks, observed for the first time here, display nonlinear dependences on temperature and THz laser field that differ from those of the second harmonic peak (Figs. 2 (d) and (e)). We attribute them to the THz-driven time delayed synchronization of a continuum of pseudo-spin oscillators whose phases lock in a way analogous to Dicke superradiance. While in synthetic matter with ultracold atoms order parameters governed by soliton oscillations have been identified, solitons in solid state superconductors have eluded observation until now. A grand challenge of fundamental quantum science and information technology lies in overcoming the dephasing bottlenecks that impede high-coherence of solid state systems. Our demonstration of THz solitons controllable by the laser field holds promise for quantum memory and sensing applications utilizing the enhanced coherence of a macroscopic pseudo-spin. At the same time, our demonstration of a temporal Higgs grating of the superconductor order parameter, controlled by the relative phase of a THz pulse-pair, paves the way for steering a quantum system during cycles of THz wave oscillations towards eigenstates that can form a temporal Floquet lattice.

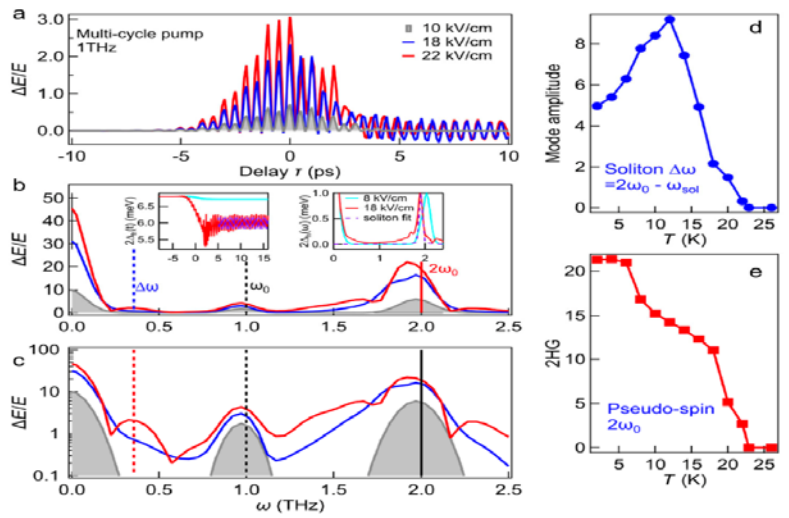

Fig. 2. Emergence of soliton sideband peak in pump-probe spectra *for* ω_0=1THz *driving of iron-based superconductors.* ***(a):*** *High field pump-probe signal develops new persistent oscillations after the pulse has peaked.* ***(b)*** *Soliton sideband peak develops in pump-probe spectrum at frequency* $\Delta\omega$ *well below the superconductor energy gap at ~6.8meV. Compare with the fundamental and second harmonic peaks.* ***Inset:*** *Time and frequency dependence of order parameter for low and high pump fields. Soliton state emerges during the second part of multi-cycle THz pump in multi-band superconductors with strong inter-band interactions.* ***(c)*** *Comparison of pump-probe spectra in log-linear scale for pump fields as in* ***(a)****.* ***(d),(e):****Comparison of temperature dependencies between soliton sideband (d) and second harmonic* ***(e)*** *peaks.*

By using THz-MDCS to observe such processes with a resolution superior to that of previous experiments, one can provide missing steps towards practical Floquet engineering and quantum coherent tomography in a wide range of quantum systems. Future coherent control experiments could contribute to transformative advances in quantum logic and electronic functionalities that can reach the ultimate sub-cycle speed limit.

References

[1] L. Luo, M. Mootz, J. H. Kang, C. Huang, K. Eom, J. W. Lee, C. Vaswani, Y. G. Collantes, E. E. Hellstrom, I. E. Perakis, C. B. Eom, J. Wang *Nature Physics* **19**, 201 (2023).
[2] M. Mootz, L. Luo, J. Wang, I. E. Perakis, *Communications Physics* **5,** 47 (2022).
[3] M. Mootz, L. Luo, C. Huang, J. Wang, I. E. Perakis, *Physical Review* B **109**, 014515 (2024).
[4] B. Cheng, D. Cheng, K. Lee, M. Mootz, C. Huang, L. Luo, Z. Chen, Y. Lee, B. Y. Wang, I. E. Perakis, Z.-X. Shen, H. Y. Hwang, J. Wang *arXiv:2310.02589v1* (2023).
[5] B. Cheng, D. Cheng, K. Lee, M. Mootz, C. Huang, L. Luo, Z. Chen, Y. Lee, B. Y. Wang, I. E. Perakis, Z.-X. Shen, H. Y. Hwang, J. Wang *Nature Materials*, https://doi.org/10.1038/s41563-023-01766-z (2024).
[6] C. Huang, M. Mootz, L. Luo, D. Cheng, J. M. Park, R. H. J. Kim, Y. Qiang, V. L. Quito, Y. Yao, P. P. Orth, I. E. Perakis, J. Wang *arXiv:2312.10912v1* (2024).
[7] M. Mootz, C. Vaswani, J. H. Kang, C. Huang, L. Luo, A. Khatri, I. E. Perakis, C. B. Eom, J. Wang, *submitted* (2024).

Optical Properties of two-dimensional materials

V. Perebeinos

University at Buffalo SUNY, Buffalo, NY 14260, USA

Atomically thin two-dimensional materials are direct bandgap semiconductors with a rich interplay of the valley and spin degrees of freedom, which offer the potential for electronics and optoelectronics. A strong Coulomb interaction leads to tightly bound electron-hole pairs or excitons and two-electron one-hole quasiparticles or trions. We solve the two-particle and three-particle problems for the wavefunctions for excitons and trions in the basis set of the model- Hamiltonian for single particles. The calculated linear absorptions [1], photoluminescence spectra [2], and polariton spectra [3] as a function of doping and temperature explain the experimental data in 2D monolayers and predict novel spectroscopic features due to the many-body Coulomb interactions.

Fig. 1. Left*:* ***Temperature dependence of the photoluminescence*** *trion peak in MoS2, where non-monotonic behavior is due to the low-lying dark trion states [2].*
Right*: Doping dependence of the transition energies in MoS2. The size of the circles are proportional to the oscillator strengths of the excited states [4].*

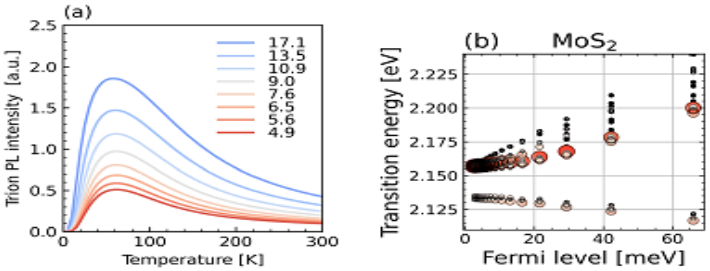

Exciton lifetime plays a crucial role in optoelectronic applications. I will also discuss the phonon-assisted Auger non-radiative decay mechanism of excitons in doped 2D materials.

References

[1] Y.V. Zhumagulov, A. Vagov, N.Y. Senkevich, D.R. Gulevich, V. Perebeinos, *Physical Review* B **101**, 245433 (2020).
[2] Y.V. Zhumagulov, A. Vagov, P.F. Junior, D.R. Gulevich, V. Perebeinos, *Journal of . Physical Chemistry* **153**, 044132 (2020)
[3] Y. V. Zhumagulov, S. Chiavazzo, D. R. Gulevich, V. Perebeinos, I. A. Shelykh, O. Kyriienko, *npj Computational Materials* **8**, 92 (2022).
[4] Y.V. Zhumagulov, A. Vagov, P.F. Junior, D.R. Gulevich, V. Perebeinos, *Journal of . Physical Chemistry* **153**, 044132 (2020).

* Acknowledgement:this material is based upon work supported by Air Force Office of Scientific Research under award number FA9550-22-1-0312.

Parametric quantum control for superconducting and hybrid quantum devices

W. Pfaff
University of Illinois at Urbana Champaign, Urbana, IL 61801, USA

Hybrid quantum systems provide a unique opportunity for combining the advantages of different physical degrees of freedom into a single device; for instance, coupling qubits to ultra-coherent solid-state spins could unlock quantum memories with unprecedented coherence times [1]. Conversely, combining qubit degrees of freedom with other systems is a promising path toward new, quantum-limited sensing techniques. It remains an outstanding problem, however, to realize efficient interfaces between different degrees of freedom such that benefits outweigh the challenges. Recently, parametric control of superconducting quantum circuits has emerged as a promising route for interfacing weakly coupled, highly coherent circuit modes [2-4]. Here, the Josephson junction of superconducting qubit devices is effectively employed as a nonlinear medium, allowing pumped mode-conversion. Crucially, this leads to drive-controlled, fast exchange of excitations at rates that may exceed static coupling strengths. This raises the opportunity for fast and efficient control of hybrid circuits as well. Specifically, we are interested in realizing systems in which collective excitations of solid-state spins, such as magnons [5] or collective modes in highly coherent rare-earth (RE) dopant spins [6], are controlled through superconducting quantum circuits.

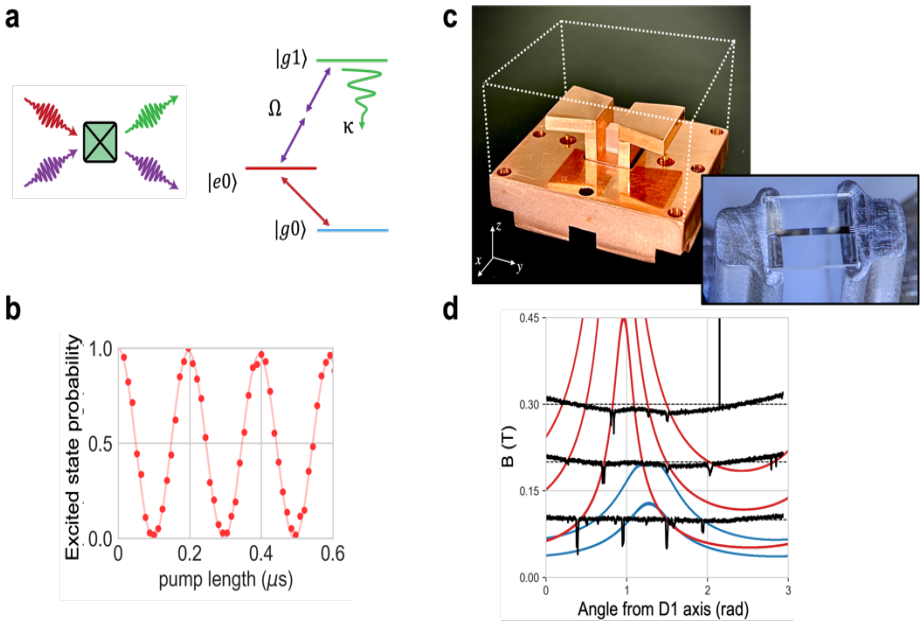

Fig. 1.a. Four-wave mixing in Josephson junctions *enables fast mode conversion, akin to driven sidebands;* ***b****, fast and high-fidelity swaps of excitations between a superconducting qubit and a resonator; this enables fast inter-qubit gates through bus modes;* ***c,*** *hybrid quantum circuits are composed of a 3D cavity, rare-earth doped crystal* ***(seen in between the 'bowties')****, and on-chip quantum circuit;* ***d,*** *RE spins of Yb171 dopants detected through hybridization with the cavity. Black lines: cavity readout signal at various magnetic field magnitudes and angles; detection results in 'dips' in cavity signal when cavity hybridized with spins* ***(predicted by intersections with the solid lines)****.*

I will discuss our recent progress in developing parametrically controlled superconducting circuits, and how this effort has enabled a flexible toolkit for interfacing weakly coupled quantum degrees of freedom. Enabled by strong parametric pumping, we have realized fast and high-fidelity two-qubit gates between superconducting transmon qubits located on different chips, coupled only through a detachable cable connection. This result shows that parametric control enables highly efficient quantum interfaces for composite systems. To transfer this approach to the platform of hybrid circuits, we have combined solid-state spins with microwave cavities, which in turn are coupled to parametrically controllable Josephson circuits. Initial results have shown coherent interactions between all components of these devices, and we have shown sensitive spin-detection as well as controlled hybridization between spins and circuit modes. These results lay the foundation for a powerful and versatile interface for hybrid quantum systems and will enable us to realize new classes of quantum devices, such as spin memory-enhanced quantum circuits.

References

[1] A. A. Clerk, K.W. Lehnert, P. Bertet, J.R. Petta, Y. Nakamura, *Nature Physics* **16**, 257 (2020).
[2] E. Zakka-Bajjani, F. Nguyen, M.Lee, L.R. Vale, R.W. Simmonds, J. Aumentado, *Nature Physics* **7**, 599 (2011).
[3] W. Pfaff, C.J. Axline, L. D. Burkhart, U. Vool, P. Reinhold, L. Frunzio, L. Jiang, M.H. Devoret, R. J. Schoelkopf, *Nature Physics* **13**, 882 (2017).
[4] Y. Zhou, B. Xiao, M.D. Li, O. Zhao, Z.S. Yuan, X. Ma, J.-W. Pan, *Npj Quantum Information* **9**, 54 (2023).
[5] D. Lachance-Quirion, Y Tabuchi, A Gloppe, K Usami, Y Nakamura, *Applied Physics Express* **12**, 070101 (2019).
[6] V. Ranjan, J. O'Sullivan, E. Albertinale, B. Albanese, T. Chanelière, T. Schenkel, D. Vion, D. Esteve, E. Flurin, J. J. L. Morton, P. Bertet**,** *Physical Review Letters* **125,** 210505 (2020).

* Acknowledgment: We acknowledge support from the NSF QLCI-HQAN, the DOE (grant DE-SC0022060), and IBM.

Understanding the ultrafast emergence of a Skyrmion phase in a ferromagnet

B. Pfau
Max Born Institute for Nonlinear Optics and Short Pulse Spectroscopy, 12489 Berlin, Germany

Femtosecond lasers provide a unique tool to excite and investigate matter in highly excited, non-equilibrium states. In magnetic materials, laser excitation can result in transient ultrafast demagnetization or even permanent magnetization switching. Highly excited states may also transition into magnetic states which remain hidden during adiabatic field sweeps or after slow excitation. I will report on a recently discovered phase transition in ferromagnetic Co-based multilayers with perpendicular magnetic anisotropy where laser excitation leads to the formation of a topological skyrmion phase [1]. The skyrmions formed are solitonic nanometer-scale spin textures that are intrinsically stabilized even at room temperature by stray fields and asymmetric exchange (Dzyaloshinskii–Moriya interaction, DMI) in the ferromagnetic material.Insight into the laser-induced formation mechanism comes from pump–probe resonant scattering experiments at x-ray free-electron lasers. These experiments have demonstrated that the transition proceeds at unprecedented speed, with the topology change completed after 300 ps (Fig. 1) [1]. In concert with atomistic simulation, our experiments further reveal that a fluctuation state created by the laser pulse mediates the topological phase transition. During this transient, high-temperature state, the lateral ferromagnetic order and the coupling between the magnetic layers are dissolved, leading to the effective elimination of the energy barrier for topological transitions. Skyrmions then freeze out from this fluctuation phase by an increasing imbalance of the skyrmion nucleation rate and their decay rate during cool down. In this process, the strong dependence of the nucleation rate on the applied field provides a knob to tune the density of the final skyrmion phase. We are able to produce states raging from densely packed skyrmions down to states with single skyrmions in the excited area, providing perspectives for applications [2]. As the skyrmions nucleate from magnetic fluctuations, they appear randomly distributed in the material. We have developed two methods to control the position of the nucleation sites in the material. The first method is based on focused-ion beam modification of the local magnetic anisotropy using He-ions (Fig. 1) [3]. In our second approach, we use metallic nanostructures on the backside of the magnetic films that lead to a local modification of the laser excitation amplitudes [4]. Both methods allow for reliable nanoscale localization of the skyrmions.

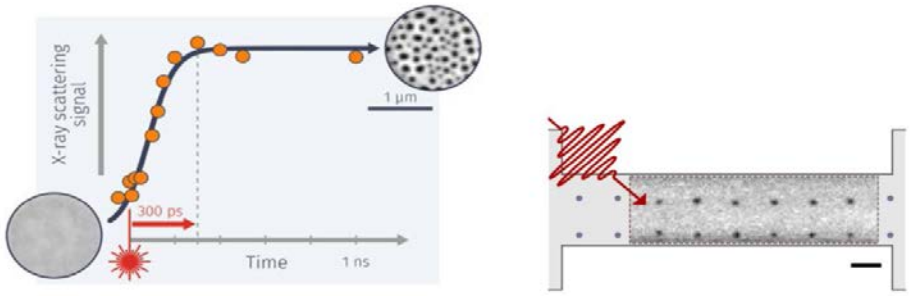

Fig.1.Left:Time-resolved scattering signal *tracking the formation of the skyrmion phase after ultrafast laser excitation. The images of the initial homogenously magnetized state and the final skyrmion state were recorded separately with x-ray imaging. [1].* ***Right****: Laser-induce formation of skyrmions controlled by local He-ion irradiation. [3]*

In the future, these developments may provide the control required for pump–probe experiments to image the ultrafast formation of a single skyrmion.

References

[1] F. Büttner, B. Pfau, M.Böttcher, M.Schneider, G.Mercurio, C.M. Günther, P.Hessing, C.Klose, A. Wittmann, K.Gerlinger, L.-M. Kern,C. C.Strüber C. von Korff Schmising, J. Fuchs, D. Engel, A. Churikova, S. Huang, D.Suzuki, I.Lemesh, M.Huang, L.Caretta, D.Weder, J.H. Gaida, M. Möller T. R.Harvey, S. Zayko, K. Bagschik, R. Carley, L. Mercadier, J. Schlappa, A. Yaroslavtsev, L. Le Guyarder, N. Gerasimova, A. Scherz, C. Deiter R. Gort, D.Hickin, J.Zhu, M.Turcato, D.Lomidze, F. Erdinger, A.Castoldi, S.Maffessanti, M.Porro, A. Samartsev, J. Sinova, C. Ropers, J. H.Mentink B. Dupé, G.S. D. Beach, S. Eisebitt, *Nature Materials* **20**, 30 (2021).

[2] K. Gerlinger, B.Pfau, F.Büttner, M.Schneider, L.-M. Kern,J.Fuchs, D. Engel, C. M. Günther, M. Huang, I. Lemesh, L.Caretta, A. Churikova, P.Hessing C. Klose, C.Strüber, C.von Korff Schmising, S.Huang, A. Wittmann, K.Litzius, D.Metternich, R. Battistelli, K. Bagschik, A.Sadovnikov, G.S. D. Beach S. Eisebitt, *Applied Physics Letters* **118**, 192403(2021).

[3] L. Kern, B.Pfau,V.Deinhart, M.Schneider, C. Klose, K. Gerlinger, S.Wittrock, D.Engel, I.Will, C. M. Günther, R.Liefferink, J.H. Mentink, S.Wintz M.Weigand,M.-J. Huang,R. Battistelli,D.Metternich,F. Büttner,K. Höflich,S. Eisebitt, *Nano Letters* **22**, 4028 (2022).

[4] L. Kern, B. Pfau, M. Schneider, K. Gerlinger, V. Deinhart, S. Wittrock, T. Sidiropoulos, D. Engel, I. Will, C. M. Günther, K. Litzius, S. Wintz M.Weigand, F. Büttner, S. Eisebitt, *Physical Review* B **106,** 054435(2022).

Light-driven deterministic control of magnetism

I. Radu
European X-ray Free-Electron Laser, 22869 Schenefeld, Germany

A long sought-after phenomenon and a core scientific driver in ultrafast science is the light-driven deterministic control of order parameters in solids (magnetism, ferroelectricity etc) on timescales comparable or even faster than the optical cycle of the photo-exciting light field. In this context, a particularly appealing approach is the use of strong THz and mid-IR fields (MV/cm and higher) that can drive elementary excitations (phonons, magnons), long-range quantum phases as well as phase transitions on their intrinsic energy- and time-scales [1-3]. Here, I will showcase the latest developments in our projects on ultrafast magnetism by employing light-spin interactions in a strong-field regime and demonstrate THz-driven ultrafast magnetization reversal of a magnetically ordered material *using linearly polarized, single-cycle THz pulses*. We observe a fully deterministic switching event occurring upon each single-shot THz pulse excitation of the investigated ferrimagnetic GdFe alloys, i.e. the so-called toggle magnetization switching [4,5] – see Figure 1. The magnetization switching process evolves at unprecedented speeds down to sub-picosecond timescales, as stroboscopically probed with time-resolved magneto-optics in the extreme ultraviolet (XUV) and visible (VIS) spectral range. Reaching switching amplitudes close to 100% within a few picoseconds our measurements reveal a highly efficient non-equilibrium energy transfer mechanism from the THz light pulse to the spin system, this novel spin switching behavior being solely driven by the electric (E) field of the THz pump pulse.

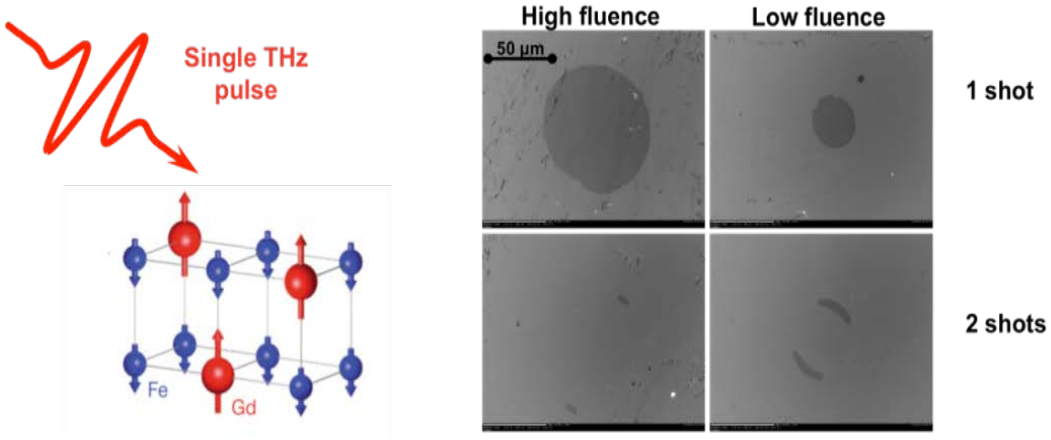

***Fig. 1: Left Schematic depiction of the experimental approach**: Single-cycle THz pulses with variable central frequency and field strengths are used to photoexcitethe ferromagnetic GdFe alloys (Gd and Fe magnetic moments are anti -ferro-magnetically coupled in the ground state) in a single shot manner. **Right**: Magneto-optical imaging of the GdFe sample after a single-shot and two-shot THz exposure at two different incident THz fluences. The magnetization orientation of the sample is fully controlled back and forth by a linearly polarized, single-cycle THz pulse excitation (i.e. toggle magnetization reversal) in the absence of an external magnetic field,demonstrating the THz- driven all-optical magnetization switching phenomenon.*

Our findings demonstrate the ultrafast and deterministic control of magnetization using single THz pulses in the absence of a symmetry-breaking magnetic field, paving the way for an entire class of new experiments employing nonlinear light-spin interactions at THz frequencies. I will conclude with our future plans on implementing such strong-field THz/mid-IR sources in combination with ultrashort X-ray pulses at the European XFEL.

References

[1] I. Radu, J. Lloyd-Hughes, P. M. Oppeneer, T. Pereira dos Santos, A. Schleife, S. Meng, M. A. Sentef, M. Ruggenthaler, A. Rubio, I. Radu M.Murnane, X. Shi, H. Kapteyn, B. Stadtmüller, K M Dani, F. H. da Jornada, E. Prinz, M. Aeschlimann, R. L. Milot, M. Burdanova, J. Boland T. Cocker, F. Hegmann, *Journal of. Physics: Condenced Matter* **33**, 353001 (2021).
[2] K.Carva, P. Balasz, I. Radu,*Handbook of Magnetic Materials* **26**, 29 (2017).
[3] T. Kampfrath, K. Tanaka, K. Nelson, *Nature Photonics* **7**, 680 (2013)
[4] I. Radu, K. Vahaplar, C. Stamm, T. Kachel, N. Pontius, H. A. Du¨rr, T. A. Ostler, J. Barker, R. F. L. Evans, R.W. Chantrell, A. Tsukamoto A. Itoh , A. Kirilyuk, Th. Rasing, A. V. Kimel *Nature* **472**, 205 (2011)
[5] T. A. Ostler, J. Barker, R. F. L. Evans, R.W. Chantrell, U. Atxitia, O. Chubykalo-Fesenko, S. El Moussaoui, L. Le Guyader, E. Mengotti L. J. Heyderman, F. Nolting, A. Tsukamoto, A. Itoh, D. Afanasiev, B.A. Ivanov, A.M. Kalashnikova, K. Vahaplar, J. Mentink, A. Kirilyuk T. Rasing , A.V. Kimel, *Nature Communications* **3**, 666 (2012) .

Carrier dynamics in semiconductor structures under Photonic and electronic excitations

M.K. Rafailov
University of Alberta, Edmonton, Alberta, Canada T6G 1H9

One of the critical issues Ultrafast Dynamics is the maintaining the metastability of light-induced nonequlibrium. It is an idea to use relatively long lasting processes that is linked to nonequlibrium - ones like acoustic phonons, carrier motion, specifically in semiconductors, the processes in the inner shell of the atoms, and so on, to envelope the nonequlibrium to make it lasting longer. It may provide a solution to nonequlibrium metastability. It is also may help to solve a problem of non-photonic nonequlibrium excitation leading to numerous technology applications. As matter of fact in low dimentionals structures the timing of even very slow processes like carrier motion and acoustic phonons run the same as photoinduced nonequlibrium in electronic structures-timing, say acoustic phonons in molecular-size (sub-nm) structure may be well below ps, that bring the use of features specific to the nonequlibrium to practical technology applications, like above THz electronics on chip and so on. Here we will discuss one of such processes - negative photoresponse-NPR, induced by below ps-pulse laser excitation. A nonintuitive result of the experimentally observed response [1] -Fig.1, a where instead of predicted unipolar response [2], has been demonstrates voltage polarity change. As a matter of fact it does not affect the regular excitation with low intensity modulated signal-see the inset that in its turn, offers great opportunities for remote applications, like EO-IR sensing, optical communications, EW and so on. NPR that is lasting up to ms and depends only on pump pulse intensity, is a combination of two factors-electronic system excitation and low dimensionality (2D) defined by the nature of fs-excitation-resulted bleaching.

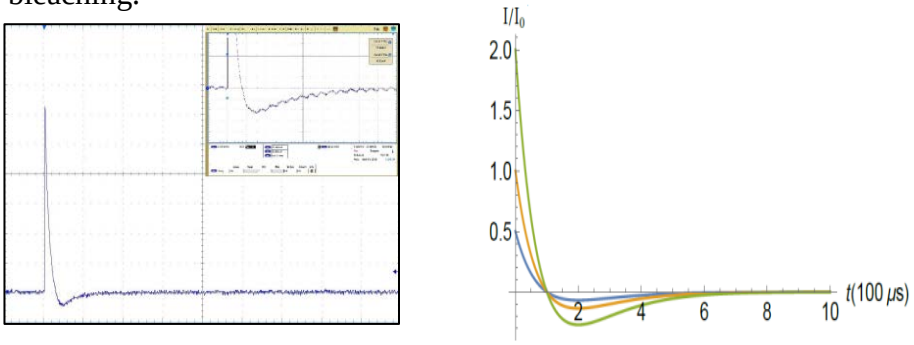

Fig.1. NPR-excitation by fs-laser irradiation of that is lasting up to ms. *a. experimental observation in Ge p-i-n diode structure;*
b. nonequlibrium modeling results based on theoretical model. From [3].

Recent discovery that "if, following ultrafast excitation, the carrier density and temperature are increased, and during relaxation the system reaches a state sufficiently close to the quasi-thermal equilibrium in which the carrier density is still elevated, but smaller than the intrinsic thermal equilibrium density at the elevated temperature, then the signal can become negative" [3]-Fig.1.b. That result open a new opportunity for extending nonequlibrium lifetime in semiconductor structures-specifically ones with p-n junctions. Despite the effect has been observed in bulk material the pulse propagation in semiconductors that demonstrates so called bleaching effect depending on pulse flight time -which is for 10fs in Ge it is~0.75μm and with respect to Ge absorption is modeled in [4]Fig.2. Therefore, with respect to p-n junction lay out the dynamics in the structure pretty much follows to 2D.

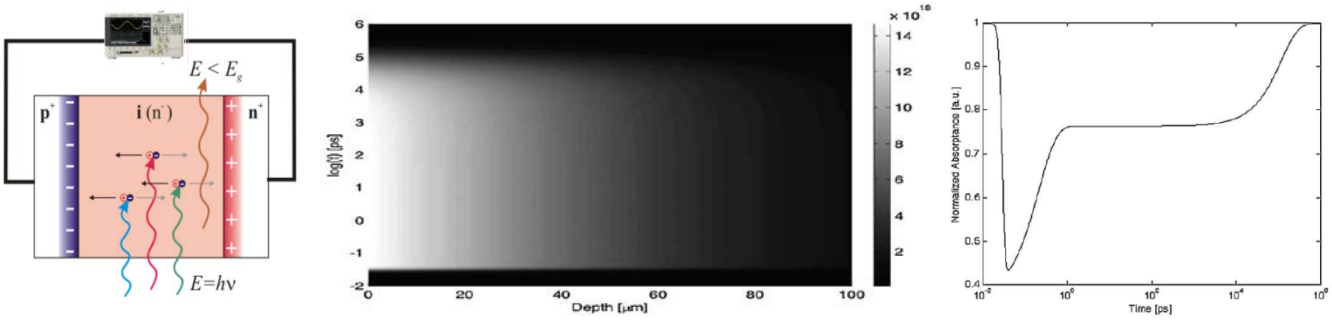

Fig. 2. Bleaching in semiconductors*. a. bulk p-i-n diode bleaching schematic; b, c calculated bleaching effects in bulk Ge. From [4].*

And it is plausible to maintain such a quasi-metastability with a train of relatively low pulse repetition rate ultrashort pulses. Making a layered structure where each layer is comparable with pulse time of flight and the NPR timing, it is possible to build layered structure maintaining practically indefinite metastability. If we look at that from the other side it is possible with respect to bleaching time and pulse time of flight to build a photovoltaic structure that can be used to maintain such qualities with very long pulses excitation or even wih CW sources. The same principle also can be used while train of electric pulses is used as a pumping source [7]. In such a case the only limitations for pulse width and, thereto pumping power will be the capacitance-C which is directly depends on layer thickness. And in such a case we may need a potential or bias to move pulses across a layer. While results of positive response is strongly depending on R-C parameters it will be plausible in low dimentionals semiconductor structures to see above mentioned enveloping of nonequlibrium with carrier velocity. Farther considering electronic pumping of such low dimensional structures Once tested in organic light emitting diodes [5] electronic pumping that strongly depends on capacitance-size of the structure demonstrated high efficiency in maintain nonequlibrium even in relatively thick materials.

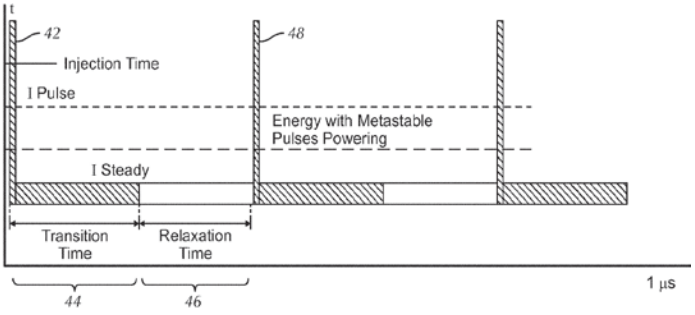

Fig.3. Schematic of thing layered heterostructure electrically pumped by train of electric pulses. *From [5]*

Electronic phase-transition with electric pumping was experimentally demonstrated in double pump-probe experiment [6], where phase transition were measured with respect to X-ray probe diffraction pattern with pumping both optically-100fs laser pulse and electrically with different step-voltages applied to the structure.

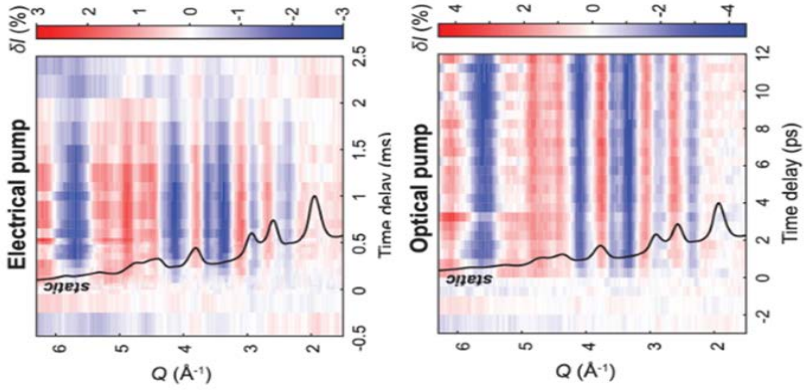

Fig.4 .Similarity of transient structures formed under electrical and optical excitation*. The static diffraction pattern is shown by the black curve. From [7].*

Switching to electronic pumping and using layered structures, like similar to twisted vdW structures, may allow on-chip broadband electronics using the principles of Ultrafast Dynamics and Ultrafast Bandgap Photonics.Not only electric pumping in combination with layered material structures is a plausible way to induce nonequlibrium but any other non-ultrashort laser pulse pumping is a way to pump high intensity pulse into a such structured material and it makes great prospective for proliferating nonequlibrium-related phenomena and effects in multiple applications: from peta-Hz electronics to remote sensing, photovoltaics in general, like the Sun-powered batteries, high-temperature superconductivity, magnetic switches and so on.

References

[1] I. K. Zakharova, M.K. Rafailov, *Proceedings SPIE* **9467**, 946726-1 (2015).
[2] X-A. Dou; X-Q. Sun; L. Shao, *Lasers in Engineering* **25,** 117 (2013).
[3] M. Yuan, M. K. Rafailov, R. Binder, *Journal of Applied Physics* 134, 174503 (2023).
[4] X.-A. Dou, X. Sun, X.Li, X. Chen, *Optik* **126,** 3267 (2015).
[5] M. K. Rafailov, US Patent 10242618, *US Patent ad Trademark Office* (2019).
[6] A. Sood, X. Chen, Y.Shi, S.Kumar, S.J. Park,M.Zajac,Y.Sun,L.Q.Chen,S.Ramanathan,X.Wang,W.C.Chueh,A.M. Lindenberg, *Science* **373**, 352 (2021).
[7] A. Lindenberg, *Ultrafast Dynamics and Ultrafast Bandgap Photonics* **VIII**, Georgetown Washington DC, 14 (2021).

Advanced electronics for the clean energy future

M. Ringer
National Renewable Energy Laboratory, Golden, CO80401, USA

Power electronics, and related semiconductor-based devices, are critical elements as increased renewable energy technologies are deployed globally. It is imperative that these devices are readily available, manufactured efficiently, and comprised of elements that do not further constrict global supply chains for critical materials. NREL, along with Department of Energy (DOE) collaborators, developed scenarios that demonstrated the increased in renewable generation required to meet the aggressive decarbonization goals targeted by the U.S. government. Figure 1a shows that between 300 and 400 GW of onshore wind, 100-300 GW of solar photovoltaics, and 75-175 GW of offshore wind will be required to meet an 80% renewable energy penetration scenario [1]. With that penetration of renewables, increased power electronics to convert generated electricity (DC to AC in the U.S.) and to optimize the operation of these variable assets is critical to achieving the adoption of these technologies, and of the audacious carbon reduction targets that each will drive [2]. Estimates suggest that up to 80% of the generated power will flow through power electronics [3].

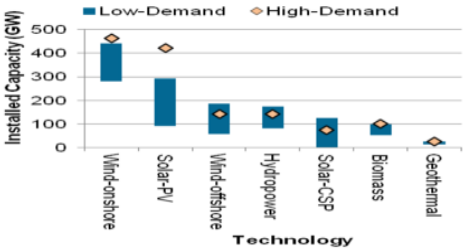

(a) 2050 installed capacity by technology

Fig. 1. *- Installed renewable capacity in the U.S. to .meet an 80% renewable energy 2050[1]*

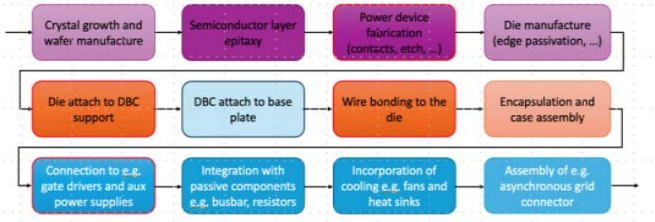

Fig. 2. *– Development of grid-ready power electronics at NREL – from material discovery to device fabrication (**Source**: NREL planning presentation, 2023)meet an 80% renewable energy 2050[1].*

The development of the next generation of power electronics will require a multi-pronged research effort. In addition to the materials science discoveries, the new devices that will evolve from these discoveries will need to be developed into devices that are resilient, manufactured effectively and evaluated at relevant power levels for operation. NREL has developed a multi-disciplined team that is collaborating to get these next generation wide-bandgap power electronic devices commercialized. The team at NREL is utilizing the process illustrated in Fig. 2 to move from material discovery to devices validation.

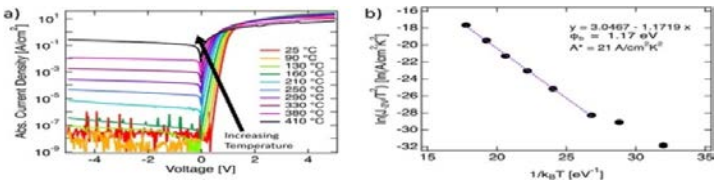

Fig. 3 *(a)* ***J-V results of a Schottky diode*** *with a diameter of 1 mm, measured as the temperature is brought up to 410 °C.*
(b) *Plot of ln(J_{-2V}/T^2) vs 1/k_bT from fitting the J-V data from part (a). Resulting barrier height from fitting this line is around 1.2 eV [4]*

NREL is looking at gallium oxide devices, at the materials level, to help lower costs, improve performance, operate at higher efficiencies, and increase reliability. Recent work has demonstrated Fig. 3 that certain gallium oxides can reduce turn-on voltage by a factor of 10, with a corresponding reduction in on/off ratio [4]. These results show the potential impact that novel materials can achieve towards improve power electronic performance. Any material that shows promising results must also be able to handle challenging (high temperature, aggressive operating environments) conditions. NREL's researchers have worked with a commercial partner to develop a 200kW, 1050 VDC SiC-based inverted to power a hybrid motor in a heavy-duty construction vehicle. Similar to the work completed for other vehicle-based power electronics, the evaluation for thermal management systems is required to remove the large amounts of heat that are produced by next generation power electronics [5]. Finally, once a material has been identified, and scaled to handle its operating environment, it must be evaluated at scale. Modeling has demonstrated that a multilevel, back-to-back, inverter can be used successfully in grid forming applications [6]. The presentation associated with this abstract will discuss the importance of a balanced approach to scientific discovery, device scale-up and inevitable scale-up at relevant operating conditions. The scientific community must be able to simultaneously identify new materials, and scale-up current technology to meet the stringent needs of a decarbonized energy future.

References

[1] M. M. Hand, Renewable Electricity Futures Study, *National Renewable Energy Laboratory*, NREL/TP-6A20-52409, (2012).
[2] F. Blaabjerg, I. Romero, *Hitachi Perspectives*, (2023).
[3] S. Reese, T Remo, J Green, A Zakutayev, *Joule* **3**(2019)
[4] K. Heinselman, P. Walker, A. Norman, P.Parilla, D.Ginley, A. Zakutayev, *Journal Vacuum Science* A **39**, 040402 (2021).
[5] G. Moreno, S. Narumanchi, X. Feng, P. Anschel, S. Myers, P. KellerG, *Journal Electronic Packaging* **144,** (2022).
[6] V. R. Chowdury, B. Mather, IEEE Conference Energy Conversion and Exposition. (2023).

Ultrafast pump-probe nano-imaging: nano-movies of coupled polaron-cation Dynamics in triple cation perovskites

M. B. Raschke
University of Colorado, Boulder, CO 80309, USA

Ultrafast infrared spectroscopy in its extension to nano-imaging provides access to vibrational and low energy carrier dynamics in molecular, semiconductor, quantum, or polaritonic materials. In addition, to simultaneously probe both ground and excited state dynamics we have developed ultrafast heterodyne pump-probe nano-imaging with far-from-equilibrium excitation. In ultrafast movies with simultaneous spatial, spectral, and temporal resolution we can image heterogeneities in electron-phonon, cation-lattice, and coupled polaron dynamics on their elementary time and length scales (Fig. 1) [1,2].

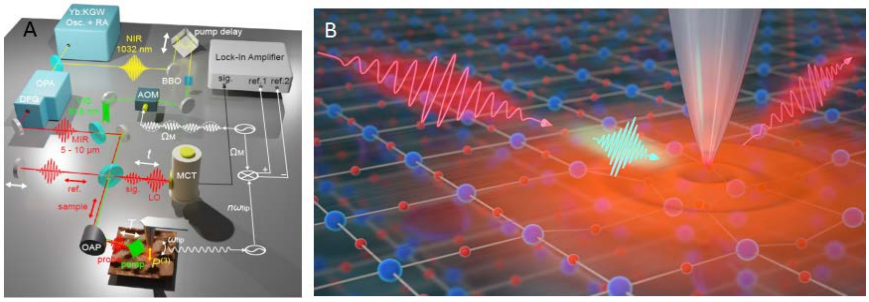

Fig. 1. (A) Development of ultrafast nano-imaging in heterodyne *fs s-SNOM resolving excited state dynamics with fs-nm spatio-spectral-temporal resolution. (**B**). In ultrafast movies with electronic pump and low-energy IR probe spectroscopy heterogeneities in electron-phonon, cation-lattice, and coupled polaron dynamics can be resolved on the elementary time and length scales.*

As exemplary application we use this approach of ultrafast pump-probe nanoimaging to provide a real-space and real-time view of the coupled electron-lattice dynamics underlying the photophysical response of hybrid organic-inorganic perovskites. Their photovoltaic performance and other photonic functions are still poorly understood in part because of the multi-scale chemical and structural heterogeneities. While polaron formation following the photoexcitation is believed to relate to the effective carrier transport observed, the elementary physical processes underlying electron-phonon coupling to both the perovskite lattice and molecular cations constituents have not yet been resolved. First, in ultrafast visible-pump infrared-probe nano-imaging we resolve the photoinduced carrier dynamics in triple cation perovskite films, with a ~20 % variation in sub-ns relaxation dynamics with spatial disorder on tens to hundreds of nanometer which we attribute to the heterogeneous evolution of polaron delocalization and increasing lifetime (Fig. 2) [3].

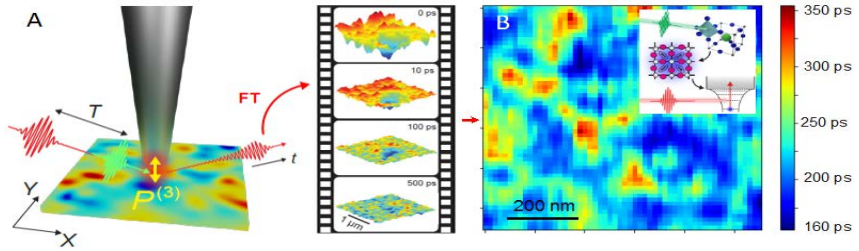

Fig. 2. (A) Ultrafast nano-imaging of photoinduced polaron dynamics *in triple cation perovskites.*
(B)*Ultrafast movie resolving heterogeneity in carrier dynamics and polaron radius underlying the performance of perovskite-based photophysical devices of solar cells, lasers, and light emitting diodes.*

We then apply a combination of ground and excited state spectroscopic nanoimaging of the formamidinium (FA) cation vibration where we use vibrational solvatochromism as a probe of the static and dynamic evolution of the local molecular environment. A transient vibrational blueshift we model as signature of nano-scale spatial variations in the polaron-cation coupling based on a combination of vibrational Stark shift, FA orientation, and lattice-field effects [4].
The high degree of local variation in polaron-cation coupling dynamics points towards the missing link between the optoelectronic heterogeneity and associated carrier dynamics. The results suggest that there is a lot of room for improved synthesis and device engineering and that perovskite photonics performance is far from any fundamental limits.

References

[1] J. Nishida, A.H. Alfaifi, T.P. Gray, S.E. Shaheen, M.B. Raschke , *ACS Energy Letters* **5**, 1636 (2020).
[2] J. Nishida, P.T.S. Chang, J.Y. Ye, P. Sharma, D.M. Wharton, S.C. Johnson, S.E. Shaheen, M. Raschke, *Nature Communications* **13**, 6582 (2022).
[3] J. Nishida, S. C. Johnson, P. T. S. Chang, D. M. Wharton, S. A. Dönges, O. Khatib, M. B. Raschke, *Nature Communications* **13**, 1083 (2022).
[4] E.Wilcken, B. Esses, M. B. Raschke, *to be submitted*, (2024).

* Acknowledgement: project supported by National Science Foundation (NSF) Science and Technology Center on Real-Time Functional Imaging (STROBE) under Grant DMR 1548924.

Ultrafast dynamics of athermal electrons in metals

T. Held[1], C. Seibel[1], S. Roden[1], M. Uehlein[1], P.D. Ndione[1], S.T. Weber[1], D.O. Gericke[2], B. Rethfeld[1]
[1]*Rheinland-Pfälzische Technische Universität Kaiserslautern-Landau, 67663 Kaiserslautern, Germany*
[2]*University of Warwick, Coventry CV4 7AL, United Kingdom*

Femtosecond laser pulses irradiating solid materials induce a cascade of processes starting with the excitation of so-called hot electrons, proceeding through various relaxation processes and, at sufficiently high energies, inducing ultrafast structural dynamics. During irradiation, the energy is mainly absorbed by the electrons, which collectively reach a state far from equilibrium with an energy distribution deviating strongly from a Fermi distribution. The relaxation of such electrons to an equilibrated situation may include complex pathways since several scattering mechanisms act on different timescales. As a result, thermal electron distributions as well as highly excited electrons can exist much longer than the single-electron lifetime predicts. We simulate the dynamics of a large ensemble of excited electrons using complete Boltzmann collision integrals. We consider the density of states of the given metal and are able to identify characteristic features in the excited electron distributions. Figure 1a) shows athermal electron distributions in gold at different timesteps after an ultrashort excitation with visible light. Here, all electrons in the density of states indicated in the figure have been considered to belong to one effective band. Moreover, only electron-electron collisions have been activated. Our approach allows to extract spectral electron densities [1], i.e. the occupation of certain energy ranges. Figure 1b) shows examples of such spectral electron densities in different energy ranges, as indicated in the figure. Depending on the energy, we identify two regions with qualitatively different behavior and a transition between them at a certain transition energy. Between the Fermi energy and the transition energy, the spectral densities continue to rise after the laser excitation.

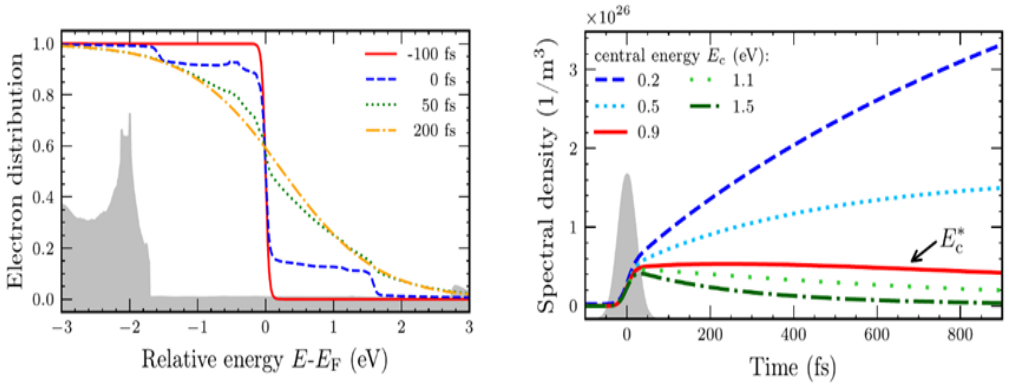

Fig. 1. a) Electron distribution *of gold at various times after ultrashort laser excitation with visible light.*
b) *Development of spectral electron densities at various energies arising due to the interplay of various relaxation processes [1].*

The transition energy is characterized by an almost constant electron density after the pulse, and we found it to be close to half the photon energy of the exciting laser. Above the transition energy, the spectral densities decrease after the excitation. We find that this complex behavior is caused by the interplay of electron lifetimes and secondary excitation mechanisms [1]. These results reveal that the temporal dynamics cannot be matched with a simple relaxation time approach. For noble metals, sp- and d-electrons may have to be considered separately. Moreover, an occupational nonequilibrium may persist even after Fermi-distributions have been established. We have studied such case in a temperature-based approach and have determined the optical response of laser-excited gold over a broad range of timescales [2]. We now reconsider the dynamics from the initial athermal distribution to the occupational nonequilibrium with help of band-resolved Boltzmann collision integrals. First results on the electron dynamics will be discussed in the presentation. Moreover, we investigate how an occupational nonequilibrium affects the electron-phonon coupling strength. We find a strong dependence of the coupling parameter on the band occupation reflecting features of the band-resolved density of states [3]. Our results demonstrate the importance of nonequilibrium electron distributions on the heating of the crystal lattice and subsequent phase transitions.

References

[1] C. Seibel, M. Uehlein, T. Held, P.N. Terekhin. S.T. Weber, B. Rethfeld, *Journal of Physical Chemistry C* **127**, 23349, (2023)
[2] P. D. Ndione, S.T. Weber, D.O. Gericke, B. Rethfeld, *Scientific Reports* **12**, 4693, (2022)
[3] T. Held, S.T. Weber, B. Rethfeld, *arXiv:2308.01067* (2023).

Unpacking photoinduced phase transition in quantum materials: from Equilibrium to nonequilibrium

C.-Y. Ruan
Michigan State University, East Lansing, MI 48824, USA

Early pioneering studies of photoinduced phase transition (PIPT) identified hallmark behaviors, such as domino effects, sensitivity to the initial condition, and the density-dependence [1], as keys to bring light-induced metastable or even long-lived hidden phases with properties never seen under equilibrium conditions [2]. Such distinct signatures of PIPT were often identified in low-dimensional charge-transfer organic crystals that are prototypical correlated electron systems [3]. For inorganic systems, such as quais-1D and quasi-2D inorganic quantum materials, the PIPT dynamics demonstrated by recent ultrafast investigations seemed also to embody similar phenomenology but in a more subtle way [4,5]. In this talk, I will seek to connect the hallmark PIPT behaviors with nonequilibrium many-body physics as a general framework [6] for understanding emergent behavior and nonequilibrium controls of hidden, metastable phases in quantum materials [5-9].

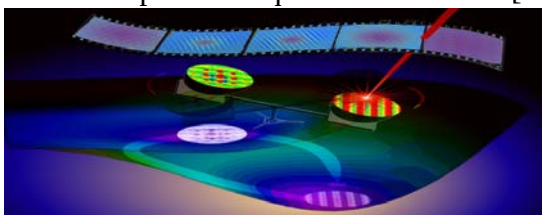

Fig.1. *Quantum material systems upon applying ultrashort laser pulses provide a rich platform to access excited material phases and their transformations that are not entirely like their equilibrium counterparts [9, 15].*

The methodology we primarily draw to investigate the emergent behavior in PIPT is multi-message ultrafast measurements to probe the evolutionary process from nonequilibrium to equilibrium regimes and back. The term evolution here may have two connotations: (1) the photoexcited state evolves from a locally extended complex system into a more homogeneous macroscopic entity, but without a directly traceable linkage between the two functioning bodies; (2) the law of physics underpinning this phase transitions itself also evolves. Thus, the PIPT phenomenology naturally includes two key aspects behind the nonequilibrium many-body physics, namely the emergent phenomena and scale-dependent physics [7]. To identify the key traits of nonequilibrium evolution and scale-dependent physics, the datasets we employed to illustrate the phenomenology comes from correlative measurements uniting structural and electronic probes together [8], to map the property evolution based on local and global structure correlation functions [9]. In particular, the recent advances that achieved an improved spatiotemporal resolution based on diffraction contrast in high-brightness microscope systems critically aided the effort to push the nonequilibrium windows of observation down to sub-100 fs temporal and sub-picometer noise floor [10] – namely the few-particle excitation regime. This new sensitivity hence makes it possible to bridge between the ultrafast photo-seeding process, the incubation stage (metastable), and the down-fall dynamics characteristic of the domino effects at later stage under a broad range of excitation to identify the multi-pronged and multi-thresholded processes behind PIPT [11].Two examples will be given to illustrate this phenomenology: (1) Scale-dependent self-organization in vanadium dioxide thermally induced and photoinduced phase transitions [12,13]. (2) Disorder to order: Nonequilibrium universal dynamics in the condensation of 2D charge-density waves [14,15]. We hope to illustrate that while in all thermodynamical phase transitions converge to the familiar equilibrium dynamics and phase diagrams, upon driven far from equilibrium the systems may display various routes towards nonthermal phases and there is no single overarching principle governing the entire evolutionary process from equilibrium to nonequilibrium stages.

References

[1] K. Nasu, *Photoinduced Phase Transitions. World Scientific* (2004).
[2] S. Koshihara, T. Ishikawa, Y. Okimoto, K. Onda, R. Fukaya, M. Hada, Y. Hayashi, S. Ishihara, T. Luty, *Physics Reports* **942**, 1 (2022).
[3] S. Iwai, S. Tanaka, K. Fujiiuma, H. Kishida, H. Okamoto, Y. Tokura, *Physical Review Letters* **88**, 057402 (2002).
[4] J. Ravnik, M. Diego, Y. Gerasimenko, Y. Vaskivskyi, I. Vaskivskyi, T. Mertelj, J. Vodeb, D. Mihailovic,*Nature Communication* **12**, 2323 (2021).
[5] A De La Torre, DM Kennes, M Claassen, S Gerber, JW McIver, MA Sentef, *Reviews of Modern Physics* **93**, 041002 (2021).
[6] U. C. Tauber, *Annual Review of Condenced Matter Physics* **8**, 185 (2017).
[7] P. W. Anderson, *Science* **177**, 393 (1972).
[8] C.-H. Ryan, The Many Facets of Ultrafast Electron Diffraction and Microscopy:Development and Applications, Royal Society of Cmemistry,2023
[9] X. Sun, S. Sun, C.-Y. Ruan, *Comptes Rendus Physique* **22**, 15 (2023).
[10] X. Sun, J. William, S. Sharma, S.Kuniir, D. Morris, S. Zhao, C.Y. Ruan, *Structural Dynamics* **11**, arXiv:2401.00915 (2024).
[11] Q. M. Liu, D.Wu, Z.Li, L.Shi, Z.Wang, S. Zhang,T.Lin, T.C.Hu, H.F. Tian, J.Q. Li, T. Dong, N.L.Wang, *Nature Communications* 12, 2050 (2021).
[12] X Sun, S Sun, I Gonzalezafanador, GM Torres, NA Sepulveda, CY Ruan, *CLEO:Fundamental Science 2023* (2023).
[13] Z. Tao, F. Zhou, T.R.T. Han, D. Torres, T. Wang, N. Sepulveda, K. Chang, M. Young, R.R. Lunt, C.-Y. Ruan, *Scientific Reports* **6**, 38514 (2016).
[14] C. Y. Ruan, S. Sun, J. Williams, F. Zhou, M. Zhang, X.Sun, C.Malliakas, M.Kanatzidis, M. Mahgrebi, *Microscopy and Microanalysis* **26**, 1(2020).
[15] F. Zhou, J. Williams, S. Sun, C.D. Malliakas, M. G. Kanatzidis, A. F. Kemper, C.-Y. Ruan, *Nature Communications* **12**, 566 (2021).

* Acknowledgements: author acknowledge support from by the U.S. Department of Energy Basic Energy Sciences Program (Grant Nos. DE-FG0206ER46309 and SC0018529).

Quest to reveal the Higgs excitation in superconductors by NEARS

M. Rübhausen[1], T. Glier[1], D. Manske[2] , S. Kaiser[3]
[1]Universität Hamburg, 22761 Hamburg, Germany
[2]Dresden University of Technology, 01062 Dresden, Germany
[3] Max Planck Institute for Solid State Research, 70569 Stuttgart, Germany

The U(1) gauge invariant version of the superconducting BCS state as formulated by P.W. Anderson is characterized by the Higgs mode as the elementary excitation of the superconductor in the two particle channel [1]. This mechanism inspired Y. Nambu and in particular P. Higgs to formulate the Higgs mechanism for elementary particle physics leading subsequentially to the discovery of the Higgs particle.[2-3] Varma pointed out early that the Higgs particle is a Raman active excitation. [4] Indeed experiments by Sooryakumar and Klein showed the first measurement of the Higgs mode in superconductors already in 1980 – a finding later confirmed in 2014. [5,6] Due to its weak coupling to light the Higgs mode remained quite elusive to experiments, despite the case in $NbSe_2$ where it gained strength in the Raman cross section by coupling to a CDW. However, over the past 20 years there was a continuous build up of experimental evidence for the Higgs mode in Raman scattering of HTCs. Already in 2005 Budelmann et al. noticed by using resonance Raman spectroscopy a distinct in-gap quasiparticle excitation as part of the overall gap feature seen in HTCs.[7] In 2009 Saichu et al. obseverd and in gap feature reacting on a pump on a different time scale as compared to the expected pair breaking peak suggesting the presence of a distinct in-gap excitation.[8] Since then many studies by different techniques in particular THz measurements have provided a growing body of evidence for the presence of the Higgs mode [9].

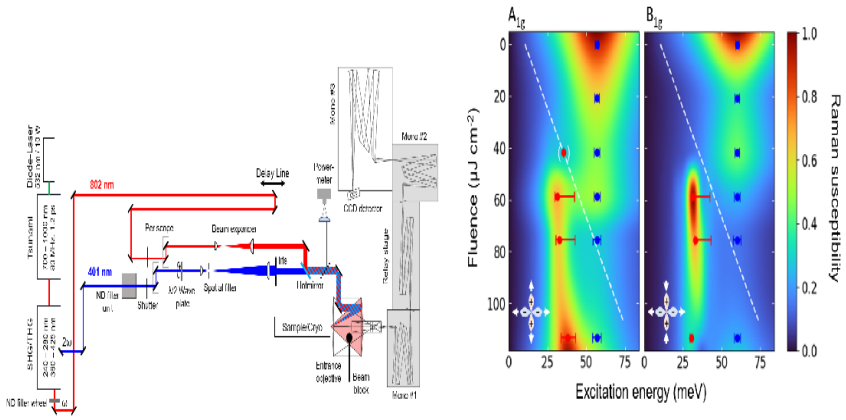

Fig.1. Left :Nonequilibrium Raman instrument *for the simultaneous measurement of energy gain and energy loss data. At infinite temperatures the energy gain and energy loss data would be equal. The NEARS measurements show a stronger Anti-Stokes (energy gain) contribution compared to the Stokes contribution which is only possible when pumping a novel state in the superconductor leading to population inversion. We assign this state tentatively to the Higgs mode and derive the excitation landscape of a superconductor in the single particle and two-particle channel (see panel on the* ***Right****). Figures are taken from Ref. [1].*

However, Raman scattering is susceptible to a combination of pair breaking excitations and superconducting quasiparticle excitations. The development of non-equilibrium Raman scattering (NEARS) allows to discriminate the different contributions by comparing the Anti-Stokes and Stokes (energy gain / energy loss) spectra in order to identify modes that get populated in a superconductor after a quench of the Mexican hat potential (see Fig. 1 – left) . We will discuss the detailed measurement procedure and will outline the presence of a new in-gap mode in the superconducting state. Its symmetry dependent behavior is consistent with the Higgs mode in the superconductor and incompatible with other excitations. From the fits it is then possible to determine the excitations landscape of a superconductor (see Fig. 1, right). We will also outline future plans to further support our assignment and what needs to be done to systematically evaluate the presence of the Higgs mode in HTCs.

References

[1] Y. Nambu, *Physical Review* **117**, 648 (1960).
[2] P. Anderson, *Physical Review* **110**, 827 (1958).
[3] P. Higgs, *Comptes Rendus Physique* **8**, 970 (2007).
[4] C. M. Varma, *Journal of Low Temperature Physics* **126**, 901 (2002).
[5] R. Sooryakumar, M. V. Klein, *Physical Review Letters* **45**, 660 (1980).
[6] M.-A. Measson, Y. Gallais, M. Cazayous, B. Clair, P. Rodiere, L. Cario, A. SacutoM. *Physical Review* B **89**, 060503 (2014).
[7] D. Budelmann, P.Maioli, T.Meunier, S.Gleyzes, A.Auffeves, G.Nogues, M.Brune, J. Raimond, S.Haroche, *Physical Review Letters* **95**, 057003 (2005)
[8] R. P. Saichu, I. Mahns, A. Goos, S. Binder, P. May, S. G. Singer, B. Schulz, A. Rusydi, J. Unterhinninghofen, D. Manske, P. Guptasarma M. S. Williamsen, M. Rübhausen, *Physical Review Letters* **102**, 177004 (2009).
[9] R. Shimano, N. Tsuji, *Annual Review of Condensed Matter Physics* **11**, 103 (2020).
[10] T. E. Glier, M. Rerrer, L. Westphal, G. Lüllau, L. Feng, S. Tian, J. Dolgner, R. Haenel, M.Zonno, H. Eisaki, M. Greven, A. Damascelli, S.Kaiser D. Manske, M. Rübhausen, *arXiv 2310.08162* (2024).

* Acknowledgements: we acknowledge many scientific discussions with Mika Rerrer, Lea Westphal, Garret Lüllau, Liwen Feng, Sida Tian Jakob Dolgner, Rafael Haenel, Marta Zonno, Hiroshi Eisaki, Martin Greven, and Andrea Damascelli.

Ultrafast anisotropic electronic properties of ZnAs2 semiconductor

N. T. Samani, N. Mignani, A. Crepaldi, E. Carpene, C.Dallera
Politecnico di Milano, 20133 Milano, Italy

Comprehension of anisotropic materials is crucial for developing polarization-sensitive photodetectors and polarizers [1]. Binary II-V semiconductors are among the most promising candidates to reach this goal, exhibiting anisotropic optical and electronic responses [2]. This family includes $ZnAs_2$: its energy absorption edge varies by more than 30 meV when light polarization is rotated from parallel to orthogonal to the crystallographic c-axis, while reflectivity is 1.5 times larger when the electric field is parallel to the c-axis, both in the region of transparency [1.2 um - 20 um] and at energies larger than the optical gap [2, 3, 4]. What gives rise to these properties is still an open question. To address this inquiry, we have mapped the band structure of ZnAs2 using angle-resolved photoemission spectroscopy (ARPES): the different effective masses of the valence band along ΓB and ΓZ directions of the Brillouin zone are the clear fingerprint of the optical anisotropy previously outlined.

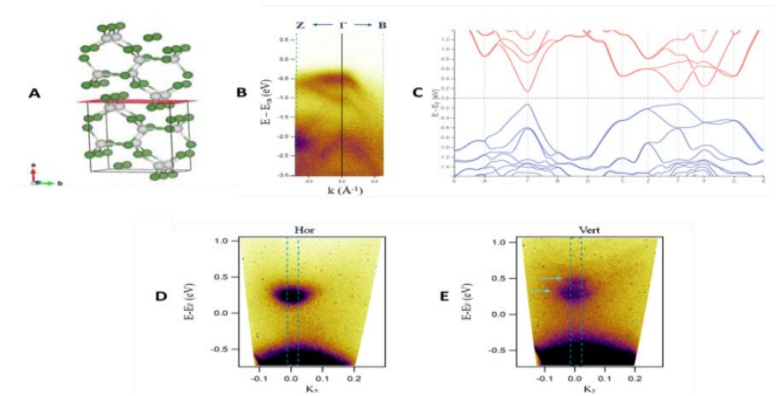

Fig. 1. (A) Crystal structure of ZnAs2 *showing in red the cleave plane [3].*
(B) *Occupied valence band structure measured with 56 eV photon energy, the zero energy scale is set to the maximum of the valence band (VB).* ***(C)*** *Calculated band structure is adapted.* ***(D)*** *and* ***(E)*** *Conduction band transiently populated by an above gap (1.8 eV) optical excitation (pump). The polarization of the probe, with an energy of 6 eV, is horizontal (**D**) and vertical (**E**), respectively.*

Furthermore, to disclose the unoccupied states, we have carried out time-resolved ARPES measurements, revealing lifetimes of several tens of picoseconds and a unique splitting in the transiently populated conduction band while probing with vertical polarization that cannot be reproduced by *ab initio* calculations. The goal of our activity is to clarify the origin of this behavior in the conduction band which may pave the way to the use of ZnAs2, and II-V semiconductors, in optoelectronic devices, leveraging their large anisotropic properties, and the long-lasting charge populations induced by light absorption in the visible spectral range.

References

[1] W. Ran, Z. Ren, P. Wang, Y. Yan, K. Zhao, L. Li, Z. Li, L. Wang, J.Yang, Z. Wei, Z. Lou, G. Shen, *Nature Communications* **12** 6476 (2021).
[2] W. J. Turner, A.S. Fischler, W.E. Reese, *Physical Review* **121**, 759 (1961).
[3] A. V. Mudryi A. I. Patuk, I. A. Shakin, A. E. Kalmykov, S. F. Marenkin, A.M. Raukhman, *Materials Chemistry and Physics* **44**, 151 (1996).
[4] V. V.Sobolev, N. N. Syrbu, *Physica Status Solidi (b)* **51**, 863(1972).

Exploring supersolid formation in polariton condensates

D. Sanvitto
Instituto di Nanotechnologia, 73100 Leece, Italy

Polaritons are unique quasiparticles resulting from the coupling of excitons with confined photons in semiconductors. Their hybrid light-matter nature has facilitated the study of various fundamental phenomena and the proposal of numerous technologically relevant applications, offering advantages such as low energy consumption, dissipation-less operation, and high clock frequencies [1]. Moreover, polaritons exhibit captivating macroscopic quantum phenomena, including superfluidity, quantized circulation, and parametric effects, to name a few. In this work, we explore the potential observation of supersolid formation in a polariton condensate. By utilizing patterned waveguides to fold propagating polariton modes within the light cone, we induce the creation of topologically protected states where condensation occurs at very low thresholds. [2-4] Through the spontaneous parametric scattering into higher modes within the waveguide, we observe a modulation atop the condensate, suggesting the emergence of a supersolid phase. These findings are pioneering in demonstrating the feasibility of realizing a supersolid in a photonic structure and could pave the way for discovering new regimes and physical phenomena.

References

[1] D. Sanvitto, S. Kena-Cohen, *Nature Materials* **15,** 1061 (2016).
[2] V. Ardizzone, F. Riminucci, S. Zanotti, A. Gianfrate, M. Efthymiou - Tsironi, D. G. Suarez-Forero, F. Todisco, M. De Giorgi, D. Trypogeorgos G. Gigli K. Baldwin, L. Pfeiffer, D. Ballarini, H. S. Nguyen,D. Gerace, D. Sanvitto, *Nature* **605**, 447 (2022).
[3] F. Riminucci, A. Gianfrate, D. Nigro, V. Ardizzone, S. Dhuey, L. Francaviglia, K.W. Baldwin, L. N. Pfeiffer, D. Ballarini, D. Trypogeorgos A. Schwartzberg D. Gerace, D. Sanvitto, *Physica Review Letters* **131,** 246901 (2023)
[4] A. Gianfrate, H. Sigurðsson, V. Ardizzone, H. C. Nguyen, F. Riminucci, M. Efthymiou - Tsironi, K. W. Baldwin, L. N. Pfeiffer, D. Trypogeorgos M. De Giorgi, D.Ballarini, H. S.Nguyen D. Sanvitto , *Nature Physics* **20**, 61 (2024).

An ultrafast and depth-resolved view on all-optical Switching of in-plane magnetization

D. Schick
Max-Born-Institut für Nichtlineare Optik und Kurzzeitspektroskopie,12489 Berlin, Germany

All-optical magnetic switching (AOS) describes the ability to deterministically switch the magnetization of a nanolayer exclusively by light and without applied magnetic fields [1]. Typical laser pulse durations of femto- to few picoseconds render this approach orders of magnitude faster than current field-driven technology, e.g., in state-of-the-art magnetic hard drives. AOS has so far been observed for a range of nanoscale transition metal (TM) and rare earth (RE) based alloys and multilayers, but the underlying mechanisms are still under investigation [2,3]. Ultrashort pulses of soft-X-ray radiation have been an inevitable tool for disentangling the dynamics of the different magnetic elements in materials exhibiting AOS [4] and their short wavelength also enabled AOS on a nanometer lateral scale [5]. In this work, we reveal the spatiotemporal evolution of AOS along the depth of a magnetic heterostructure consisting of a 10-nm thin, in-plane magnetized, ferrimagnetic GdCo layer [6]. To this end, we perform femtosecond transverse magneto-optical Kerr effect (TMOKE) spectroscopy at the Gd $N_{5,4}$ resonance at a laser-driven high-harmonic generation (HHG) source [7]. The comparison of the angle- and energy-resolved data with magnetic scattering simulations [8] enables a depth-resolved view of the photoexcited dynamics. Results being recorded for different excitation fluences, below and above the AOS threshold, show that the magnetization reversal is governed by the formation and propagation of a transient domain along the depth of the nanolayer with reversed in-plane magnetization, which - within a few picoseconds and depending on the fluence - either expands from the top through the entire depth of the magnetic thin film or is quenched back to the initial state.

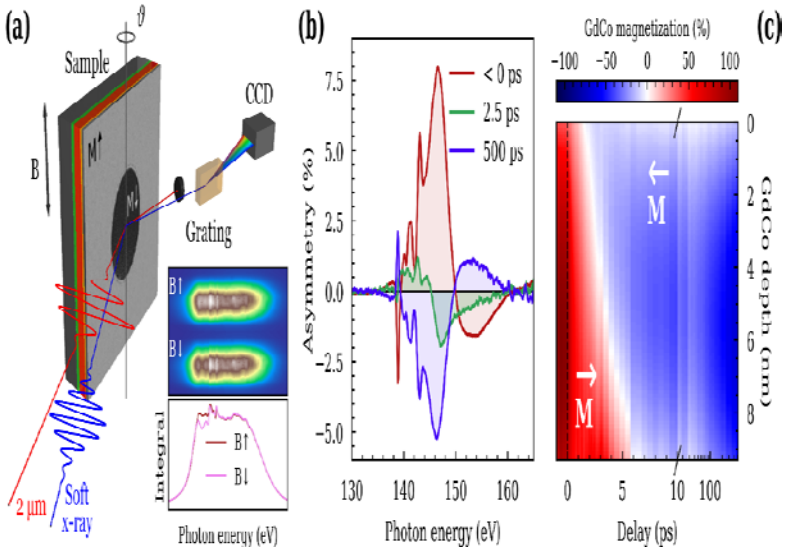

Fig. 1(a) Schematic of the ϑ-2ϑ spectroscopy setup *used for the time-resolved pump-probe measurements. The all-optical switching dynamics of an in-plane magnetized GdCo sample are excited by 27 fs (FWHM), 2.1 µm mid-infrared laser pulses and probed at the Gd $N_{5,4}$ resonance via broadband TMOKE spectroscopy, employing > 27 fs (FWHM) soft x-ray pulses. The magnetic contrast is achieved by flipping a saturating magnetic field B applied to the sample.* ***(b)*** *Magnetic asymmetry spectra are recorded as a function of pump-probe delay, capturing the depth-dependent magnetization dynamics of the GdCo layer due to a strongly photon energy-dependent information depth.* ***(c)*** *Fitting the time-resolved spectra with magnetic scattering simulations allows retrieving the transient magnetization distribution within the GdCo layer, relating ultrafast pump-induced changes within the asymmetry spectrum to real-space changes of the magnetization depth profile.*

The time-resolved profiling of the laser-induced switching process provides a direct insight into the microscopic mechanisms and spatial propagation of the ultrafast magnetization reversal within a magnetic thin film system. This enables a better understanding of the dynamics in the different material classes and sample geometries exhibiting AOS.

References

[1] C. Stanciu, F. Hansteen, A. Kimel, A. Kirilyuk, A. Tsukamoto, A. Itoh, T. Rasing, *Physical Review Letters* **99**, 047601 (2007).
[2] M. Beens, M. L. M. Lalieu, A. J. M. Deenen, R. A. Duine, B. Koopmans, *Physical Review* B **100**, 220409 (2019).
[3] Y. Peng, D. Salomoni, G. Malinowski, W. Zhang, J. Hohlfeld, L. D. Buda-Prejbeanu, J. Gorchon, M. Vergès, J. X. Lin, D. Lacour, R. C. Sousa I. L. Prejbeanu, S. Mangin, M. Hehn, *Nature Communications* **14**, (2023).
[4] I. Radu, K. Vahaplar, C. Stamm, T. Kachel, N. Pontius, H. A. Durr, T. A. Ostler, J. Barker, R. F. L. Evans, R. W. Chantrell, A. Tsukamoto A. Itoh, A. Kirilyuk, Th. Rasing, A. V. Kimel, *Nature* **472**, 205 (2011).
[5] K. Yao, F.Steinbach,M. Borchert,D. Schick,D.Engel,F.Bencivenga,R.Mincigrucci,L.Foglia,E. Pedersoli,D. De Angelis, M. Pankaldi, B. Wehinger F. Capotondi,C.Masciovecchio,S.Eisebitt,C. von Korff Schmising, *Nano Letters* **3** (2022).
[6] J.- X. Lin, M. Hehn, T.Hauet, Y. Peng, J.Igarashi, Y.Le Gen, Q.Remy, J.Gorchon, G.Malinowski, S.Mangin, J. Hohlfeld, *Physical Review* B **108** L220403 (2023).
[7] M. Hennecke, D. Schick, T. Sidiropoulos , F. Willems, A. Heilmann, M. Bock, L. Ehrentraut, D. Engel, P. Hessing, B. Pfau ,M. Schmidbauer A. Furchner, M. Schnuerer,C.von Korff Schmising, S.Eisebitt,, *Physical Review Research* **4**, L022062 (2022).
[8] D. Schick, *Computer Physics Communications* **266**, 108031 (2021).

Light-induced superconducting-like state in $La_{2-x-y}Nd_ySr_xCuO_4$

R. Shimano
The University of Tokyo, 113-0033 Tokyo, Japan

In high-T_c cuprate superconductors, the charge order phase has been widely identified in the temperature region above the superconducting phase in their phase diagram. Here a crucial question arises as to whether the charge order is related to the emergence of superconductivity or not. A common example of the charge order in cuprate SCs is the so-called stripe order where charges and spins are aligned in a form of stripes in CuO_2 planes. A substantial reduction of T_c in the stripe phase suggests that the charge/spin stipe is a competing order with the superconductivity. Along with this picture, the initial studies of the light-induced superconductivity have been performed in the stripe phase of $La_{2-x-y}Eu_ySr_xCuO_4$ (LESCO) [1] and $La_{2-x}Ba_xCuO_4$ (LBCO) [2]. The phenomena have been understood as the light-induced suppression of the stripe order which leads to the revival of initially prohibited c-axis interlayer Josephson couplings in equilibrium. However, there still remains a number of ambiguities about the origin of the light-induced superconductivity phenomena, and how the charge order states, including the stripe order, are correlated or uncorrelated with the superconductivity.In this work, we performed comprehensive studies of light-induced superconductivity in another archetypical La-214 system, $La_{2-x-y}Nd_ySr_xCuO_4$, by optical pump-terahertz probe spectroscopy. We found that the plasma edge appears in the c-axis THz reflectivity spectrum after the photo-excitation near below the onset of charge order temperature but far above T_c, whereas the 1/ω-divergence of the imaginary part optical conductivity was lacked in all the investigated doping samples [3]. Based on the experimental results, we discuss the interplay between the charge order and the superconductivity in La-based cuprates.

References

[1] D. Fausti, R. I. Tobey, N. Dean, S. Kaiser, A. Dienst, M. C. Hoffmann, S. Pyon, T. Takayama, H. Takagi A. Cavalleri, *Science* **331**, 189 (2011).
[2] D. Nicoletti, E. Casandruc, Y. Laplace, V. Khanna, C. R. Hunt, S. Kaiser, S. S. Dhesi, G. D. Gu, J. P. Hill, A. Cavalleri, *Physical Review* B **90** 100503(R) (2014).
[3] M. Nishida, K. Katsumi, D. Song , H. Eisaki, R. Shimano, *Physical Review* B **107**, 174523 (2023).
* The author acknowledges the collaboration with M. Nishida, K. Katsumi, D. Song, A. Hallas, and H. Eisaki. This work was in part supported by JST CREST Grant No. JPMJCR19T3..

Femtosecond electron diffuse scattering reveals two distinct non-thermal Phonon populations in bulk MoS_2

Y. Pan[1], P. Hildebrandt[2], D. Zahn[2], M. Zacharias[3], R. Ernstorfer[4], F. Caruso[1]
H. Seiler[5]
[1] *Christian-Albrechts-Universität zu Kiel, 24118 Kiel, Germany*
[2] *Fritz-Haber-Institut, 14195 Berlin, Germany*
[3] *FOTON Institute, 35708 Rennes, France*
[4] *Technische Universität Berlin, 10623 Berlin, Germany*
[5] *Freie Universität Berlin,14195 Berlin, Germany*

Femtosecond electron diffuse scattering has recently emerged as a powerful method to investigate electron-phonon and phonon-phonon couplings in time- and momentum-spaces [1-3]. Here we employ femtosecond electron diffuse scattering (FEDS) to investigate the momentum-resolved phonon dynamics in bulk MoS_2 [4]. Our data reveal that the non-equilibrium lattice dynamics after photo-excitation with a 2.14 eV pump pulse occurs in two successive stages involving qualitatively distinct non-thermal phonon populations before the lattice finally reaches a hot but quasi-thermal state. These stages are seen in Fig. 1. **a-c**, displaying intensity difference maps at 3 chosen pump-probe time delays. The first of these populations, seen in Fig.1. **a**, is established on the 500 fs timescale, and is dominated by K and M phonons generated through electron-phonon thermalization. A second nonthermal phonon distribution, seen in Fig. 1. **b** emerges with a timescale of roughly 3 ps, featuring hot Q phonons in addition to K and M phonons. Finally, over a timescale of around 40 ps, a hot but quasi-thermal phonon distribution is observed, seen in Fig. 1. **c**. To rationalize the observed phonon dynamics, we combine ab initio computations of the structure factor with time-dependent Boltzmann equations [3,5]. By combining these tools, we are able to reproduce the two-step relaxation process of the nonequilibrium lattice in MoS_2 seen in the FEDS experiments. For the first step, we identify some particularly strongly coupled acoustic modes at M and K which are coupled to the electrons.

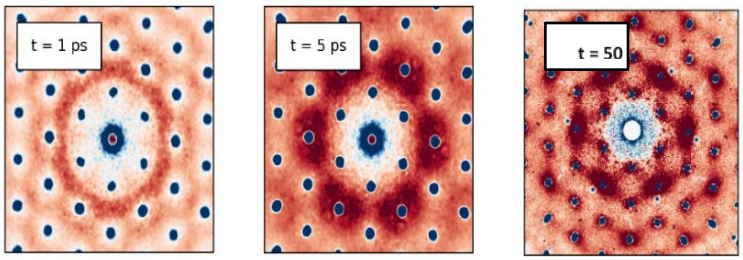

Fig. 1. a-c. Momentum-resolved electron diffraction signals*, I(q, t) - I(q, t < t_0), at pump–probe delays of 1, 5, and 50 ps. The Bragg reflections (**blue dots**) are negative due to the Debye-Waller effect. The diffuse background (**red**) qualitatively evolves as a function of pump–probe delay. The inelastic signals at 5 ps qualitatively depart from the non-thermal signals at 1 ps and quasi-thermal signals at 50 ps. This indicates that MoS_2 undergoes two qualitatively distinct non-thermal phonon populations before the lattice reaches a hot but thermal state.*

These results demonstrate the richness of nonequilibrium lattice dynamics in layered materials.

References

[1] H. A. Dürr, R. Ernstorfer, B. Siwick, *MRS Bulletin* **46,** 731, (2021).
[2] T. L. Britt, Q. Li, L. P. de Cotret, N. Olsen, M. Otto, S. Ali Hassan, M. Zacharias, F. Caruso, X. Zhu, B. J. Siwick, *Nano Letters* **22**, 4718, (2022).
[3] H. Seiler, D. Zahn, M. Zacharias, P. Hildebrandt, T. Vasileiadis, Y. W. Windsor, Y. Qi, C. Carbogno, C. Draxl, R. Ernstorfer, F. Caruso *Nano Letters* **21,** 6171, (2021).
[4] Y. Pan, P. Hildebrandt, D. Zahn, M. Zacharias, R. Ernstorfer, F. Caruso, H. Seiler, *submitted* (2024).
[5] M. Zacharias, H. Seiler, F. Caruso, D. Zahn, F. Giustino, P. C. Kelires, R. Ernstorfer, *Physical Review Letters* **127**, 207401, (2021).

he quantum Boltzmann equation in exciton, polariton and hot carrier dynamics

D. Snoke[1], V. Hartwell[2], H. Alnatah[1]
[1] *University of Pittsburgh, Pittsburgh, PA 15218, USA*
[2] *Skibo Energy Systems, Pittsburgh, PA 15208, USA*

The quantum Boltzmann equation has been used successfully in modeling the nonequilibrium behavior of electrons, holes, and polaritons in laser-excited semiconductors. As far back as 1991, the quantum Boltzmann equation was used to model the path to equilibrium of an exciton gas (see Fig.1) and free electrons and holes.

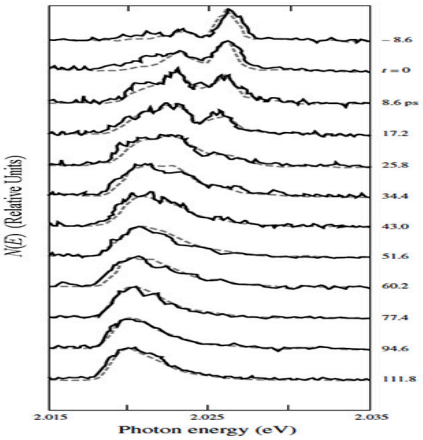

Fig. 1. Solid lines*: time-resolved photoluminescence from excitons in Cu_2O. **Dashed lines**: the results of a fit to the quantum Boltzmann equation for phonon emission and absorption. From[1].*

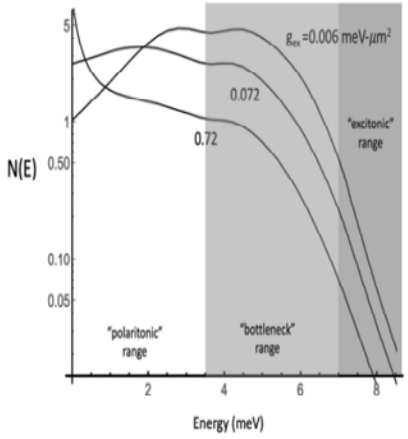

Fig. 2. The steady-state distribution of polaritons in a microcavity *for three different choices of exciton-exciton interaction strength From[3].*

More recently, it has been extended to a Boltzmann-like equation for the phase coherence as a function of time in fermion and boson gases, which helps us to understand how a fully quantum mechanical description can give irreversible behavior in time [2]. The quantum Boltzmann equation depends sensitively on the scattering rates of particles, which in turn depend on the interaction constants. In the past few years a quantum Boltzmann equation model has been used to constrain the polariton-polariton scattering rate in microcavities [3] (see Fig.2), which has been a controversial topic in polariton optics. It has also been used to model the transfer of momentum from free electrons to polaritons in one-dimensional drag experiments in which electric current is passed through a polariton condensate. This talk will give a review of quantum Boltzmann methods and discuss recent work.

References

[1] D. Snoke, D. Braun, M. Cardona, *Physical Review* B **44**, 2991 (1991).
[2] D. W. Snoke, G.-Q. Liu, S.M. Girvin, *Annals of Physics* **327**, 1825 (2012).
[3] D. W. Snoke, V. Hartwell, J. Beaumariage, S. Mukherjee, Y. Yoon, D. M. Myers , M. Steger , Z. Sun, K. A. Nelson, L. N. Pfeiffer, *Physical Review* B **107**, 165302 (2023).
* Acknowledgment: the authors acknowledge support from the US National Science Foundation grant DMR-2306977.

Prototype polariton superfluid qubit analog in an annular trap

J. Barrat[1], A. F. Tzortzakakis[4], M. Niu[2], X. Zhou[2], G.G. Paschos[2], D. Petrosyan[3], P.G. Savvidis[2]
[1]*Fudan University, Shanghai 200433, China*
[2]*Westlake University, Hangzhou 310030, China*
[3]*Institute of Electronic Structure and Laser, 70013 Heraklion, Greece*
[4]*National and Kapodistrian University of Athens, 157072 Athens, Greece*

Exciton-polaritons are hybrid light-matter quasi-particles resulting from the strong coupling of semiconductor excitons and microcavity photon. Being bosons polaritons can exhibit macroscopic spatial coherence and form out-of-equilibrium condensates exhibiting superfluid behavior when pumped above threshold. A promising recent theoretical proposal for polaritonic qubit utilizes split-ring polariton-condensate in an annular ring involving quantized circular currents[1,2]. This system relies on the formation of vortices in superfluids arising from the quantization of circulation, where the phase accumulation around a supercurrent loop can only take discrete values. Closely related physics governs the principles of operation of superconducting flux or phase qubits involving superconducting loops interrupted by Josephson junction. Here we show that, under appropriate conditions, optically trapped out-of-equilibrium polariton condensates can populate two well-characterized states corresponding to the clockwise and counterclockwise circulating currents. We demonstrate coherent coupling between these states, due to the partial reflection of the circulating superfluid from a weakly disordered laser potential or an external control laser beam, while simultaneously maintaining long coherence times. We can control the coupling and thereby the energy splitting between the two eigenmodes of the system. Inspired by the theoretical proposal to realise qubit analogs and quantum computing with two-mode BECs [4], we formallyidentify the two polaritonic eigenmodes with the basis states of a qubit. Supplemented with controllable coupling between individual polaritonic qubits, such systems hold great potential for simulating a subset of quantum algorithms that do not rely on entanglement.

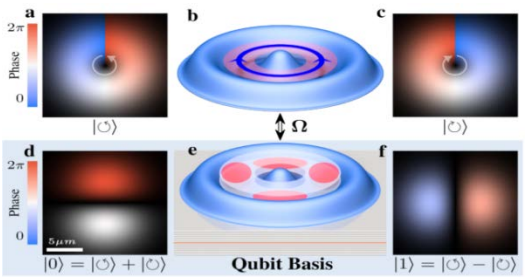

Fig 1. Polaritonic qubit analog

References
[1] Y. Xue, I. Chestnov, E. Sedov, E. Kiktenko, A. K. Fedorov, S. Schumacher, X. Ma, A. Kavokin, *Physical Review Research* **3**, 013099 (2021).
[2] A. Kavokin, T.C.H. Liew, C. Schneider, P.G. Lagoudakis, S. Klembt, S. Hoeflinget, *Nature Review Physics* **4**, 435 (2022).
[3] J. Barrat, A.F. Tzortzakakis, M.Niu, X.Zhou, G.G. Paschos, D. Petrosyan, P.G. Savvidis, a*rXiv:2308.05555* (2023).
[4] T. Byrnes, K. Wen, Y. Yamamoto, *Physical Review* A **85**, 040306(R) (2012).

Sub-wavelength time- and spatially resolved electron and spin dynamics in solids

M. Schultze
Graz University of Technology, 8010 Graz, Austria

The enormous electric field strength of ultrafast laser waveforms allows to steer electronic motion and control electronic excitation so fast, that secondary processes disrupting coherence and striving for an equilibrium have hard time catching up – even in condensed phase systems. We investigate the opportunities this temporal segregation offers to transfer coherent control ideas as demonstrated in atomic and molecular ensembles to solids. This talk will discuss two experiments demonstrating that ultrafast optical fields at optical frequencies allow manipulating electronic and spin degrees of freedom in solid state systems at optical clock rates faster than de-coherence.

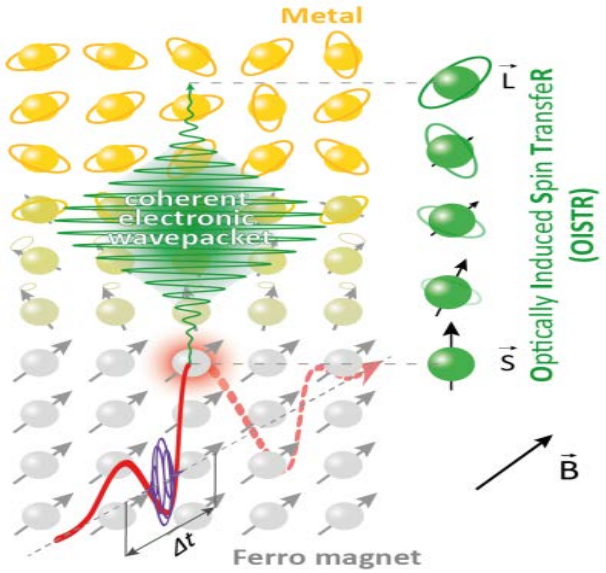

Fig.1: Ultrafast wave-packet creation by an ultraviolet light-field.

Ultrafast wave-packet creation by an ultraviolet light-field in the band-structure of wide-gap dielectrics proves the early times reversibility of electronic excitations and holds promise of novel ultrafast, coherent optoelectronic applications up to the petahertz frontier that we identified as the ultimate limit of optoelectronic signal manipulation [1].
As a corollary of this ultrafast coherent modification of the electronic system, in suitably chosen heterostructures also the spin system can be manipulated coherently. Optically induced spin transfer is demonstrated as a route to the direct, all-optical manipulation of macroscopic magnetic moments on previously inaccessible attosecond timescales [2].

References

[1] M. Ossiander, K. Golyari, K. Scharl, L. Lehnert, F. Siegrist, J. P. Bürger, D. Zimin, J. A. Gessner, M. Weidman, I. Floss, V. Smejkal, S. Donsa C. Lemell, F. Libisch, N. Karpowicz, J. Burgdörfer, F. Krausz, M. Schultze, *Nature Communications* **13**, 1620 (2022).

[2] F. Siegrist, J. A. Gessner, M. Ossiander, C. Denker, Y.-P. Chang, M. C. Schröder, A. Guggenmos, Y. Cui, J. Walowski, U.Martens, J. K. Dewhurst U. Kleineberg, M. Münzenberg, S. Sharma, M. Schultze, *Nature* **571**, 240 (2019).

Advanced laser technology for THz generation

C. J. Saraceno

Ruhr University Bochum, 44801 Bochum, *Germany*

Ultrafast lasers have become ubiquitous for fundamental research. However, many applications could benefit from long driving wavelengths with comparable performance to the more well-established 1µm laser systems. For example, long driving wavelengths are of interest as drivers for secondary sources, for nonlinear conversion schemes from the XUV to the THz. We focus our attention on the advantages of long-wavelength pulses to increase the conversion efficiency in THz generation.: they allow in many materials to reduce the impact of multi-photon absorption, as well as enable to reach high conversion efficiencies in two-color plasma sources, thanks to a stronger ponderomotive force. Traditionally, high-power ultrafast sources were restricted to complex and inefficient parametric conversion stages, allowing to reach tens of watts of average power, using pumps with several hundreds of watts based on Yb systems [3]. A much more elegant and simple approach is to use gain media directly emitting in this wavelength range for high-power oscillators and amplifiers. As shown in Fig. 1, many advances have been realized in bulk and fiber-based amplifier systems in this wavelength range. Some remarkable achievements in the wider area of high-power 2 µm ultrafast lasers are the demonstration of a Tm-fiber based chirped pulse amplifier systems, with an average power of 1060 W at 80-MHz pulse repetition frequency, corresponding to a pulse energy of 13.2 µJ [4]. Nevertheless, compared with ultrafast lasers in the 1-µm wavelength range, the average power of 2 µm ultrafast lasers are at least one order of magnitude lower as show in Fig. 1, showing large potential for further progress. In particular, very few results have been achieved in this wavelength range with disk lasers -both oscillators and amplifiers- therefore representing an area of unexplored potential in ultrafast source development. We will discuss during our presentation the current development in high-power 2 µm disk and bulk lasers and current challenges and application possibilities, in particular with a focus towards THz generation using these sources.We will discuss during our presentation the current development in high-power 2 µm disk and bulk lasers and current challenges and application possibilities, in particular with a focus towards THz generation using these sources.

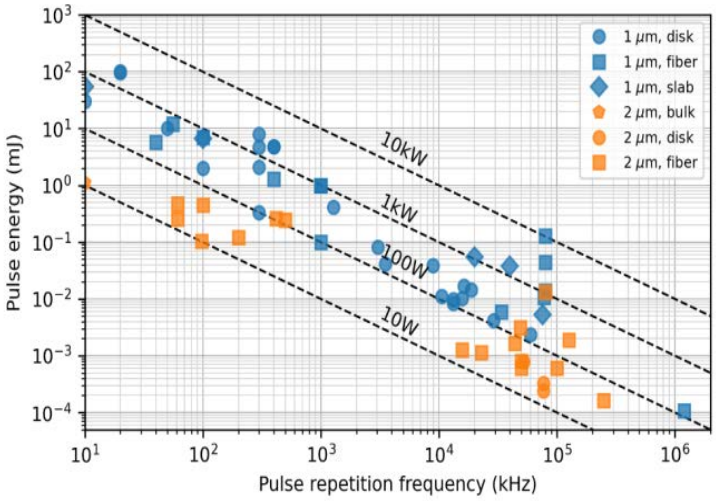

References

[1] I. Mingareev, F. Weirauch, A. Olowinsky, L. Shah, P. Kadwani, M. Richardson, *Optics and Laser Technology* **44**, 2095 (2012).

[2] R. A. Richter, N. Tolstik, S. Rigaud, P. D. Valle, A. Erbe, P. Ebbinghaus, I. Astrauskas, V. Kalashnikov, E. Sorokin, I. Sorokina, *Journal of Optical Society of America* B **37**, 2543 (2020).

[3] J. Buss, M. Schulz, I. Grguras, T. Golz, M. J. Prandolini, R. Riedel, *SPIE Proceedings* **11278**, (2020).

[4] C. Gaida, M. Gebhardt, T. Heuermann, F. Stutzki, C. Jauregui, J. Limpert, *Optics Letters* **43**, 5853 (2018).

Continuous-wave and pulsed operation of rare-earth ion-doped Fluoride crystal waveguide lasers in the near and mid-infrared spectral region

A. Sennaroglu[1], Y. Morova[1], B. Ayevi[1], M.Tonelli[3]
[1]*Koç University, Istanbul 34450, Turkey*
[2]*Università di Pisa, 56127 Pisa Italy*

Fluoride based crystal hosts have numerous favorable optical properties, including low phonon energies that help reduce unwanted non-radiative decay processes, wide transparency window from ultraviolet to mid-infrared and the possibility to fabricate low-loss waveguides by femtosecond laser inscription. In addition, various rare-earth ions can be doped into the crystal to generate laser emission in the near and mid-infrared wavelengths. In this study, we describe our recent experiments in which low-loss channeled waveguides were fabricated in Tm^{3+}:BaY_2F_8 and Er^{3+}:$YLiF_4$ to obtain laser operation near 2 µm and 2.7-2.8 µm, respectively [1, 2]. Fig. 1(a) shows a photograph of the Tm^{3+}:BaY_2F_8 waveguide laser setup. Channeled waveguides with diameters of 30 µm and 50 µm were inscribed inside the crystal, with propagation loss of as low as 0.22 dB/cm for the 50-µm waveguide at the non-resonant pump wavelength of 731 nm. By using 680 mW of pump power at 781 nm and a 6% transmitting output coupler, 73 mW of continuous-wave (cw) output power was obtained with a slope efficiency of 13% as can be seen in the measured efficiency curve in Fig. 1(b). The output spectrum was centered at 1.86 µm (Fig. 1(c)).

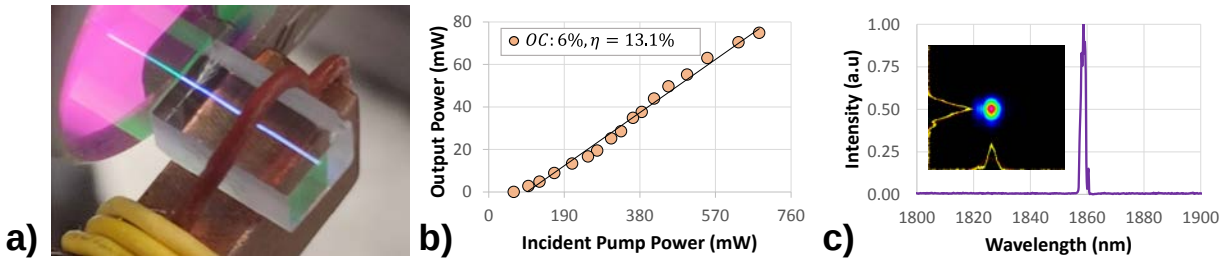

Fig. 1. (a) Photograph, (b) measured efficiency curve, and (c) output beam profile*/spectrum of the Tm^{3+}:BaY_2F_8 waveguide operating at 1.86 µm.*

In a second experiment, low-loss channeled waveguides with diameters of 50 µm and 70 µm were inscribed inside a Er^{3+}:$YLiF_4$ crystal. The propagation loss of the 70-µm waveguide, shown in Fig. 2(a) was measured as 0.23 dB/cm. The waveguide laser was pumped at 798 nm and could be operated either in cw or self-Q-switched (SQS) regime. The output wavelength and power slope efficiency were 2808 nm and 19.6% during cw operation, respectively. During SQS operation, the output wavelength shifted to 2717 nm (Fig. 2(b)) and pulses as short as 240 ns could be generated with a repetition rate of 368 kHz.

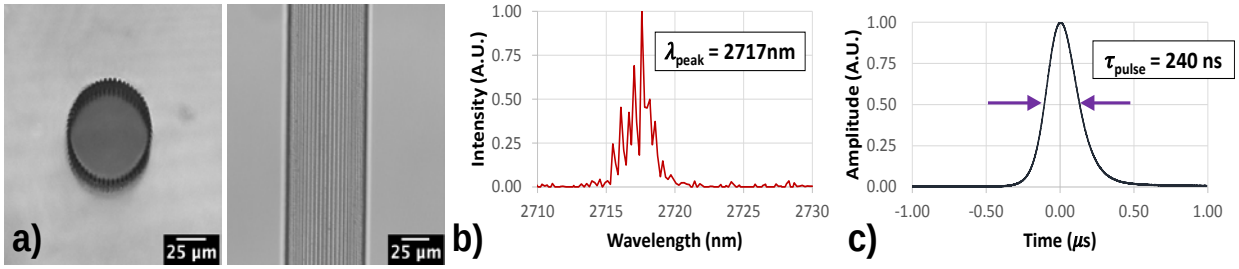

Fig. 2. (a) Confocal microscope image of the 70-µm channeled waveguide *inside Er^{3+}:$YLiF_4$ crystal. Measured (**b**) output spectrum and (**c**) temporal pulse profile of the self-Q-switched Er^{3+}:$YLiF_4$ waveguide laser operating at the wavelength of 2717 nm.*

The measured temporal profile of the 240-ns pulses is shown in Fig. 2(c).

References

[1] Y. Morova, M. Tonelli, A. Sennaroglu, *Optical Materials* **126**, 112121 (2022).
[2] B. Ayevi, Y. Morova, M. Tonelli, A. Sennaroglu, *Optics Letters* **49**, 1017 (2024).

Ultrafast 2-3 micron laser sources: towards silicon photonics Integration and applications

I. T. Sorokina[1], M. Demesh[1], A. Rudenkov[1], N. Gusakova[1], E. Einmo[1]
V. L. Kalashnikov[1], C. Grivas[1], E. Sorokin[2]
[1] Norwegian University of Science and Technology, 7034 Trondheim, Norway
[4] Technische Universität Wien, 1040 Vienna, Austria

In the last 15 years silicon (Si) photonics has received tremendous attention, mainly from the telecom industry. Such areas as Si optical interconnects and other passive devices have matured to the degree that they find applications in the mega-scale datacenters in the research and industrial giants like Intel. The light emitters, however, could not be directly fabricated in Si, neither as a laser/LED (Si is an indirect bandgap semiconductor) nor by doping. Most of the demonstrated silicon photonic systems still rely on external light sources such as VECSELs [1]. Interestingly, Cr^{2+}-doped ZnS may provide a path for direct integration with Si photonics, because ZnS is one of the few semiconductors lattice-matched to Si and because the Cr^{2+}: ZnS operation wavelength range of 2-3.1 μm [2-4] lies well in the transparency window of Si and allows for high-power broadest tunable and few-cycle ultrafast laser operation, including frequency combs [3,5] even in the directly diode-pumped setups [6]. The works on power scaling have enabled generation, via nonlinear frequency conversion, of mid-IR light that spans the entire "molecular fingerprint" region between 3 and 14 μm [5,6]. For ultrashort-pulse Si photonics, it is also advantageous that Cr:ZnS wavelength range lies beyond the two-photon absorption range of Si below 2.1 μm. At the same time, the development of energetic 0.1-10 μJ ultrafast mid-IR sources opens possibilities for sub-wavelength 3-D sub-surface processing of silicon and other semiconductor materials [7,8].This talk reviews the state-of-the-art in the field with a particular emphasis on our recent advances towards the challenging goal of development of integrable ultrashort-pulsed waveguide laser systems in the 2–3 μm wavelength range. We will discuss approaches for generating and amplification with a high gain factor of CW and pulsed mid-IR radiation in depressed-cladding buried waveguide lasers. We demonstrate that a relaxation of higher-order spatial modes to the lowest-order mode ("mode condensation" [9]), initialized by spatially profiled gain, allows energy harvesting in a waveguide solid-state amplifier with a good mode with M^2<1.3. *1. Cr:ZnS processing with 2.1μm ultra-short pulsed laser:* For the direct laser writing of the waveguide we used an integrated MOPA Ho:YAG picosecond laser system (ATLA Lasers AS) at 2090 nm central wavelength and compared the results with previously written structures using sub-ps pulses at 1030 nm. We fabricated circular waveguides with different diameters of 20–50 μm (Fig. 1) that were inscribed in a 34-mm long polycrystalline Cr:ZnS sample using a NA=0.85 objective. The waveguides possess estimated single pass losses of about 0.6±0.1 dB/cm at 30–50 μm diameter and refractive index change of about $\Delta n = (-2.5 \pm 0.5) \times 10^{-3}$ at 1030 nm and noticeably higher index change at 2090 nm. The modification traces at 2090 nm were nearly spherical, while the 1030-nm traces were 5–10 times longer in the direction of writing beam propagation. An investigation of this phenomenon is underway.

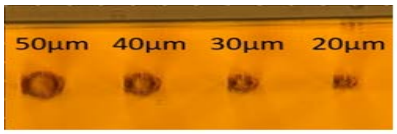

Fig. 1. End view of waveguides *in Cr:ZnS crystal at ~200 μm depth (2090 nm writing). Laser beam is focused from above. Writing direction is perpendicular to the view plane. Since the index change in ZnS is negative, all waveguides are of depressed-cladding type, where the waveguide is formed by many lines of traces written around the unchanged core.*

2. CW operation of waveguide Cr:ZnS laser/ We have built a simple laser cavity with flat cavity mirrors butt-coupled to the polished uncoated facets of the samples. The active waveguide was pumped at 1550 nm by the emission of an Erbium-fiber laser focused on the waveguide facet through the dichroic mirror, highly reflective in the 2100–2500 nm range and transmitting at the pump wavelength. The output coupler mirror had about 40% transmittance. Typical output characteristics are shown in Fig 2.

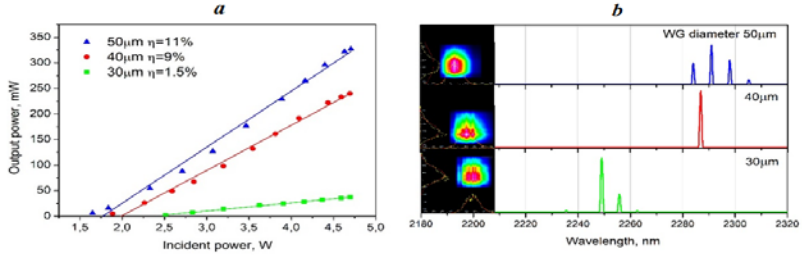

Fig. 2. Top*: **a) comparison of CW laser** operation of polycrystalline Cr:ZnS depressed cladding buried waveguide lasers with different geometry; **b)** effect of waveguide size on the spatial distribution of the output radiation and spectral characteristics of waveguide lasers.*

We measured the highest slope efficiency of 11% and 300 mW output at the incident pump power of 4.7 W for the 50-μm waveguide. We aim to reduce the propagation loss by optimizing the writing conditions and depressed cladding geometry. *3. Chirped pulse amplification in waveguide laser.*In our previous report [8] we proposed a novel technique to provide hybrid CPO-CPA pulse energy scaling, preserving

the output spectrum high-fidelity compression. In this work, we study a robust technique of high repetition rate chirped pulses amplification in a laser written depressed-cladding buried waveguide active media in a single pass configuration. A schematic of the experimental setup is shown in Fig. 3a. It consists of a Cr:ZnS mode-locked seed laser operating in an anomalous dispersion regime (30fs, 10nJ, 68MHz), chirped volume Bragg grating stretcher, a Faraday isolator, the waveguide Cr:ZnS gain element, Er-fiber laser as a pump source, and dichroic mirror based signal/ pump separator at the output. The results are presented for the most representative cases - waveguides with diameters of 50, 40, and 20 μm. Fig. 3b shows beam quality measurements for the 50 μm waveguide with an M^2 factor of 1.13×1.25. Fig. 3c shows the power performance of the same samples. The maximum output power of 2.3 W and the gain factor G=61 (5.2 dB/cm) was obtained for a 50 μm waveguide with power added optical efficiency of 10.2%. The other waveguides demonstrated the following parameters: 1.5 W output power and G=62 for the 40 μm waveguide, 0.2 W output power, and G=3.8 for the 20 μm waveguide. Fig. 3d illustrates the normalized spectra of the seed, amplified pulse, and ASE in the 50 μm waveguide amplifier. One can see the onset of gain-narrowing, where the longer wavelength components are suppressed, while components near the gain maximum (cf. the ASE spectrum) are enhanced.

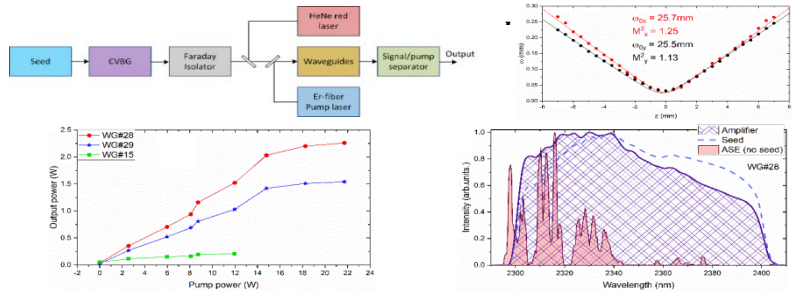

***Fig. 3. Top**: **a) experimental setup**: Seed is the femtosecond Cr:ZnS laser, CVBG is the chirped volume Bragg grating, Signal/ pump separator at the output is a dichroic mirror; **b)** M^2 factor measurements results for 50 μm waveguide). **Bottom: c)** output power versus pump power characteristics for waveguides with three different diameters (50, 40, and 20 μm); **d)** seed, amplified pulse, and amplified spontaneous emission (ASE) spectra for 50 μm waveguide.*

The results of numerical simulations based on the dissipative Lugiato–Lefever model [11] are shown in Fig. 4a, b

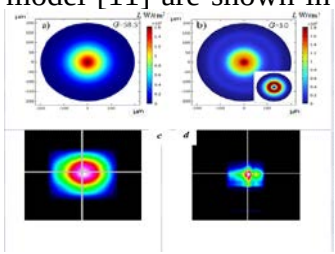

***Fig. 4. Intensity I profiles of the amplified field** after 3.4 cm Cr:ZnS waveguide of 50 μm **(a)**, and 20 μm **(b)** diameters. The input energy of the 500 ps seed pulse is 1.47 nJ and the pump powers are 22 W **(a)** and 12 **(b)** W. Inset in **(b)** shows the field profile after 3.28 cm propagation distance in a waveguide. G is a gain factor (arb.un.). **(c)** and **(d)**: output beam profiles for 50μm **(c)**, and 20 μm **(d)** waveguide diameters.*

The calculated gain factor G up to ~60 (Fig. 4a) agrees with the experiment for the largest waveguide cross-sections 50 μm (Fig. 3c). The beam profile is close to the Gaussian (Figs. 3b and 4a,c). The mode quality and gain factor degrade with a decrease in the waveguide diameter due to the excitation of higher-order transverse modes (Fig. 3c and 4b,d). In this case, the impact of the soft aperture induced by a transversely profiled pump beam is not sufficient for their suppression. In the experiment, the gain factor is noticeably lower than the calculated, as we guess, due to higher propagation losses (Figs. 2a and 3c) and oversimplified (parabolic-like) graded refractive index profile with Δn =0.003. We demonstrate that using a large cross-section multimode Cr^{2+}:ZnS waveguide allows reaching the gain factors up to ~60 in a single pass. Experiments and calculations show the interplay between the non-dissipative (transversely graded refractive index) and dissipative (graded gain) confinement potentials. This results in integrating higher-order modes into lower-order ones (spatial mode synthesis or “mode condensation” [9]), potentially allowing effective use of the whole gain volume and energy harvesting in the compact multimode waveguides. As an outlook, one may anticipate realizing a high-repetition-rate waveguide self-mode-locked oscillator [11] and a photonic crystal-like amplifier in a laser-processed Cr^{2+}:ZnS bulk medium.

References

[1] Z. Wang, A. Abbasi, U. Dave, A. De Groote, S. Kumari, B. Kunert, C.Merckling, M. Pantouvaki, Y. Shi, B. Tian, K.van Gasse, J. Verbist R. Wang W. Xie, J. Zhang, Y. Zhu, J. Bauwelinck, X. Yin, Z. Hens, J. van Campenhout, B. Kuyken, R. Baets, G. Morthier, D. van Thourhout G. Roelkens, *Laser Photonics Review* **11**, 1700063 (2017).
[2] I. T. Sorokina, *Optical Materials* **26,** 395 (2004).
[3] I. T. Sorokina, E. Sorokin, IEEE Journal Selected Topics Quantum Electronics **21,** 1601519 (2015).
[4] S. B. Mirov, V.V. Fedorov, D. Martyshkin, I. S. Moskalev, M. Mirov, S. Vasilyev, *IEEE Journal Selected Topics Quantum Electronics* **21,** 292 (2015)
[5] S. B. Mirov, I. S. Moskalev , S. Vasilyev, V. Smolski , V. V. Fedorov, IEEE Journal Selected Topics Quantum Electronics **24,** 1601829 (2018)
[6] N. Nagl, “A New Generation of Ultrafast Oscillators for Mid-Infrared Applications”, *PhD thesis, Springer* (2021).
[7] N. Tolstik E. Sorokin, J.C. Mac-Cragh, R. Richter, I.T. Sorokina, *CLEO Application and Technology* AM41.8 (2022).
[8] I. T. Sorokina, E. Sorokin, *OPIC’2022*, (2022).
[9] W. H. Renninger, F. W. Wise, *Nature Communications* **4,** 1719 (2013).
[10] A. Rudenkov, V.L. Kalashnikov, E. Sorokin, M. Demesh, I.T. Sorokin, *Optics Express* **31,** 17820 (2023).
[11] M. Demesh, V. L. Kalashnikov, E. Sorokin, N. Gusakova, A. Rudenkov, I. T. Sorokina, *Journal Optical Society America* B **40,** 1717 (2023).

* Acknowledgement(s): authors ITS, VLK, AR, MD, CG, and NG acknowledge support from the Norwegian Research Council projects #303347 (UNLOCK), 326503 (MIR) and #326241(LAMMO-3D), as well as from ATLA Lasers AS.

Ultrafast spin and charge carrier dynamics in heterostructures with Hidden spin polarization

B. Stadtmüller
Rheinland-Pfälzische Technische Universität Kaiserslautern-Landau, 67663 Kaiserslautern, Germany

Developing innovative concepts to control charge and spin carriers in active functional units on increasingly smaller length scales and faster timescales is one of the major challenges in information technology. One approach to achieve this is by using intrinsic two-dimensional (2D) materials like transition metal dichalcogenides (TMDs) and designing their spin-dependent band structure through chemical functionalization or optical engineering. For TMDs, this is primarily achieved by creating aligned or twisted 2D heterostructures with either other TMDs or 2D honeycomb materials, such as graphene. Although this method has been successfully used to adjust the interfacial properties of 2D heterostructures, it still has limitations in terms of tuneability of the interfacial energy level alignment and the lateral dimensions of the heterostructures. In this contribution, we will introduce heterostructures consisting of molecules and TMDs (see Fig. 1a) as a highly tunable platform to control the evolution of optically excited charge and spin carriers at hybrid interfaces. This carrier dynamics can have a profound influence on the transient interfacial energy level alignment.

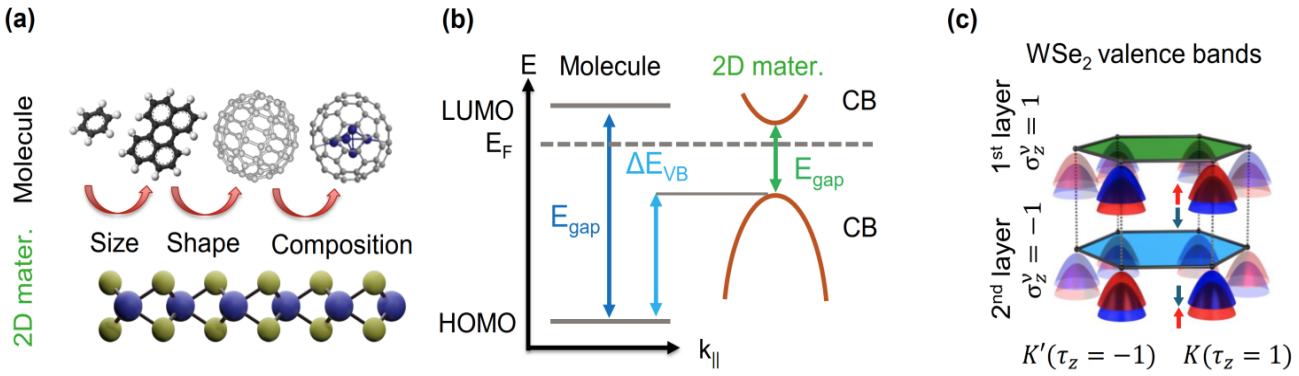

Fig.1 (a). Graphical representation of the tunability of molecule-TMD heterostructures*. The electronic properties of such interfaces can be chemically designed by choosing molecules that can exhibit different sizes, structural shapes, and chemical compositions. These distinct properties enable a fine-tuning of the energy level alignment in the molecular layer as well as at the hybrid interface* ***(b)****. (****c****) Sketch of the local layer- and spin-dependent valence band structure of the two non-interacting WSe_2 layers of the bulk unit cell in which the spin polarization vanishes at every point in the Brillouin zone.*

The key to this approach is the highly tunability of molecular materials. As illustrated in Fig 1b, this allows one to control not only the optical band gaps (E_{gap}) of both sides of the interface but also to design the energy level alignment at the interfaces (ΔE_{VB}). We will focus on heterostructures that combine the TMD bulk crystal WSe_2 with fullerenes and metal-phthalocyanines (MPcs). WSe_2 has a *hidden spin polarization* [1,2], as illustrated in Fig. 1c. This means that the valence bands of the individual WSe_2 layers show the well-known spin polarization at the Brillouin zone boundary. polarization of neighboring layers cancels each other out due to the centrosymmetric bulk structure, leading to an overall spin-degenerate band structure. On the other hand, the excited state dynamics of fullerenes such as C_{60} are dominated by charge transfer excitons [3,4] that can act as precursors for a highly efficient interlayer charge transfer across the hybrid interfaces. Using time-, spin—and momentum-resolved photoemission [5], we will show how different types of energy level alignment at the interface between molecules and bulk crystals of WSe_2 influence the interfacial charge and spin transfer dynamics and the transient interfacial energy level alignment. For the case of C_{60}/WSe_2, optical excitation of the molecular layer leads to the formation of charge transfer excitons followed by an ultrafast electron transfer into WSe_2, as sketched in Fig. 2a. This population dynamics can be identified by the characteristic signatures in the time- and momentum-resolved photoemission (tr-ARPES) data set

that is shown in Fig. 2b. Most importantly, the ultrafast electron transfer from the molecular layer into WSe_2 leads to a transient charging of the interfacial layers. The corresponding interfacial dipole fields can transiently alter the interfacial energy level alignment. Most importantly, the strength of these transient interfacial dipoles reduces with increasing distance from the interface thus affecting the WSe_2 layers within the bulk unit cell differently. This causes a spin- and layer-dependent modification of the WSe_2 valence bands (see Fig. 2c) that transiently reveals the hidden spin polarization of WSe_2 [6].
In the context of hybrid interfaces between metal phthalocyanines (MPcs) and WSe_2, we have uncovered an interesting energy level alignment with two competing resonant optical excitation pathways.

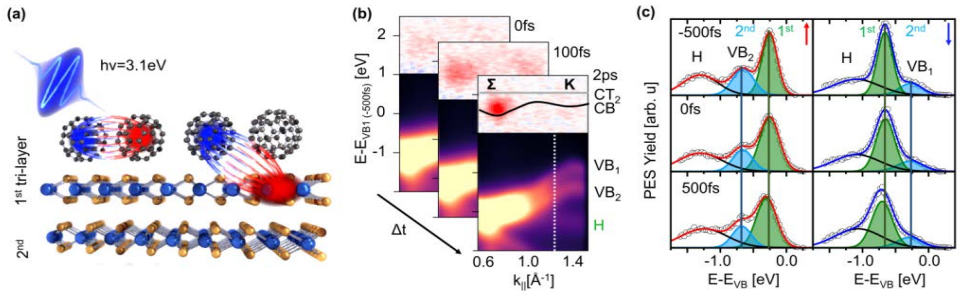

Fig.2 (a) Illustration of the C_{60}/WSe_2 heterostructure *as well as the interfacial charge transfer after the optical excitation of the C_{60} layer.* ***(b)*** *Snapshots of the time resolved ARPES data set.* ***(c)*** *Spin-resolved spectral yield of the valence band structure at selected time delays illustrating the transient layer dependent WSe_2 valence band shift.*

When we use IR photons, we observe an optical transition either across the fundamental band gap of WSe_2 or across the hybrid interface from the MPc into the WSe_2 layer as shown in Fig. 3.

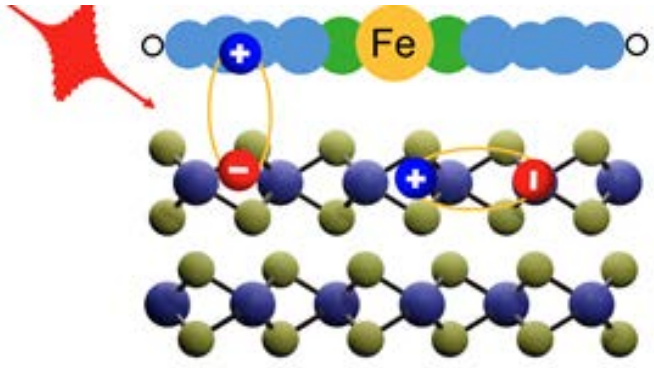

Fig.3 Illustration of the optically excited intra- and interlayer charge transfer *processes occurring for the MPc/WSe_2 heterostructures.*

This generates charge and spin carrier populations that can undergo various competing interlayer charge transfer processes. We will focus on the ultrafast dynamics of the interfacial charge transfer processes and their impact on the transient interfacial energy level alignment. Furthermore, we will demonstrate how we can adjust the optically generated charge and spin carrier populations by polarizing the excitation light pulses.
Our results will thus provide a clear pathway toward manipulating spin functionalities in molecular/TMDC heterostructures by chemically and optically steering the evolution of ultrafast spin and charge carriers in hybrid systems.

References

[1] X. Zhang, Q. Liu, J. W. Luo, A. J. Freeman, A. Zungeret, *Nature Physics* **10**, 387(2014).
[2] M. Riley, F. Mazzola, M. Dendzik, M. Michiardi, T. Takayama, L. Bawden, C. Granerød, M. Leandersson, T. Balasubramanian, M. Hoesch T. K. Kim, H. Takagi, W. Meevasana, Ph. Hofmann, M. S. Bahramy, J. W. Wells P. D. C. King, *Nature Physics* **10,** 835 (2014).
[3] B. Stadtmüller, S .Emmerich, D. Jungkenn, N. Haag, M. Rollinger, S. Eich, M. Maniraj, M. Aeschlimann, M. Cinchetti, S.Mathias, *Nature Communications* **10**, 1470 (2019).
[4] S. Emmerich, S. Hedwig, B. Arnoldi, J. Stöckl, F. Haag, R. Hemm, M. Cinchetti, S. Mathias, B. Stadtmüller**,** M.Aeschlimann, *Journal of Physical Chemistry* C **124**, 23579 (2020).
[5] B. Stadtmüller, *Journal of Physics. Condensed Matter* **33**, 353001 (2021)
[6] B. Arnoldi, S.L. Zachritz, S. Hedwig, M.Aeschlimann, O.L.A. Monti, B. Stadtmüller, *arXiv:2304.10237* (2023).

Ultrafast laser-induced shear phonons in layered vdW materials revealed by Ultrafast electron microscopy

S. Sun, W. Gao, Y. Zhang, K. Zhu, W. Wang, H. Tian, H. Yang, J. Li
Institute of Physics, Beijing, 100190, People's Republic of China

Coherent phonons generated by optical excitation have been extensively studied for their potential application in characterizing and manipulating the fascinating properties of low-dimensional electronic materials. The detection of coherent phonons has gradually matured with the development of various ultrafast experimental methods, especially through techniques like ultrafast electron diffraction and microcopy, providing direct structural sensitivity and high spatial resolution [1]. Optical phonons and longitudinal acoustic (LA) phonons spanning gigahertz to terahertz frequencies have been reported in a wide range of materials. However, the generation of transverse acoustic (TA) shear modes is less common, as it requires a specific choice of excitation symmetry breaking.Firstly, ultrafast selected-area electron diffraction was used to investigate laser-induced LA phonons in hexagonal 2*H*-$MoTe_2$ film [2]. Experimental and simulation results demonstrate that the inhomogeneous laser excitation can induce the second harmonic component of the LA strain wave, while no TA phonons can be excited. We theoretically analyzed the influence of coherent LA and TA phonons on diffraction intensity to provide a guide for identification of different type of phonons [3]. Then, we explored the shear phonons in monoclinic 1*T*'-$MoTe_2$ [4], which underwent a phase transition into the orthorhombic *Td* phase below around 250K. In the *Td* phase, a ~0.37 THz interlayer optical shear phonon (Fig. 1a) was observed, disappearing as the temperature rises above 250K. Within the 1*T*' phase, two coherent acoustic phonons were measured with frequency of 13.5 GHz (TA) and 39 GHz (LA) respectively (Fig. 1c). The LA phonon represents a common breathing mode that can be excited in both *Td* and 1*T*' phase; in contrast, TA phonons can only be detectable in the 1*T*' phase. The presence of optical shear mode in *Td* phase and acoustic shear mode in 1*T*' phase serves as valuable indicators for characterizing thermal phase transition (Fig. 1e). Further experiments will focus on the pathway of ultrafast light-induced *Td* to 1*T*' phase transition.

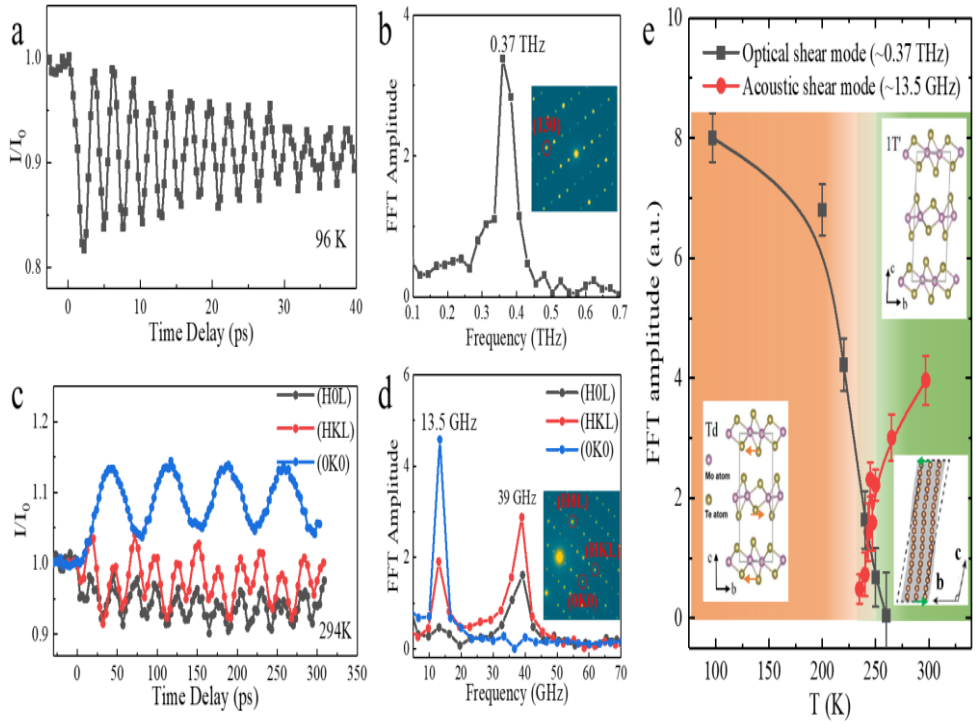

Fig. 1. Laser-excited coherent shear phonons in $MoTe_2$. ***(a)*** *Diffraction intensity oscillation of optical shear mode and* ***(b)*** *the corresponding FFT in Td phase;* ***(c)*** *Diffraction intensity oscillation of acoustic shear and breathing mode and* ***(d)*** *the corresponding FFT in 1T' phase, the acoustic shear mode can only be detected in the Bragg peak with k≠0, which was also cross-checked by the bend contour movement in dark-filed imaging;* ***(e)*** *Temperature dependence of optical and acoustic shear mode amplitude indicating the thermal phase transition.*

Further experiments will focus on the pathway of ultrafast light-induced *Td* to 1*T*' phase transition.

References

[1] W. Wang, S. Sun, J. Li, D. Zheng, S. Huang, H. Tian, H. Yang, J. Li, *Chinese Physics* B **33,** 010701 (2023).
[2] Y. Zhang, S. Sun, W. Wang, H. Tian, J. Li, J. Li, H. Yang, *Physical Review* B **108,** 245426 (2023).
[3] Y. Zhang, J. Li, W. Wang, H. Tian, W. Gao, J. Li, S. Sun, H. Yang, *Structural Dynamics* **10,** 064102 (2023).
[4] W. Gao, S. Sun, Y. Zhang, *to be submitted* (2024).
* Acknowledgement(s): this work is supported by Synergetic Extreme Condition User Facility (SECUF).

Sum-frequency ionic Raman scattering at finite wavevector

J. Stanton[1], M. Fechner[2], G. Orenstein[2], V. Krapivin[2], Y. Huang[3], Z.Zhan[5], G. de la Pena Munoz[3]
R. A Duncan[4] ,Q. Nguyen[3], H. Yavas[3], T. Sato[3], M. C Hoffmann[3], P.Kramer[3], J. Zhang[5], R. Comin[5]
A. S Disa[6] M. P.M. Dean[7], M. Forst[2], S. L Johnson[8], M. Mitrano[9], A. M Rappe[10], D. Reis[4], D. Zhu[5]
K. A Nelson[5], A. Cavalleri[2], M. Trigo[3], S. Teitelbaum[1]
[1]*Arizona State University, Tempe, AZ 75287, USA*
[2]*Max Planck Institute for the Structure and Dynamics of Matter, 22761 Hamburg, Germany*
[3]*SLAC National Accelerator Laboratory, Menlo Park, CA94025, USA*
[4]*Stanford University, Stanford, CA94035, USA*
[5]*Massachusetts Institute of Technology, Cambridge, MA02139, USA*
[6]*Cornell University, Ithaca, NY14850, USA*
[7]*Brookhaven National Laboratory, Upton, NY 11973, USA*
[8]*ETH Zurich, 8093 Zurich, Switzerland*
[9]*Harvard University, Cambridge, MA 02138, USA*
[10]*University of Pennsylvania, Philadelphia, PA19104, USA*

Third-order anharmonicity is the lowest symmetry-allowed anharmonic interaction in homogeneous solids, and thus the lowest-order description of phonon-phonon interaction. In many solids three-phonon scattering is the primary interaction that describes processes as diverse as thermal conductivity, phase transitions and light-driven superconducting-like states [1-3]. Historically, nonlinear photonics is often implemented by driving a high-frequency IR-active drive mode, producing a coherent response in a lower-frequency Raman-active mode. Here, the rectified (quasi-DC) component of the RMS displacement of the IR mode u^2 results in an impulsive force on the lower-frequency mode, leading to displacive excitation [4]. However, in general, a third-order anharmonic process driving a low-frequency mode can also drive a mode with double the drive frequency, and the drive modes to not, in general have to be at finite wavevector, as long as the total crystal momentum is conserved.X-ray free electron lasers (XFELs) are uniquely suited to probe the nonlinear interactions between finite-wavevector modes. The combination of sensitivity to finite-wavevector motions, quantitative measurement of mode displacements, and time-domain measurements which allow for nonlinear spectroscopy are key to revealing these interactions [5].

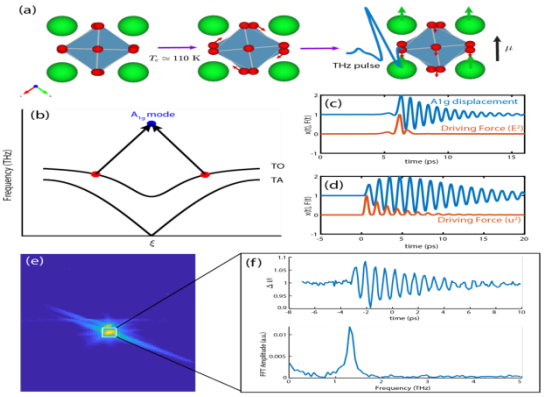

Fig, 1: Ionic Raman Scattering *in SrTiO3. **(a)** Structure of STO and Excitation scheme. The A1g mode is illustrated in red (**center panel**) and the TO phonon at zone-center is illustrated on the right panel. **(b)** Schematic of the Ionic Raman scattering process in reciprocal space. Two TO phonons (**red**) combine and produce a single A1g phonon (**blue**). **(c)** Predicted A1g displacements based on a THz drive field (electronic Raman scattering). **(d)** Predicted A1g displacements (**blue**) based on an Ionic Raman scattering drive force (**orange**) for a single oscillating mode. **(e)** X-ray diffraction of a peak sensitive to octahedral rotation of the A1g mode. **(f)** Time-dependent displacement of the A1g mode. Note the slow buildup of amplitude over two cycles, indicating a resonant drive force.*

In particular, THz pump, x-ray probe experimental modalities are a powerful approach, as direct excitation of IR-active vibrations ensures that all of the energy delivered by the pump pulse is delivered to the vibrational degrees of freedom that are of interest in these experiments [6, 7]. Here, we investigate strontium titanate ($SrTiO_3$) a crystal with low-lying IR-active modes that can be driven to high amplitude with THz radiation. In this experiment, we use THz radiation to excite finite-wavevector TO phonons in $SrTiO_3$. Subsequently, using time-resolved x-ray diffraction, we observe a coherent oscillation of the Raman-active A_{1g} mode that corresponds to the octahedral rotation of the TiO_6 octahedra away from their high-temperature symmetric phase. There are two possibilities for how this mode is driven – either by a direct Raman transition, or by a (sum-frequency Ionic Raman scattering) [8]. Both processes have the same nonlinearity, and therefore we distinguish between them by the shape of the expected drive field and displacement. Based on the buildup of oscillations in the Raman-active mode, we conclude that the A_{1g} mode in SrTiO3 is primarily driven by Ionic Raman scattering that couples the low-frequency TO phonon modes at finite wavevector $+q$ to the zone-center A_{1g} mode. To our knowledge, this is the first observation of finite-wavevector ionic Raman upconversion. We further

quantify the coupling strength by estimating the amplitude of the TO and A_{1g} phonon mode displacements. Since this anharmonicity is the lowest-order nonlinear coupling between the phonon branches that control octahedral rotation and ferroelectric displacement, a measurement of this coupling provides powerful insight into the nature of tolerance factor tuning in ferroelectrics – using the octahedral rotation to control the ferroelectric order parameter. Beyond ferroelectrics, our approach should be generalizable to a wide variety of systems with coupled structural degrees of freedom. This points the way to a powerful quantitative tool to disentangle the underlying couplings that result in the phase diagrams of complex quantum matter.

References

[1] W. Zhong, D. Vanderbilt, K. M. Rabe, *Physical Review* B **52**, 6301 (1995).
[2] M. Zebarjadi, K. Esfarjani, M. S. Dresselhaus, Z. F. Ren, G. Chen, *Energy and Environmental Science* **5**, 5147 (2012).
[3] M. Mitrano, A. Cantaluppi, D. Nicoletti, S. Kaiser, A. Perucchi, S. Lupi, P. Di Pietro, D. Pontiroli, M. Riccò, S. R. Clark, D. Jaksch A. Cavalleri *Nature* **530**, 461 (2016).
[4] M. Först, C. Manzoni, S. Kaiser, Y. Tomioka, Y. Tokura, R. Merlin, A. Cavalleri, *Nature Physics* **7**, 854 (2011).
[5] S. W. Teitelbaum, T. Henighan, Y. Huang, H. Liu, M. P. Jiang, D. Zhu, M. Chollet, T. Sato, É. D.Murray, S. Fahy, S. O'Mahony, T. P. Bailey C. Uher, M.Trigo, D. A. Reis, *Physical Review Letters* **121**, 125901 (2018).
[6] M. Kozina, M. Fechner, P. Marsik , T. van Driel, J. M. Glownia, C. Bernhard, M. Radovic, D. Zhu, S. Bonetti, U. Staub, M.C. Hoffmann, *Nature Physics* **15**, 387 (2019).
[7] R. Mankowsky, A. Subedi, M. Först, S.O.Mariager,M.Chollet,H.T.Lemke, J.S. Robinson, J.M. Glownia, M.P. Minitti, A. Frano, M.Fechner, T. Loew N. A.Spaldin, B. Keimer, A. Georges, A. Cavalleri, *Nature* **516**, 71 (2014).
[8] D. M. Juraschek, S. F. Maehrlein, *Physical Review* B **97**, 174302 (2018).

Electric-pulse-induced spin and charge dynamics in doped Mott insulators

T. Tohyama

Tokyo University of Science, Tokyo 125-0051, Japan

Electric pulse applied to the Mott insulators induces insulator-to-metal transitions. The nature of the insulator-to-metal transition depends on the shape of pulses. The Keldysh crossover serves as an indicator that distinguishes between excitations resulting from photon absorption triggered by near-infrared multicycle pulses and those arising from quantum tunneling induced by terahertz pulses. The crossover has been theoretically demonstrated for a one-dimensional (1D) Mott insulator [1]. In doped Mott insulator, however, metallic excitations due to doped carriers will cause electric-pulse-induced phenomena different from the Mott insulator. In doped 1D Mott insulators, only Drude component dominates low-energy excitation. When space dimension is higher than 1D, spin degrees of freedom contribute to charge excitations. Therefore, not only the Drude weight but also spin-related excitations emerge above the Drude excitation in energy. To clarify the nature of electric-pulse-induced charge dynamics in the low-energy region below the Mott gap in doped Mott insulators as wll as the difference of nonequilibrium responses between Drude and spin-related excitations, we study a doped two-leg ladder Hubbard model with strong on-site Coulomb interaction. We calculate time-resolved optical conductivity for the hole-doped two-leg ladder Hubbard model driven by electric field. The time-dependent density-matrix renormalization group is used for the calculation of the optical conductivity in a 16x2 ladder [2]. Fig. 1 shows a preliminary result of the real part of optical conductivity before and after pumping by electric pulses [3].

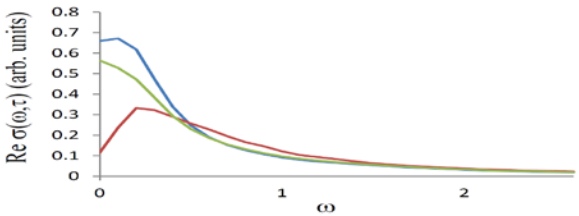

Fig. 1. Time-dependent optical conductivity *excited by pump pulses for a four-hole doped two-leg ladder Hubbard lattice with 16x2=32 sites and on-site Coulomb interaction U=10 in the unit of hopping energy. The amplitude of the vector potential is set to be A_0=0.5. Blue line is for time τ<0 (before pumping). Red line represents spectrum for a monocycle pulse with pump frequency ω_p=0 calculated at time τ=12 when pump pulse is finished. Green line is for a pump pulse with ω_p=1.*

Before pumping, low-energy metallic excitations form a peak structure close to the energy ω=0. Together with this low-energy peak, there is a broad excitation near ω=1 accompanied by spin excitations. By pumping these two structures using the pump frequency ω_p=0 and ω_p=1, we find suppression of the peak for both cases. The peak structure remains for ω_p=0, while the peak position shifts to ω=0 for the ω_p=1 case. The latter suggests that pumping the broad ω=1 spin-related structure induces a strong Drude-like feature, i.e., coherent metallic state.

This work was done in collaboration with Sumal Chandra, Kazuya Shinjo, and Shigetoshi Sota.

References

[1] K. Shinjo , T. Tohyama, *APL Materials*, in print *arXiv:2401.12584* (2024).
[2] T. Tohyama, K. Shinjo, S. Sota, S. Yunoki, *Physical Review* B **108**, 035113 (2023).
[3] S. Chandra, K. Shinjo, S. Sota, T. Tohyama, *(to be submitted)* (2024).

Polariton formation and interactions in van der Waals metasurfaces

J. Tollerud[1], T. Weber[2], L. Sortino[2], S. Maier[3], J. Davis[1]
[1] *Swinburne University, Hawthorn, 3122VIC, Australia*
[2] *Ludwig-Maximilians-Universität München, Munich, Germany*
[3] *Department of Physics, Imperial College London, London, UK*

Intrinsic strong light-matter coupling was recently demonstrated in a nano-patterned multi-layer WS_2 flake by engineering a bound-state in the continuum (BIC) energetically resonant with the bulk exciton[1]. This all-dielectric approach (shown in Fig 1 a-c) supports a photonic mode that is independent of material-intrinsic losses, and the coupling can thus be precisely tuned via the details of the BIC structure. The polariton (a coupled exciton/photon) energy can be tuned further via the choice of dielectric material which makes this a potentially ideal platform for polaritonic devices operating at room temperature. A polariton's photonic origin imbues on it a dispersion relation in which the band energy can vary considerably even below 1 μm^{-1}, a regime which is relevant to wave-vector sensitive ultrafast spectroscopy techniques. BIC-WS_2 polaritons are characterized by an anomalous dispersion relation in which the polariton energy decreases as wave-vector increases, an inversion of the dispersion relation typically seen in micro-cavity based polariton systems. Zero momentum polaritons can thus scatter into higher wavevectors that are both energetically favourable and more weakly coupled, reducing polariton lifetimes. Polariton scattering to larger wave vectors relies on interactions with other polaritons, uncoupled excitons, and/or phonons, and depend strongly on the detuning between the exciton transition energy and the energy of the trapped photonic mode. Understanding how these interactions underpin fast polariton relaxation is vital for eventual implementation of monolithic polaritonic devices.

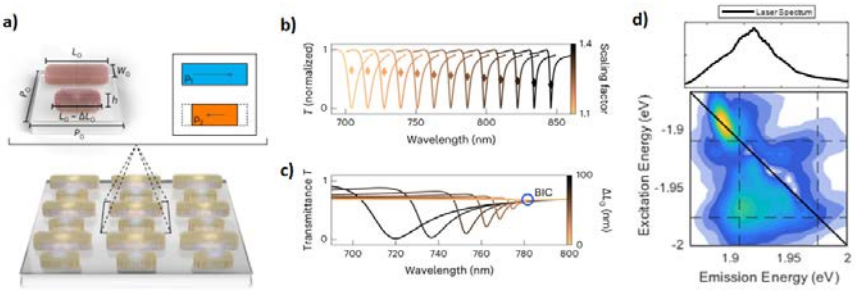

Fig. 1. (a) WS_2 - BIC metasurface *[1]. **(b)** BIC energy can be tuned by changing the unit cell scaling factor [1]. **(c)** BIC linewidth can be tuned by changing the length difference between the islands in a unit cell [1]. **(d)** Example WS2-BIC 2D spectrum showing polariton at ~1.90eV and exciton at 1.97eV*

Multi-dimensional coherent spectroscopy (MDCS) is an incisive ultrafast tool which can be used to reveal and quantify interactions in diverse material systems. In this work, we simultaneously track excitation and emission at both exciton and polariton energies and observe coherent dynamics that occur on the femtosecond timescale. By examining lineshape and linewidth of the polariton resonance, we can extract both homogeneous and inhomogeneous linewidth as a function of a variety of other controllable parameters (e.g. detuning, wavevector, temperature) to understand how they impact the polariton dynamics. For example, we can understand the relevance of polariton-phonon interactions by looking at the polariton homogeneous line-width at different temperatures -Fig 2.

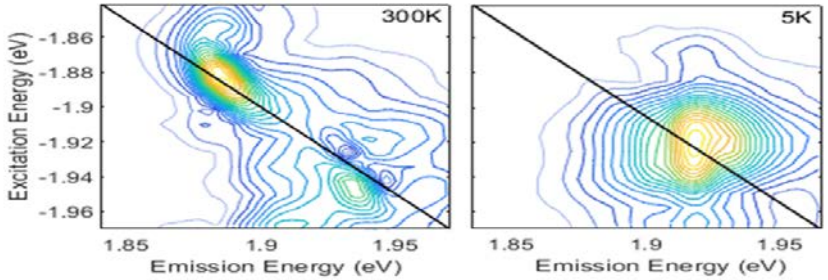

Fig. 2. 2D spectra of the polariton resonance *at 300K and 5K, showing no decrease in linewidth at low temperature. The blueshift of the polariton transition is due to the change in energy of the exciton resonance, which is also observed in transmission measurements in [1]*

We observe no decrease in the linewidth at low temperature, which indicates that phonon-polariton interactions do not play a dominant role in polariton decoherence. By performing measurements at different excitation densities, we also find that polariton-polariton and exciton-polariton interactions are also not a significant factor. With these decoherence pathways ruled out, we conclude that non-radiative population relaxation pathways and radiative recombination are the dominant factors governing the homogeneous linewidth and thus the polariton line-shape. We find significant dependence of the

polariton linewidth and shape on the wavevector and phonon- exciton detuning -Fig 3, with the longest decoherence times near normal incidence and zero detuning, respectively.

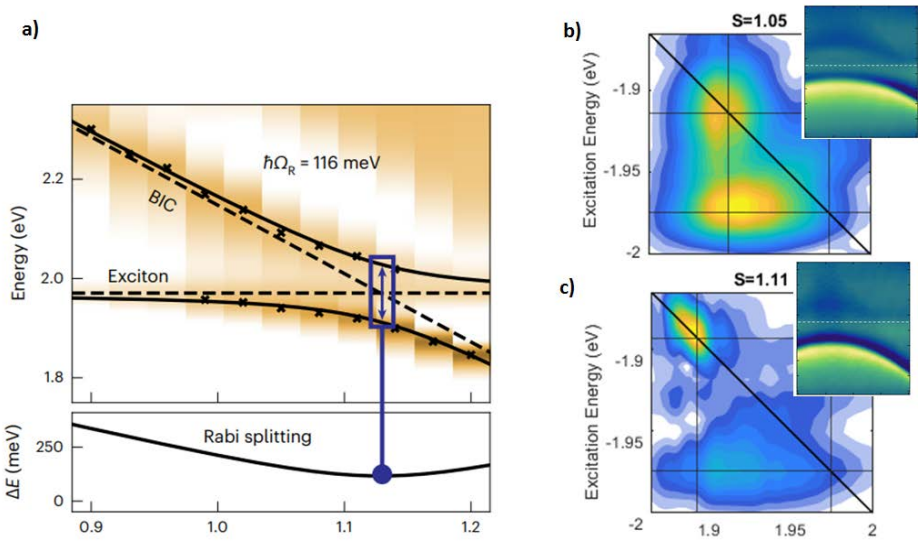

Fig. 3. (a) Transmission measurements as a function of detuning *(scaling factor) [1].* ***(b-c)****2D rephasing spectra of WS2-BICwith moderate positive and near zero detuning,respectively. Insets show the polariton dispersion curve for each detuning.*

We explain the former as being caused by the exciton-photon coupling being reduced, enabling scattering of the polariton to higher wave-vectors where the photon confinement is reduced, increasing leakage from the BIC. As wavevector increases, the effective detuning is also increased, similarly leading to reduced exciton-phonon coupling. MDCS can also be used to study relaxation and coupling between different bright transitions through the presence and dynamics of cross peaks – signals that appears at different excitation and detection energies. We utilize this capability to investigate the timescale over which resonantly excited excitons form into polaritons. Understanding this process will likely be very important for devices where polaritons would be formed using electrical rather than optical means. Our results show polariton formation and relaxation occurring over 10s and 100s of fs, respectively, and hint at slower hybridization due to inherent aperiodicity at the edge of the structure.

Reference

[1] T. Weber, L. Kühner, L. Sortino, A. Mhenni, N. Wilson, J. Kühne, J. Finley, S. Maier, A. Tittl, *Nature Materials* **22,** 970 (2023).

* Acknowledgement(s) : this work was supported by the Australian Research Council Center of Excellence in Future Low-Energy Electronics Technologies (CE170100039), the Deutsche Forschungsgemeinschaft (DFG, German Research Foundation) under Germany's Excellence Strategy (EXC 2089/1—390776260 and EXC-2111—390814868) , the Emmy Noether Programme (TI 1063/1), the Bavarian programme Solar Energies Go Hybrid (SolTech), the Center for NanoScience (CeNS), the Alexander von Humboldt Foundation (Humboldt Research Fellowship to L.S.), the International Max Planck Research School for Quantum Science and Technology (IMPRS-QST) (funding to A.B.M.), the EPSRC (EP/W017075/1 to S.A.M.) and the Lee-Lucas Chair in Physics (to S.A.M.).

Polarization density waves in $SrTiO_3$

G. Orenstein[1], V. Krapivin,[1] Y. Huang[3], Z. Zhang[4], G.de la Peña Muñoz[1], R. A. Duncan[1], Q. Nguyen[1], J. Stanton[2]
S. Teitelbaum[5], H. Yavas[1], T.Sato[1], M. C. Hoffmann[1], P.Kramer[1], J. Zhang[6], A. Cavalleri[7], R.Comin[4]
M.P. M. Dean[8], A. S. Disa[9], M. Först[7], S. L. Johnson[10], M. Mitrano[11], A. M. Rappe[6]
D. Reis[2], D. Zhu[1], K. A. Nelson[4], M. Trigo[1]
[1]*SLAC National Accelerator Laboratory, Menlo Park, California 94025, USA*
[2]*Stanford University, Stanford, California 94305, USA*
[3]*University of Illinois at Urbana-Champaign, Urbana, Illinois 61820, USA*
[4] *Massachusetts Institute of Technology, Cambridge, Massachusetts 02139, USA*
[5]*Arizona State University, Tempe, Arizona 85281, USA.*
[6]*University of Pennsylvania, Philadelphia 19104, USA*
[7]*Max Planck Institute for the Structure and Dynamics of Matter, Hamburg, Germany*
[8]*Brookhaven National Laboratory, Upton, New York 11973, USA*
[9]*Cornell University, Ithaca, NY 14853, USA*
[10]*ETH Zurich, CH-8093 Zurich, Switzerland*
[11]*Harvard University, Cambridge, Massachusetts 02138, USA*

Recent measurements on $SrTiO_3$ showed that strong single- and multi-cycle terahertz (THz) fields can induce transient ferroelectricity [1-2], raising the prospects for ultrafast, reversible control of structure. However, recent equilibrium measurements show hints of a different instability towards an incipient phase with spatially modulated polarization at low temperature [3–5], highlighting the need for

microscopic structural information of the transient ferroelectric state. We present ultrafast x-ray scattering from THz-driven $SrTiO_3$ in the quantum paraelectric regime. We developed a novel approach to probe inversion symmetry breaking that reveals polar-acoustic excitations that are particularly soft at lengthscales of tens of nanometers. This indicates a structural instability with spatially-modulated polarization distinct from the homogeneous ferroelectric [5,6]. Our results highlight the importance of probing fluctuations with momentum resolution and provide new insight into the microscopic structure of transient phases [1,2]. Fig. 1 summarizes the x-ray scattering response of $SrTiO_3$ upon excitation with a single-cycle THz pulse.

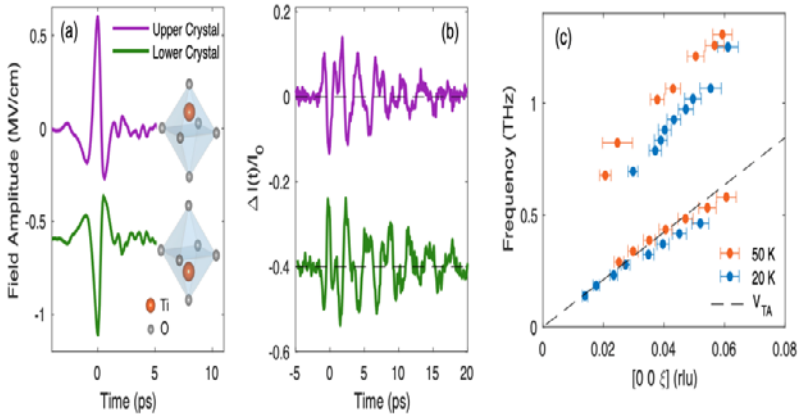

***Fig. 1. (a) Intensity of the** (3,3,3) **Bragg reflection** of SrTiO3 at T=20 K along the [0,0,1] direction (pseudo-cubic lattice). The inset is a reciprocal space map of the peak in a plane perpendicular to [1,-1,0]. **(b)** Dynamics of the relative intensity for representative wavevectors indicated with colored dots above the intensity in **(a)**. The corresponding wavevectors are indicated next to each trace. **(c)** Dispersion relation obtained by Fourier transform of the coherent oscillations like those in (**b**). Note that the response is localized at finite wavevector corresponding to wavelengths of order 10-50 nm.*

The coherent oscillations generated by the THz pulse, shown in Fig. 1(b), are primarily localized in the range of wavevectors ξ = 0.03 - 0.06 rlu, corresponding to wavelengths of 10-20 nm. This is surprising since the strongest resonant mode is expected to be the 0.4 THz zone-center ferroelectric soft mode, yet the strongest response is away from ξ = 0, indicating that momentum conservation is broken by a nanoscale modulation of the absorption, i.e. polar nanoregions that modulate the infrared absorption at short lenghscale. To characterize the inversion symmetry of excitations in Fig. 1 we devised a scheme to invert the polarity of the generated THz based on two identical $LiNbO_3$ prisms with ferroelectric axes pointing in opposite directions [7]. Fig. 2 (a) shows the electro-optic sampling of the THz field from the two prisms. In Fig. 2(b) we show a representative x-ray intensity response for the two incident fields sowing that the entire response is inverted when the field polarity inverts (purple and green traces, respectively). This indicates that the coherent excitations that result in the dispersion of Fig. 1(c) are polar and infrared active, and especially the acoustic branch. Importantly, Fig. 2(c) shows that the dispersion of this polar-acoustic mode softens upon cooling. This softening at finite momentum is distinct from the known ferroelectric precursor that originates from the collapse of the TO mode at ξ = 0. Here, the eventual collapse of the acoustic branch at finite ξ would correspond to a state with a spatially modulated polarization [5].

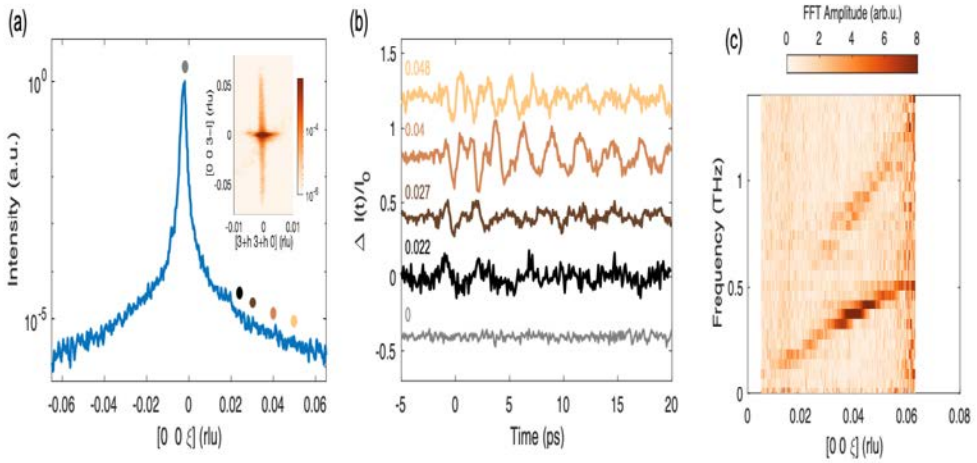

***Fig. 2. (a) Electro-optic sampling of the THz waveforms** generated by two LiNbO3 prisms oriented with ferroelectric axis in opposite directions. The inset illustrates how the inversion of the field is expected to produce an inverted distortion of the crystal. **(b)** differential X-ray intensity integrated over x = 0.03 - 0.06 rlu for the two fields shown in **(a)**. **(c)** the temperature dependence of the dispersion obtained from the peak of the Fourier transform similar to that in **Fig. 1(c)**.*

Our ultrafast x-ray measurements reveal the polar nature of acoustic excitations in the quantum paraelectric phase of $SrTiO_3$ measurements. Our data indicates that this behavior arises from a flexoelectric coupling that is linear in both optical and acoustic displacements. The softening of this acoustic polar branch at finite wavevector implies a potential instability of the structure related to an incipient modulated polar-acoustic regime.

References

[1] X. Li, T. Qiu, J. Zhang, E. Baldini, J. Lu, A. M. Rappe, K. A. Nelson, *Science* **364**, 1079 (2019).
[2] T. F. Nova, A. S. Disa, M. Fechner, A. Cavalleri, *Science* **364**, 1075 (2019).
[3] M. J. Coak, C. R. S. Haines, C. Liu, S. E. Rowley, G. G. Lonzarich, S. S. Saxena, *Proceedings of the NAS* **117**, 12707(2020).
[4] S. E. Rowley, L. J. Spalek, R. P. Smith, M. P. M. Dean, M. Itoh, J. F. Scott, G. G. Lonzarich, S. S. Saxena, *Nature Physics* **10**, 367 (2014).
[5] G. .Guzmán-Verri, C. H. Liang, P. B. Littlewood, *Physical Review Letters* **131**, 046801 (2023).
[6] B. Fauqué, P. Bourges, A. Subedi, K. Behnia, B. Baptiste, B. Roessli, T. Fennell, S. Raymond, P. Steffens, *Physical Review* B **106**, L140301 (2022)
[7] G. Orenstein, V. Krapivin, Y. Huang, Z. Zhang, G. de la Peña Muñoz, R. A. Duncan, Q. Nguyen, J. tanton, S. Teitelbaum,H. Yavas, T.Sato M. C. Hoffmann, P.Kramer, J. Zhang, A. Cavalleri, R.Comin, M.P. M. Dean, A. S. Disa, M. Först, S. L. Johnson, M. Mitrano, A. M. Rappe, D.Reiss D. Zhu, K. A. Nelson, M. Trigo , arXiv.org/abs/2403.17203 (2024).

* Acknowledgement(s): The experimental work was supported by the U.S. Depart- ment of Energy, Office of Science, Office of Basic Energy Sciences through the Division of Materials Sciences and Engineering through Contract No. DE-AC02-76SF00515 (G. O., V. K., Y. H., G.dP., R. D., D. A. R. and M. T.) and Contract No. DE-SC0019126 (Z. Z., R. C. and K. A. N.). Work at Brookhaven is supported by the Office of Basic Energy Sciences, Materials Sciences and Engineering Division, U.S. Department of Energy (DOE) under Contract No. DE-SC0012704. Use of the LCLS was supported by the U.S. Department of Energy, Office of Science, Office of Basic Energy Sciences under Contract No. DE-AC02-76SF00515. S. L. J. acknowledges support from the Swiss National Science Foundation under project grant 200020_192337. Work at Harvard University was supported by the U.S. Department of Energy, Office of Basic Energy Sciences, Early Career Award Program, under Award No. DE-SC0022883. J.S. acknowledges supported by the NSF under REU supplement 2133686 under award 2019014.

Ultrafast quench of the electronic order in the strongly coupled Charge-density-wave system VTe_2

M. Tuniz[1], D. Puntel[1], W.Bronsch[2], F.Sammartino[1], G. M. Pierantozzi[3], R. Cucini[3], F. Parmigiani[1] F. Cilento[2]

[1] *Università degli Studi di Trieste, 34127 Trieste, Italy*
[2]*Elettra - Sincrotrone Trieste 34149 Trieste, Italy*
[3]*Istituto Officina dei Materiali 34149 Trieste, Italy*

The coexistence of strong electron-phonon coupling and non-trivial topological physics in quantum materials can lead to new exciting phenomena, and the study of the interplay of these multiple quantum orders constitute a new paradigm in condensed matter. Here, by combining time and angle-resolved photoemission spectroscopy (TR-ARPES) and broadband time-resolved optical spectroscopy (TR-OS), we investigate the effect of an optical excitation on the electronic and structural properties of the strong-coupling charge-density-wave (CDW) system VTe_2. Using TR-OS measurements we unveil the presence of two independent amplitude modes (AM) of the CDW phase [1]. Moreover, by performing TR-ARPES experiments, we show that at high pump fluence the closure of the electronic gap is not controlled by the excitation of the CDW amplitude modes, but it takes place on a slower time scale of the order 500 fs, as shown in Fig. 1.

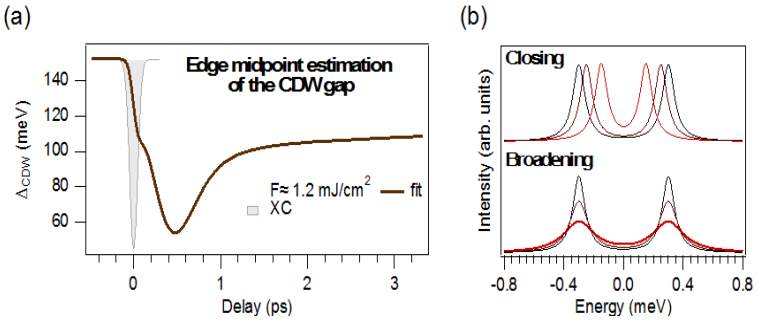

Fig. 1. (a) Dynamics of the CDW gap *magntiude as a function of the pump-probe delay. The grey trace shows the cross-correlation between pump and probe pulses. The measurement has been performed at an absorbed fluence of 1.2 mJ/cm^2.* ***(b)*** *Schematic representation of the two main effects contributing to the dynamics of the CDW gap.*

This timescale suggests that the gap dynamics is mostly governed by the excitation of high-frequency strongly-coupled optical phonons, which result in a loss of long range order of the CDW phase [2].

References

[1] M. Tuniz, D. Soranzio, D. Bidoggia , D. Puntel , W. Bronsch, S. L. Johnson, M. Peressi , F. Parmigiani, F. Cilento, *Physical Review Research* **5** 043276 (2023).
[2] J. Maklar, Y. W. Windsor, C. W. Nicholson, M. Puppin, P. Walmsley, V. Esposito, M. Porer, J. Rittmann, D. Leuenberger, M. Kubli, M. Savoini E. Abreu, S. L. Johnson, P. Beaud, G. Ingold, U. Staub, I. R. Fisher, R. Ernstorfer, M. Wolf, L. Rettig, *Nature Communications* **12**, 2499 (2021).

Nonlinear emission from dressed excitons in thin layer WSe_2

K. Uchida[1], S. Kusaba[1], K. Nagai[1], T. N. Ikeda[2], K. Tanaka[1]
[1] *Kyoto University, Kyoto 606-8501, Japan.*
[2] *RIKEN Center, Saitama 351-0198, Japan.*

Under intense periodic driving by light, an electronic system undergoes photon-dressing and its energy structure changes strongly depending on the light properties (field strength, polarization, wavelength). Such concept of photon-dressed states, in other words Floquet states, is considered as a promising way to manipulate material properties on an ultrafast time scale [1]. So far, there have been many reports on characteristic energy structure changes of Floquet states in solids [2-4]. However, in real experiments, where ultrashort pulses are usually used, the above Floquet picture becomes an approximate one, and we need to consider the dynamics of Floquet states in both the adiabatic and non-adiabatic regime [5,6]. The understanding of their dynamics provide us with additional knob for control of Floquet state. Here, we focus on the coherent emission from Floquet state as a probe of Floquet state dynamics, and chose monolayer WSe_2 as a target sample to induce Floquet state [7]. Monolayer WSe_2 hosts excitons with a large binding energy of several hundred meV, providing us with an ideal platform to study electronic structure modification effect on nonlinear coherent emission process [3,4]. As a driving field, we used mid-infrared (MIR) pulses, whose photon energy and pulse are set to be 0.26 eV and 60 fs (full width of half maximum), respectively.Fig.1(a) shows the measured emission spectrum in the vicinity of exciton level (1.65 eV) with MIR intensity of 0.17 TW cm^{-2}. We observed the clear 5th and 7th harmonic emission (dotted lines), which has been reported in the previous study [8]. In addition to the high harmonics, we found coherent emission resonant with the excitonic level (dashed line). When the quantum state is described by single Floquet eigenstate, coherent emission is only allowed near high harmonic emission energy reflecting the temporal periodicity. Our observation of coherent emission far from harmonic emission suggests that the quantum state during the MIR pulse duration becomes the superposition of Floquet states, breaking the temporal periodicity. To understand the Floquet state dynamics in detail, we performed the numerical simulation of the two-level model. As shown in Fig. 1(b), the calculated coherent emission spectrum is similar to the experimentally observed one. By analyzing the simulated results, we obtained the overview of dressed exciton dynamics. First, exciton resonance is dynamical shifted toward higher energy through Floquet state formation with an increase of MIR field amplitude. Second, dynamical shift of the excitonic energy satisfies seven-photon resonance condition with MIR photon, leading to diabatic transition from dressed vacuum to dressed excitonic states. Finally, dressed excitonic states are adiabatically transformed to bare excitonic state with a decrease of MIR field amplitude, emitting coherent excitonic emission.

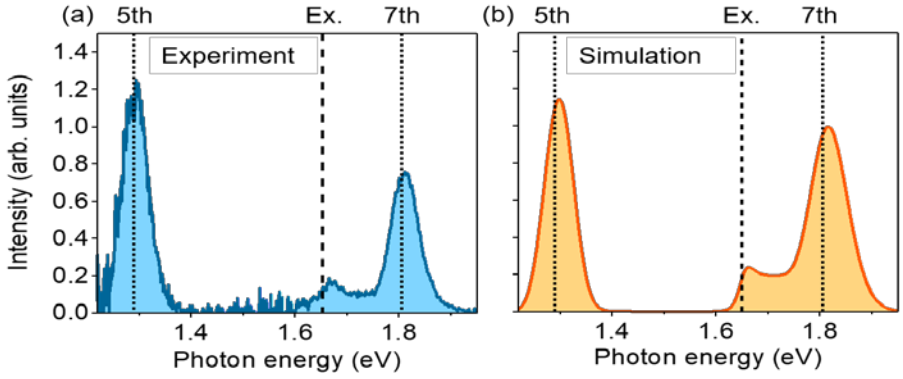

Fig. 1. (a) Measured coherent emission spectrum *from monolayer WSe_2 sample driven by MIR pulses.* ***(b)*** *Simulated emission spectrum using the two-level model. Dotted lines indicate high harmonic emission energy. Dashed lines (l****abelled as Ex.****) indicate the excitonic level.*

Our observation clearly demonstrates novel nonlinear optical response induced by Floquet state formation under MIR pulse. Time-resolved measurement of the coherent emission may allow us to capture Floquet state dynamics in more detail.

References

[1] T. Oka, S. Kitamura, *Annual Review of Condensed Matter Physics* **10**, 387 (2019).
[2] Y. H. Wang, H. Steinberg, P. Jarillo-Herrero, N. Gedik, *Science* **342**, 453 (2013).
[3] J. Kim, X. Hong, C. Jin, S.F. Shi, C.Y.S. Chang, M.H. Chiu, L.J. Li, F. Wang, *Science* **346**, 1205 (2014).
[4] E. J. Sie, James W. McIver,Y.-H. Lee,L. Fu,J.Kong, N.Gedik, Nature Material **14**, 290 (2014).
[5] K. Drese, M. Holthaus, *European Physical Journal* D **5**, 119 (1999).
[6] T. N. Ikeda, S. Tanaka, Y. Kayanuma, *Physical Review Research* **4**, 033075 (2022).
[7] K. Uchida, S.Kusaba, K. Nagai, T.N. Ikeda, K. Tanaka,*Science Advances* **8**, eabq7281(2022).
[8] N. Yoshikawa, K. Nagai, K. Uchida, Y. Takaguchi, S. Sasaki, Y. Miyata, K. Tanaka, *Nature Communication* **10**, 3709 (2019).

Driving superconducting collective modes with terahertz light pulses

M. Udina[1], J. Fiore[1], K. Katsumi[2], N. Sellati[1], G. Seibold[3], C. Castellani[1], N. P. Armitage[2], L. Benfatto[1]
[1] Sapienza University of Rome, P.le A. Moro 5, 00185 Rome, Italy
[2] The Johns Hopkins University, Baltimore, MD 21218, USA
[3] Brandenburgische Technische Universität Cottbus-Senftenberg, 03013 Cottbus, Germany

The latest advances in time-resolved spectroscopic techniques, based on the generation of intense THz pulses, have paved intriguing new ways for the investigation of ultrafast collective phenomena in many complex systems. As an example, recent experiments showed the possibility to selectively excite electronic collective modes in broken-symmetry phases of matter, such as amplitude (Higgs) or phase (plasma) fluctuations of the superconducting order parameter. Despite the great interest and the huge experimental progress, a general framework able to describe THz-driven collective excitations in ultrafast experiments is still lacking. In this talk I will present some recent advances in the theoretical modelling of the superconducting response at THz frequencies, shedding light on the microscopic mechanism at the basis of the Higgs mode visibility in conventional superconductors and on the nonlinear excitation of out-of-plane Josephson plasma modes in superconducting cuprates.

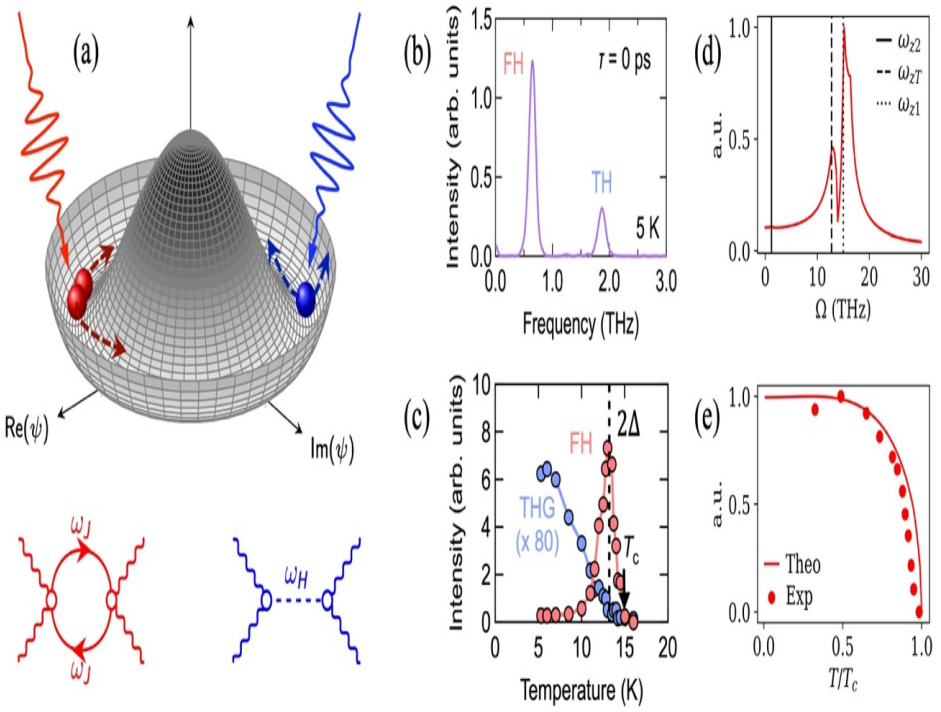

Fig.1. ***(a) Nonlinear excitation of the superconducting (Higgs) amplitude and (plasma) phase modes*** *[3]. While strong THz pulses drive a single Higgs fluctuation (blue), two plasma modes at opposite momenta (red) are simultaneously excited.* ***(b)*** *Nonlinear response at fixed time delay τ in 2D THz spectroscopy on superconducting NbN samples [2].* ***(c)*** *When the incident THz frequency matches 2Δ, the first harmonic (FH) component shows a divergence ascribed to the paramagnetic light-matter coupling.* ***(d)*** *Out-of-plane nonlinear response in bilayer superconducting YBCO [4]. Due to dispersion effects, the signal is flat close to the lower plasma edge $\omega_{z2} \sim 1$ THz while it is maximized close to the upper plasma edge $\omega_{z2} \sim 15$ THz.* ***(e)*** *When pumping the system close to ω_{z2}, the nonlinear response scales monotonically with the superfluid stiffness as a function of temperature [5].*

In particular, while the Higgs mode is very elusive in conventional spectroscopies, amplitude fluctuations become sizable in disordered superconductors due to a finite paramagnetic coupling with strong THz pulses [1]. Whit this respect, we have recently demonstrated that 2D THz spectroscopy appears as a preferential tool to unambiguously identify the paramagnetic (current-current) response and decouple it from the diamagnetic (density-density) one [2]. For what concerns the superconducting phase mode, instead, we have shown that the simultaneous excitation of two Josephson plasmons in superconducting cuprates dominates the out-of-plane nonlinear response at THz frequencies [3]. We have demonstrated [4] that an accurate description of dispersion effects, and the subsequent mixing between in-plane and out-of-plane plasmons, is crucial to understand what marks the difference between single-layer and bilayer cuprates [5].

References

[1] G. Seibold, M. Udina, C. Castellani, L. Benfatto, *Physical Review B* **103**, 014512, (2021).
[2] K. Katsumi, J. Fiore, M. Udina, R. Romero, D. Barbalas, J. Jesudasan, P.Raychaudhuri, G.Seibold, L.Benfatto, N. P. Armitag, *arXiv:2311.16449* (2023).
[3] F. Gabriele, M. Udina, L. Benfatto, *Nature Communications* **12**, 752, (2021).
[4] J. Fiore, N. Sellati, C. Castellani, G. Seibold, M. Udina, L. Benfatto, *arXiv:2310.16815* (2023).
[5] K. Katsumi, M. Nishida, S. Kaiser, S. Miyasaka, S. Tajima, R. Shimano, *Physical Review* B **107**, 214506 (2023).
* Acknowledgement: Mattia Udina acknowledges support from EU under program MORE-TEM ERC-SYN (grant agreement No 951215).

Spin to charge conversion mechanisms down to picosecond timescales

A. Levchuk[1], A. El Hamdi[1], J.-Y. Chauleau[1], V. Juvé[2], T. O. Otomalo[2], G. Vaudel[2], P. Ruello[2], S.Gariglio[3]
M. Boselli[3], C. Thibault[3], J.M.Triscone[3], C.Gorini[1], A. Smogunov[1], C. Barreteau[1], M. Viret[1]
[1]*Université Paris-Saclay, 91190 Gif-sur-Yvette, France*
[2]*Le Mans Université, 72085 Le Mans, France*
[3]*University of Geneva, 1205 Geneva, Switzerland*

Creating and manipulating dissipation-less pure spin currents have been crucial challenges for the spintronic community for the past ten years. A central handle to achieve low consumption pure spin based computing is the inter-conversion of spin and charge, if possible at very short timescales. All known mechanisms rely here on the Spin-Orbit Coupling (SOC) interaction, whereby spins couple with moving charges [1]. So far, the most reliable mechanism in the DC range is the (inverse) Spin Hall effect (ISHE) obtained in the bulk of metallic heavy elements like Pt or W. Recently another type of SOC, called spin galvanic or (inverse) Edelstein effect (IEE), has been used based on the Rashba interaction [2,3]. It stems from the action of an electrical built-in potential onto the two-dimensional electron systems existing at interfaces between two different materials [4]. To evidence the conversion effect, one needs an injector, i.e. a ferromagnetic layer, in contact with the convertor. Here, I will compare the two effects pushed to the picosecond regime. The injection is realized by ultra-fast demagnetization of a metallic ferromagnet, a mechanism appropriate for generating a picosecond angular spin burst. Different systems are assessed, either with a heavy metal as the strong spin-orbit material insuring the conversion into charge (ISHE), or relying on the behavior of interface states between two materials (IEE). In particular, bilayers like CoFeB/MgO [4] or the record efficiency system (in the DC range): $SrTiO_3/LaAlO_3$ /NiFe [5, 6] are studied. The latter relies on the 2D electron liquid created by the polar discontinuity between the two band gap insulators, allowing for the Rashba splitting to be tuned using an electric field [7,8].

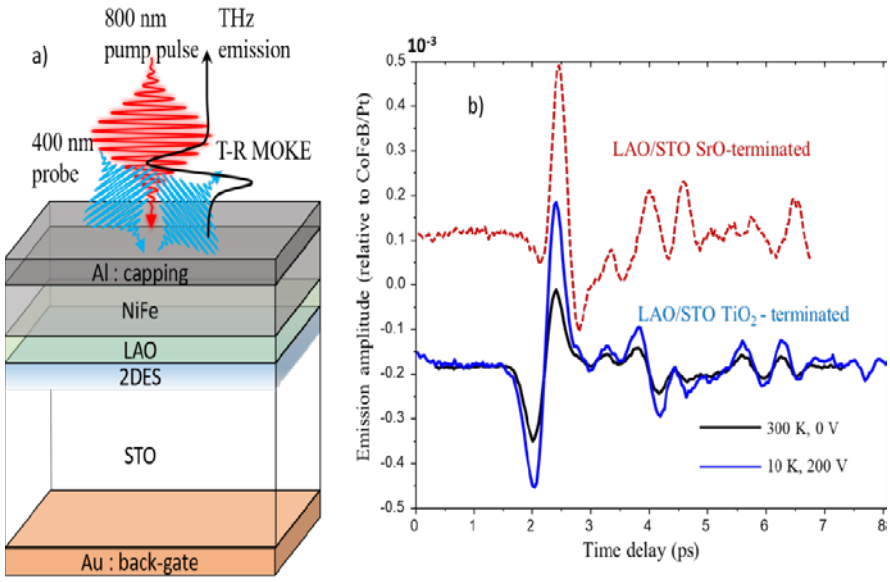

Fig. 1: THz response of the LAO/STO interface. ***a)*** *shows the schematics of the measurement setup and* ***b)*** *is the THz emission of the system. The signal is 1000 smaller than that of the reference system CoFeB/Pt and is equivalent to that obtained on a sample without the 2D electron state.*

I will discuss the (lack of) efficiency of the Rashba-based systems in the THz range (Fig. 1) in the light of the timescales of the different characteristic phenomena occurring around the picosecond, emphasizing the salient features necessary for an efficient THz emission. I will also address the potential importance of orbital effects that dominate the angular momentum conversion in the STO/LAO system [9].

References

[1] M. Dyakonov, V. Perel, *Journal of Experimental and Theoretical Physics Letters* **13**, 467 (1971).
[2] E. I Rashba, Fizika Tverdogo Tela **1,** 368/407 (1959).
[3] J.- C. Rojas-Sanchez, L. Vila, G. Desfonds, S. Gambarelli, J. P. Attané, J. M. De Teresa, C. Magén, A. Fert, *Nature Communications* **4**, 2944 (2013).
[4] A. Levchuk, V. Juvé, T. O. Otomalo, T. Chirac, O. Rousseau, A. Solignac, G. Vaudel, P. Ruello, J.-Y. Chauleau, M. Viret, *Applied Physics Letters* **123** 012407 (2023).
[5] E. Lesne, Y. Fu, S. Oyarzun, J. C. Rojas-Sanchez, D. C. Vaz, H. Naganuma, G. Sicoli, J.-P. Attané, M. Jamet , E. Jacquet , J.-M. George A. Barthélémy1 , H. Jaffrès1 . A. Fert1 . M. Bibes1. L. Vilaet. *Nature Materials* **15**. 1261 (2016).
[6] J.- Y. Chauleau, J. Y Chauleau, M Boselli, S Gariglio, R. Weil, G. De Loubens, J.M. Triscone, M Viret, *Europhysics Letters* **116**, 17006 (2016).
[7] S. Thiel, G. Hammerl, A. Schmehl, C. W. Schneider, J. Mannhart, *Science* **313**, 1942 (2006).
[8] A. D. Caviglia, M. Gabay, S. Gariglio, N. Reyren, C. Cancellieri, J.M .Triscone, *Physical Review Letters* **104**, 126803 (2010).
[9] A. El Hamdi, J.-Y. Chauleau, M. Boselli, C.Thibault, C.Gorini, A. Smogunov, C.Barreteau, S. Gariglio, J.-M. Triscone, M. Viret, *Nature Physics* **19** 1855 (2023).

GHz diamond spin-mechanical Lamb wave resonators protected by a Phononic band gap

X. Li, I. Lekavicius, J. Noeckel, H. Wang
University of Oregon, Eugene, OR 97403, USA

Spin-mechanical resonators, in which electron spins are coupled to vibrations of a mechanical oscillator, provide an experimental platform for exploring coherent interactions between single phonons and spins and for exploiting these interactions to mediate coherent coupling between distant spins. Recent experimental studies on spin-mechanics have used negatively charged nitrogen vacancy (NV) centers and silicon vacancy (SiV) centers in diamond as suitable spin systems. A variety of mechanical resonators such as beams and cantilevers, bulk acoustic wave resonators, surface acoustic wave (SAW) resonators, microdisks, and optomechanical crystals have been explored [1]. Further experimental advance of quantum spin-mechanics, however, requires the development of ultracoherent diamond nanomechanical resonators at a GHz frequency. A mechanical resonator can be characterized by three key parameters: linewidth γ_m (or quality factor Q), effective mass m_{eff}, and resonance frequency f_m. Ultrasmall γ_m and m_{eff} are essential for reaching the quantum regime of spin-mechanics, while f_m at a GHz frequency is important for reducing effects of thermal phonons and for matching the mechanical resonance with a spin transition. Ultracoherent GHz nanomechanical resonators have been realized with a silicon optomechanical crystal embedded in a phononic crystal lattice. Fabricating a diamond optomechanical crystal, which integrates a nanomechanical resonator with a photonic crystal optical cavity, especially embedding the diamond optomechanical crystal in a phononic band gap shield, however, remains difficult. A Lamb wave resonator (LWR), which is essentially a thin elastic plate with free boundaries, provides a simple geometric structure for GHz nanomechanical resonators. As illustrated in Fig. 1a, a thin rectangular diamond plate with a length of 9.5 μm, embedded in a phononic crystal lattice, features a fundamental compression mode with f_m near 1 GHz. For the square lattice in Fig. 1a, the phononic band structure of the symmetric (with respect to the midplane of the plate) compression modes features a large energy gap that protects the fundamental compression mode (see Fig. 1b). Without an integrated photonic crystal, this type of structures is relatively straightforward to fabricate. Figure 1c shows a scanning electron micrograph (SEM) of a diamond phononic structure fabricated with the design given in Fig.1a [2].

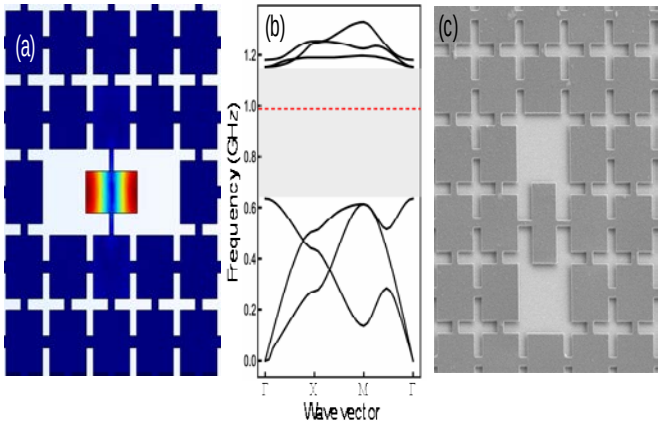

Fig. 1. (a) A LWR with dimension *(9.5, 4.5) μm, along with the calculated displacement pattern of the fundamental compression mode, embedded in a square phononic crystal lattice with a period of 8 μm.* ***(b)*** *Phononic band structure of the symmetric modes of the square lattice. The phononic band gap shields the fundamental compression mode with a frequency near 1 GHz (**the dashed line**). **(c)** Scanning electron micrograph of a LWR embedded in a phononic square lattice fabricated from a diamond thin film with the dimension given in **(a)**.*

A major obstacle that has hindered the development of LWRs as ultracoherent nanomechanical resonators is the excitation and detection of compression modes without making physical contact with the resonators, since unlike in a cavity optomechanical system, these modes do not couple to an optical cavity. We have developed an all-optical technique to excite and detect the fundamental compression mode in a LWR [3]. Specifically, a LWR is placed in a sharply focused laser beam (see Fig. 2a). A temporally modulated optical gradient force is employed to resonantly excite the fundamental compression mode. The induced mechanical vibrations are probed through their coupling to a SiV center. Mechanical vibrations with an amplitude as small as a picometer can be detected through sideband, instead of conventional, optical interferometry and through sideband optical transitions of a SiV center.

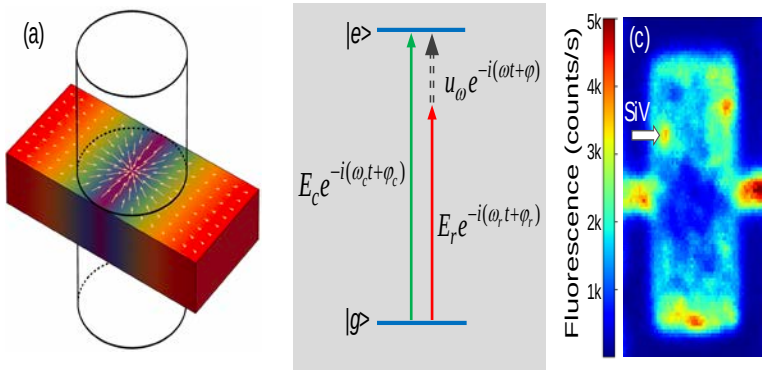

Fig. 2. (a) A LWR placed at the waist of a laser beam. *The arrows illustrate the directions of the gradient force. (**b**) schematic illustrating the interference between the direct dipole transition and the first red sideband transition. (**c**) A confocal fluorescence microscopy image of the LWR indicating the SiV used for the experiment.*

Using this all-optical approach, we have demonstrated a diamond LWR featuring a fundamental compressional mode with f_m near 1 GHz and with $Q > 10^7$ at temperatures near 7 K. The Qf_m product achieved is comparable to or exceed that of the state-of-the-art silicon optomechanical crystals embedded in a phononic band gap acoustic shield at similar temperatures [4]. As illustrated in Fig. 2b, both the direct dipole transition and the phonon-assisted transition of a SiV can excite the two-level system from $|g\rangle$ to $|e\rangle$. Optical emissions from the excited state depend on the relative phase of the two corresponding transition amplitudes. The compression mechanical vibrations can thus be detected through the interference between these two transition pathways, i.e. through sideband optical interferometry. For our experimental studies, a SiV center slightly offset from the center of the resonator is used, with the SiV position indicated in a confocal fluorescence microscopy image of the LWR in Fig. 2c. An intensity-modulated 1550 nm laser beam is used to resonantly excite the fundamental compression mode via the optical gradient force. Optical emissions from the SiV center are measured as a function of the phase of the intensity modulation, i.e., φ in Fig. 2b. The resulting interference fringes shown in Fig. 3a demonstrate the coherent excitation of the compression mechanical mode in the LWR.

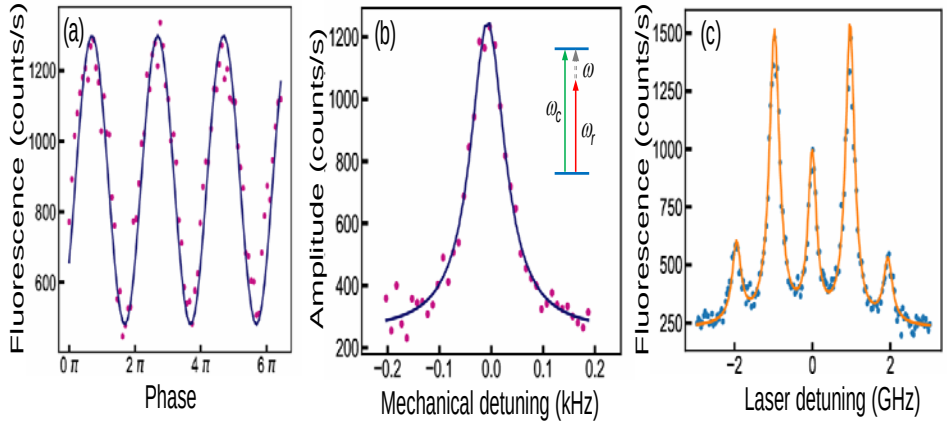

Fig. 3. (a) Fluorescence from the SiV center *as function of j, the phase of the intensity modulation of the 1550 nm laser. The solid line is a numerical fit to a sinusoidal with a period of 2p. (**b**) The oscillation amplitude derived from the interference fringes as a function of the detuning from the mechanical resonance. (**c**) Phonon sidebands in the PLE spectrum induced by the excitation of the fundamental compression mode.*

Multiple phonon sidebands can be observed in the PLE spectrum, indicating the relatively strong excitation of the compression mechanical mode by the resonant gradient force. More detailed experimental results along with a theoretical analysis will be presented.

References

[1] H. L. Wang, I. Lekavicius, *Applied Physics Letters* **117**, 230501 (2020).
[2] I. Lekavicius, T. Oo, H. L. Wang, *Journal of Applied Physics* **126**, 214301 (2019).
[3] H. L. Wang, *submitted* (2024).
[4] G. S. MacCabe, H. J. Ren, J. Luo, J. D. Cohen, H. Y. Zhou, A. Sipahigil, M. Mirhosseini, O. Painter, *Science* **370**, 840 (2020).
* Acknowledgement: this work is supported by NSF and AFOSR.

Robust spin order and fragile charge order in $Na_{0.5}CoO_2$ as revealed by Time-resolved terahertz spectroscopy

N.-L. Wang
Peking University, Beijing 100871, China

Near-infrared (NIR) pump-terahertz (THz) probe spectroscopy is used to investigate the charge and spin excitations in a strongly correlated electron compound $Na_{0.5}CoO_2$. The compound shows a coexistence of multiple charge and spin orders due to the intricate interactions between charge, spin, and orbital degrees of freedom (Fig.1). Our findings unequivocally illustrate that ultrashort laser pulses facilitate the disentanglement of different interactions within complex systems characterized by multiple orders, providing a fresh perspective on the interplay between itinerant and localized electrons within the Co 3d t_{2g} multiplets [1].

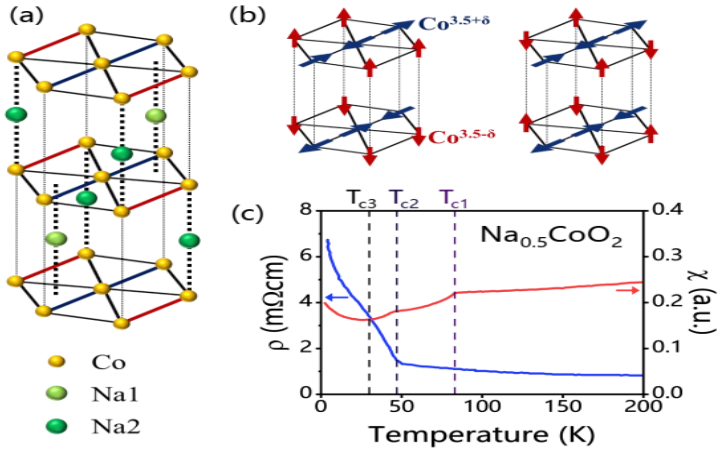

***Fig. 1: (a) Crystal structure of $Na_{0.5}CoO_2$, with oxygen sites undisplayed**. The ordered occupation of Na ions leads to inequivalent Co valent states of $Co^{3.5+\delta}$ and $Co^{3.5-\delta}$ within each CoO_2 layer. **(b)** The $Co^{3.5+\delta}$ ion has larger magnetic moment, while the $Co^{3.5-\delta}$ ion has smaller magnetic moment. They form antiferromagnetic orders at T_{c1} and T_{c3}, respectively, with two possible configuration. A charge order is formed near T_{c2}~50 K. **(c)** Resistivity and magnetic susceptibility measurement of $Na_{0.5}CoO_2$.*

NIR pulses create significantly diverse effects on the charge and spin orders; while the charge order is easily melted, coherent magnon excitations are present in all fluences examined. Furthermore, a π-phase shift of the coherent magnon oscillations is observed in the pump-induced change of the terahertz electric field between regions of increasing and decreasing field change (Fig. 2).

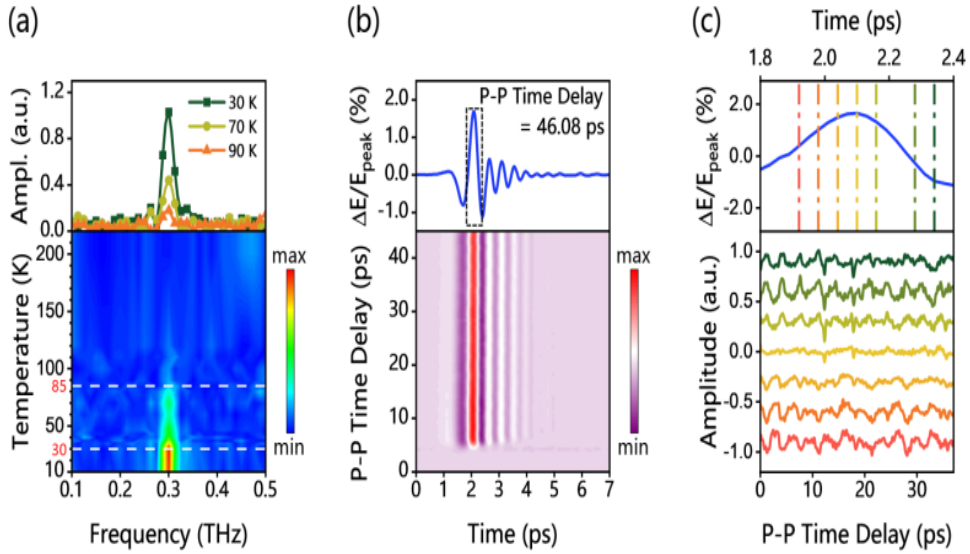

***Fig.2: (a) The coherent magnon mode at several temperatures**. **(b)** Upper panel: $\Delta E/E_{peak}$ along pump-probe time delay τ= 46.08 ps. Lower panel: Two-dimensional scanning of $\Delta E(t,\tau)/E_{peak}$ signal along t and τ. **(c)** A π-phase shift of the oscillations between the region when $\Delta E/E_{peak}$ is increasing or decreasing. At the gate time when ΔE reaches the maximum, the oscillation becomes invisible.*

Work done in collaboration with X. Y. Zhou, S. J. Zhang and other team members in Peking University and Beijing Academy of Quantum Information Sciences-BAQIS.

Reference

[1] X. Y.Zhou, S. J.Zhang, D. Wu, H. Wang, B.H. Li, S.F.Wu, Q. M. Liu, T. C. Hu, R. S. Li, J. Y. Yuan, S. X. Xu, Q. Wu, L. Yue, T. Dong , N. L. Wang, *arXiv*:2404.09185 (2024).

* Acknowledgement:this work was supported by National Science Foundation of China and National Key Research and Development Program of China.

Using ultrafast x-ray spectroscopies to probe and control many-body Entanglement in quantum materials

Y. Wang
Emory University, Atlanta, GA30322,USA

Quantum materials are at the forefront of both scientific research and technological development. One of the defining features of these materials is that their electrons exhibit collective behavior underpinned by quantum entanglement, which sets them apart from classical band theory. The quest to understand, control, and design quantum materials for specific functionalities, such as superconductors and batteries, stands as a crucial research domain in the field of energy science. Achieving these groundbreaking applications requires precise and efficient characterization of the collective properties of electrons using advanced experimental techniques and theoretical analysis. In this talk, I will combine the recent progress in quantum optics and ultrafast x-ray spectroscopy in the probe and control of many-body entanglements. My talk will start with probing entangled states in cold-atom-based quantum simulators for a doped Hubbard model. Through multi-partite correlations, we discovered an exotic crossover from spin polarons to Fermi liquid, possibly addressing the recent ARPES observations in cuprates [see Fig.1(a)]. I will then generalize the notions to quantum materials and discuss the spectral probe of entanglement using time-resolved resonant inelastic x-ray scattering (trRIXS). We find that the instantaneous short-range magnetic excitations can be manipulated by pulsed laser in a predictive manner. The entanglement depth of the transient state can be witnessed by the quantum Fisher information and quantified by trRIXS snapshots via a self-consistent iteration [see Fig.1(b)].

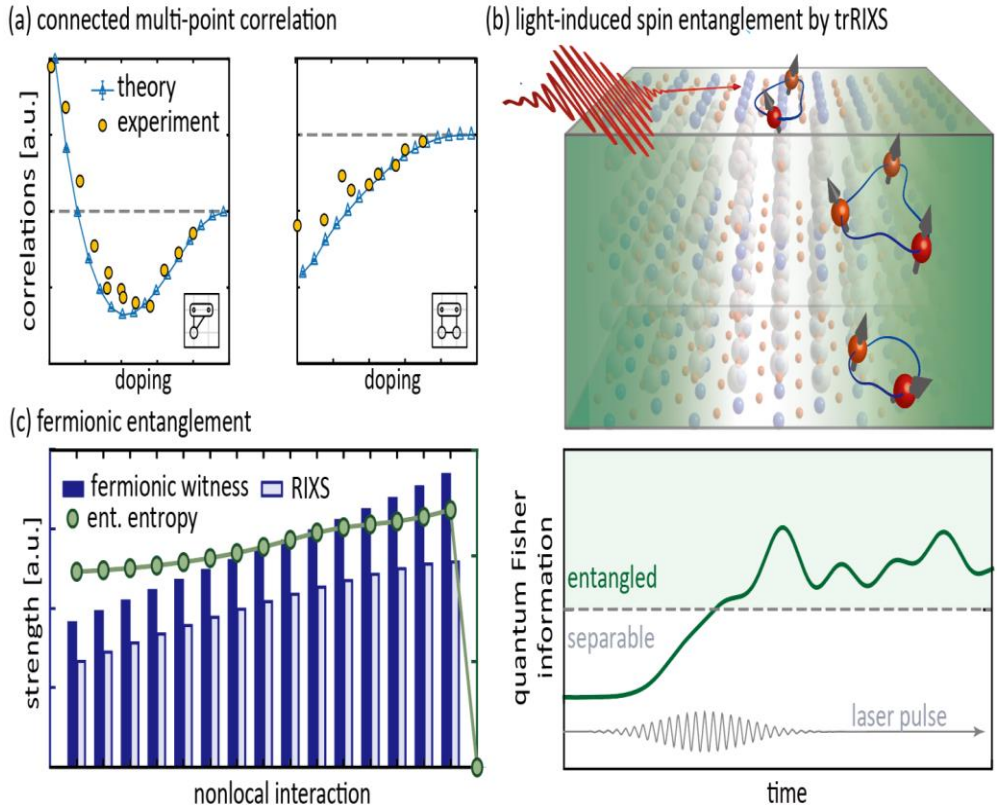

Fig. 1. (a). *The simulated three-point (left) and four-point (right) correlations for doped Hubbard models, compared against the cold-atom experimental data (yellow circles).* ***(b).*** *Light-induced spin quantum Fisher information in a strongly correlated system, describbed by the single-band extended Hubbard model. The gray dashed line indicates the boundary between witnessed separable and entangled state.* ***(c):*** *fermionic entanglement witness extracted from RIXS spectrum, compared with the entanglement entropy. The simulation uses an extended Hubbard model as an example.*

Finally, I will discuss the possibility of enhancing many-body entanglement using an ultrafast laser pulse and generalizing the spectral witness to indistinguishable fermions via the ideas in cold atoms [see Fig.1(c)].

References

[1] S. Ding, S. Li, Y. Wang, *arXiv*:2403.18246 (2024).
[2] J. Hales, U. Bajpai, T. Liu, D.R. Baykusheva, M. Li, M. Mitrano, Y. Wang, *Nature Communications* **14**, 3512 (2023).
[3] T. Liu, L. Xu, J. Liu, Y. Wang, *to be submitted* (2024)

* Acknowledgement(s) : Y.W. acknowledges support from U.S. Department of Energy, Office of Science, Basic Energy Sciences, under Early Career Award No. DE-SC0024524.

Ultrafast spin-shear coupling in van der Waals antiferromagnets

H. Wen
Argonne National Laboratory, Lemont, IL, 60439, USA

The interlay of magnetic orders and lattice structures in van der Waals magnets gives rise to a plethora of exotic phenomena. However, among multiple structural degrees of freedom, it remains elusive which structural parameters primarily couple to magnetism and how this coupling impacts the ultrafast dynamics of vdW magnets. Here, we discover a strong coupling between interlayer shear and magnetic orders in vdW antiferromagnets using a set of ultrafast measurements including ultrafast electron diffraction and microscopy, ultrafast x-ray diffraction, and optical linear dichroism. On picosecond time scale, a seesaw-like motion of the reciprocal lattice is observed in $FePS_3$, which exhibits a thirty-fold amplification upon cooling of the sample below the Neel temperature (Fig. 1a,b) [1]. The rotation in reciprocal space is a result of an unusually large interlayer shear in real space, where individual micro-patches of the film behave as synchronized shear oscillators along the same in-plane axis. Ultrafast electron microscopy further reveals shear acoustic harmonics up to the 4th order that arise from structural heterogeneities (Fig. 1c) [2]. On nanosecond time scales, the recovery of the lattice shear and magnetic order exhibit concurrent slowing down at the Neel temperature with the same critical components (Fig. 1d) [3]

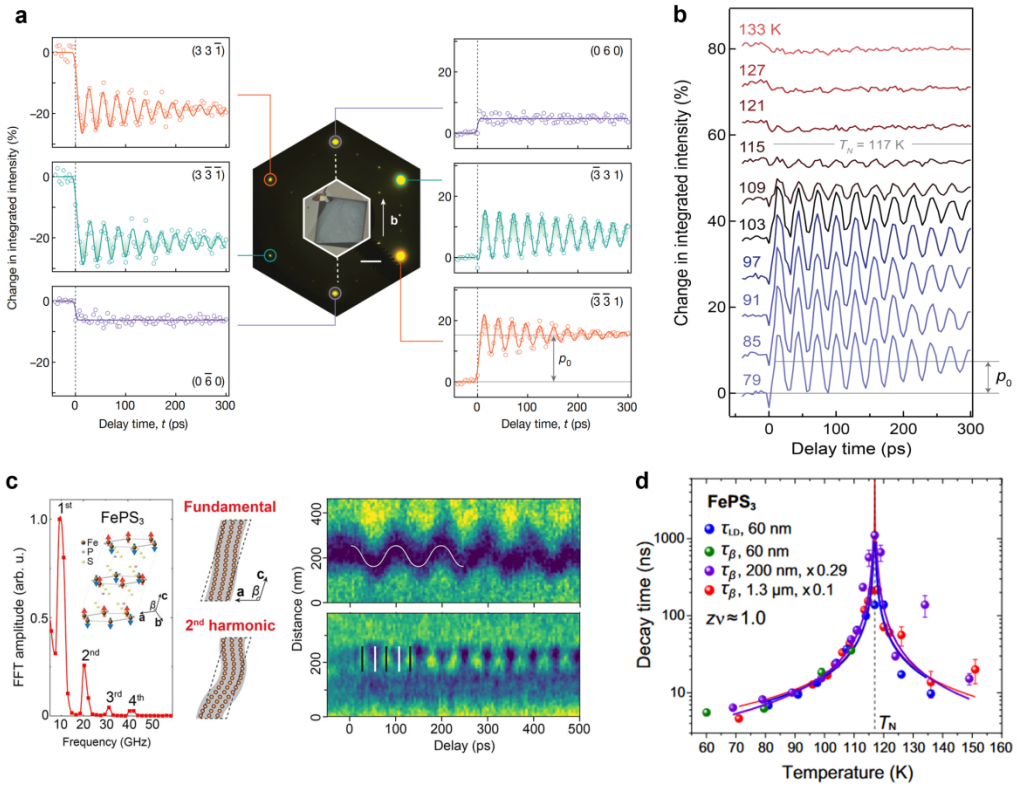

Fig. 1 ***a****, Ultrafast electron diffraction measurement of FPS_3 films at the sample temperature of 79 K. Diffraction pattern and sample image are shown as the middle inset).* ***b****, Diffraction intensity oscillations of -331 peak at various temperatures.* ***c****, Harmonics of acoustic waves and the corresponding space-time maps.* ***d****, Recovery time constants as a function of temperature shows coupled critical slowing down of spin (τ_{LD}) and lattice (τ_β) degrees of freedom.*

The time-dependent Ginzburg-Landau theory shows that this concurrent critical slowing down arises from a linear coupling of the interlayer shear to the magnetic order, which is dictated by the broken mirror symmetry intrinsic to the monoclinic stacking. Our work not only offers the first microscopic view of the spin-mediated mechanical motion of an antiferromagnet but also identifies a new route towards realizing high-frequency resonators up to the millimeter band, where the capability of controlling magnetic states at the ultrafast timescale can be readily transferred to engineering the mechanical properties of nano-devices.

Reference

[1] A. Zong, Q. Zhang,F.Zhou,Y.Su, K.Hwangbo, X.Shen, Q.Jiang, H.Liu, T.E. Gage, D. A. Walko, M. E. Kozina, D. Luo, A. H. Reid, J.Yang, S.Park S. H. Lapidus, J.-H.Chu, I. Arslan, X.Wang, D.Xiao, X. Xu, N.Gedik, H.Wen, *Nature* **620**, 988 (2023).
[2] F. Zhou, H.Liu, M. Zajac, K. Hwangbo, Q. Jiang, J.H. Chu, X. Xu, I. Arslan, T.E. Gage, H. Wen, *Nano Letters* **23**, 10213 (2023).
[3] F. Zhou, K.Hwangbo, Q.Zhang, C Wang, L.Shen, J. Zhang, Q Jiang, A.Zong, Y. Su, M.Zajac,Y.Ahn,D. A. Walko, R. D. Schaller, J.-H. Chu, N. Gedik X. Xu, D.Xiao,H.Wen, *Nature Communications* **13**, 6598 (2022).
* Acknoledgements: this work is primarily supported by the US Department of Energy, Office of Science, Basic Energy Sciences, Materials Sciences and Engineering Division, under award no. DE-SC-0012509.

Ultrafast dynamics of iron-based superconductors and High pressure ultrafast spectroscopy

J. Zhao
Institute of Physics, Beijing 100190, China

I will address two parts of our recent ultrafast spectroscopy investigation of quantum materials. First, I will talk about our ultrafast spectroscopy investigations of iron-based high temperature superconductors. Ultrafast dynamics of single-unit cell layer FeSe/$SrTiO_3$ [1], intercalated iron-based superconductors $(Li_{0.84}Fe_{0.16})OHFe_{0.98}Se$, $Fe_{1.05}Se_{0.2}Te_{0.8}$, and $Fe_{1.01}Se_{0.2}Te_{0.8}$ [2] have also been investigated, for which the e-phonon coupling strengths are experimentally obtained. With these, for the first time a universal positive correlation between the superconducting transition temperature $\boldsymbol{T_c}$ and the e-phonon coupling strength λ_{A1g} or λ is discovered to exist among all known optimally doped iron-based superconductors (including FeSe-based, FeAs-based, and monolayer FeSe systems). Thus, we found that the e-phonon coupling may play an important role in all iron-based superconductors, especially including the single-layer system.

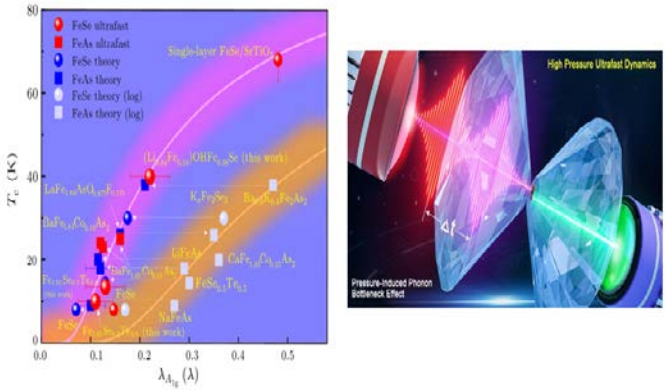

Fig.1. Left. Universal positive correlation between T_c and λ(λ_{A1g}) in iron-based superconductors [2,1].
***Right**: On-site in situ high-pressure ultrafast spectroscopy and ultrafast dynamics [3,4].*

Then I will talk about our recent innovation of on-site in situ high pressure ultrafast pump-probe spectroscopy. Both ultrafast spectroscopy and high-pressure physics is important fields of materials physics. Combining the two is nontrivial, because conventional efforts cannot remove potential artifacts caused by repositioning fluctuations. In conventional ways, usually the DAC is taken out of the light path to tune and calibrate pressure and then put back. This will often introduce sample motion and rotation (i.e. repositioning fluctuation), which likely introduces artifacts in signals. We innovated and realized an on-site in situ high pressure pump-probe ultrafast spectroscopy technique, for which the DACs and samples remain within the light path, thus successfully removing repositioning fluctuation. With such, we successfully constructed an on-site in situ high pressure ultrafast pump-probe spectroscopy instrument [3]. Before, colleagues report mainly normalized data. Now this achievement allows for precision measurements in both the amplitude and lifetime. Standard description has also been initiated to greatly enhance the data comparability among different groups [3]. Using this instrument we studied the ultrafast dynamics of strongly correlated iridate Sr_2IrO_4 under high pressure. For the first time we found pressure-induced phonon-bottleneck effect (needs experimental data in both amplitude and lifetime), whereby conventional phonon-bottleneck effects are all driven by temperature [4,5]. These achievements critically help the inauguration of high-pressure ultrafast dynamics—to become a new branch of material physics research. This will also greatly contribute to the investigations of material physics under extreme conditions.

References

[1] Y. C. Tian, W. H. Zhang, F. S. Li, Y. L. Wu, Q. Wu, F. Sun, G. Y. Zhou, L. L. Wang, X. C. Ma, Q. K. Xue, J. Zhao, *Physical Review Letters* **116** 107001 (2016).
[2] Q. Wu, H. X. Zhou, Y. L. Wu, L. L. Hu, S. L. Ni, Y. C. Tian, F. Sun, F. Zhou, X. L. Dong, Z. X. Zhao, J. Zhao, *Chinese Physics Letters* **37** 097802 (2020).
[3] Y. L. Wu, X. Yin, J. Z. L. Hasaien, Z. Y. Tian, Y. Ding, J.Zhao, *Review of Scientific Instruments* **92**, 113002 (2021).
[4] Y. L. Wu, X. Yin, J. Z. L. Hasaien, Y. Ding, J. Zhao, *Chinese Physics Letters* **37**, 047801 (2020).
[5] X. N. Lin, S. H. Fu, Y. N. Zhai, W. H. Wang, H. C. Li, R. Z. Zhang, S. Meng, J. Zhao, *The Innovation* **5**, 100614 (2024).

* Acknowledgement(s) : authors (J.Z.) acknowledge support from the National Key Research and Development Program of China (grants 2021YFA 1400201 and 2017YFA0303603), the CAS Project for Young Scientists in Basic Research (grant YSBR-059), the Strategic Priority Research Program of CAS (grant XDB30000000), the National Natural Science Foundation of China (grant 11774408 and 11574383), the Beijing Natural Science Foundation (grant 4191003), the International Partnership Program of Chinese Academy of Sciences (grant GJHZ1826), and the CAS Interdisciplinary Innovation Team.

Nonlinear photonics and excitonics in van der Waals heterostructures

L. Gu[1], L.Zhang[1], R.Ni[1], M.Xie[1], D. S. Wild[2], S. Park[3], H.Jang[3], T. Taniguchi[4], K. Watanabe[4], M,Hafezi[1], Y. Zhou[1]
[1]*University of Maryland, College Park, MD 20742, USA*
[2]*Max Plank Institute of Quantum Optics, Garching, 85748, Germany*
[3]*Brookhaven National Laboratory, Upton, NY 11973, USA*
[4]*National Institute for Materials Science, 1-1 Namiki, Tsukuba 305-0044, Japan*

Heterostructures of atomically thin semiconductors, such as transition metal dichalcogenides (TMDs), have recently emerged as an exciting platform for exploring strongly interacting many-body systems of electrons and excitons. This talk focuses on our recent research investigating strong interactions among excitons and free carriers within these systems, shedding light on their relevance to Mott-Hubbard physics and applications in nonlinear optics and nanophotonics.First, I will discuss how optical pumping in TMD trilayers can induce giant excitonic optical nonlinearity, as much as ~10 meV of resonance blueshifts of Fermi polarons [1]. Intriguingly, we observe a remarkable asymmetry in the optical nonlinearity between electron and hole doping, which is tunable by the applied electric field. We attribute these features to the optically induced valley polarization due to the interactions between excitons and free charges, which open new avenues for photon blockade. Combining multiple layers of atomically thin excitonic materials, we envision the realization of chiral optical nano-cavities [2] featuring a strong nonlinear response.

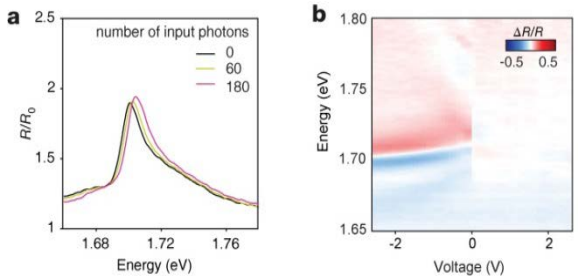

Fig. 1. Giant optical nonlinearity from exciton-hole interactions. a*. Our results show strong oscillator strength and giant nonlinearity of Fermi polarons in trilayer WSe_2, where hundreds of photons lead to a strong blueshift of the polaron resonance [Ref. 1].*
b. *Reflectance change induced by optical pumping in trilayer WSe_2, showing drastically different behaviors in the hole vs. electron-doped regimes (negative vs. positive gate voltages).*

Furthermore, I will discuss our recent demonstration of ultrasharp, tightly bound interlayer excitons with energy tunable over a ~180 meV range. Remarkably, we demonstrate the long-range transport of interlayer excitons with a characteristic diffusion length exceeding ten micrometers, which can be attributed, in part, to their dipolar repulsive interactions. The formation and transport of tightly bound interlayer excitons with narrow linewidth, coupled with the ability to electrically manipulate their properties, open exciting new avenues for exploring quantum many-body physics, including excitonic condensate and superfluidity.

References

[1] L. Gu, L. Zhang, R. Ni, M. Xie, D. S. Wild, S. Park, H. Jang, T. Taniguchi, K. Watanabe, M. Hafezi, Y. Zhou, in print *Nature Photonics*, (2024). .
[2] D. G. Suárez-Forero, R. Ni, S. Sarkar, M. J. Mehrabad, E. Mechtel, V. Simonyan, A. Grankin, K. Watanabe, T. Taniguchi, S. Park, H. Jang, M. Hafezi Y. Zhou, *arXiv*:2308.04574 (2023).
[3] L. Zhang, L. Gu, R. Ni, M. Xie, S. Park, H. Jang, R. Ma, T. Taniguchi, K.Watanabe, Y. Zhou, *Physical Review Letters*, in print arXiv:2312.02446 (2024).
* Acknowledgement(s): we acknowledge support from the U.S. Department of Energy, Office of Science, the U.S. National Science Foundation, and the Oak Ridge Associated Universities.

Angular momentum dynamics on ultrashort timescales in ferromagnets: Electron-magnon vs. spin-orbit interactions

F. Dusabirane[2], K. Leckron[1], B. Rethfeld[1], H. C. Schneider[1]
[1] *University of Kaiserslautern-Landau, 67653 Kaiserslautern, Germany*
[2] *University of Rwanda, P.O. Box 3900, Kigali, Rwanda*

Ultrafast demagnetization dynamics in 3d-ferromagnets, such as Nickel, were discovered more than 25 years ago, yet there still is no consensus as to how the angular momentum is dissipated on a timescale of about 100fs. I will give a brief overview of old and new theoretical approaches that have been suggested as a microscopic mechanism for ferromagnetic ultrafast demagnetization. I will review our own work on the Elliott-Yafet mechanism and then focus on electron-magnon interactions, which have received increasing attention recently. To study the influence of electron-magnon scattering processes on the carrier dynamics in itinerant ferromagnets on ultrafast timescales, we employ a model band structure ("Stoner model") for the electronic single-particle states. The electron magnon-interaction is formally obtained as coupling to a Heisenberg model, which incorporates the magnetic properties of the itinerant ferromagnet [1]. Importantly, we compute the dynamics of momentum resolved electron and magnon distributions including electron-magnon and electron-electron scattering, which are both treated at the level of Boltzmann scattering integrals. We also include an Elliott-Yafet like spin relaxation mechanism due to spin-orbit coupling [2]. We find that electron-magnon scattering leads to a pronounced non-equilibrium for magnon modes at higher energies and wave vectors that couple directly to Stoner transitions as shown in the Figure. For reasonable parameters that

capture some of the properties of magnons in iron, the electronic spin-flip scattering with magnons results in a momentum dependent absorption/emission of magnons and a transient increase of the electron spin polarization on a timescale of a few ten femtoseconds, which is then removed by the Elliott-Yafet spin relaxation. Such an increase of the spin polarization is also found in the dM/dt model, which has been introduced to model ferromagnetic demagnetization dynamics and spin current generation [3]. As we do not make its quasi-equilibrium assumption, we can go beyond the dM/dt model and demonstrate the non-equilibrium features inherent in the demagnetization dynamics due to the interplay of electron-magnon and electron-electron scattering processes [4].

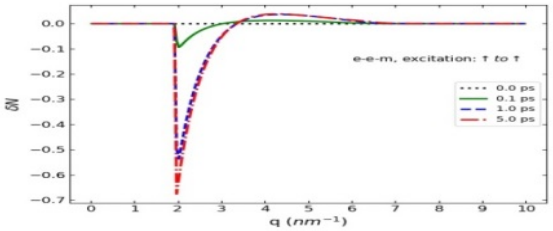

Fig. 1. Change of magnon distribution *δN(q,t) due to electron-magnon and electron-electron scattering after excitation by an instantaneous heating process. The region of q values, for which electronic spin flip transitions are possible, starts around 2 nm^{-1}.*

We study the influence of magnon-phonon relaxation processes and different excitation conditions. Finally, we compare our results to recent experiments [5].

References

[1] B. Woolsey, R. M. White, *Physical Review* B **1**, 4474 (1970).
[2] K. Leckron, S. Vollmar, H. C. Schneider, *Physical Review* B **96**, 140408 (2017).
[3] M. Beens, R. A. Duine. B. Koopmans. *Physical Review* B **102**, 054442 (2020).
[4] F Dusabirane, K Leckron, B. Rethfeld, H.C. Schneider, *arXiv:2304.14978* (2023).
[5] M. Stiehl, M. Weber, C. Seibel, J. Hoefer, S. T. Weber, D. M. Nenno, H. C. Schneider, B. Rethfeld, B. Stadtmüller, M. Aeschlimann, *Applied Physics Letters* **120**, 062410 (2022).

* Acknowledgment: we acknowledge funding by the Deutsche Forschungsgemeinschaft (DFG, German Research Foundation) through grant TRR 173- 268565370 (project B03).

Ultrafast magnetization from the perspective of phonon

N.Wu [2],Y.Wang[1]

[1]*Institute of Physics, Chinese Academy of Sciences, Beijing 100190, China*
[2]*University of Chinese Academy of Sciences, Beijing 100190, China*

Ultrafast magnetism upon photoexcitation in magnetic quantum materials inspires new device concepts based on nonequilibrium phenomena, yet meanwhile poses great challenges in capturing the coupled spin-lattice and spin-electron dynamics. Here we present a full ab initio dynamics description of the photoinduced ultrafast demagnetization of a monolayer ferromagnet, using Fe_3GeTe_2 as a prototype system. We observe a three-stage demagnetization process, namely, an ultrafast and substantial demagnetization on a timescale of 100 fs, after which the light-induced coherent A1g phonon modes significantly couple to the spin dynamics in the next 200-800 fs. In the third stage, nonlinear phonons drive chiral in-plane and out-of-plane lattice motions and results in significant spin precession. The nonadiabatic effect causes significant phonon hardening and suppresses the spin-phonon coupling during demagnetization. Our work provides a general understanding of the dynamic charge-spin-lattice coupling in ultrafast demagnetization and evidences angular momentum transfer between phonons and the spin degrees of freedom.

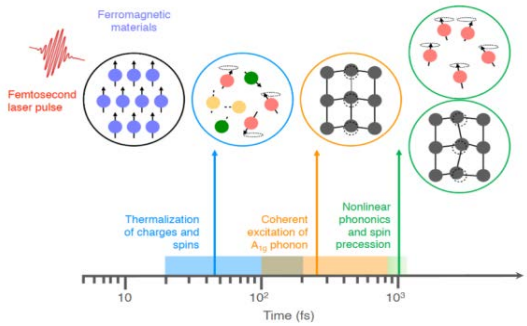

Fig. 1. The three-stage demagnetization mechanism *in two-dimensional ferromagnet.*

Finally, we discuss the proposal of manipulating magnons and chiral phonons via light which we hope to spark further experimental study.

References:

[1] E. Beaurepaire, J.-C. Merle, A. Daunois, J.-Y. Bigot, *Physical Review Letters* **76**, 4250 (1996).
[2] A.S. Disa, M. Fechner, T. F. Nova, B. Liu, M. Först, D. Prabhakaran, P. G. Radaelli, A. Cavalleri, *Nature Physics* **16**, 937 (2020).
[3] D. Chen, P. You, Z. Nie, Na Wu, C. Lian, C. Zhang, S. Meng, *Chinese Science Bulletin* **66**, 3088 (2021).
[4] N. Wu, S. Zhang, Y. Wang, S. Meng, *Progress in Surface Science* 100709 (2023).
[5] N. Wu, S. Zhang, D.Chen, Y.Wang, S.Meng. *Nature Communications* **15**, 2804 (2024).

Waveform measurement of propagating ultrashort graphene Plasmon wavepackets using on-chip THz spectroscopy

K.Yoshioka
NTT Corporation, 243-0198 Atsugi, Japan

Graphene plasmons within the terahertz (THz) spectrum have attracted significant interest as potential next-generation information carriers due to their strong confinement capabilities, active functionalities, and minimal loss characteristics [1]. The development of graphene-based plasmonic circuitry necessitates the ability to dynamically generate, control, and manipulate signal propagation, as well as to conduct on-chip remote measurements of these signals in terms of their amplitude and phase. However, existing methodologies that employ optical excitation via subwavelength configurations are predominantly constrained to stationary assessments of localized plasmonic fields.Here, through the application of state-of-the-art THz electronic techniques [2,3], we have achieved the dynamic on-chip transmission of ultrashort graphene plasmon wavepackets [4]. Our approach, centered on electrical excitation, facilitates the direct conversion of ultrashort electrical pulses into plasmon wavepackets, effectively eliminating the momentum mismatch that notably reduces the efficiency of plasmon generation and detection in optical strategies.Fig. 1(a) shows the schematic of our THz circuit, made by inserting hexagonal boron nitride (hBN) encapsulated graphene into a coplanar waveguide. This configuration allows an ultrashort current pulse of approximately 1 ps, generated using a photoconductive switch, to be injected from ohmic contacts while the signal propagating through the graphene is read out from the opposite ohmic contact. The measurement temperature was 4K. Fig. 1(b) shows the measured waveform of an acoustic plasmon after propagation of 12 μm length in the circuit.

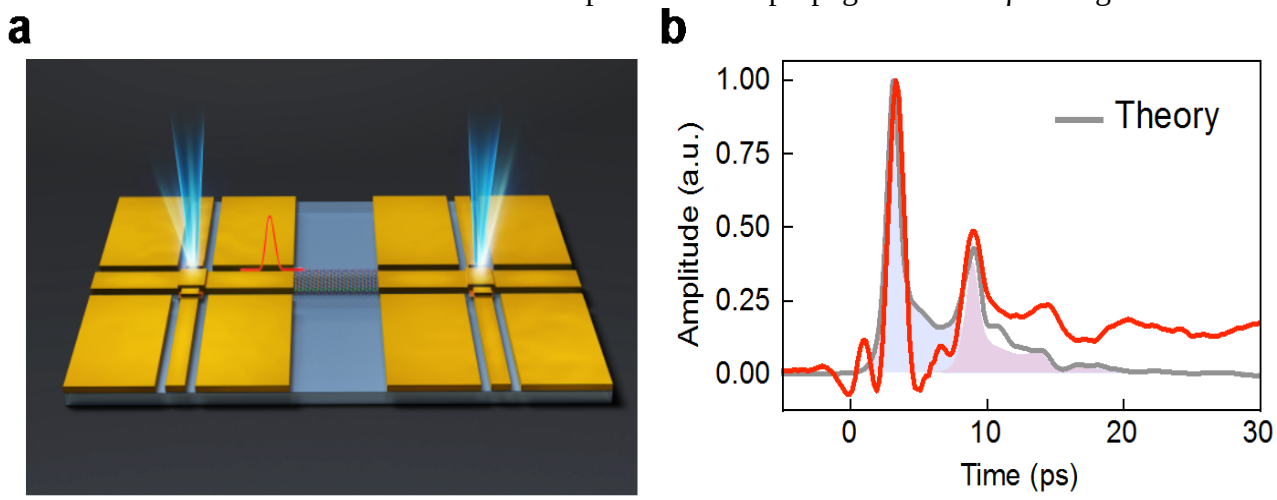

Fig. 1. a. Schematic of the on-chip THz spectroscopy setup *used to investigate the dynamic transfer of ultrashort graphene plasmon wavepackets.*
b*. Time-domain waveform of the plasmon wavepackets, showcasing a pulse duration of 1.2 ps. The waveform is reproduced using a plasmon theory that accounts for the first echo pulse due to impedance mismatch in the circuit.*

The pulse duration of the main pulse was only 1.2 ps, to the best of our knowledge, this is the shortest electrically generated plasmon wavepacket in any material. Following echo pulses come from multiple reflections in the circuit. Furthermore, we succeeded in reproducing the plasmon waveform with a theory based on the telegrapher's equation [5] without adjustable parameters. This enabled us to understand detailed transport properties of ultrashort wavepackets such as propagation mode, velocity, and length. With the estimated propagation length of 21 μm and wavepacket size of 4.0 μm, more than five wavepackets can be transferred before decoherence. We envision that our THz-electronics approach will accelerate the progress of polariton studies in various van der Waals heterostructures, not limited to graphene, and therefore unlock new capabilities for controlling ultrafast signals on-chip.

References

[1] D. N. Basov, M. M. Fogler, F. J. García de Abajo, *Science* **354**, aag1992 (2016).
[2] K. Yoshioka, N. Kumada, K. Muraki, M. Hashisaka, *Applied Physics Letters* **117**, 161103 (2020).
[3] K. Yoshioka, T. Wakamura, M. Hashisaka, K. Watanabe, T. Taniguchi, N. Kumada, *Nature Photonics* **16**, 718 (2022).
[4] K. Yoshioka, G. Bernard, T. Wakamura, M. Hashisaka, K. Sasaki, S. Sasaki, K. Watanabe, T. Taniguchi, N. Kumada, *arXiv* 2311.02821 (2023).
[5] K. Sasaki, N. Kumada, *Physical Review* B **90**, 035449 (2014).

Ultrafast formation of topological defects in a 2D charge density wave

A. Zong
University of California Berkeley, Berkeley, California 94720, USA

Topological defects play a key role in nonequilibrium phase transitions, ranging from birth of the early universe [1] to quantum critical behavior of ultracold atoms [2]. In solids, transient defects are known to generate a variety of hidden orders not accessible in equilibrium [3–5], but how defects are formed at the nanometer lengthscale and femtosecond timescale remains unknown. Here, we employ an intense laser pulse to create topological defects in a 2D charge density wave (CDW) in 1*T*-$TiSe_2$, and we track their morphology and dynamics with ultrafast electron diffraction (Fig. 1a–d).

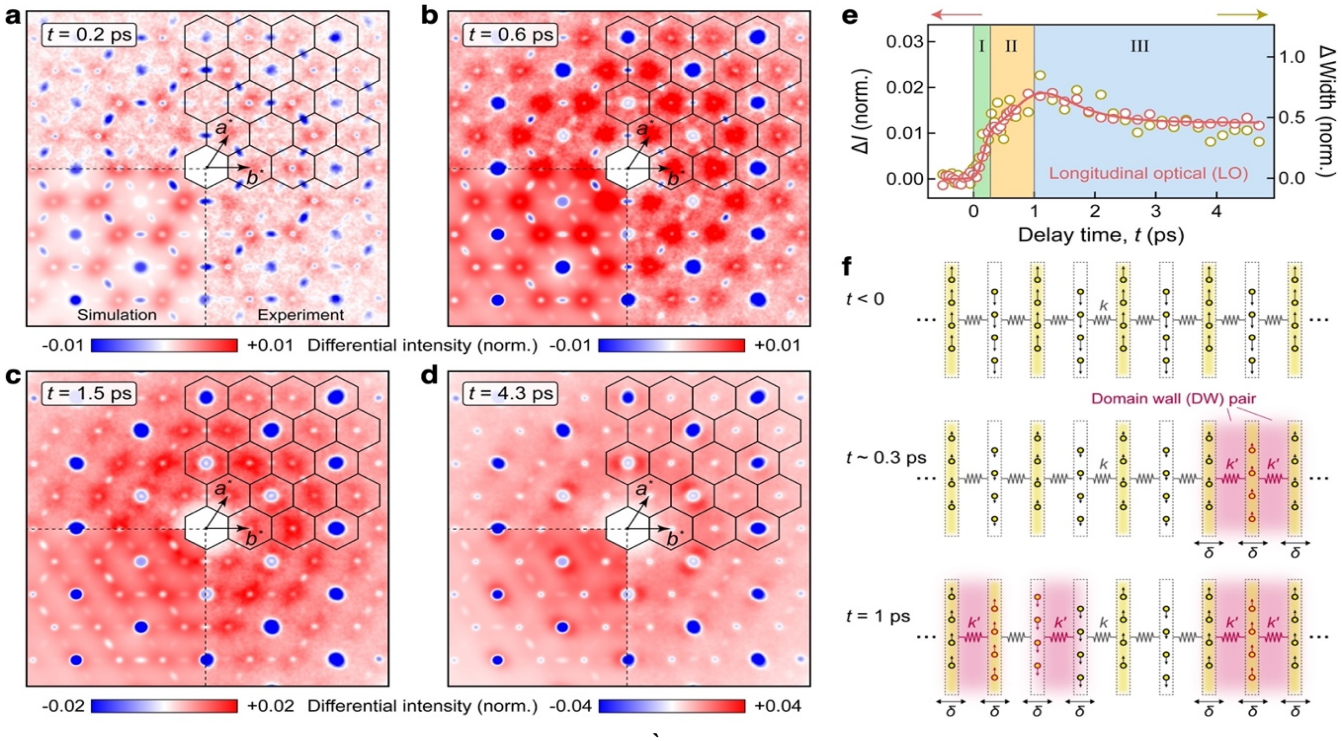

Fig. 1. a–d. Differential electron diffraction intensity *at four time delays after photoexcitation at 210 K by a 3-mJ/cm^2, 800-nm pulse. The lower left quadrant shows the simulation result.* ***e****. Time evolution of diffuse intensities for the longitudinal optical phonon (**red markers, left axis**) and change in the peak width of the 2D CDW at the M point (**yellow markers, right axis**). Solid curves are guides to the eye. Both the width and LO phonon population show similar three-part dynamics, labeled I–III.* ***f.*** *Schematic of dual-stage formation of CDW domain walls mediated by LO phonons. Only Ti atoms are shown (**circles**), where arrows denote CDW displacements. In the first stage (up to ~0.3 ps), the CDW amplitude decreases, represented by the shrinking arrow length; in the second stage (up to 1 ps), the CDW amplitude partially recovers. Pairs of domain walls are indicated by red shades, where CDW displacements in the opposite direction compared to the t < 0 configuration are highlighted by red arrows. Domain wall formation modifies the local inter-chain coupling (k → k'), leading to local displacements (δ) that constitute the LO phonons. All panels reproduced from ref. [6].*

Leveraging its high temporal resolution and sensitivity in detecting weak diffuse signals, we discover a dual-stage growth of 1D domain walls within 1 ps, a process not dictated by the order parameter amplitude but instead mediated by a nonthermal population of longitudinal optical phonons (Fig. 1e,f). Our work provides a framework for the ultrafast engineering of topological defects that are coupled to specific collective modes, which will prove useful for the dynamical control of non-equilibrium phases in correlated materials [6].

References

[1] W. H. Zurek, *Nature* **317**, 505 (1985).
[2] A. Keesling, A. Omran, H. Levine, H. Bernien, H. Pichler, S. Choi, R. Samajdar, S. Schwartz, P. Silvi, S. Sachdev, P. Zoller, M. Endres M. Greiner, V. Vuleti, M. D. Lukin, *Nature* **568**, 207 (2019).
[3] L. Stojchevska, I. Vaskivskyi, T. Mertelj, P. Kusar, D. Svetin, S. Brazovskii, D. Mihailovic, *Science* **344**, 177 (2014).
[4] S. Duan, Y.Cheng, W.Xia, Y.Yang, C.Xu, F.Qi, C.Huang, T. Tang, Y. Guo, W. Luo, D. Qian, D. Xiang, J. Zhang, W. Zhang, *Nature* **595**, 239 (2021)
[5] A. Kogar, A.Zong, P.E.Dolgirev, X.Shen, J.Straquadine, Y.-Q.Bie, X. Wang, T. Rohwer, I.-C. Tung, Y. Yang, R. Li, J. Yang, S. Weathersby S. Park M. E. Kozina, E. J. Sie, H. Wen, P. Jarillo-Herrero, I. R. Fisher, X. Wang, N. Gedik, *Nature Physics* **16**, 159 (2020).
[6] Y. Cheng, A. Zong, L. Wu, Q. Meng, W. Xia, F. Qi, P. Zhu, X. Zou, T. Jiang, Y. Guo, J. van Wezel, A. Kogar, M. W. Zuerch, J. Zhang, Y. Zhu D. Xiang, *Nature Physics* **20,** 54 (2024).

Effective magnetic field and magnetization from chiral phonons

H. Zhu
Rice University, Houston TX 77025, USA

Controlling time-reversal symmetry (TRS) on very short time scales may enable novel non-equilibrium phases of matter, as well as ultrafast spintronics for energy-efficient information processing. Strongly driven phonons directly influence the interatomic distances, orbital symmetry, and exchange interactions that are closely related to magnetism in materials. Chiral phonons, where atoms rotate unidirectionally around the equilibrium position inside crystalline lattice, break time reversal symmetry and are expected to directly couple with magnetization. We excited chiral phonons using circular-polarized terahertz pulses and observed a prominent transient magneto-optic Kerr effect in cerium trihalide[1], which was known to have unusually large spin-phonon coupling [2]. We developed the technique for the generation and nonlinear imaging of coherent chiral phonons in the spectral range around 10 THz to reveal the phonon dynamics [3]. The effective magnetic field needed to polarize the paramagnetic spins is on the order of 1 tesla under a moderate absorbed fluence of 0.2 mJ/cm^2. The temperature dependence of the spin dynamics indicates the magnetic field indeed is generated by the phonons, as opposed to a pure electromagnetic inverse Faraday effect.

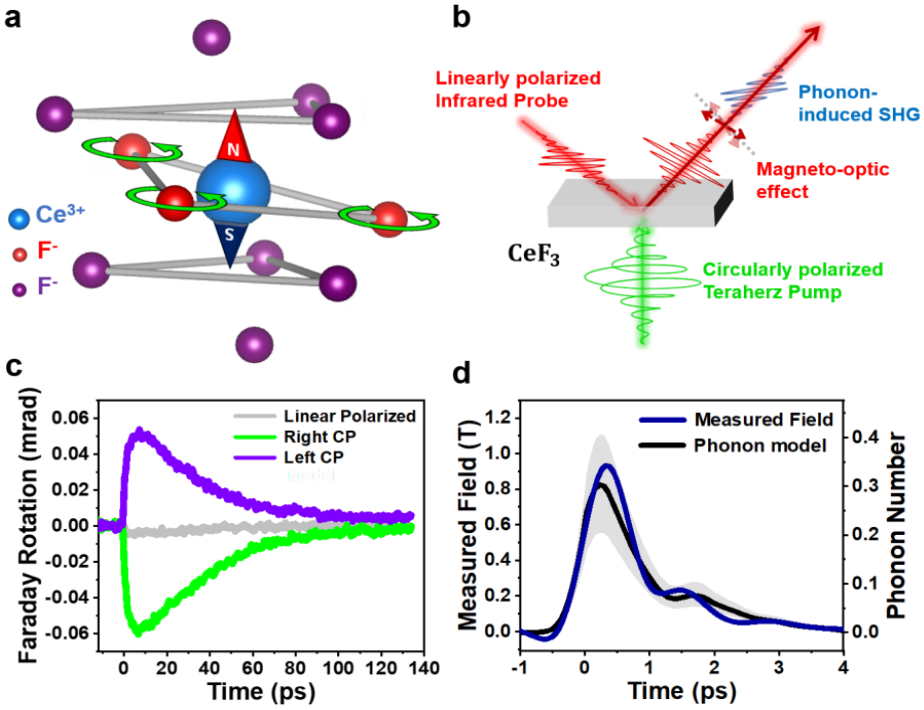

Fig. 1. (a) Illustration of part of the unit cell centered around a Ce^{3+} ion *and the atomic displacement of E_u chiral phonon mode centered around 10.5 THz according to DFT calculations. The F^- ions are denoted in red and purple according to their difference in effective charge tensor. (**b**) Schematic of the time-resolved Kerr ellipticity and Faraday rotation for spin dynamics, and second harmonic generation for phonon dynamics. (**c**) Faraday rotation as a function of delay time is opposite under left CP and right CP THz excitation, evidencing TRS breaking at 10 K. (**d**) Time-dependent effective magnetic field derived from measured magnetization dynamics aligns with that derived from phonon dynamics. The shadowed region indicates uncertainty from the measurement of the phonons' effective magnetic moment.*

The quasi-static magnetic field from TRS-broken phonons, as opposed to magnetoelectric and magnetoelastic effect that causes linear magnon-phonon coupling [4,5],or phonon-enhanced magnetism [6], may be enhanced by polaritonic cavities [7] and open a new route to investigate spin-phonon interaction in a broad range of quantum materials [8,9].

References

[1] J. Luo, T. Lin, J. Zhang, X. Chen, E.R. Blackert, R. Xu, B.I. Yakobson, H. Zhu, *Science* **382**, 698 (2023).
[2] D. M. Juraschek. T. Neuman. P. Narang. *Physical Review Research* **4**, 013129 (2022).
[3] T. Lin. R. Xu. X. Chen. Y. Guan. M. Yao. J. Zhang. X. Li. H. Zhu. *ACS Photonics* **11**. 33 (2024).
[4] A. S. Disa, M. Fechner, T.F. Nova, B. Liu, M. Först, D. Prabhakaran, P.G. Radaelli, A. Cavalleri, *Nature Physics* **16**, 937(2020).
[5] J. Luo, S. Li, Z. Ye, R. Xu, H.Yan, J. Zhang, G. Ye, L. Chen, D. Hu, X.Teng, W. A. Smith, B. I. Yakobson, P. Dai, A. H. Nevidomskyy, R. He H. Zhu, *Nano Letters* **23**. 2023 (2023).
[6] A. Disa, J Curtis, M. Fechner, A. Liu, A. Von Hoegen, M Först, T.F Nova, P Narang, A Maljuk, A.V. Boris, B. Keimer, A. Cavalleri, *Nature* **617** 73 (2023).
[7] R. Xu. T Lin. J Luo. X Chen. ER Blackert. AR Moon. KM JeBailev. H Zhu. *Advanced Materials* **35**. 2302974 (2023).
[8] M. Basini, M. Pancaldi, B. Wehinger, M. Udina, T. Tadano, M. C. Hoffmann, A. V. Balatsky, S. Bonetti, *Nature* **628**, 534 (2024).
[9] C. S. Davies, F.G.N. Fennema, A.Tsukamoto, I. Razdolski, A.V. Kimel, A. Kirilyuk, *Nature* **628**, 534 (2024).

* Acknowledgement: Hanyu Zhu acknowledges support from the NSF (grant No. DMR-2240106), Welch Foundation (grant No. C-2128), and Keck Foundation (grant No. 995764).

AUTHOR INDEX

AUTHOR INDEX

AUTHOR INDEX

MILESTONES 2016-2024

Ultrafast Dynamics and Metastability
Ultrafast Bandgap Photonics

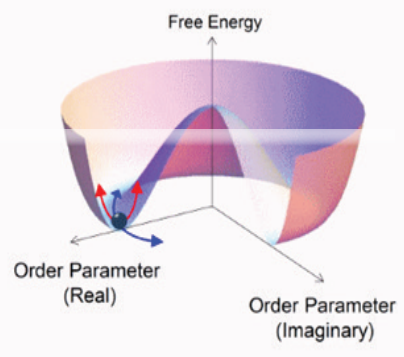

Physica Scripta – 2017
Focus: Ultrafast Bandgap Photonics
Guest Editors: Michael K. Rafailov and Luca Perfetti, 2017
http://iopscience.iop.org/journal/1402-4896/page/Focus-issue-on-Ultrafast-Bandgap-Photonics

Ultrafast Bandgap Photonics
Baltimore, 2016
http://spie.org/Publications/Proceedings/Volume/9835
Anaheim, 2017
http://spie.org/Publications/Proceedings/Volume/10193
Orlando, 2018
https://spie.org/Publications/Proceedings/Volume/10638

Ultrafast Dynamics and Metastability 2017 Workshop
Washington, DC, 2018
https://sites.google.com/a/georgetown.edu/ultrafast-dynamics-and-metastability-archive-2017/

Ultrafast Dynamics and Metastability & Ultrafast Bandgap Photonics 2019
V International Workshop
Washington, DC, April 2019

Ultrafast Bandgap Photonics: Dynamics and Metastability of Transient States 2019
VI International Conference
St. Petersburg, 2019

Ultrafast Bandgap Photonics: Dynamics and Metastability of Transient States 2020
VII International Symposium
Hersonissos, Crete, Greece June 2022

Ultrafast Dynamics and Metastability & Ultrafast Bandgap Photonics 2021
VIII International Workshop
Washington, DC, November 2021

Ultrafast Dynamics and Metastability & Ultrafast Bandgap Photonics 2022
IX International Workshop
Washington, DC, November 2022

Ultrafast Bandgap Photonics: Dynamics and Metastability of Transient States 2023
X International Symposium
Hersonissos-Crete, Greece June 04-10 2023

Ultrafast Dynamics & Metastability : Ultrafast Bandgap Photonics 2024
XI International Symposium 2023
Hersonissos-Crete, Greece June 16-21 2024

Ultrafast Dynamics & Metastability : Ultrafast Bandgap Photonics 2024
XII International Conference
Tucson, AZ, September 25-28, 2024